The role of type I regulatory cells in regulating immune responses to influenza infection

Caitlin Abbott BSc(adv)

A thesis submitted to the University of Adelaide in fulfillment of the requirements for the degree of Doctor of Philosophy.

THE UNIVERSITY *of* ADELAIDE

The University of Adelaide
Department of Biological Sciences
School of Molecular and Biological Sciences
Jan 2022

Declaration

I certify that this work contains no material which has been accepted for the award of any other degree or diploma in my name, in any university or other tertiary institution and, to the best of my knowledge and belief, contains no material previously published or written by another person, except where due reference has been made in the text. In addition, I certify that no part of this work will, in the future, be used in a submission in my name, for any other degree or diploma in any university or other tertiary institution without the prior approval of the University of Adelaide and where applicable, any partner institution responsible for the joint award of this degree. I give permission for the digital version of my thesis to be made available on the web, via the University's digital research repository, the Library Search and also through web search engines, unless permission has been granted by the University to restrict access for a period of time. I acknowledge the support I have received for my research through the provision of an Australian Government Research Training Program Scholarship.

Caitlin Abbott

Acknowledgements

“There is a fifth dimension beyond that which is known to man. It is a dimension as vast as space and as timeless as infinity. It is the middle ground between light and shadow, between science and superstition, and it lies between the pit of man’s fears and the summit of his knowledge. This is the dimension of imagination. It is an area which we call the twilight zone”- Rod Serling. This is known to others as PhD candidature.

Iain, first and foremost I sincerely apologise for the countless times I was far too tired for a meeting and ended up overwhelmed and crying in your office. This occurred more than I would like to admit. Thank you for allowing me to work through my emotions and for not judging me for these incidents. I appreciate the countless hours you have spent with me freaking out about having no data and no project. Thank you for giving me the licence to develop a project independently and assisting me with direction and experimental design. I also need to thank you for all the times you helped me take apart the ARIA and get it working for sorts which became quite frequent towards the end of her life.

Shaun, thank you for guiding me think to about postgraduate research as an undergraduate student. I remember at the time finding the idea of continuing in science exciting and an option I had not seriously considered before our conversations. Thank you for allowing me to be an independent and highly critical scientist and for believing in me and the Tr1 project. Although, maybe I shouldn’t thank you for letting me work on such a finicky cell type... Thank you for helping to develop my scientific writing. I got a lot out of our thesis meetings and have come a long way since starting in the lab. More recently, thank you for allowing me to help steer the direction of future Tr1 cell work in the lab.

Past and present members of the chemokine biology lab thank you for all the help and support over the years. Thank you Adriana for all the cake, for sharing my dream of a clean and tidy lab, for holiday advice, and for listening to me when I’m annoyed. Special mentions include Carly and Jade for being mentors for me from the start, Maleika for moral support and always finding time for tea with me, Kerrie for introducing me to the wonderful world of birds and supporting me when I had no project and no data. Todd, Jaz, and Tim thanks for being my scientific advice panel, for

listening to my project ideas, telling me when they are rubbish, and for helping with experimental design. Aaron thank you for all the bioinformatics help and for always being enthusiastic. Emily, thanks for being the only other person excited about Tr1 cells.

To my family, I have finally finished my PhD so you can stop asking when I will be a doctor now. In all seriousness thank you Mum and Dad for believing in me. Thank you for being endlessly supportive and encouraging me to pursue science. Thank you for always being proud of me, even when I had no data, no project, and no money. Will, Harry, and Annie thank you for listening to me waffle on about science.

Babs, Gertie, and Richard III thank you for being the most ridiculous chickens I have ever had the pleasure of meeting and for the daily cuddles and emotional support.

Last and most importantly, Jesse I don't know why you put up with me but thank you for doing so. There are not enough words to express how much you have supported me and kept me sane during this PhD. You have had to live with outrageous scientific jargon, almost constant complaining, and more recently a rather severe chicken obsession. I can't thank you enough for all the ways you support and inspire me. You are my world and I am excited for our next adventure together.

“Sitting on a cornflake, waiting for the van to come”
- John Lennon

Contents

List of Figures

List of Tables

Abbreviations

ADCC	Antibody dependent cellular cytotoxicity
APC	Antigen presenting cell
ARDS	Acute respiratory distress syndrome
AREG	Amphiregulin
AIRE	Autoimmune regulator
AhR	Aryl hydrocarbon receptor
BALF	Broncho-alveolar lavage fluid
BATF	Basic leucine transcription factor, ATF-like
B6	C57Bl/6
Blimp-1	B-lymphocyte induced maturation protein-1
C-MAF	Musculoaponeurotic fibrosarcoma proto-oncogene
CFA	Complete Freund's Adjuvant
CNS	central nervous system
cTEC	cortico-thymic epithelial cells
CTL	Cytotoxic T lymphocyte
CO_2	Carbon dioxide
CSF1	Colony stimulating factor 1
CCR2	C-C Chemokine receptor type 2
CCR5	C-C Chemokine receptor type 5
CCR7	C-C Chemokine receptor type 7
CXCR3	CXC Chemokine receptor type 3
CXCR4	CXC Chemokine receptor type 4
CXCR5	CXC Chemokine receptor type 5
CXCR6	CXC Chemokine receptor type 6
CTLA-4	Cytotoxic T lymphocyte associated antigen 4
DAMP	Damage associated molecular pattern
DE	Differentially expressed
DC	Dendritic cell
DMEM	Dulbecco's Minimal Essential Medium
DNAM-1	DNAX accessory molecule 1
DN	Double negative
DP	Double positive
EDTA	Ethylenediamine tetraacetic acid
EGFR	Epidermal growth factor receptor
Ebi3	Estein-Barr induced gene 3 (subunit of IL-27)
EAE	Experimental Autoimmune Encepthalomyelitis
Eomes	Eomesodermin
ERK1/2	Extracellular signal regulated kinase
Egr2	Early growth response gene
FOXP3	Forkhead box P3
FACS	Fluorescence activated cell sorting
GATA-3	GATA binding protein 3
GzmB	Granzyme B
GFP	Green fluorescent protein
GM-CSF	Granulocyte-monocyte colony stimulating factor
GvHD	Graft versus host disease
HLA	Human leukocyte antigen
HDM	House dust-mite
Het	Heterozygous
HSCT	Haematopoietic stem cell transfer
ID2/3	Inhibitor of DNA binding 2/3
IL-2	Interleukin 2
IL-4	Interleukin 4
IL-5	Interleukin 5
IL-6	Interleukin 6
IL-10	Interleukin 10
IL-12	Interleukin 12
IL-17	Interleukin 17
IL-21	Interleukin 21
IL-22	Interleukin 22
IL-23	Interleukin 23
IL-27	Interleukin 27
IL-27p28	Interleukin 27 protein 28 (subunit of IL-27)
IL-10Rα	Interleukin 10 receptor alpha
IL-27Ra	Interleukin 27 receptor a
IRF1,4	Interferon regulatory factor 1,4
IAV	Influenza A virus
IEL	Intra-epithelial lymphocytes
IFNγ	Interferon gamma
ICOS/L	Inducible costimulator/ligand
ITK	Inducible T cell kinase

i.n	Intra-nasal
i.p	Intra-peritoneal
i.v	Intra-vascular
IMDM	Iscove's modified Dulbecco's medium
KO	Knockout
LAG-3	Lymphocyte Activation Gene 3
LI	Large Intestine
LPL	Lamina propria lymphocytes
MHC	Major histocompatability complex
mRCLB	Mouse red cell lysis buffer
MLN	Mesenteric lymph nodes
mLN	Mediastinal lymph node
mTEC	Medullary thymic epithelial cells
MOG	Myelin oligodendrocyte protein
nAB	Neutralising antibody
NFAT	Nuclear factor of activated T cells
NOD mice	Non-obese diabetic mice
OVA	Ovalbumin from chicken egg
PAMP	Pathogen associated molecular pattern
PCR	Polymerase chain reaction
PBMC	Peripheral blood mononuclear cells
PBS	Phosphate buffered saline
PB	Peripheral blood
PP	Peyer's patches
Prf1	Perforin
P2RX7	Purinoceptor 7
p-MHC	Peptide-major histocompatibility complex
PD-1	Programmed cell death protein 1
rm	Recombinant mouse
RUNX2	Runt-related transcription factor 2
RORγT	RAR-related orphan receptor gammaT
RT-qPCR	Real Time quantitative polymerase chain reaction
RFP	Red fluorescent protein
SLO	Secondary lymphoid organ
STAT1,2,3,4	Signal transducer and activator of transcription 1,2,3,4
SI	Small Intestine
SIT	Specific allergen immunotherapy
T_H	T helper
TNFα	Tumour necrosis factor alpha
Tbet	T box transcription factor
TOX	Thymocyte selection-associated high mobility group box protein
Treg	T regulatory cell
Tr1	Type 1 regulatory cell
TGFβ	Transforming growth factor beta
TIM-3	T cell immunoglobulin mucin-3
TIGIT	T cell immunoreceptor with Ig and and ITIM domain
TCDD	2,3,7,8-tetrachloro-dibenzo-p-dioxin (AhR ligand)
TLR	Toll like receptor
WT	Wildtype

The role of type I regulatory cells in the regulation of the immune response to influenza infection

Caitlin Abbott

Abstract

The resolution of influenza A virus (IAV) infection requires T cell-dependent immune regulation. In severe cases, without appropriate control of the immune response, the inflammation resulting from respiratory viral infection can lead to pneumonia and death. It is known that regulatory T cells are important for many aspects of immune regulation including preventing uncontrolled inflammation and limiting tissue damage. The quintessential and most studied regulatory T cell is the FOXP3^{+} Treg. Type I regulatory (Tr1) cells are also known to be present in different infection settings but are far less understood. Tr1 cells are defined as IL-10^{+} FOXP3^{-} CD4^{+} T cells, enriched for co-inhibitory molecule expression, and capable of suppressing effector T cell responses. In the present study Tr1-like cells accumulated in the parenchyma of the IAV-infected lungs at day 7 post infection where they represented the dominant source of T cell-derived IL-10. IAV infection of a known model of Tr1 deficiency (*Il27ra*$^{-/-}$ mice) resulted in increased weight loss and delayed recovery from maximum infection-induced weight loss. Adoptive transfer of *in vitro*-derived polyclonal Tr1 cells into *Il27ra*$^{-/-}$ mice led to Tr1 cell recruitment to the lungs and significantly improved recovery from infection-induced weight loss. This established a role for Tr1 cells in the resolution of inflammation in IAV infection. Detailed investigation found four distinct *bona fide* Tr1 cell populations based on expression of the surface molecules LAG-3 and CD49b. Although all four populations were suppressive, however, only CD49b-expressing Tr1 cells exhibited IL-10-dependent suppression of effector T cell division. These results determined that Tr1 populations from the IAV-infected lungs exhibited differences in kinetics of accumulation, localisation, suppressive capacity, mechanism of suppression, and molecular profile. Overall, this study points toward a role for Tr1 cells in the resolution of inflammation in IAV infection.

Publications and Presentations

Manuscript in preparation

Distinct sub-populations of Tr1 cells infiltrate the influenza-infected lungs. **Caitlin Abbott**, Aaron Heng, Todd Norton, Timona Tyllis, Jade Foeng, Mark A. Armstrong, Stephen M. Pederson, Mohammed Alsharifi, Shaun R. McColl and Iain Comerford.

Conference Oral Presentations

- 2021- "Type I regulatory cells contribute to the recovery-phase of the immune response to influenza A-infection", The Annual Immunology retreat for the SA/NT branch of the Australian and New Zealand Society for Immunology, *SA*
  Award for Best Oral Presentation by a PhD Student.
- 2020- "The role of Tr1 cells in acute infection", Invited Seminar Speaker at the Babraham Institute Cambridge, Cancelled due to COVID-19 (Invited speaker at the Liston Lab Retreat via Zoom instead) *Cambridge, UK*
- 2019- "Tr1 cells contribute to the regulation of the immune response against Influenza infection", The 48th Annual scientific meeting of the Australian and New Zealand Society for Immunology, *Adelaide, AU*
- 2017-2019- "Tr1 Cells in Influenza A infection", The Annual Immunology retreat for the SA/NT branch of the Australian and New Zealand Society for Immunology, *SA* : *2018- Award for Best Oral Presentation by an Honours or Masters Student.*

Conference Poster Presentations

- 2021- "The role of Tr1 Cells in the resolution of Influenza A infection", The Australian and New Zealand Society for Immunology Conference, *Online*
  Australian and New Zealand Society for Immunology-British Society for Immunology Poster Award.
- 2020- "Tr1 cells contribute to the regulation of the immune response against Influenza infection", Immunochemistry and Immunobiology- Gordon Research Conference, Cancelled due to COVID-19 *Castelldefels, Spain*
- 2018- "Tr1 Cells in Influenza A infection", The Australian and New Zealand Society for Immunology Conference, *Perth, AU*

Chapter 1: Introduction

1.1 The immune response to IAV infection

The immune system is responsible for protecting the body from a deluge of microbial challenges. The innate and adaptive immune systems collaborate to sense threats and elicit a tailored and appropriate immune response. Influenza A virus (IAV) is a major human pathogen, responsible for between 294,000 and 518,000 fatalities per year worldwide [1]. Yearly vaccination is required to control IAV infection rates. This is due to IAV vaccines providing limited strain coverage as they predominately target B cell epitopes in combination with the virus itself having a high rate of antigenic drift and shift. In addition, the emergence of new variants of IAV regularly cause serious pandemics [2]. The immune response to IAV infection incorporates both innate and adaptive responses to control and clear the virus. While these responses are elicited for pathogen elimination they are accompanied by tissue damage, which can also be detrimental to the host by facilitating secondary infection or irreparable airway destruction leading to respiratory failure [3], [4]. Understanding how immune responses are regulated in the face of acute infectious challenge such as IAV is not completely understood and will be the main focus of this thesis.

IAV generally enters the respiratory tract via inhaled droplets after which it can productively infect host respiratory epithelial cells [5]. These cells provide a first line of defence against IAV infection. Aside from acting as a physical barrier to microbial challenge the respiratory epithelium is armed with a number of innate defence strategies to maintain homeostasis including cilia, mucins, and toll-like receptors (TLRs). Most respiratory epithelial cells have cilia on their surface. These luminal projections can beat in unison to promote mucus flow to expel foreign bodies and protect the underlying epithelial cells from contact with foreign and microbial particles [6]. Mucins are produced by a number of epithelial cell types within the respiratory tract and form the protective mucous layer. In addition to acting as a physical barrier, mucins also exhibit anti-microbial properties [7]. As indicated above, respiratory epithelial cells also express TLRs which recognise pathogen- and damage- associated molecular patterns (PAMPs and DAMPs) [8], [9], [10]. TLR signalling leads to activation of the downstream mediator NF-κB which in turn activates transcription factors in the interferon regulatory factor (IRF) family resulting in activation of anti-microbial gene expression, pro-inflammatory cytokine production, and chemokine production [11], [12]. The cytokines produced via this pathway are from the type I interferon (IFN) family, namely IFNα and IFNβ. These type I IFNs, when bound to the type I IFN receptor, induce expression of interferon stimulated genes (ISGs). There are a multitude of different ISGs, the products of which have the capacity to target different stages of the "life cycle" of the virus by targeting viral attachment, entry, nuclear import, mRNA synthesis, protein synthesis, replication, degradation, assembly, and egress [13].

Pathogen or damage recognition, as would occur in the event of IAV infection, results in the rapid recruitment of a range of innate cells tasked with combating the challenge including neutrophils, macrophages, and innate lymphoid cells (ILCs). Phagocytes are cells such as macrophages which are specialised to engulf the virus and promote clearance. ILCs consist of ILC1, ILC2, and ILC3s in addition to cytotoxic NK cells. In IAV infection NK cells can kill virally infected cells via natural and antibody dependent cellular cytotoxicity (ADCC) [14], [15], [16]. Natural and ADCC both rely on killing via perforin and granzyme dependent mechanisms [17], [18]. This potent killing function is kept in check as the killer-like leptin receptors (KLR) expressed by NK cells bind to major histocompatability complex class I (MHC-I) on uninfected cells and results in signalling to inhibit cytotoxic function against healthy cells. In contrast virally infected cells will often down-regulate MHC-I and hence, become susceptible to NK-mediated cytotoxicity [19], [20]. Both NK cells and ILCs are an early source of inflammatory cytokine IFNγ. Type I IFN signalling in NK cells is required for IFNγ production and cytotoxic function in IAV infection [21].

Specialised populations of macrophages and dendritic cells (DCs) reside within the respiratory epithelium. DCs are the sentinel cells of the immune system which link innate and adaptive immunity. DCs express TLRs to sense PAMPs and DAMPs and upon recognition of these molecules the resulting signalling leads to activation and maturation of DCs [22], [23], [24]. Once activated, DCs migrate to the draining lymph nodes where they can present processed antigen to T cells in the context of MHC molecules. In contrast B cells do not require antigen presentation and instead recognise native antigen which drains into the lymph node during infection. T and B cells express receptors that are specific for a single antigen. Diversity in antigen receptor specificity is achieved through a complex process of somatic recombination and clonal selection to provide an essentially unlimited repertoire of antigen binding specificities. Upon recognising their cognate antigen, lymphocytes carrying a single receptor specificity undergo clonal selection resulting in their expansion and differentiation.

In response to IAV infection a type I immune response is generated including anti-IAV antibody producing B cells, as well as $CD4^+$ helper and $CD8^+$ cytotoxic T cells. $CD4^+$ T cells produce IFNγ which further enhances $CD8^+$ T cell cytotoxicity. B cells which have undergone clonal selection and maturation can further specialise by undergoing class-switch recombination and affinity maturation. Antigen specific B cells, with help from T follicular helper (Tfh) cells can form germinal centres (GCs) which are required to generate large pools of high affinity and memory B cells. Other B cells can differentiate into antibody secreting plasma cells. Antibodies specific for IAV bind to the virus, enhance visibility for phagocytic cells, and neutralise the virus by preventing entry into host cells [25].

With regard to T cell responses to IAV, $CD4^+$ T cells are known to further assist in DC maturation via CD40:CD40L ligation, which "licences" DCs to more effectively prime $CD8^+$ cytotoxic T cells (CTLs) [26], [27], [28], [29]. $CD8^+$ T cells are able to directly kill virally infected cells via secretory pathways (e.g. production of granzymes and perforin) and non-secretory pathways (eg. FAS-FASL cell death signalling) [30]. Activated virus-specific $CD8^+$ T cells also produce inflammatory cytokines such as IFNγ which contributes to further recruitment of DCs and macrophages to the site of infection. In addition to recruitment, IFNγ is also critical for macrophage activation [31], [32], [33], [34], [35], [36] and upregulation of MHC-I molecules on the surface of antigen presenting cells (APCs) [37], [38] further potentiating the CTL response to viral infection. The robust anti-viral CTL response is effective in clearing infection, however, without appropriate control these responses can lead to exacerbated tissue damage. To prevent excessive tissue damage there are populations of $CD4^+$ T cells which act to restrain inflammation and promote tissue repair. These $CD4^+$ T cells with regulatory function are aptly named regulatory T cells. In order to convey the importance of the regulation elicited by $CD4^+$ T cells, the activation, differentiation, and effector functions of this multifarious group of T cells will be described in the following sections.

1.2 $CD4^+$ T cells

T cells complete their development in the thymus where they undergo positive and negative selection. The process of thymic selection ensures that developing T cells (thymocytes) express a functional, MHC-restricted, non-self reactive TCR prior to their release into the periphery. Post-thymic development T cells are considered mature naive cells, having completed antigen-independent development. To become activated and subsequently participate in an immune response, naive T cells must recognise their cognate antigen in the context of MHC presented by APCs in combination with co-stimulation and soluble signals to result in activation, proliferation and differentiation [39], [22], [23], [40], [41], [42], [43], [44], [45].

$CD4^+$ T cells have a diverse array of functions in the immune system during health and disease. The functional specialisation for distinct immune activities has given rise to the classification of these cells into discrete subsets. Each $CD4^+$ T cell subset is specified by a single lineage-defining master transcription factor which is both necessary and sufficient to drive cell fate by imprinting a specific gene expression profile including, a unique cytokine signature which is tailored for dealing with specific challenges. Mosmann and Coffman were the first to divide $CD4^+$ T cell subsets into Th1 and Th2 cells based on their stable expression of distinct sets of cytokines [46]. Th1 cells were thought to regulate immunity to intracellular pathogens (such as viruses including IAV) while Th2

cells supported immunity to extracellular pathogens such as helminths. This is now known to be a great oversimplification and various other $CD4^+$ T cell subsets that control distinct aspects of adaptive immunity are now known. With accumulating evidence other subsets were later designated as Th17, Th9, Th22 cells, and Tfh. Each of these $CD4^+$ T cells is specialised to combat specific types of microbial challenge as will be discussed in this section (refer to **Figure 1.1**).

1.2.1 Th1 cells

The role of Th1 cells is to assist with the clearance of intracellular pathogens such as viruses and intracellular bacteria, and this is predominately mediated through IFNγ production [47]. Th1 cells can be polarised in the presence of IFNγ derived from NK cells in the lymph node as this promotes STAT-1 activation [48], [49], [50]. This leads to upregulation of the lineage specific transcription factor T-BET which in turn, promotes expression of the IL-12Rβ2 [51], [52], [50]. It was demonstrated that T-BET is necessary and sufficient for Th1 cell IFNγ-production [51], [53], [54]. IL-12 received from APCs can then activate STAT-4 to increase and stabilise production of IFNγ in addition to promoting growth and survival of Th1 cells [52], [55], [56]. As previously mentioned IFNγ is known to activate macrophages enhancing their anti-microbial activity [31], [32], [33], [34], [35], [36] in addition to up-regulating MHC expression on APCs [37], [38]. IFNγ is also an important signal for B cells which drives class switching to IgG2 isotypes [57],[58]. These IgG2 antibodies can bind high affinity Fcγ receptors to contribute to opsonisation and phagocytosis of microbial pathogens [59]. Therefore, Th1 cell function is critical for promoting CTL responses directed against intracellular pathogens, and via antibody production, enhancing pathogen phagocytosis.

1.2.2 Th2 cells

Th2 cells promote responses targeted towards expulsion of extracellular bodies such as protozoa and helminths. The lineage specific transcription factor for Th2 lineage commitment is GATA-3 [60], [61], [62], [63], [64]. GATA-3 is induced during Th2 polarisation via IL-4 dependent pathways following STAT6 activation and IL-4 production [65], [55], [66]. There are also IL-4/STAT6 independent pathways in which TCR signalling with co-stimulation and IL-2 can also lead to IL-4 production albeit, with sub-optimal expression of GATA-3 [67], [68], [69], [70]. This pathway of Th2 induction relies on IL-2 signalling which activates STAT5 leading to IL-4R expression and GATA-3 activation [71], [72], [73]. GATA-3 is common to all Th2 cells and is known to promote the production of IL-4, IL-5, and IL-13 [61], [74]. These effector cytokines are critical for Th2 cell function

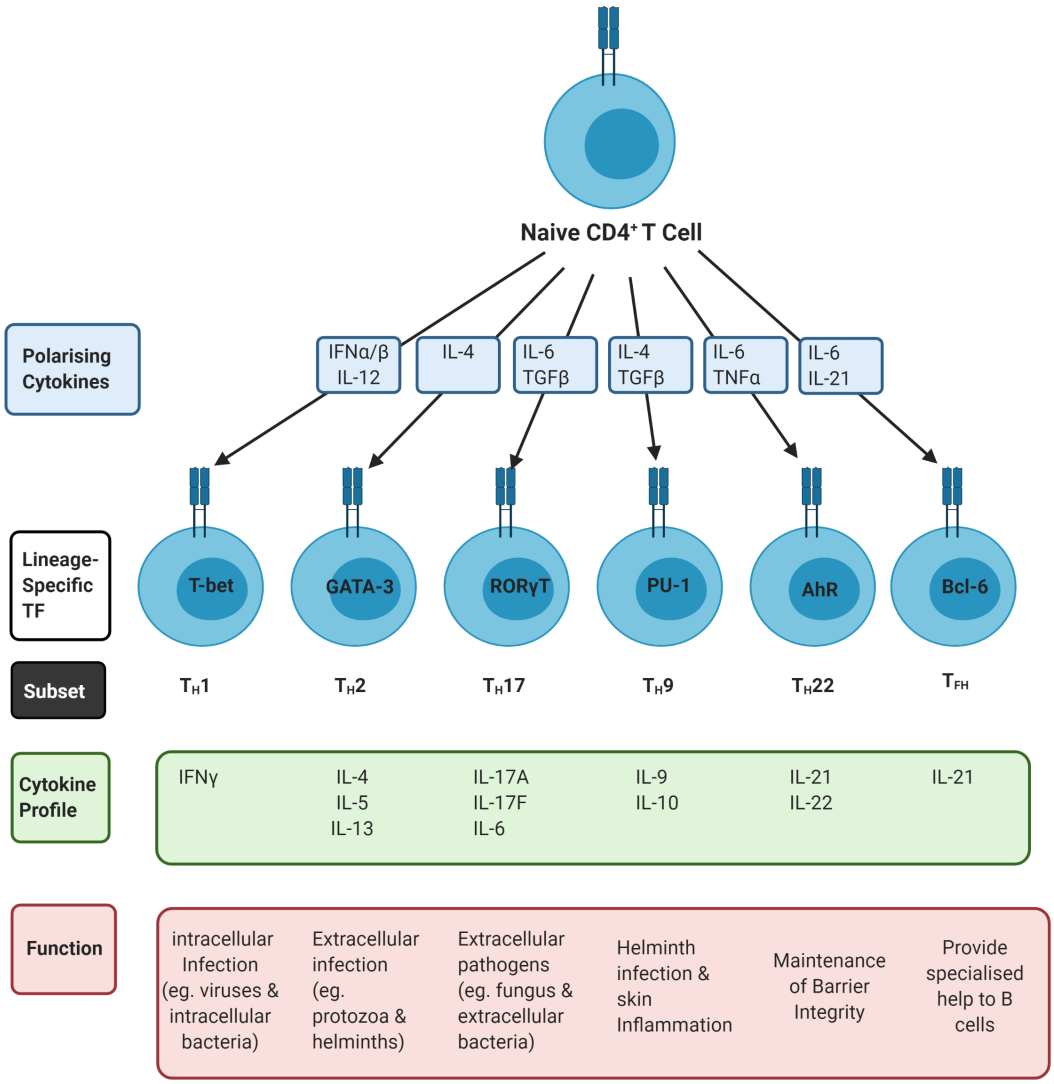

Figure 1.1: The CD4⁺ T cell subsets.

Summary of CD4⁺ T cell subset specification. Each subset is identified and characterised based on polarising cytokine conditions and lineage specific transcription factor expression. This unique combination gives rise to a specialised cytokine production profile which dictates the effector function of each population against a specific challenge. (Created with BioRender.com)

in combating helminth challenge. Th2 cells can promote B cell activation, antibody production and isotype switching to IgE, IgG1, and IgG4, as well as promoting basophil and eosinophil accumulation at the site of challenge [75], [76], [76], [77], [78]. This allows Th2 cells to efficiently drive clearance of helminth pathogens while limiting tissue damage through production of IL-10. In addition, Th2 cells can also promote tissue repair processes elicited by macrophages [79].

1.2.3 Th17 cells

Th17 cells are an important cell type for combating extracellular pathogens such as yeast, fungi, and extracellular bacteria. Th17 cells promote inflammation and recruit neutrophils to the site of challenge to assist in clearance of extracellular pathogens [80], [81]. This $CD4^+$ T cell population relies on the transcription factor RORγt which defines the Th17 lineage [82], [83]. Despite being known as predominately pro-inflammatory cells, relatively benign Th17 cells maintain the integrity of barrier tissues (eg. mucous membranes of the intestinal and respiratory tracts) [84], [85], [86]. These cells are induced by TGF-β and IL-6, and co-express IL-17A, IL-17F, IL-22, and IL-10. More inflammatory subsets of Th17 cells are induced by IL-23 signalling in the presence of chronic antigen activation. It is these pathogenic Th17 cells which are known to be required for the development of chronic inflammation and autoimmune disease and these cells express IL-22, IFNγ, and GM-CSF in addition to IL-17 [87], [88], [89], [90], [91], [92], [93]. IL-6 and IL-23 both induce signalling through STAT3 which is known to bind and activate the IL-17A/F promoter an essential gene for Th17 development [94], [95], [96]. Therefore, the Th17 lineage relies on STAT3 and RORγT to drive a fate specialised for combating extracellular pathogens.

1.2.4 Th9 cells

Th9 cells are an IL-9 producing $CD4^+$ T cell population with varied contributions to immune responses. IL-9 producing $CD4^+$ T cells are implicated in skin homeostasis [97] and anti-tumour immunity [97], [98]. Th9 cells have also been implicated in immunity to helminth infection which was found to be dependent on the expression of IL-9 and recruitment of mast cells [99]. The lineage specific transcription factor driving expression of IL-9 and Th9 development is PU.1 [100]. In mice with a T-cell specific deletion of PU.1, Th9 development is inhibited and IL-9 production abrogated [100]. Naive $CD4^+$ T cells can be polarised to a Th9 fate by activation in the presence of TGF-β and IL-4 [101], [99]. The resultant cells produce IL-9 and IL-10 but are not suppressive and instead promote inflammation [101]. IL-4 signalling activates STAT6 leading to the up-regulation of PU.1, production of IL-9, and activation of IRF4 leading to IL-10 production [101], [102], [100], [103].

Th9 cells have been shown to contribute to a broad range of immune responses in which they promote inflammation.

1.2.5 Th22 cells

Th22 cells are known for producing the cytokine IL-22. The IL-22 receptor is expressed by cells of the barrier tissues (eg. skin, lung epithelium, and intestinal epithelium) [104]. In the epithelial cells of the intestine and skin IL-22 signalling is known to promote the expression of anti-microbial proteins to protect against infection [105], [106], [107]. This barrier protection function of Th22 cells aids in the defense against bacterial pathogens and defines this $CD4^+$ T cell subset [108]. The Th22 lineage can be polarised by the cytokines IL-6 and TNFα which promote IL-22 production and expression of the lineage-specific transcription factor AHR [109], [110]. Th22 cells are not the only $CD4^+$ T cell subset capable of expressing IL-22. The difference between Th17 cells expressing IL-22, and Th22 cells is the latter do not express IL-17 or rely on RORγT [109], [108], [111]. Both Th17 and Th22 cells are polarised via IL-6 signalling. However, unlike Th17 cells, Th22 cells are inhibited by TGF-β signalling [111], [112], [108]. For Th22 cells, IL-6 signalling activates STAT3 and this drives the production of the lineage specific cytokine IL-22 [113]. In the absence of IL-22-producing $CD4^+$ T cells (*Il6*$^{-/-}$mouse) there was reduced survival of deficient mice compared to wildtype in *C. rodentium* infection [108]. This highlights the critical role for Th22 cells in the maintenance of barrier integrity to prevent exacerbated tissue pathology.

1.2.6 Tfh cells

Tfh cells provide specialised help to B cells and are required for the development of GC reactions. GCs are the critical niche in which antigen-experienced B cells undergo expansion and affinity maturation. Tfh cells were initially characterised as a non Th1 or Th2 cell which expressed a high level of CXCR5 and stimulated production of antibodies by B cells [114], [115], [116]. CXCR5 is a chemokine receptor that directs Tfh cells to the B cell follicle where the ligand for this receptor is abundant [117], [118]. High co-expression of the surface receptors CXCR5 and PD-1 is known as an efficient method for Tfh identification [119], [120]. The transcription factor responsible for driving the Tfh lineage is *Bcl6* [121], [122], [123]. Tfh cell polarisation is promoted by the cytokines IL-6 and IL-21 as mice deficient in both of these cytokines exhibit significantly reduced generation of Tfh cells compared to loss of either cytokine alone [124],[125]. Both IL-6 and IL-21 in combination with co-stimulation via CD28, and ICOS-ICOSL ligation can activate STAT1 and STAT3 which can drive cells toward a Tfh cell lineage by initiating and maintaining activation of the transcription factor BCL-6 [126]. Murine T cells require *Bcl6* for Tfh cell

development. In the absence of *Bcl6* there is a lack of T cell help for B cells and germinal centres fail to form as a result [121], [122], [123].

1.3 Immune regulation by CD4$^+$ T cells

CD4$^+$ T cell populations play important roles in immune responses combating pathogens, however, when misdirected virtually all of these subsets have been implicated in the development of pathologies. Th1 cells are known to contribute to lethality in models of high dose acute infection via overproduction of type I cytokines [127], [128]. Th2 cells are known to drive allergy when inappropriately activated within barrier tissues such as the respiratory tract resulting in allergic asthma, and in the skin leading to atopic dermatitis [129], [130], [131], [132], [133]. Th17 cells, when misdirected are known to drive autoimmune diseases such as experimental autoimmune encephalomyelitis (EAE, a mouse model of multiple sclerosis), autoimmune arthritis, and Crohn's disease/inflammatory bowel disease (IBD) [92], [93], [87], [134], [135]. Misguided Th9 responses can drive skin inflammation [136], allergic airway inflammation [100], [137], [138], autoimmune disease [139], [140], [141], [142], and T-cell driven colitis [143], [101]. Th22 cells have been associated with autoimmune arthritis and autoimmune thyroid disorders when inappropriately activated [144], [145], [146], [147]. Dysregulation of Tfh cell responses is known to exacerbate autoimmune pathologies by facilitating the production of auto-antibodies [148], [149], [150]. To prevent the development of the pathologies listed above, there is a requirement for regulation by specialised populations of immune cells.

The deletion of self-reactive T cells during thymic development is not perfect. Some self-reactive cells will inevitably escape into the periphery where further regulation is required to limit their activation and expansion. In addition, T cells activated appropriately in response to pathogens also require constraint to prevent unnecessary tissue damage as a repercussion of robust effector responses. For these reasons T cells with regulatory function exist to limit both the activation of self-reactive lymphocytes that escape deletion in the thymus and to maintain control over appropriate effector T cell responses. This prevents immune responses from continuing when they are no longer required and causing tissue pathology. A landmark study by Sakaguchi and colleagues described the importance of regulatory T cells for self-tolerance, as mice lacking CD25$^+$ CD4$^+$ T cells exhibited systemic autoimmune disease and adoptive transfer of CD25$^+$ CD4$^+$ T cells into *Cd25*$^{-/-}$ mice ameliorated disease [151]. Consequently, these cells were named T regulatory (Treg) cells. The Treg lineage-specific master transcription factor was subsequently shown to be FOXP3 [152], [153]. During T cell development, thymic Treg (tTreg) are generated from self-reactive T cells in the thymus [154], [155], that bind to self-peptide:MHC complexes

with moderate affinity and are programmed to up-regulate FOXP3 [156]. This diverts these self-reactive T cells towards a regulatory fate. It was later identified that a subset of the regulatory T cell compartment was generated from naive precursors in the periphery. These peripheral regulatory T cells are now named peripheral or inducible Treg cells (pTreg or iTreg). These are generated during activation in response to persistent low-dose antigen exposure [157], [158], [159], antigen presentation in the context of TGF-β supplied by APCs [160], and in the absence of appropriate co-stimulation upon recognition of cognate antigen [161].

FOXP3$^+$ CD25$^+$ tTregs are the most characterised of the regulatory T cell populations identified to date. However, there are many populations of peripherally-induced regulatory T cells and some do not require FOXP3 expression to maintain their regulatory function such as Th3 cells, and type I regulatory (Tr1) cells [162]. Th3 cells express high levels of TGF-β, IL-4, and some IL-10 [163]. These cells are implicated in the development of FOXP3$^+$ Treg cells in the periphery due to their production of TGF-β1 [164], [165]. Tr1 cells are instead characterised by high production of IL-10 and are known to contribute to peripheral tolerance [166]. These FOXP3$^-$ IL-10$^+$ regulatory T cells will form the main focus of this thesis and will be discussed in depth in the following sections.

Overall, regulatory T cells are defined on the basis of their ability to inhibit immune responses. To do this, regulatory T cells exploit a number of different mechanisms, including co-inhibitory molecule expression, competition with other cell types for growth factors, disruption of cell metabolism, and regulatory cytokine production [167], [168], [169]. One of the main cytokines which has been associated with Treg suppressor function is IL-10 [170]. This cytokine is most commonly associated with immunosuppression in the literature, however, it is pleiotrophic and the effects it elicits are highly context dependent [171]. The function and significance of IL-10, the main effector cytokine produced by Tr1 cells, will be discussed in the next section.

1.4 IL-10 in homeostasis and infection

IL-10 was first identified as a secreted molecule produced by Th2 cells capable of inhibiting cytokine production by Th1 cells [172]. IL-10 binds the IL-10R, composed of IL-10Rα and IL-10Rβ with the alpha-subunit as a high affinity component [173], [174]. IL-10 is usually categorised as anti-inflammatory, however, this is entirely context-dependent as it can also have pro-inflammatory effects. For mast cells, IL-10 acts as a growth factor during stimulation [175]. The combination of IL-10 with IL-2 promotes cytotoxic T cell proliferation and differentiation [176], and IL-10 also stimulates activated B cell

proliferation, differentiation, and antibody secretion [177]. This highlights the importance of context for the function of IL-10. Treg within the niche of the B cell follicle are called T follicular regulatory T cells (Tfr). These cells are known to inhibit the activation and expansion of Tfh and B cells through CTLA-4 [178], [179], however, their function is not solely to suppress immune responses. IL-10 derived from Tfr cells has been implicated in promoting B cell differentiation and the GC response in mouse models of infection [180], [181]. In acute LCMV this Tfr-derived IL-10 was found to drive GC-B cells to proliferate and differentiate thus, expanding the pool of these cells in an infection setting [181]. The above examples demonstrate stimulatory and pro-inflammatory functions of IL-10 in a number of contexts, however, most of the literature exploring the function of IL-10 is focused on the suppressive activity of this cytokine.

In APCs, IL-10 signalling through the IL-10R decreases MHC expression and antigen presentation [182], [183], [184], [185], [186], co-stimulatory molecule expression [187], [188], [183], [184], and inflammatory cytokine production [189], [190], [184]. IL-10R signalling in T cells inhibits proliferation and abrogates the production of inflammatory cytokines [191], [192], [193], [194], [195]. During the resolution of acute infection, IL-10 is also known to promote the maturation of effector $CD8^+$ T cells into functional memory cells [196], [197], [198]. In fact, IL-10 signalling activates STAT3 and SOCS3, which are proposed to limit the responsiveness of memory precursor cells to inflammatory cytokines [197]. Therefore, IL-10 promotes the generation of functional memory cells via dampening the response to inflammatory cytokines [197], [198]. As previously alluded to, Tr1 cells are regulatory T cells known to express high levels of IL-10. This unconventional regulatory T cell subset will be discussed in detail in the following sections.

1.5 The discovery of type I regulatory cells

The field of Tr1 cell biology began with studies conducted by the Roncarolo Lab [199], [200]. These studies were the first description of cells now considered to be Tr1 cells and were observed in human patients with severe combined immunodeficiency (SCID). SCID patients have no functional B or T cells and as such are severely immuno-compromised. In the original study, a one-year old SCID patient received a fetal liver and thymus transplant. It was later determined that there was a complete MHC mis-match between donor and recipient. Despite this incompatibility intriguingly, GvHD did not develop in this individual. The patient exhibited chimerism as their T cells were donor-derived but their B cells and monocytes were host-derived. At the 10 year follow-up, T cells were cloned from the patient's blood. Upon stimulation with host antigen, $CD8^+$ T cells proliferated and expressed cytotoxic molecules, suggesting host reactivity. It was puzzling that although

these host-reactive T cells were not deleted in the thymus, they were not causing GvHD in the periphery. This led authors to conclude that there was an unidentified mode of peripheral tolerance occurring [199]. Later studies aiming to identify the mechanism for this observed tolerance to host antigen again investigated SCID patients, this time with mis-matched hematopoietic stem cell transplants (HSCT). Again, stimulation of donor-derived $CD8^+$ T cell clones from recipient patient blood with recipient-antigen resulted in proliferation of some clones. However, this study also cloned donor-derived $CD4^+$ T cells from recipient patient blood. These $CD4^+$ T cells produced high levels of IL-10 when activated by host antigen. The combined observations of host-reactive cytotoxic $CD8^+$ T cells and host reactive IL-10^+ $CD4^+$ T cells suggested that these IL-10^+ $CD4^+$ T cells may be important for maintaining tolerance in these patients [200].

A subsequent study by the Roncarolo Lab revealed that chronic antigen stimulation of human and mouse $CD4^+$ T cells in the presence of IL-10 resulted in the differentiation of T cells that produced high levels of IL-10 but no IL-2 or IL-4. This study named these $CD4^+$ T cells, Tr1 cells [191]. This work established both the suppressive capacity of Tr1 cells, as well as a requirement for antigen-specific activation for their function. Both human and mouse Tr1 cells strongly suppressed the proliferation of naive $CD4^+$ T cells in response to alloantigen. This suppression was shown to be dependent in part on IL-10 and TGF-β. This suggested that IL-10 and TGF-β production are both important for the suppressive function of Tr1 cells but also indicated that other mechanisms were involved [191]. The work by the Roncarolo Lab established the field of Tr1 cell biology and re-ignited interest in novel regulatory T cell populations with the potential for these cells to be applied in clinical settings to mediate tolerance and control inflammation.

There was an explosion of interest in the cytokine IL-10 during the 1990s and it was Locksley and Reed who first identified IL-10^+ $CD4^+$ T cells in human and mouse models of parasite infection. It was found that treatment with anti-IL-4 antibody increased IFNγ-producing $CD4^+$ T cells and led to mice with healing leishmaniasis. Conversely, IL-4 and IL-10 were markedly increased in progressive disease, suggesting an immunosuppressive role of IL-4 and IL-10 during *Leishmania major* infection [201]. Furthermore, in human acute visceral leishmania patients, PBMCs were shown to produce IL-10 in response to leishmania antigen which could inhibit proliferative responses [202]. A similar role for IL-10 was shown for human patients with *Leishmania donovani* infection [203]. Building on these initial studies $CD4^+$ T cells have been shown to be a major source of T cell-derived IL-10 during parasite infection which is important for susceptibility to parasite infection and subsequent disease progression [204], [205], [206], [207].

The initial studies from the Roncarolo Lab were published prior to the development of the $FOXP3^+$ Treg field and further progress in Tr1 biology was hampered by difficulty

in identifying and isolating Tr1 cells. Following the generation of tools such as FOXP3 and IL-10 fluorescent reporter mice [208], [209], Tr1 cells are more recently defined as FOXP3$^-$ IL-10$^+$ CD4$^+$ T cells. However, this definition is not strict enough to encompass Tr1 cells in all scenarios [210], [101]. Fundamentally, Tr1 cells must be capable of suppressing effector T cell division [191], [211], [212], [213], [214], [215], [194], [195], [162], [192], [193]. Tr1 cells can also express Th1 associated cytokines but must not express core cytokines for other Th lineages [216], [191]. As is true for Treg cells, co-inhibitory molecule expression contributes to the suppressive function of Tr1 cells [192], [213], [210]. Accordingly, Tr1 cells are known to be enriched for co-inhibitory molecule expression including the receptors LAG-3, TIM-3, PD-1, TIGIT, and CTLA-4 and a combination of these surface markers have been described as sufficient for their identification [210], [217]. In addition, co-expression of the surface markers LAG-3 and CD49b have been shown to reproducibly identify Tr1 cells in humans and mice [194], [210], [218]. LAG-3 is a known CD4 homolog which binds with higher affinity to MHC-II and so out-competes CD4 for binding [219]. This receptor is required for the suppressive function of some Treg populations [220]. LAG-3 on the surface of Treg cells binds to MHC-II expressed by DCs, inhibiting activation and maturation of the DC [221]. CD49b is expressed by highly activated, functionally mature Treg cells [222]. CD49b has been shown to be induced by co-stimulation and can be indicative of the extent of activation in CD8$^+$ T cells [223]. However, the specificity of these markers for Tr1 cells has been questioned in other settings [224], [225].

Since these landmark studies Tr1-like cells have been identified in type I diabetes (T1D) [226], [227], [228], [229], [230], multiple sclerosis [231], [232], [233], EAE [234], [235], [236],[237], IBD [238], [239], [240], [241], [210], [225], [194], [195], [242], transplantation and GvHD [199], [200], [243], [244], [245], [246], α-CD3 treatment [247], [248], [194], [236], [195], [230], [210], allergy [192], [249], [250], [251] and infection [128], [252], [253], [254], [255], [254], [256], [218], [257], [258]. As the definition of Tr1 cells was only outlined extensively in 2018 [217], there are many studies preceding this review that have not sufficiently characterised and assessed the function of IL-10$^+$ CD4$^+$ T cells to allow for designation as Tr1 cells. This confounds past literature assessing the role of Tr1 cells because IL-10$^+$ CD4$^+$ T cells is not a specific enough definition to exclude Treg cells or effector T cells which are capable of IL-10 expression. The studies mentioned above, the role of Tr1 cells in each disease setting, and the definition used for identification of these cells are summarised in **Table 1.1**. The sheer extent of the different Tr1 cell definitions employed in human disease and mouse models highlights the complexity of the field and the lack of consensus concerning what a Tr1 cell is and what their roles are during disease. In the next section, the current body of knowledge on Tr1 cells will be described with the caveat that most previous studies did not use the currently accepted criteria to define Tr1 cells.

Table 1.1: Definitions of Tr1 cells studied in human diseases and mouse models.

Tr1 definition	Disease-specific effects	References
GvHD		
Human IL-10$^+$ CD4$^+$ T cells	Establish tolerance dependent on IL-10 in SCID patients who had received mis-matched HSCT. These patients did not develop GVHD.	[199],[200]
Human IL-10$^+$ CD4$^+$ T cells	In a clinical trial Tr1 cells were given to HSCT recipients and showed efficacy in promoting tolerance and preventing chronic GVHD in some patients.	[243]
Mouse IL-10$^+$ CD4$^+$ T cells	Donor IL-10$^+$ T cells are required to suppress development of GVHD.	[244],[245]
Mouse FOXP3$^-$ IL-10$^+$ CD4$^+$ T cells	Tr1 cells are the main regulatory population after allogenic bone marrow transfer. Blocking the development of Tr1 cells exacerbated GVHD.	[246]
Acute Intestinal Inflammation (α-CD3 treatment)		
Mouse CD4$^+$ FOXP3$^-$ IL-10$^+$ LAG-3$^+$ CD49b$^+$ T cells	Tr1 cells aid in the resolution of inflammation in EAE.	[236]
Mouse CD4$^+$IL-10$^+$IL-2^{lo}IL-4$^-$	Tr1 cells prevent development of colitis.	[191]
Mouse CD4$^+$ FOXP3$^-$ IL-10$^+$ LAG-3$^+$ CD49b$^+$ T cells	Tr1 cells inhibit the development of T cell transfer colitis.	[194], [195], [210]
IBD and Crohn's Disease		
Human CD4$^+$IL-10^{hi} T cells	Tr1 cells inhibited effector T cell division and myeloid cell production of IL-1β and TNF. Healthy individuals had Tr1 cells which produced IL-22 and maintained intestinal barrier integrity.	[225]

Continued on next page...

Table 1.1 – continued from previous page.

Tr1 definition	Disease-specific effects	References
Human $CD4^+$ IL-10^+ T cells	Reduction in frequency of Tr1 cells in patients with ulcerative colitis and Crohn's Disease.	[241]
Human $CD4^+$ $CD45RA^-$ IL-10^+ T cells	Upon isolation from peripheral blood mononuclear cells (PBMCs) and expansion, Tr1 cells from ulcerative colitis and Crohn's Disease patients exhibit no phenotypic or functional abnormalities and could be useful in treating patients.	[225]
Mouse $CD4^+$ $FOXP3^-$ IL-10^+ LAG-3^+ $CD49b^+$ co-inhibitory receptor enriched Tr1 cells	Co-inhibitory receptor enriched-Tr1 cells are deficient in ulcerative colitis and Crohn's Disease patients.	[210]
Mouse $CD4^+$ $FOXP3^-$ IL-10^+ LAG-3^+ $CD49b^+$ T cells	Tr1 cells inhibit the development of T cell transfer colitis.	[194], [195], [210]
Allergy		
Human IL-10^+ $CD4^+$ T cells	In humans Tr1 cells are responsible for mediating control over allergic Th2 responses.	[192]
Human $CD4^+$ $CD25^+$ IL-10^+ TGF-β^+ T cells	IL-10^+ $CD4^+$ T cells induced by specific immunotherapy suppressed allergen specific immune responses in allergic patients.	[249]
Mouse $CD4^+$ IL-10^+ T cells	Tr1 cells abrogated OVA-induced airway hypersensitivity.	[250], [251]
EAE		
Mouse $CD4^+$ $FOXP3^-$ IL-10^+	Tr1 cells can suppress disease severity in EAE.	[237]
Mouse $CD4^+$ $FOXP3^-$ IL-10^+ LAG-3^+ $CD49b^+$ T cells	Tr1 cells aid in the resolution of inflammation in EAE.	[236]

Continued on next page...

Table 1.1 – continued from previous page.

Tr1 definition	Disease-specific effects	References
Infection		
IL-10^{+} CD3^{+} T cells	*Il27ra*$^{-/-}$ mice have uncontrolled effector T cell proliferation, increased tissue damage, and lethality post *Toxoplasma gondii* infection.	[128]
Mouse FOXP3^{-} CD25^{-} IL-10^{+} CD4^{+} T cells	*Il27ra*$^{-/-}$ mice have increased tissue damage and lethality post *Leishmania major* infection.	[254]
Mouse IL-10^{+} CD4^{+} T cells	*Il27ra*$^{-/-}$ mice have increased tissue damage and lethality post IAV infection.	[256]
Mouse IFNγ^{+} Tbet^{+} IL-10^{+} CD4^{+} T cells	*Il27ra*$^{-/-}$ mice have increased tissue damage and lethality post *Leishmania donovani* infection.	[252]
Mouse FOXP3^{-} IL-10^{+} CD4^{+} T cells	*L. monocytogenes* induced a robust population of IL-10^{+} T cells.	[253]
Mouse CD4^{+} IL-10^{+} T cells	In *Rag*$^{-/-}$ mice infected with *T. gondii*, only reconstitution with IL-10-sufficient CD4^{+} T cells was able to rescue survival post infection.	[255]
Mouse CD4^{+} & CD8^{+} IL-10^{+} effector T cells	IL-10 was required to prevent lethal immunopathology at time points coinciding with the expansion and peak of the T cell response in the IAV-infected lungs.	[259]
Mouse CD4^{+} FOXP3^{-} IL-10^{+} CD49b^{+} LAG-3^{+}	The *Itk*$^{-/-}$ mouse exhibited defects in Tr1 generation post high dose infection. Led to increased mortality and pathology.	[218]
T1D		
Human IL-10^{+} T cells	Increased IL-10^{+} T cells at onset predicted better control in later disease stages.	[260]

Continued on next page...

Table 1.1 – continued from previous page.

Tr1 definition	Disease-specific effects	References
Human IL-10^{+} T cells	Much greater IL-10 produced by T cells from healthy patients compared to newly diagnosed T1D patients in response to islet antigen stimulation.	[228]
Human IL-10^{+} CD4^{+} T cells	Increased IL-10 produced by CD4^{+} T cells from healthy donors compared to T1D patients in response to islet auto-antigen.	[226], [227]
Mouse CD4^{+} FOXP3^{-} IL-10^{+} Tr1 cells	Increasing Tr1 cells in the gut of NOD mice inhibited onset of T1D & antigen-specific Tr1 cells can inhibit diabetes development in T cell transfer systems.	[230]
Mouse CD4^{+} IL-10^{+} IL-4^{-} CD45RB^{low} T cells	Treatment of NOD mice with rapamycin + IL-10 promoted Tr1 development in the spleens of long-term tolerant mice.	[229]

1.6 Phenotype and function of Tr1 cells

As outlined above, a fundamental feature of Tr1 cells is their ability to suppress effector T cells. This suppressive capacity is known to be elicited by Tr1 cells through inhibition of co-stimulatory molecule expression, antigen presentation, and inflammatory cytokine production by the APCs [187], [188], [190], [182], [189], [183], [184]. Tr1 cells also possess the ability to directly suppress effector T cells. In suppression assays using irradiated APCs it was shown that IL-10 and TGF-β were required for suppression of effector T cell division by Tr1 cells *in vitro* [191], [192], whereas *in vivo* efficacy of Tr1 suppression has been shown to be predominately dependent on IL-10 in T cell transfer colitis models [194], [195]. In contrast to Treg cells, Tr1 cells have also been shown to inhibit IL-1β transcription and suppress caspase-I activation, and in turn inflammasome activation in macrophages via production of IL-10 in both mice and humans [261], [225]. The main point of difference between Treg and Tr1 cells is that unlike Treg, FOXP3 expression is not required by Tr1 cells to maintain their suppressive capacity [162]. However, in contrast with Treg cells there is much less known regarding trafficking, localisation, and transcriptional landscape of Tr1

cells in disease settings. To expand on the current understanding of Tr1 cell biology an extensive molecular characterisation of Tr1 cells in specific disease settings is required.

1.6.1 Transcriptional regulation of Tr1 development

As previously mentioned, the first method described for polarising naive $CD4^+$ T cells to a Tr1 lineage employed chronic activation of naive human and mouse $CD4^+$ T cells in the presence of IL-10 [191]. Another method described for generating human Tr1 cells employed the use of IL-10-producing myeloid-derived DCs found naturally in human peripheral blood. These tolerogenic DCs could be differentiated *in vitro* and were found to induce Tr1 cells via ILT4/HLA-G signalling. This was proposed as an important mechanism for generation of Tr1 cells *in vivo* [215]. In this scenario, T cell HLA-G binding to the inhibitory receptor ILT4 leads to the development of anergic or suppressive $CD4^+$ T cells that exhibit Tr1-like properties [262], [263]. In subsequent studies using α-CD3 and α-CD28 with IL-27 stimulation, it was observed that $CD4^+$ T cells could be polarised towards IL-10 production [264], [265]. This finding was surprising as IL-27 had previously been implicated in driving a Th1 phenotype [266], [267], [268], [269]. The cytokine IL-27 is a heterodimeric protein consisting of IL-27p28 and Ebi3 subunits. IL-27 signals through the IL-27R which is composed of IL-27RA and gp130 [270]. Addition of TGF-β in combination with IL-27 resulted in enhanced and stable production of IL-10 from *in vitro*-polarised Tr1-like cells [264]. Further interrogation of IL-27-mediated signalling found that STAT1 [266] and STAT3 are activated in response to IL-27 signalling [271]. Furthermore, deficiency in STAT1 or STAT3 significantly reduced induction of IL-10 due to IL-27 signalling in both human and mouse $CD4^+$ T cells [265], [272]. This suggests that IL-27, via STAT1 and STAT3, is required for the generation of IL-10^+ $CD4^+$ T cells.

Building on these studies it was demonstrated that IL-27-driven expansion of Tr1 cells occurred via induction of c-MAF, IL-21, and ICOS [273]. ICOS is a co-stimulatory molecule known to be highly expressed by IL-10^+ T cells and ICOS driven signalling induces much greater IL-10 production compared to the classical co-stimulatory molecule CD28 [274]. IL-27 is known to activate STAT3 which promotes both IL-10 and IL-21 production. Combining IL-27 with ICOS signalling which activates c-MAF driving Tr1 development [273]. Accordingly, with abrogation of IL-21R, ICOS, or c-MAF there is a significant defect in the generation of Tr1 cells [273]. Signalling via the IL-27R also leads to activation of AHR. In response to treatment of naive $CD4^+$ T cells with IL-27 and TGF-β1 AHR expression is increased and this in turn, drives Tr1 generation [275]. It was concluded that both c-MAF and AHR interact together and act in concert to transactivate both the IL-10 and IL-21 promoters to drive Tr1 polarisation [273], [275]. Further investigation into the establishment of a Tr1 cell transcriptional landscape led to discovery of the “pioneer

factors" IRF1 and BATF. These transcription factors were found to establish the chromatin structure required for IL-10 production and Tr1 development [237]. IL-27 signalling in naive T cells leads to activation of STAT1 which activates IRF1, and STAT3 which in turn activates BATF. In the absence of either IRF1 or BATF, AHR was unable to bind to the IL-10 locus and drive Tr1 fate (Refer to **Figure 1.2**). This study highlighted the importance of IRF1 and BATF as transcription factors, which established the chromatin state required for the induction of a Tr1 cell lineage [237]. In infection settings IL-27 is produced by activated populations of monocytes, macrophages, and DCs [270], [276], [277]. Myeloid-cell derived IL-27 was shown to be critical in the lungs and BALF of IAV-infected mice for the early effector functions of NK cells [278]. In human cells, IL-27 was shown to be expressed by IAV-infected epithelial cells and PBMCs and may limit IAV replication [277].

Much of the early work on IL-10-producing $CD4^+$ T cells utilised cells in which induction of IL-10 in Th1 cells was mediated by chronic TCR stimulation and IL-12. In contrast, more recent work that has focused specifically on Tr1 cells, which are superficially quite similar to Th1 cells, have instead used cells polarised with IL-27 (refer to **Figure. 1.2**). Signalling through the IL-27R induces BLIMP-1 through STAT1 and STAT3 [265] whereas, IL-12-mediated signalling induces BLIMP-1 through STAT4 [279]. BLIMP-1 is known to promote EOMES expression and together they induce IL-10 production in $CD4^+$ T cells [246]. Taken together, these studies exemplify the key signalling pathway differences between effector T cell- and Tr1 cell-derived IL-10 production.

One way in which Tr1 cell generation can be promoted is through high levels of TCR stimulation [280]. In Th1 cells, high levels of TCR stimulation activates ERK1 and ERK2 signalling. This signalling in combination with IL-12, activates STAT4, and together promotes c-MAF expression and IL-10 production. In the absence of IL-12 or the presence of ERK inhibitors there is abrogation of IL-10 production from Th1, Th2, and Th17 cells [280]. The link between c-MAF and IL-10 production by all $CD4^+$ Th cell subsets was consolidated by Gabrysova and colleagues using a T-cell specific *Cmaf*$^{-/-}$ which exhibited a deficiency in IL-10-producing T cells. Transcriptional analysis determined that IL-2 is suppressed by c-MAF and this has been suggested to be a mechanism of limiting type 1 and 2 immune responses, which depend on this growth factor, with induction of IL-10 likely acting as a further level of control [281]. c-MAF is also known to promote Th17 responses leading to a differential disease-specific role for c-MAF in different settings [281]. However, it is not clear if the IL-10^+ T cells from the study by Gabrysova et al., were in-fact Tr1 cells as the five Tr1-defining criteria outlined in the previous section were not adequately assessed.

TCR signalling was further highlighted as a critical factor for Tr1 differentiation as *Itk*$^{-/-}$ mice exhibited a defect in Tr1 cell differentiation in experimental models including

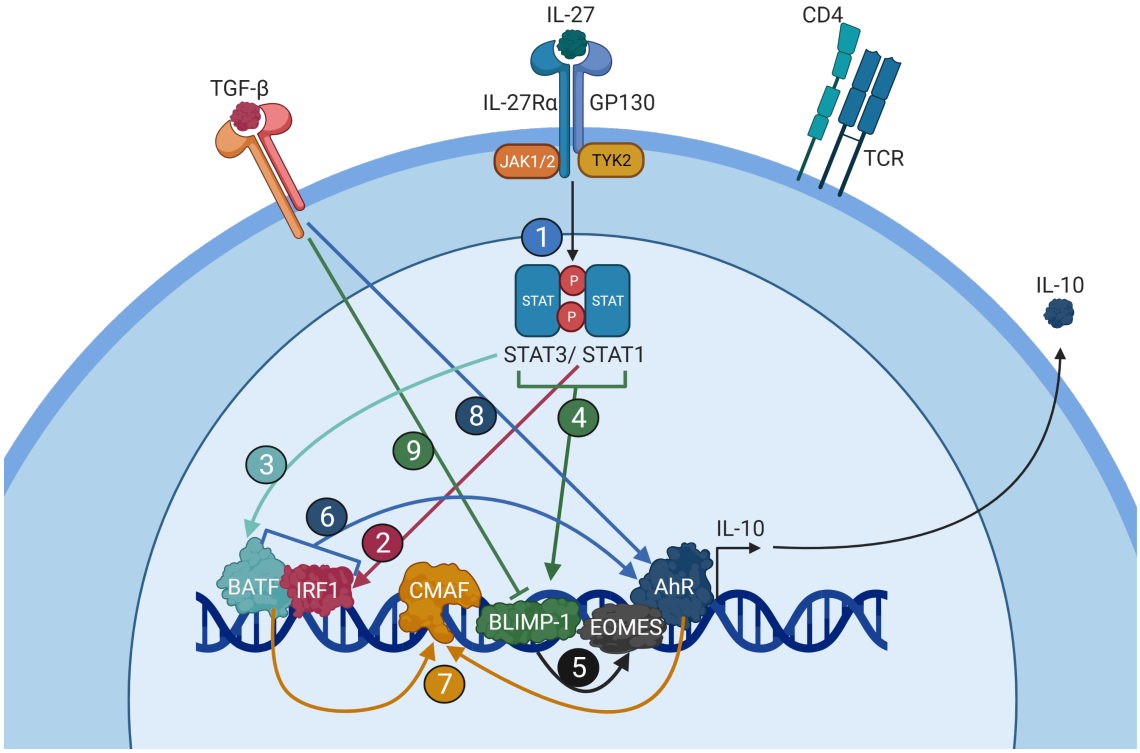

Figure 1.2: IL-27-mediated induction of Tr1 cell development.

(1) IL-27R signalling results in activation of STAT1 and STAT3. (2) STAT1 activates the transcription factor IRF1 and (3) STAT3 activates BATF. (4) STAT3 and STAT1 also activate BLIMP-1 initiating IL-10 expression. (5) BLIMP-1 in turn, activates EOMES again reinforcing the expression of IL-10. (6) Together the pioneer factors IRF1 and BATF establish the chromatin landscape required for Tr1 polarisation and activate AHR. (7) Both BATF and AHR can then activate c-MAF and stabilise IL-10 production. (8) TGF-β1 signalling activates AHR. (9) TGF-β also inhibits BLIMP-1 switching IL-10 production to a BLIMP-1 and EOMES- independent pathway relying on c-MAF. This results in the initiation and stabilisation of IL-10 production and drives the Tr1 cell lineage. (Created with BioRender.com)

α-CD3 treatment, parasite infection, and IAV infection [218]. ITK activates HRas in order to induce IRF4 expression. Restoring IRF4 or HRas expression in *Itk*$^{-/-}$ rescues AHR activation, Tr1 development, and IL-10 expression [218]. This contrasts earlier findings that found IRF4 to be dispensable for Tr1 development [237]. This may be explained by discrepancies between the Tr1 polarising conditions used between these studies, with one study using TGF-β [218] and the other not [237]. It is known TGF-β1 antagonises BLIMP-1 to allow IL-10 production by Th17 and Tr1 cells to be driven instead by c-MAF and AHR [282], [279].

As previously mentioned, an important aspect of Tr1 cell biology is the expression of a range of co-inhibitory receptors that contribute to their suppressive function. IL-27 has been implicated in the expression of LAG-3, TIM-3, and TIGIT [283], [284]. In addition to IL-27 signalling, LAG-3 and CTLA-4 expression can be increased with greater TCR signalling strength [283]. Mice deficient in both *Prdm1* and *Cmaf* have reduced expression of co-inhibitory molecules PD-1, TIM-3, TIGIT, PDPN, PROCR, and LAG-3. The genes for these co-inhibitory molecules were determined to be coordinately regulated by IL-27 signalling via BLIMP-1 and C-maf and have been named "the co-inhibitory gene module" [284]. Furthermore, both *Prdm1* and *Cmaf* were necessary during *in vitro* Tr1 differentiation to establish and maintain the IL-10 producing phenotype. Loss of both *Prdm1* and *Cmaf* resulted in the development of spontaneous colitis, which recapitulates the *Il10*$^{-/-}$ mouse phenotype [285].

To date, the transcription factors implicated in the development of Tr1 cells were studied as they are required for IL-10 production however, this is not the only molecule important for Tr1 function. Transcription factors expressed by Tr1 cells that do not drive IL-10 production are potentially required to drive other aspects of Tr1 development and function [191], [210]. Two transcription factors fitting this category are RUNX2 and ID2 as they are known to be highly expressed by Tr1 cells but are not required for IL-10 production [210], [285]. *Runx2* has been extensively characterised in plasmacytoid dendritic cells (pDCs) as it is important for the differentiation of this cell type [286]. ID2 was found to specifically mark Th1 cells when stained in combination with ID3 which delineates Tfh cells. *Id2* expression was found to be critical for the expression of a number of Th1 genes [287]. These transcription factors could be involved with regulatory functions elicited by Tr1 cells independent of IL-10 and further investigation is required to elucidate their role in Tr1 biology.

Despite these previous studies, the transcriptional landscape of Tr1 cells is still not entirely understood. This T cell subset requires elegant coordination of a variety of factors to initiate, stabilise, and maintain expression of IL-10. Although c-MAF and BLIMP-1 have been identified as critical factors for the development of Tr1 cells in some settings

[285], further interrogation is required to determine what factors drive the development of Tr1 cells as opposed to other Th cell subsets capable of IL-10 production. In summary, although the transcriptional landscape of Tr1 cell development has been investigated there is still much to explore with regard to transcription factors which may not regulate IL-10 production but are involved in driving Tr1 cell development and function.

1.6.2 Chemokine receptor profile of Tr1 cells

Exquisite control of highly specific immune responses is achieved through coordination of the spatiotemporal localisation of immune cells. This is orchestrated by the chemokine system. Chemokines are small protein ligands which are recognised and bound by chemokine receptors. Chemokine receptors are surface bound seven-transmembrane G-protein coupled receptors. Upon binding to their cognate ligands, chemokine receptors uncouple their bound small G-proteins which leads to cell signalling events resulting in directed migration, generally towards higher concentrations of a specific chemokine [288], [289], [290]. *In vivo* this system allows cells to recirculate through secondary lymphoid organs, access inflamed tissues and also organises the microanatomical localisation of immune cells within discrete tissue niches for their activation, differentiation, and effector functions [291] (Refer to **Figure 1.3**). There is little known about chemokine receptor expression by Tr1 cells. Most of what has been documented to date has focused on *in vitro*-derived cells or Tr1 cells from the small intestine. A comparison between the migratory receptors employed by Tr1 cells compared to Treg or effector T cells has not been assessed. Indeed, *in vivo*, it is not yet understood whether Tr1 cells are purely derived from effector T cells at the site of infection/inflammation or whether they differentiate directly from naive precursors within secondary lymphoid organs and migrate to the site of challenge. Uncovering this could contribute to the current understanding of how Tr1 cells are generated and whether they rely on cell migration to reach the effector sites.

Chemokine receptors reported to be expressed by Tr1 cells include CCR1, CCR4, CCR5, CCR7, CCR9, and CXCR6 [194], [230], [292]. Tr1 cells polarised from naive $CD4^+$ T cells exhibited low expression of CCR7 and high levels of CXCR6. The CXCR6 expressed by *in vitro*-derived Tr1 cells was shown to be functional in chemotaxis assays [292]. Tr1 cells polarised from mouse and human naive $CD4^+$ T cells were shown to express more CCR1 compared to unpolarised Th0 cells [194]. However, it is not known if Tr1 cells express CCR1 or CXCR6 *in vivo*. Tr1 cells localised within the intestine commonly co-express of CCR5 and PD-1 [241], [230]. In a mouse model of T1D, islet antigen-specific Tr1 cells from the intestine were injected intra-rectally and their subsequent distribution assessed. Tr1 cells were found in the spleen, lymph nodes, small intestine, colon and the pancreas. They expressed CCR4, CCR5, CCR7 and CCR9 but whether any or all of

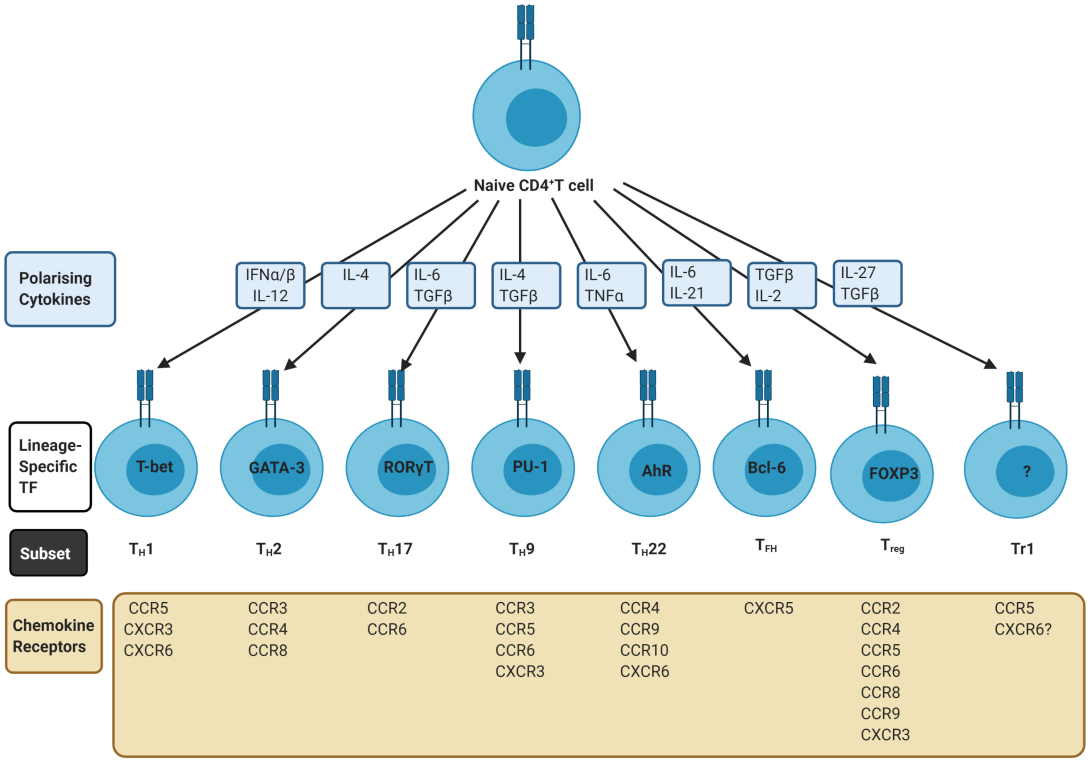

Figure 1.3: Chemokine receptor expression by CD4$^+$ T cells

Each CD4$^+$ T cell population expresses characteristic chemokine receptors important for the localisation in a specific niche relevant to the type of microbial challenge encountered. (Created with BioRender.com)

these receptors are required for their migration to those tissues was not directly assessed [230]. Overall, despite some limited studies, further characterisation of the migratory axes employed by Tr1 cells is required to unravel their trafficking capacity and understand their localisation in homeostasis and disease.

1.7 Models of Tr1 deficiency

In order to robustly interrogate the function of Tr1 cells *in vivo*, models in which Tr1 cells are specifically and selectively ablated are required. This is important to provide information on Tr1 cell function not only due to the inability of the host to produce them, but also providing the opportunity to study their function in transfer (gain-of-function) experiments. This has been a challenge in the field. As no single lineage specific transcription factor has been defined for Tr1 cell differentiation, this is an area of contention. One model used has been the broad *Il10*$^{-/-}$ mouse. An issue with this model is that Tr1 cells are not the only cells which produce IL-10. In *Il10*$^{-/-}$ mice colitis develops spontaneously [293]. This is similar to human studies showing that genetic mutations in *Il10r* or *Il10* are associated with early onset severe colitis and Crohn's disease [238], [239], [240]. Similarly, the T cell-specific deletion of IL-10 is not without complications for use in studying Tr1 cells. These mice have increased T cell responses but normal innate immunity and also spontaneously develop colitis [294]. However, even within the T cell compartment there are a diverse array of T cells in addition to Tr1 cells that produce IL-10, including CD4$^+$ effector T cells, Treg cells, CD8$^+$ T cells, NKT cells, and MAIT cells. This confounds the interpretation of T cell specific deletion of IL-10 with respect to Tr1 cell function as the deficiency in IL-10 production is not limited to Tr1 cells, and other Tr1 cell functions may still be intact independent of IL-10.

The importance of IL-27 in Tr1 cells is reinforced by experiments that show mice lacking functional IL-27RA exhibit a deficiency in IL-10 production by T cells [295], [253]. In *Il27ra*$^{-/-}$ mice overall IL-10 expression is normal. The defect in IL-10 production is contained only within the T cell compartment and does not affect Treg cell-derived IL-10 [253]. In response to infection with *T. gondii*, T cells from *Il27ra*$^{-/-}$ exhibited increased proliferation and IFNγ production compared to WT T cells, suggesting a lack of control of effector T cell responses under conditions where IL-10 derived from T cells was lacking [128]. This lack of regulation of effector responses in the absence of IL-27R extends to models of autoimmune disease. In experimental models of CNS autoimmunity, *Il27ra*$^{-/-}$ mice develop exacerbated disease, with increased inflammatory cytokine production, higher clinical disease scores, and increased demyelination of the CNS [296]. Conversely, treatment of EAE mice with IL-27 suppresses onset and clinical score in adoptive transfer

and actively induced EAE models. It was determined that IL-27 inhibited the development of Th17 cells [297]. Therefore, *Il27ra*$^{-/-}$ mice provide a system in which global IL-10 is unaffected but FOXP3^{-} CD4^{+} T cell derived IL-10 is impaired. This allows interrogation of the function of T cell-derived IL-10 in a variety of contexts.

1.8 The roles of regulatory T cells in acute infection.

A fine balance is maintained by regulatory T cells during acute infection to ensure clearance of the pathogen while minimising tissue damage. In respiratory infection, lack of control over inflammatory responses can lead to lethal lung injury. Conversely, excessive regulation could result in persistence of the pathogen and lead to secondary or chronic infections. It is known that Treg cells contribute to the regulation of immune responses during acute infection by facilitating the anti-pathogen immune response, suppressing effector T cells, promoting memory development, and initiating tissue repair processes [298], [299], [300], [301], [302], [303], [304], [305], [306]. Furthermore, Treg cells have been demonstrated to specifically inhibit the anti-viral CD8^{+} T cell response [307], [308], [309], [301], [298], [299], [302]. In contrast, the contribution of Tr1 cells to the regulation of the immune response in acute infection is not well understood. Due to the difficulty in identifying Tr1 cells it is unknown if previous studies that characterised IL-10^{+} T cells in an acute infection setting were focusing on Treg, Tr1, or effector T cells. There is much that is unknown about the biology and importance of Tr1 cells in the context of acute infection. In this setting, whether cells with a Tr1 phenotype are capable of suppression, or if they contribute to pro-inflammatory anti-pathogen responses remains a major question.

Once the activation of naive T cells is initiated in lymph nodes, these cells begin to produce IL-2. This cytokine is required in autocrine to promote T cell proliferation. The IL-2 is partially sequestered by Treg cells, which are the first cells to expand after this event [310]. Treg cell activation was shown to be dependent on the naive T cell activation, as with increasing naive T cell activation there were greater numbers of Treg cells. IL-2 stimulation increases Treg proliferation and suppressive function [310], [311]. This is an important process during homeostasis as it prevents autoimmunity. IL-2 scavenging by Treg cells increases their suppressive function and prevents immune responses that are not required by suppressing inappropriate effector T cell activation and expansion [312]. In an appropriate immune response directed against IAV, Treg numbers peak in the lung prior to effector T cells, proliferate in response to IAV hemagglutinin peptide, and are significantly more suppressive to effector T cell division and cytokine production than naive Treg and Treg cells from non-draining LNs [311]. This indicates that Treg cells are activated in response to acute infection and function to exert control over immune responses.

Treg cells are known to limit the magnitude of immune responses at the site of challenge to prevent exacerbated pathology in infection settings [298], [299]. Another important aspect of Treg function in acute infection is their contribution to tissue repair. Amphiregulin (AREG) is an epithelial cell growth factor which binds the EGF-receptor and stimulates proliferation [313]. This effector molecule is known to be produced by activated Th2 cells in response to helminth infection. This is an important mechanism used to expel helminth pathogens as increased epithelial cell proliferation increases shedding of the intestinal lining. As such, effective clearance of worms from the intestinal epithelium was dependent on AREG [313]. AREG has also been found to be produced by pathogenic Th2 cells in asthma and the remodelling induced by AREG in the context of chronic allergic inflammation is pathogenic. This is due to eosinophils "reprogrammed" by AREG signalling, leading to secretion of osteopontin which results in airway fibrosis [130]. In contrast with earlier findings [314], [315] it has been established that autocrine amphiregulin is not required for Treg cell function or suppressive capacity [306]. Using *Areg*$^{-/-}$ mice it was established that AREG did not affect antiviral immune responses in the context of weight loss or cytokine expression [306]. There was significantly increased tissue damage during viral infection in mice with a Treg-specific deletion of AREG. This identified that in IAV infection, AREG was not required for Treg cell-mediated suppression of immune responses but was critical for tissue repair [306]. However, the contribution of Tr1 cells to this repair process has not been investigated in acute infection. In the intestine it is also known that Tr1 cells can produce IL-22 which is protective, supports the maintenance of intestinal barrier integrity, and is deficient in patients with IBD [225]. However, it is not known if similar roles are performed by Tr1 cells during acute infection in the lung.

IL-10 is protective against inflammation-associated tissue damage. A study by Sun and colleagues determined that if the IL-10R is inhibited during IAV infection of Balb/c mice, this results in lethal pulmonary injury due to exacerbated immune responses [257]. This study also identified an important role for IL-10^{+} T cells in eliciting some control over the magnitude of immune responses in response to IAV infection. Whether these IL-10^{+} T cells induced during IAV infection are Treg, Tr1, or Th1 cells was not specifically addressed. Mice treated with α-IL-10R neutralising antibody (nAB) are known to exhibit dramatically reduced survival times when challenged with a lethal IAV dose [257]. IL-10 is also known to inhibit the development of Th17 responses to IAV which protects the host from excessive tissue damage [258]. Similarly, *Il27ra*$^{-/-}$ mice exhibit increased mortality post high dose IAV infection and greater weight loss that exhibits delayed recovery compared to WT mice [256]. The *Il27ra*$^{-/-}$ mice also exhibit a decreased frequency of IFNγ^{+} and an increase in IL-17A^{+} T cells [256]. As Tr1 cells require IL-27 for their development, the *Il27ra*$^{-/-}$ phenotype suggests that these cells could contribute to tissue protection during high dose challenge to prevent lethal tissue pathology. However, further investigation is required to

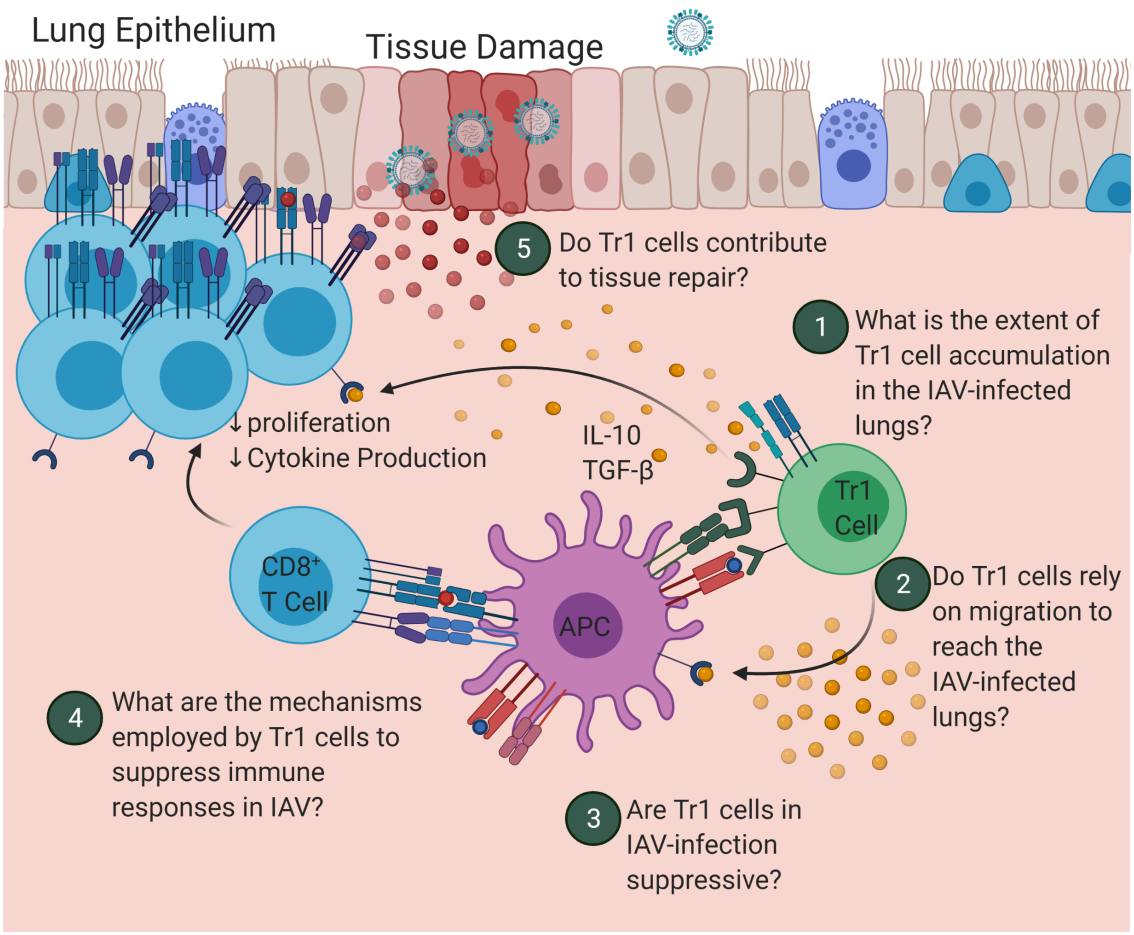

Figure 1.4: Tr1 cell contributions to the regulation of the anti-IAV immune response.

The contributions of Tr1 cells to the regulation of the immune response during acute infection were investigated in this study. The questions guiding this investigation are outlined by numbered points (1)-(5). Created with BioRender.com

determine whether restoring the Tr1 compartment in the *Il27ra*$^{-/-}$ is sufficient to rescue maximum weight loss and recovery. The contributions of Tr1 cells to the immune response against acute infection is largely unexplored compared to canonical FOXP3^{+} Treg cells (Refer to **Figure. 1.4**). In summary, while Tr1 cells are known to be suppressive in models of GVHD [246], T cell transfer colitis [191], [194], [210], and autoimmunity [230], [237], whether these cells are also suppressive in an IL-10-dependent manner in the context of acute infection remains to be determined.

1.9 The research project

Tr1 cells are an important regulatory T cell subset but their role in the resolution of acute infection is currently unknown. Controversy surrounding the classification of Tr1 cells in the literature has hindered development in the field thus far. Investigation is required to establish the suppressive potential, surface profile, and migratory axes used by Tr1 cells to further the current understanding of Tr1 biology in a resolving model of acute infection. In this project it was planned to address these questions using a model of IAV infection.

Overall Hypothesis: Tr1 cells contribute to the regulation of immune responses during acute infection.

Project Aims

1. To quantify Tr1-like cells in IAV-infected mice.
2. To determine the effect of Tr1-like cell deficiency on acute IAV infection.
3. To establish if Tr1-like cells in IAV infection express co-inhibitory markers. and suppress effector T cell division in order to classify as *bona fide* Tr1 cells.
4. To investigate mechanisms used by Tr1 cells to accumulate at the IAV-infected lung.
5. To perform extensive molecular characterisation of Tr1 cells generated during IAV infection.

Chapter 2: Materials and Methods

2.1 Mice

C57Bl/6 (B6) and Ly5.1 mice were purchased from Animal Resource Centre (ARC), Western Australia. C57BL/6J FOXP3^{RFP} IL-10^{GFP} (dual-reporter mice) (C57BL/6-*Foxp3^{tm1Flv}*x B6.129S6-*Il10^{tm1Flv}*) were originally sourced from Prof. Geoff Hill (QIMR Berghofer) and then bred at the University of Adelaide animal house. C57BL/6 N *Il27ra$^{-/-}$* (B6N.129P2-*Il27ra^{tm1Mak}* mice) and WT mice were sourced from Prof. Christian Engwerda (QIMR Berghofer). *Il27ra$^{+/-}$* mice were crossed or *Il27ra$^{+/-}$* and *Il27ra$^{-/-}$* for littermate experimental mice. *Cxcr6$^{gfp/gfp}$* mice (B6.129P2-*Cxcr6^{tm1Litt}*) were sourced from The Doherty Institute and bred as homozygous knockout mice. All mice were housed under specific pathogen-free conditions and bred in-house at the Helen Mayo Animal Facility (HMAF) or CSIRO Brailsford Robertson Building. Colony maintenance and breeding husbandry was performed by Caitlin Abbott and supported by other members of the Chemokine Biology Lab. For *Cxcr6$^{gfp/gfp}$* experiments WT C57BL/6 mice were ordered in from ARC and their microbiota was normalised over a week by swapping bedding with *Cxcr6$^{gfp/gfp}$* mice. Experiments used gender and age matched mice between 8 and 12 weeks of age. Mice were humanely killed by CO_2 asphyxiation. All experimental and breeding protocols were approved by the University of Adelaide Animal Ethics Committee under the s/2018/004, s/2017/040, and s/2019/058 ethics approvals.

2.2 Genotyping

Tail tips or ear notches from recently weaned pups were digested in 100μL of Tail tip lysis buffer supplemented with 1/200 proteinase K overnight at 55°C. The next day the tail tips were heat shocked at 95°C for 5 min and then centrifuged at 12000xg for 10 minutes. Polymerase chain reaction (PCR) was conducted using MyTaq (Bioline) according to the manufacturer's protocol. Depending on the genotyping reaction 1, 0.5μL or 0.25 μL tail tip DNA was used per reaction. Primers are listed in **Table 2.1**. PCR products were run on 1.5% agarose gels, stained with GelRed (Biotium) and visualised in a ChemiDoc (Bio-Rad). The expected product sizes and cycling conditions for each reaction are listed in **Tables 2.2-2.9**.

2.3 Phenotyping

The *Il27ra$^{-/-}$* mouse line was bred as heterozygous crosses to achieve all three genotypes. It was found there was no difference in weight loss or recovery when comparing the

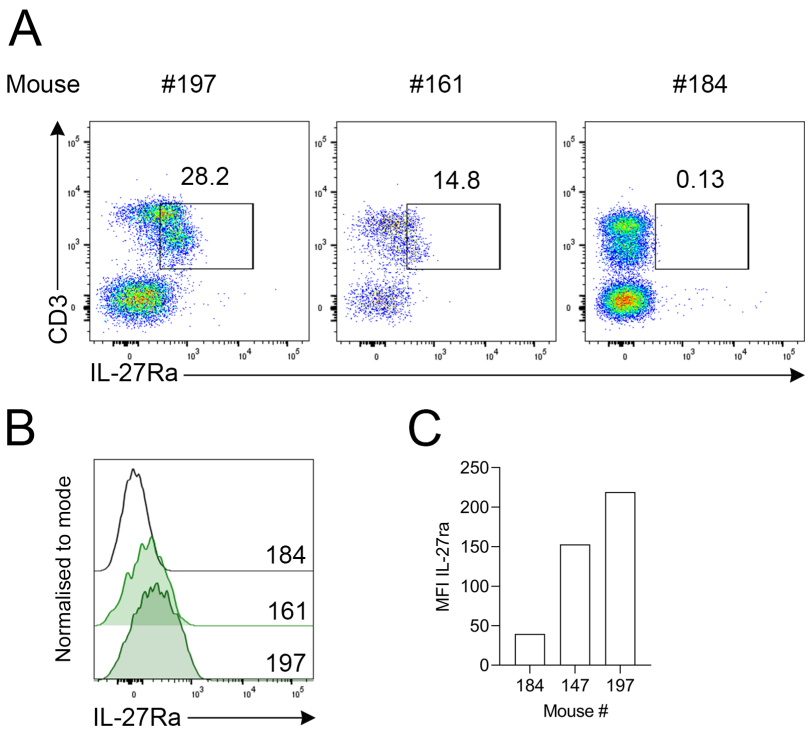

Figure 2.1: Phenotyping of *Il27ra*$^{-/-}$ *mice.*
Mice from the *Il27ra*$^{-/-}$ colony were bled by facial vein puncture to assess IL-27RA status. Blood was collected, red cells lysed, and stained for CD3 and IL-27RA for flow cytometric analysis. (A) Representative flow cytometry depicting expression of IL-27RA by CD3^{+} T cells from mouse number 197 (*Il27ra*$^{+/+}$), 161 (*Il27ra*$^{+/-}$), and 184 (*Il27ra*$^{-/-}$). (B) Histogram of IL-27RA expression by each of the three mice. (C) Quantitation of MFI of mouse number 197 (*Il27ra*$^{+/+}$), 161 (*Il27ra*$^{+/-}$), and 184 (*Il27ra*$^{-/-}$) showing the ability to discern between phenotypes.

heterozygous mice to the wildtype. Therefore, to maximise the number of experimental mice, *Il27ra*$^{-/-}$ mice were crossed to a *Il27ra*$^{+/-}$ mice, resulting in a greater proportion of *Il27ra*$^{-/-}$ mice for experiments and generation of littermate controls. To phenotype these mice, a facial vein puncture blood sample was obtained from 7-10 week old mice, lysed with mouse red cell lysis buffer (mRCLB) and the status of IL-27RA protein expression was assessed by flow cytometry. The genotype of the mouse was able to be determined based on MFI of the IL-27Ra as it is expressed by all naive CD3^{+} T cells. To double check all genotyping a separate stain was conducted on spleens at the experimental endpoint to confirm IL-27Ra status by flow cytometry (refer to **Fig 2.1**).

2.4 Murine lymphocyte isolation

2.4.1 Intestinal mucosa

Following CO_2 asphyxiation, the chest cavity was opened and mice were perfused with a 26G needle fitted to a 10mL syringe filled with PBS. The needle was inserted into the left ventricle and a small incision was made in the aorta. The small intestine was harvested and the fat and Peyer's Patches were removed. Intestinal contents and mucous were expelled, and tissue was washed extensively with PBS. The intestine was then opened longitudnally and sliced into small pieces before being placed into EDTA solution for 40 minutes at 37°C with shaking. Following incubation The supernatant containing the intra-epithelial lymphocytes was collected. The remaining small intestinal pieces were washed in PBS and transferred into gut digestion media. The intestinal pieces were mechanically minced and placed on a shaker for 1.5 hours at 37°C and pipetted up and down every 30 minutes. The lamina propria lymphocytes were then isolated by centrifuging in a discontinuous 40%/80% percoll gradient (Cytiva) at 1000xg for 20 minutes with no brake. Lymphocytes were collected from the interface and washed with PBS.

2.4.2 Lymphoid organs

Spleens were mashed through 70μm filters (BD), washed in PBS and then incubated in mRCLB for 10min at 37°C. Cells were then washed again in PBS. Skin draining inguinal lymph nodes (iLNs), mediastinal LNs (mLN), and mesenteric lymph nodes (MLN) were mashed through 70μm filters into PBS. Unless specifically stated, all cells were centrifuged at 300xg for 5-10 min.

2.4.3 Peripheral blood (PB)

Immediately following asphyxiation, the chest cavity was opened by incisions between ribs. A 29G insulin syringe was used to collect blood by cardiac puncture. The blood was collected into heparinised vacutainer tubes (BD). 250μL of blood was incubated in 10mL mRCLB for 20 min at 37°C then washed 2-3 times in PBS.

2.4.4 Broncho-alveolar lavage fluid (BALF)

The chest cavity was opened and trachea exposed. A superficial incision was made in the trachea just below the nasopharynx. For FACS analysis, a 1mL syringe filled with 1mL PBS 1mM EDTA and fitted with an insyte autoguard catheter (BD) was inserted into the tracheal incision orientated towards the lungs. Three washes were performed changing the PBS each time and fluid was collected into a 15mL falcon tube. Cells were washed 1x in PBS, then incubated in 1mL mRCLB for 5min at 37°C before a final PBS wash.

2.4.5 Lungs

Following CO_2 asphyxiation, the chest cavity was opened and mice were perfused with a 26G needle fitted to a 10mL syringe filled with PBS. The needle was inserted into the left ventricle and a small incision was made in the aorta. All five lung lobes were harvested and placed into 1mL of lung digestion medium. Lungs were mechanically minced prior to incubating at 37°C with shaking. Lungs were pipetted up and down every 15 minutes to ensure homogenisation. The lung suspensions were then passed through 70μm filters (BD), washed in PBS and then incubated in 5mL mRCLB for 7min at 37°C. Cells were then washed again in PBS.

2.5 *In vivo* techniques

2.5.1 Influenza A virus (IAV) infection

X-31 and X-31 $OVA_{323\text{-}339}$ [H3N2] IAV stocks were kindly provided by Professor Mohammed Alsharifi (The University of Adelaide). X-31 stocks were generated by Ms Jennifer Chan (The University of Adelaide). X-31 $OVA_{323\text{-}339}$ stocks were provided by Prof. Stephen Turner (Monash Biomedicine Discovery Institute, Monash University). The concentration of IAV stocks had been determined by the Alsharifi Lab by analysing the 50% tissue culture infectious dose ($TCID_{50}$) on Madin-Darby Canine Kidney cells. $TCID_{50}$ was determined using the Spearman and Karber algorithm. For infection IAV stocks were diluted in sterile PBS to 28,125 $TCID_{50}$/mL of X-31 resulting in a dose of 923 $TCID_{50}$/ mouse, or 6250 $TCID_{50}$/mL X-31 $OVA_{323\text{-}339}$ resulting in a dose of 200 $TCID_{50}$/ mouse. Virus stock concentrations are listed in **Table 2.10**. Mice were anaesthetised with pentobarbitone (Ilium) intra-peritoneally (i.p.) diluted 1/10 in sterile PBS. Anaesthetic was administered at a dose of 10μL per gram of mouse weight. Once anaesthetised, mice received 32μL of virus intranasally (i.n). Mice were placed on a 37°C heat pad and

monitored during recovery. Once recovered, mice were given wet food and monitored daily. Any mouse which lost 20% of initial weight was humanely killed in accordance with the protocol approved by the The University of Adelaide Animal Ethics Committee.

2.5.2 Intra-vascular labelling

3μg of fluorescently labelled α-TCR-β (Biolegend) was diluted in 200μL of dPBS (Sigma) per mouse. Mice were placed under a heat lamp before restraining and administering the antibody solution via tail vein injection 3 minutes prior to humane killing.

2.5.3 Adoptive transfer of Tr1 cells into Tr1-deficient recipients

Il27ra$^{-/-}$ and *Il27r*$\alpha^{+/-}$ littermates were infected with X-31-OVA$_{323\text{-}339}$ IAV intranasally. On day 5 post-infection, *Il27ra*$^{-/-}$ mice received Tr1 cells or PBS intravenously (i.v.). The transferred Tr1 cells were generated from isolated naive CD4$^+$ T cells (StemCell) from dual-reporter mice SLOs. Isolated naive CD4$^+$ T cells were cultured under Tr1 polarising conditions for 3 days, labelled with Efluor670 proliferation dye and sorted based on Efluor670$^+$ CD4$^+$ FOXP3$^-$ IL-10$^+$ prior to transfer. Transfer of Tr1 cells consisted of 2x10^5 sorted Tr1 cells from cultures. *Il27ra*$^{-/-}$ mice were separated into groups to ensure roughly equal weight loss on day 5. Post transfer the experiment was blinded as mice were weighed and monitored daily by a researcher who was not aware of the groups to avoid bias during measurement of recovery from infection. On day 7 post-infection a sample of *Il27ra*$^{-/-}$ Tr1 and PBS recipients were humanely killed and PB, BALF, lungs, mLN, and spleen were harvested to quantify the presence of transferred cells. All other mice were monitored for recovery.

2.6 *Ex-vivo* techniques

2.6.1 Flow cytometry for acquisition

Single cell suspensions were stained in 96 well round- or v-bottom plates (Corning) at 2x10^6 lymphocytes per well using antibodies and other reagents detailed in **Table 2.11**. A basic gating strategy for Tr1 cells is shown in **Figure 2.2**.

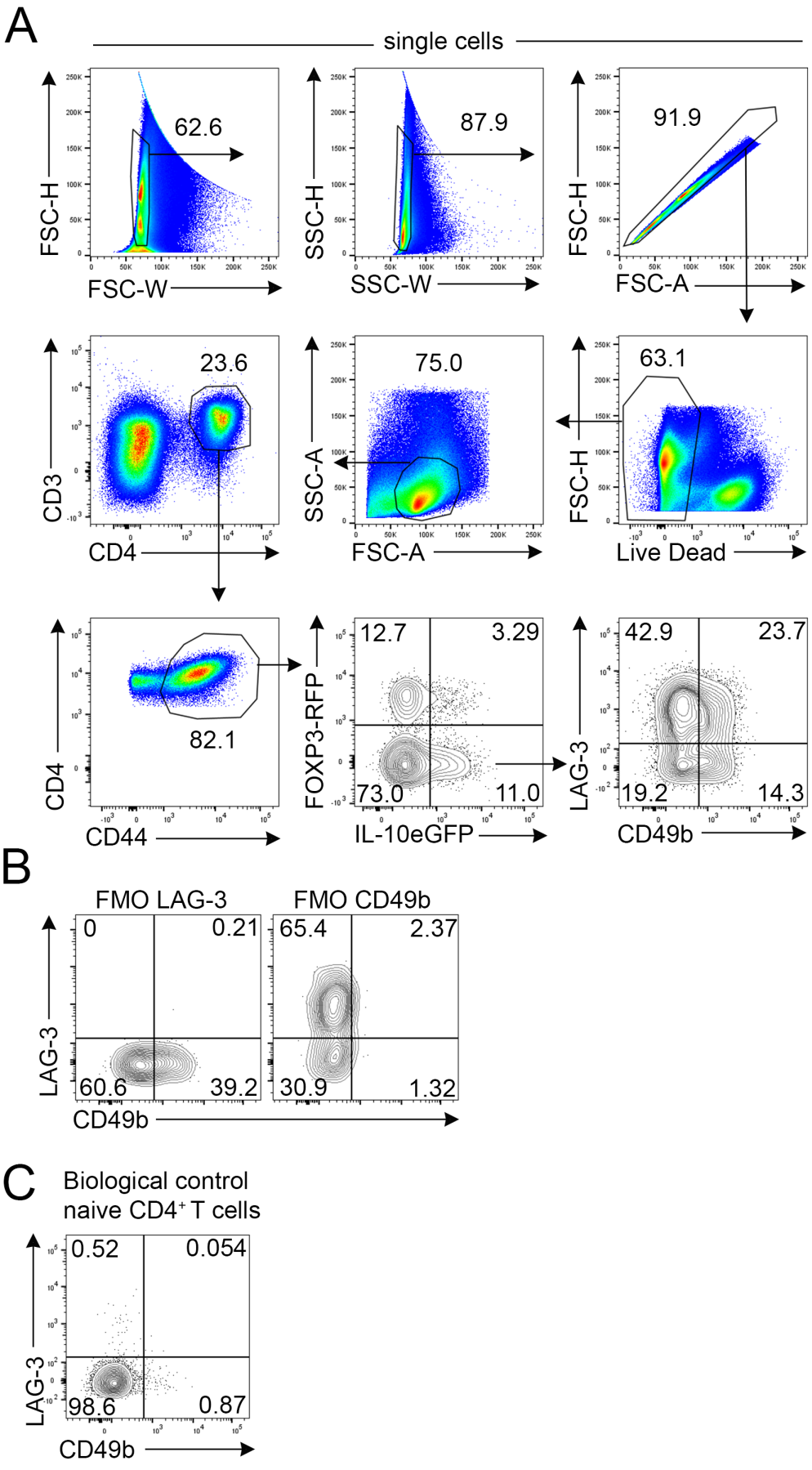
A
single cells
FSC-H
FSC-W
62.6
SSC-H
SSC-W
87.9
FSC-H
FSC-A
91.9
CD3
CD4
23.6
SSC-A
FSC-A
75.0
FSC-H
Live Dead
63.1
CD4
CD44
82.1
FOXP3-RFP
IL-10eGFP
12.7
3.29
73.0
11.0
LAG-3
CD49b
42.9
23.7
19.2
14.3
B
FMO LAG-3
FMO CD49b
0
0.21
60.6
39.2
65.4
2.37
30.9
1.32
LAG-3
CD49b
C
Biological control
naive CD4+ T cells
0.52
0.054
98.6
0.87
LAG-3
CD49b

Figure 2.2: Basic Tr1 cell gating strategy for analysis of flow cytometry data.

(A) Flow cytometry gating strategy outlining pre-gating on single cells, live, lymphocytes, $CD3^+$ $CD4^+$ T cells prior to activated ($CD44^+$), $FOXP3^-$ IL-10^+ Tr1-like cells. Finally LAG-3 and CD49b are defined with a quadrant gate. (B) Fluorescence minus one (FMO) controls for LAG-3 and CD49b are used in combination with (C) Biological negative control for LAG-3 and CD49b expression (naive $CD4^+$ T cells) to set gates.

2.6.2 Intranuclear/intracelluar staining of transcription factors and cytokines with WT and dual-reporter mice.

For intranuclear/intracelluar cytokine staining of dual-reporter mice, lymphocytes were incubated in complete IMDM with 50ng/mL Phorbol 12-Myristate 13-Acetate (PMA) (Sigma), 1μM ionomycin (Sigma), 10μg/mL brefeldin A (ebioscience) and 10μM monensin(BD) for 4 hours at 37°C and 5% CO_2. For amphiregulin staining, lymphocytes were instead incubated in complete IMDM with 50ng/mL PMA, 1nM ionomycin, 10μg/mL brefeldin A (ebioscience) and 10μg/mL monensin (BD) for 3 hours at 37°C and 5% CO_2. Cells were washed once in PBS then re-suspended in fixable viability stain 780 (BD) diluted 1/1000 in PBS and blocked with mouse γ-globulin (mγg) (200μg/ml) for 5 min at room temperature, in the dark. For purified antibodies, cells were stained with purified antibody for 60min at 4°C, washed in FACS buffer (FB), stained with secondary antibody in mγg (200μg/ml) and normal mouse serum (NMS) (1%) for 20min, washed in FACS buffer and blocked with rat γ-globulin for 15 min at 4°C. Cells were stained with directly conjugated and biotinylated antibodies for 20min at 4°C. This was the staining process for directly conjugated antibodies with the exception of anti-mouse CD49b (BD, HMα2) and LAG-3 (Biolegend, C9B7W), which were stained for 60min at 37°C in PBS + 2% FCS, 1mM EDTA. For biotinylated antibodies, cells were then washed in FB and stained with streptavidin for 15min at 4°C. Cells were then washed in PBS 0.04% azide. For all panels which included more than one violet or ultraviolet fluorophore, antibody cocktails were made up in Brilliant Stain Buffer plus (1/6 of well volume) (BD) to minimise interactions between violet fluorophores. For intracellular cytokine staining, cells were incubated in 85 μL of Cytofix/Cytoperm solution (BD) for 20min at room temperature in the dark. Cells were then washed in Permwash twice (BD) before staining with directly conjugated intracellular antibodies diluted in Permwash for 30 min at 4°C. For amphiregulin staining purified α-Areg (R&D) antibody was labelled with a PE-Cy7 lightning link kit (Novus Biologicals).

For co-staining of FOXP3 and IL-10 in WT mice, lymphocytes were incubated in complete IMDM with 10μg/mL plate bound α-CD3 (BioXcell, 2C11) and 2μg/mL soluble α-CD28

at 37°C and 5% CO_2 for 2 hours. 10μg/mL brefeldin A (ebioscience) and 10μM monensin (BD) was added to the cells after 2 hours in 20μL and mixed gently. The cells were then incubated for a further 4 hours at 37°C and 5% CO_2. After restimulation cells were washed with sort buffer (SB) prior to surface staining. Post surface staining cells were washed once with FB cells and re-suspended in 85μL FOXP3 kit perm buffer (made up with 1/4 concentrate + 3/4 diluent) (eBioscience) for 30min at room temperature in the dark, then washed in FOXP3 Wash Buffer (FOXP3 WB) (ebioscience) twice, at 500xg for 4 minutes post permeabilisation. For transcription factor and cytokine staining, cells were stained with directly conjugated antibodies diluted in FOXP3 WB for 30min at 4°C.
For intranuclear staining of dual-reporter mice, after washing post-incubation with surface antibodies, cells were re-suspended in 100μL Cytofix solution (BD) and incubated at 37°C for 10 min. After this step intranuclear staining of WT and dual-reporter mice was the same. All stains to be acquired were washed in PBS 0.04% azide, re-suspended in PBS 0.04% Azide and acquired the same day to prevent loss of FOXP3 signal (post re-stimulation). Stained cells were acquired using the BD FACSFortessa X-20 flow cytometer.

2.6.3 Fluorescence activated cell sorting (FACS)

Single cell suspensions were stained in Sterile FACS tubes (BD) at 3x10^7 cells/mL using antibodies and other reagents detailed in (**Table 2.11**). Cells were washed once in Sort Buffer (SB) then re-suspended in fixable viability stain 780 (BD) diluted 1/1000 in SB and blocked with mouse γ-globulin (mγg) (200μg/ml) for 5 min at room temperature, in the dark. Cells were stained with directly conjugated and biotinylated antibodies on top of viability and block for 20 min at 4°C., with the exception of anti-mouse CD49b (HMα2, BD) and LAG-3 (C9B7W, Biolegend) which were stained for 60 min at 37°C. For biotinylated antibodies, cells were then washed in SB and stained with streptavidin for 15min at 4°C. Cells were then washed in SB. For all panels which included more than one violet or ultraviolet fluorophore, antibody cocktails were made up in Brilliant Stain Buffer (1/6 of tube volume) (BD) to minimise interactions between these fluorophores. Stained cells were sorted using the BD FACSAria III cell sorter or the BD Fusion flow cytometers at The University of Adelaide MLS or SAHMRI.

2.6.4 Isolation of mRNA for downstream applications.

For sequencing, lungs cells were isolated and stained (as described in section **2.4.5 and 2.6.2**) and Tr1 cell populations were FACS-sorted using a FACSAria III. Total RNA was extracted using an Pico Pure RNA Extraction Kit (Articus) and following the manufacturer's protocol. DNA digestion was performed using an RNase-free DNase Kit (Qiagen). Total RNA was eluted in 20μL elution buffer and stored in provided tubes wrapped in parafilm at -80°C until required. RNA sequencing of 150bp paired end reads at an average

of 30M reads per sample was performed by Novogene. Data QC for the RNA sequencing experiment was conducted by Stephen Pederson and Mark Armstrong at The University of Adelaide. Analysis of differentially expressed genes was conducted in consultation with Stephen Pederson, Mark Armstrong, and Aaron Heng. RNA sequencing analysis is supplied in Appendix B.

To prepare cells for reverse transcription quantitative polymerase chain reaction (RT-qPCR) single cell suspensions were generated from lung, spleen, and mLN cells and stained as described above and $CD4^+$ T cells FACS-sorted using a FACSAria III (as described in section **2.4.5 and 2.6.2**). Total RNA was extracted from sorted cells using the RNAeasy Micro Plus Kit (Qiagen) with on-column DNase I treatment. The RNA was then reverse transcribed into cDNA using a High Capacity cDNA Reverse Transcription Kit (Applied Biosystems). Then RT-qPCR was conducted using SYBR Green I Power Up Master Mix (Applied Biosystems) and run on a LightCycler480 instrument (Roche Applied Science). For viral load analysis whole lungs were snap frozen in liquid nitrogen, ground into fine powder and re-suspended in TRIzol (Ambion). RNA was then extracted with chloroform, precipitated in isopropanol, and washed in ethanol. RNA samples were DNase treated using Turbo DNA-free kit (Ambion), prior to cDNA synthesis (First Strand cDNA synthesis Kit, Roche). RT-qPCR was conducted using LightCycler-480 SYBR Green I Power Up Master mix on a LightCycler-480 instrument (Roche).

All procedures involving RNA were conducted with equipment and workspaces cleaned with RNaseZap (ThermoFisher). Primer sequences listed in **Table 2.14**. All procedures were carried out using manufacturer's instructions. Cycle threshold (CT) values were determined by the second derivative method and relative gene expression was calculated using $2^{-[CT(target)- CT(reference)]}$, where the reference gene is *Rplp0*. The melting curve of each product was also analysed to confirm the specificity of the product.

2.6.5 In vitro Th and regulatory T cell cultures

Each of the Th culture systems required naive $CD4^+$T cells stimulated with plate bound α-CD3(145-2C11) 5μg/mL and soluble α-CD28 (37.51) 2μg/mL unless otherwise stated. Reagents are detailed in **Table 2.13**.

Culture Conditions

- **Th1**: rmIL-12 10ng/mL, rmIFNγ 10ng/mL, α-IL-4 10μg/mL.
- **Th2**: rmIL-4 10ng/mL, rmIL-2 5U/mL, α-IFNγ 10μg/mL.
- **Th17**: rmTGF-β 5ng/mL, rmIL-6 20ng/mL, α-IL-4 10μg/mL, α-IFNγ 10μg/mL.
- **iTreg**: rmTGF-β 10ng/mL, IL-2 5U/mL.
- **Tr1**: rmIL-27 25ng/mL, rmTGF-β 5ng/mL, rmIL-10 5ng/mL.

Cultures were incubated at 37°C for 72hrs before analysis.

2.6.6 Preparation of antigen presenting cells for suppression assay

Per experiment one C57BL/6 CD45.2 mouse was humanely killed, and spleen harvested. The spleen was digested at 37°C and 5% CO_2 for 20min. This was done to avoid loss of antigen presenting cells (APCs) which can occur when directly passing spleen through 70μM filter. The spleen was washed in PBS and then incubated in mRCLB for 10 min at 37°C. Cells were then washed again in PBS and re-suspended in PBS supplemented with 2% FCS, 1mM EDTA. An EasySep CD11c Positive Selection Kit (Stem Cell) was used, following the manufacturer's instructions to isolate APCs. APCs were then re-suspended at 1x10^5cells/mL in complete IMDM.

2.6.7 Preparation of effector T cells for suppression assay

Per experiment four Ly5.1 (CD45.1) mice were humanely killed, and spleens and iLNs were harvested. Spleens and iLNs were mashed through 70μm filters (BD), washed with PBS and then incubated in mRCLB for 10min at 37°C. Cells were washed in PBS and re-suspended in PBS supplemented with 2% FCS and 1mM EDTA. An EasySep Pan Naive T cell Isolation Kit (Stem Cell) was used following manufacturer's instructions to isolate $CD3^+$ T cells. Cells were then re-suspended at 3x10^7 cells/mL for staining. Isolated $CD3^+$ T cells were stained in sterile FACS Tubes in SB with Fixable Viability Dye 780 (BD), α-mu CD3 PE-Cy7(BD), CD25-Biotin (eBioscience) and streptavidin BV421 (Biolegend) as previously described. Live, $CD3^+$ $CD25^-$ cells were sorted using a FACS Aria III. Post-sort cells were counted, washed twice in PBS to remove serum and re-suspended to 2x10^6 cells/mL in room temperature PBS for labelling with the Efluor670 proliferation dye (Invitrogen). Efluor670 was diluted in room temperature PBS to a concentration of 10μM in the same volume as the cells were re-suspended in. The Efluor670 solution was added at a 1:1 ratio to the cells and quickly vortexed immediately after addition. The tube was wrapped in alfoil and placed at 37°C for 10 minutes for labelling. To stop labelling, 4-5 volumes of complete IMDM was added to the cell solution and incubated on ice in the dark for 5 minutes. The cells were washed 3x in complete IMDM and spun at 300xg for 10 minutes to ensure maximum recovery of labelled cells. Finally, cells were counted and re-suspended at 4x10^5 cells/mL in complete IMDM. As a control to measure background suppression in this assay, effector T cells were co-cultured at a 1:1 ratio with effector T cells (Eff+Eff).

2.6.8 Preparation of regulatory T cells for suppression assay

One week prior to setting up the suppression assay, 4x female dual-reporter mice were infected with X-31 IAV Influenza A virus as described in section **2.5.1**. On day 7 post-

infection, the assay was set up. IAV-infected dual-reporter mice were humanely killed, and lungs were harvested and digested as described in section **2.4.5**. Cells were then stained as described in section **2.6.3**. The panel used was for sorting Tr1 cells included Fixable Viability Dye 780 (BD), CD3 BV605(BD), CD4 BV421 (BD), CD44 BV480 (BD), FOXP3-RFP, IL-10-eGFP, CD49b V786 (BD), LAG-3 APC (Biolegend). Live, $CD3^+$, $CD4^+$, $CD44^+$ $FOXP3^-$ $IL\text{-}10^+$ $CD49b^-$ $LAG\text{-}3^-$, or $CD49b^+$ $LAG\text{-}3^+$, or $CD49b^-$ $LAG\text{-}3^+$, or $CD49b^+$ $LAG\text{-}3^-$ cells were sorted using a FACS Aria III. Two mice were pooled to give one biological replicate of regulatory T cells from IAV-infected lungs. Sorted cells were counted, washed and re-suspended at $4x10^5$cells/mL in complete IMDM.

2.6.9 *Ex vivo* suppression assay via live APCs

To plate out the suppression assay via live APCs, a 96 well round bottom tissue culture grade plate was used. 50μL of APCs at $1x10^5$ cells/mL were added to ensure $5x10^3$ cells/well. Next, 1μg/mL α-CD3 (2C11 purified) was added in 50μL. Then regulatory T cells were added at $4x10^5$ cells/mL (either: Treg cells, $CD49b^+$ $LAG\text{-}3^+$, or $CD49b^-$ $LAG\text{-}3^+$, or $CD49b^+$ $LAG\text{-}3^-$, or $CD49b^-$ $LAG\text{-}3^-$). 50μL of regulatory T cells were added per well for a 1:1 regulatory T cell: effector ratio ($2x10^4$cells/well) and 25μL for 1:2 and continued for 1:4, 1:8 up to 1:16. Next 50μL of labelled effector cells were added to each well. Wells that did not receive 50μL of regulatory T cells were topped up with the appropriate volume of IMDM to ensure all wells have a final volume of 200μL. Assay was then incubated at 37°C and 5% CO_2 for approximately 3 days. Division index (DI) was calculated by adding up the total number of divisions and dividing by the total number of cells in each division including undivided cells. This gives the mean number of divisions for a population of cells. To determine the % suppression of effector T cell division the DI for effector T cells in the absence (DI_{eff}) and presence (DI_{regs}) of regulatory T cells was calculated. These could then be substituted in the formula 100*(1-DIr/DIe) to calculate the % suppression [316], [317].

2.6.10 *Ex vivo* suppression assay via live APCs with inhibitory antibodies

To plate out the suppression assay via live APCs, a 96 well round bottom tissue culture grade plate was used. 50μL of APCs at $1x10^5$ cells/mL were added to ensure $5x10^3$ cells/well. Next, 1μg/mL α-CD3 (BioXcell, 2C11) was added in 50μL. Then Regulatory T cells were added at $4x10^5$ cells/mL resulting in $1x10^4$ cells/well (either Treg cells, $CD49b^+$ $LAG\text{-}3^+$, $CD49b^-$ $LAG\text{-}3^+$, or $CD49b^+$ $LAG\text{-}3^-$, or $CD49b^-$ $LAG\text{-}3^-$). 25μL of Efluor670-labelled effector T cells (at $4x10^5$ cells/mL) were added for a 1:1 regulatory T cell:effector ratio ($1x10^4$ cells/well). Neutralising α-IL-10Rα, α-LAG-3 antibodies or isotype controls (see **Table 2.4**) were added into the wells in a volume of 50μL such that the final concentration was 50μg/mL. All wells were topped up to a final volume of

200μL with complete IMDM and pipetted up and down gently, to mix. The assay was then incubated at 37°C and 5% CO_2 for approximately 3 days.

2.7 Statistics

All statistical analysis was performed using GraphPad Prism version 8.0 for Windows and RStudio version 3.6.1. For statistical analysis of two sets of unpaired continuous data with normal distributions and similar standard deviations (SD), an unpaired Student's t-test was used. When comparing two sets of paired, continuous data with an approximately normal distribution, a paired Student's t-test was used. One-way ANOVA was used to analyse three or more groups of continuous data with approximately normal distribution, with one dependent and one independent variable. Two-way ANOVA was used to analyse three or more groups of continuous data with approximately normal distribution, with one dependent and two independent variables. In all cases, p-values $\leq$0.05 were considered significant. RStudio was used for analysis of RNA sequencing data (code used to do this is supplied as Appendix B).

2.8 Solutions

2.8.1 PBS

1x PBS was purchased from The University of Adelaide Technical Services Unit (TSU).

2.8.2 PBS Azide

1x PBS was purchased from The University of Adelaide TSU supplemented with 0.04% sodium azide (Ajax Finechem).

2.8.3 mRCLB

9 parts 155mM NH_4Cl (AnalaR) solution was mixed with 1 part 170mM TRIS (Biochemicals) solution (pH 7.65) and the pH adjusted to 7.2.

2.8.4 Lung digestion medium

Dulbecco's modified eagle medium (DMEM) with sodium pyruvate (Gibco) with 10% FCS (Sigma), 10mM HEPES (Gibco), 1X penicillin/ streptomycin (Gibco), 2.5mM $CaCl_2$ (TSU), 2.5mM MgCl (TSU), 30U/mL DNase I (Sigma) and 1mg/mL Collagenase IA from *Clostridium histolyticum* (Sigma).

2.8.5 Complete IMDM

IMDM (Gibco) with 10% FCS (Sigma), 1X penicillin/streptomycin (Gibco), 1x GlutaMax (Gibco), 54pM β-mercaptoethanol (Sigma).

2.8.6 EDTA Solution

1X HBSS (Gibco) with 5% FCS (Sigma), 15mM HEPES (Gibco), 5mM EDTA (TSU).

2.8.7 Gut digestion medium

1X HBSS (Gibco) with 10% FCS (Sigma) 15mM HEPES (Gibco), 2mg/mL Collagenase IA from *Clostridium histolyticum* (Sigma) and 30U/mL DNase I (Sigma).

2.8.8 Sort buffer

1X PBS with 2% FCS (Sigma) and 1mM EDTA (TSU).

2.8.9 FACS Buffer

1X PBS (TSU) with 1% FCS (Sigma) and 0.04% sodium azide (Ajax Finechem).

2.8.10 Tail tip lysis buffer

100mM TRIS.HCl (pH 8.5) (Biochemicals), 5mM EDTA (TSU), 0.2% SDS (TSU), 200nM NaCl (AnalaR) and 100μg/mL proteinase K (Sigma).

2.9 Tables

Table 2.1: Primers for genotyping.

Primers for Genotyping	
Primer Name	**Primer Sequence (5'to 3')**
IL-10-GFP WT	GTG TGG CCA GCC TTA GAA TAG
IL-10-GFP Common	GTG TGT ATT GAG TCT GCT GGA C
IL-10-GFP Mutant	CCA AAA GAC GGC AAT ATG GT
FOXP3-RFP WT	CAG TGC TGT TGC TGT GTA AGG GTC
FOXP3-RFP Common	CAA AAC CAA GAA AAG GTG GGC
FOXP3-RFP Mutant	GGA ATG CTC GTC AAG AAG ACA GG
CXCR6-GFP WT	ACA GGG CAA AAA GAC CTC CT
CXCR6-GFP Common	GAT GAC ACA GGA GGA ACC TGA
CXCR6-GFP Mutant	GGA CAC GCT GAA CTT GTG G

Table 2.2: PCR band sizes.

PCR	Band size WT	Band size Mutant
IL-10-GFP	350bp	485bp
FOXP3-RFP	510bp	470bp
CXCR6-GFP	384bp	420bp

Table 2.3: IL-10-GFP PCR mix.

IL-10-GFP PCR reaction	
Reagent	**X1**
H_20	35.18μL
5x MyTaq Buffer	10μL
WT primer	0.84μL
Mutant primer	1.24μL
Common primer	1.24μL
MyTaq	0.5μL
gDNA	1μL

Table 2.4: FOXP3-RFP PCR mix 1.

FOXP3-RFP common + WT PCR reaction	
Reagent	**X1**
H_20	11.5μL
5x MyTaq Buffer	4μL
WT primer	1.5μL
Common primer	1.5μL
MyTaq	0.5μL
gDNA	1μL

Table 2.5: FOXP3-RFP PCR mix 2.

FOXP3-RFP common + Mutant PCR reaction	
Reagent	**X1**
H_20	11.5μL
5x MyTaq Buffer	4μL
Mutant primer	1.5μL
Common primer	1.5μL
MyTaq	0.5μL
gDNA	1μL

Table 2.6: CXCR6 PCR mix.

CXCR6 PCR reaction	
Reagent	**X1**
H_20	11μL
5x MyTaq Buffer	4μL
Mutant primer	1μL
Common primer	1μL
WT primer	1μL
MyTaq	0.5μL
gDNA	1μL

Table 2.7: IL-10-GFP cycling conditions

IL-10-GFP PCR reaction	
1. 94$^{\circ C}$	5min

Continued on next page...

Table 2.7 – continued from previous page.

	2. 94°C	30sec
	3. 54°C	1min
	4. 72°C	1:30min
	repeat steps 2-4 35X	
5. 72°C	2min	
6. 4°C	∞	

Table 2.8: FOXP3-RFP cycling conditions- both reactions

FOXP3-RFP PCR reactions		
1. 94°C	5min	
	2. 94°C	30sec
	3. 64°C	1min
	4. 72°C	1min
	repeat steps 2-4 35X	
5. 72°C	2min	
6. 4°C	∞	

Table 2.9: CXCR6-GFP cycling conditions

CXCR6-GFP PCR reaction		
1. 94°C	2min	
	2. 94°C	20sec
	3. 65°C (decrease by 0.5°C per cycle)	15sec
	4. 72°C	10sec
	repeat steps 2-4 10X	
	5. 94°C	15sec
	6. 60°C	15sec
	7. 72°C	10sec

Continued on next page...

Table 2.9 – continued from previous page.

	repeat steps 5-7 28X	
72°C	2min	
8. 4°C	∞	

Table 2.10: IAV stock concentrations

IAV stock	concentration
X-31	$2.87x10^6$ $TCID_{50}$/mL
X-31-$OVA_{323-339}$	$3.13x10^5$ $TCID_{50}$/mL

Table 2.11: Anti-mouse directly conjugated and purified antibodies for flow cytometry.

Directly Conjugated Antibodies			
Antigen & Format	**Clone**	**Supplier**	**Final Concentration**
CD25-BV421	PC61	Biolegend	1μg/mL
CD3-Biotin	145-2C11	eBioscience	1μg/mL
CD3-BV421	145-2C11	BD	1μg/mL
CD3-BV605	145-2C11	BD	1μg/mL
CD3-BUV805	145-2C11	BD	1μg/mL
CD4-BUV395	GK1.5	BD	0.67μg/mL
CD4-BV421	GK1.5	BD	0.67μg/mL
CD4-BV786	RM4-5	BD	0.67μg/mL
CD8α-BUV395	53-6.7	BD	0.67μg/mL
CD8α-BUV805	53-6.7	BD	0.67μg/mL
CD44-BV480	IM7	BD	0.33μg/mL
CD44-BV711	IM7	BD	0.33μg/mL
CD44-FITC	IM7	BD	0.33μg/mL
CD44-BUV737	IM7	BD	0.33μg/mL
CD49b-BV480	HMα2	BD	1μg/mL
CD49b-BV711	HMα2	BD	1μg/mL
CD49b-BV786	HMα2	BD	1μg/mL
CD45.1-BV421	A20	BD	0.67μg/mL
CD45.2-BUV395	104	BD	0.67μg/mL
CD103-FITC	2E7	BD	1.67μg/mL

Continued on next page...

Table 2.11 – continued from previous page.

Antigen& Format	Clone	Supplier	Final Concentration
CD107a-BV421	1D4B	Biolegend	0.167μg/mL
CD11c-PE-Cy7	N418	Biolegend	0.67μg/mL
CXCR6-BV421	SA051D1	Biolegend	0.67μg/mL
CXCR6-PE-Cy7	SA051D1	Biolegend	0.67μg/mL
DNAM-1-BV421	TX42.1	Biolegend	0.67μg/mL
EOMES-PE-Cy7	Dan11mag	Invitrogen	1.67μg/mL
FOXP3-PE	MF-14	Biolegend	1.11μg/mL
FOXP3-AF488	MF23	BD	1.11μg/mL
FOXP3-AF647	MF23	BD	1.11μg/mL
GzmB-BV421	GB11	BD	3μL/well
IL-10-BV421	JES5-16E3	Biolegend	1.11μg/mL
IL-10-PE-Cy7	JES5-16E3	biolegend	1.11μg/mL
IFNγ-PE	XMIG1.2	BD	1.11μg/mL
IFNγ-PE-Cy7	XMG1.2	BD	1.11μg/mL
IFNγ-BV480	XMG1.2	BD	1.11μg/mL
IL-17A-BV711	TC11-18H10.1	Biolegend	1.11μg/mL
IL-4-BV421	11B11	Biolegend	0.56μg/mL
IL-27Ra-PE	2918	BD	0.67μg/mL
ID2-APC	ILCID2	Invitrogen	1.11μg/mL
Ki67-BV450	SolA15	Invitrogen	1.11μg/mL
KLRG1-BV711	2F1/KLRG1	Biolegend	0.67μg/mL
NK1.1-PE-Cy7	PK136	ebioscience	0.67μg/mL
ST2-PE-Cy7	RMST2-2	Invitrogen	0.67μg/mL
TOX-PE	TXRX10	Invitrogen	1.11μg/mL
Areg-PE-Cy7 (conjugated using Lightning Link Kit)	AREG	R&D	1μg/mL
LAG-3-APC	C9B7W	Biolgend	0.8μg/mL
LAG-3-BV421	C9B7W	Biolegend	0.8μg/mL
CCR7-Purified	home made	home made	8.3μg/mL

Table 2.12: Anti-mouse antibodies for cell culture.

Purified Antibodies for Cell Culture			
Antigen	**Clone**	**Supplier**	**Final Concentration**
CD3-Purified	145-2C11	BioXcell	1-10μg/mL
CD3-purified	145-2C11	made in house	1-10μg/mL
CD28-Purified	37.51	BD	2μg/mL
IL-10Rα-Purified	1B1.3A	BioXcell	50μg/mL
LAG-3-Purified	C9B7W	BioXcell	50μg/mL
IFNγ-Purified	XMG1.2	BioXcell	10μg/mL

Table 2.13: Recombinant mouse proteins for primary cell culture.

Recombinant proteins for Cell Culture			
Antigen	**Stock Conc**	**Supplier**	**Final Concentration**
rmIL-27	100μg/mL	R&D	25ng/mL
rmTGFβ1	50μg/mL	R&D	5ng/mL
rmIL-10	200μg/mL	Biolegend	5ng/mL
rmIL-12	100μg/mL	R&D	10ng/mL
rmIL-6	100μg/mL	R&D	20ng/mL
rmIFNγ	100μg/mL	R&D	10ng/mL

Table 2.14: Primers for RT-qPCR.

Primers for RT-qPCR		
Gene	**Forward Primer (5'to 3')**	**Reverse Primer (5'to 3')**
Rplp0 (reference gene)	TGCAGATCGGGTACCCAACT	ACGCGCTTGTACCCATTGA
Cytokines and effector molecules		
Il10	AAGCTCCAAGACCAAGGTGTCT	TTCTATGCAGTTGATGAAGATGTCAA
TGF-β1	GAGGTCACCCGCGTGCTA	TGTGTGAGATGTCTTTGGTTTTCTC
Il17a	CCTCACACGAGGCACAAGTG	TCTCCCTGGACTCATGTTTGC
Il21	CTATGAAAATGACTTGGATCCTGAAC	CATGCTCACAGTGCCCCTTT
Il22	ACTTTCCTGACCAAACTCAGCAA	TGGTCGTCACCGCTGATG
IFNγ	ATGAACGCTACACACTGCATC	CCATCCTTTTGCCAGTTCCTC
Gzmb	GACAAAGGCAGGGGAGATCAT	CGAATAAGGAAGCCCCCACA
Areg	TTGCTGCTGGTCTTAGGCTC	TGGTCCCCAGAAAGCGATTC
Chemokines		
Ccl1	TGATCCCCCAGCTGTGGTA	GTTGAGGCGCAGCTTTCTCT
Ccl2	TCTTCCTCCACCACCATGCA	CCAGCCGGCAACTGTGA
Ccl3	ACAAGTCTTCTCAGCGCCATATG	CGTGGAATCTTCCGGCTGTA
Ccl4	TGCTCGTGGCTGCCTTCT	CAGGAAGTGGGAGGGTCAGA
Ccl5	CTCGGTCCTGGGAAAATGG	TGCTGATTTCTTGGGTTTGCT
Ccl20	TGCTTTTTTGGGATGGAATTG	TGCAGTGATGTGCAGGTGAA
Cxcl9	TGGGCATCATCTTCCTGGAG	CCGGATCTAGGCAGGTTTGA
Cxcl10	CCTCATCCTGCTGGGTCTG	CTCAACACGTGGGCAGGA
Chemokine receptors		
Ccr1	TGG GAG TTC ACT CAC CGT ACC T	TCC ACT GCT TCA GGC TCT TGT
Ccr2	GTT CAT CCA CGG CAT ACT ATC AAC	GCC CCT TCA TCA AGC TCT TG
Ccr3	TTG CCT ACA CCC ACT GCT GTA T	TTT CCG GAA CCT CTC ACC AA

Continued on next page...

Table 2.14 – continued from previous page.

Gene	Forward Primer (5'to 3')	Reverse Primer (5'to 3')
Ccr4	GCA ACA CTG CAA GAA TGA GAA GA	GAC CAC CAC GGC GAA GAT
Ccr5	CAT CCG TTC CCC CTA CAA GA	GGA ACT GAC CCT TGA AAA TCC A
Ccr6	CCT GGG CAA CAT TAT GGT GGT	CAG AAC GGT AGG GTG AGG ACA
Ccr7	CAT TGC CTA TGA CGT CAC CTA CA	GAA GGC ATA CCA GAA AGG GTT GA
Ccr8	GCT CGC TCA GAT AAT TGG TCT TC	CGT GAC GTT GGG CTC CAT
Ccr9	CAG TTC TGA GGA GGA TGC TTG A	AAC CCA GCT GCA CTG ATG ATC
Ccr10	CCT CTA CTC GGC CTC TTT CCA	CGG TCG GCG CTG ATA CAG
Cxcr1	TGT CCC ACA TAT TTG GCT TCC T	GCC CGT AGC AGA CCA GCA T
Cxcr2	GCC CTG ACC TTG CCT GTC T	TGC ACA GGG TTG AGC CAA A
Cxcr3	TAC CTT GAG GTT AGT GAA CGT CA	CGC TCT CGT TTT CCC CAT AAT C
Cxcr4	ACC TCT ACA GCA GCG TTC TCA TC	TGT TGG TGG CGT GGA CAA TA
Cxcr5	GGG CTC CAT CAC ATA CAA TAT GG	GAA TCT CCG TGC TGT TAC TGT AGA AG
Cxcr6	CCG GCA GGC TAA GTG GAA	CAC CCA AAT GAG CAA GCA AA
Cxcr7	GCT ACA AAC TGC TCA GCA CTG AA	TCC TGG GCT GTG GTT TGC
Cx3cr1	F primer	R primer
	Transcription factors	
Foxp3	CCCTGCCCTTGACCTCAA	GCCTCAGTCTCATGGTTTTGG
Rorc	CAGCCAACATGTG-GAAAAGCT	GGGAAGGCGGCTTGGA
Id2	CGCTGACCACCCTGAACAC	TCGACATAAGCTCA-GAAGGGAAT
Prdm1	TGGCAGAGACTGGGATCATG	CTCGGCCTCTGTCCACAAA

Continued on next page...

Table 2.14 – continued from previous page.

Gene	Forward Primer (5'to 3')	Reverse Primer (5'to 3')
Spi1	GGAGAAAGCCATAGCGATCACT	GTGGTTCTCAGGGAAGTTCTCAA
AhR	GGAAGCCCGGCCTCTTC	TGGTATCCTGTTCCTGAATGAATTT
Tbx21	GCCAGGGAACCGCTTATATG	AACTTCCTGGCGCATCCA
Gata3	GGTGGACGTACTTTTTAACATCGA	CGTAGCCCTGACGGAGTTTC
Irf4	CGGGCAAGCAGGACTACAAT	ACAATGCCCAAGCCTTGATG
Cmaf	CCGAATTTTTCATGTGAGTGTGA	GACCCCCACGGAGCATTT
Eomes	TGAGCTTCAACATAAACGGACTCA	CGGCCAGAACCACTTCCA
Batf	GTTCTGTTTCTCCAGGTCC	GAAGAATCGCATCGCTGC
Runx2	GCCTTCAAGGTTGTAGCCCT	GTTCTCATACATTCCCGGCCA
Surface Markers		
Itga2	CTCCCTCAAGGTAACAGCCG	TCACCAATGCCATGCTCACT
Cd223	CGCGTCATTTTTTAGCTGAAACT	AGACATTGAAGCCATCTCTGTAGGT
Icos	CCTCTCTCCGTGCCTGATTC	CATACCCTTGGCATTTTTTGTAAA
Cd279	CCGCCTTCTGTAATGGTTTGA	GGGCAGCTGTATGATCTGGAA
Cd152	GGACACTAATCCATCAGGTTGGA	AGCCCTGTGACAGCCTCATC
Tigit	ACTGTACTGGCTAGAAAGAAGTC	TCAGGTTCCATTCCTGTGGC
Cd224	CCAAAAGCCCTCCTCATCGT	CTACCTCCTGGCACTCCTAC
Cd226	ATGGTTCCCCAAAAGAGGCA	TCAGGAGGTTGGACTTGATGC
Il10rα	TGAGCCTAGAATTCATTGCATACG	TCCGTACTGTTTGAGGGCCA
Il27ra	TTCTGTCCCTGTGGGGTTTG	CCTGTAGGCACCTGGTACTG
Viral RNA		
X-31-NP	TTTTCTAGCACGGTCTGCACTCATATTG	CTTGGCTGTTTTGAAGCAGTCTGAAAG

Chapter 3: IL-10-producing T cells in acute respiratory infection.

3.1 Introduction

The $CD4^+$ T cells now known as Tr1 cells were first discovered over 30 years ago [199]. However, as these rare IL-10-producing cells are difficult to detect and isolate many studies have focused on models of polyclonal and chronic TCR activation in which Tr1 cells are more frequent. There is still much to investigate with regard to their function in non-lethal, resolving infection settings. As discussed in Chapter 1, a number of studies have established the contributions of Treg cells to immune responses during acute infection, however Tr1 cells have not been subject to the same extent of detailed investigation in this context. To address these issues, experiments were designed to quantify and characterise the Tr1-like cell response in a murine model of IAV infection. Although IL-10^+ T cells have been described in IAV infection, it is not clear from most of these previous studies whether these cells were *bona fide* Tr1 cells based on current definitions of these cells (outlined in Chapter 1). Therefore, this study set out to perform a detailed investigation into the IL-10-producing $CD4^+$ T cell subsets that emerge during the response to IAV infection to understand the nature of these cells and their functional significance to immunity.

3.2 Quantitation of Tr1-like cell responses in a mouse model of respiratory infection.

Initial experiments were conducted to determine conditions under which Tr1-like cells were produced during IAV infection. Therefore, $FOXP3^{RFP}IL\text{-}10^{eGFP}$ (dual-reporter) mice [208] were infected i.n with a high dose X-31 IAV to model a severe, non-lethal, acute infection, and lungs were harvested on day 7 post-infection **(Fig 3.1 A)**. Mice infected with a dose of $923TCID_{50}$ of X-31 IAV i.n, lost between 5-10% of their initial weight by day 6, and subsequently recovered **(Fig 3.1 B)**. This dose was selected for future experimentation. The day 7 time point was chosen for initial analysis as it marks both the beginning of significant numbers of IAV-specific $CD4^+$ T cells accumulating in the infected lungs [318], and is the time point prior to when mice begin recovery from weight loss **(Fig 3.1 B)**. On day 7 post-infection, T cells from IAV-infected lungs were analysed by flow cytometry. The gating strategy for these experiments is shown in **(Fig 3.1 C)**. A substantial population of activated ($CD44^{hi}$) $CD4^+$ T cells were $FOXP3^-$ IL-10^+ in the lungs of mice infected with IAV at this time point **(Fig 3.1 C)**. Of the organs analysed post-IAV infection, $FOXP3^-$ IL-10^+ Tr1-like cells accumulated mainly within the lungs with a mean frequency of 6.8% of activated $CD4^+$ T cells **(Fig 3.1 D)** with few being detected in the mLN or the spleen **(Fig 3.1 E & F)**. Overall, these data provided initial support for the notion that Tr1-like cells emerge during the course of the response to IAV infection.

The dual-reporter mouse was then used to optimise detection of FOXP3 and IL-10 by intranuclear/intracellular staining for flow cytometry to allow their detection in non-reporter mice. It was determined following restimulation that FOXP3 and IL-10 expression could be detected by $CD4^+$ T cells in the lungs on day 7 post-IAV infection **(Fig 3.2)**, with an average of 5% $FOXP3^-$ $IL\text{-}10^+$ Tr1-like cells being detected. The level of both FOXP3 and IL-10 in $CD4^+$ T cells, in terms of the percentage of cells positive for these two markers, was higher using the dual-reporter mice (compare **Fig 3.1** and **Fig 3.2**). These data indicate that although identification of Tr1-like $CD4^+$ T cells is more sensitive using the dual-reporter mice, it is also possible to reproducibly identify these cells by intranuclear/intracellular staining for IL-10 and FOXP3. This is an important outcome as it allows identification of Tr1-like cells in experiments in which the dual-reporter mice cannot be used.

Next, to further validate the dual-reporter mice to ensure reproducible identification of both IL-10- and FOXP3-expressing cells, mice were infected with IAV, and FACS-sorting was utilised to purify double-negative (GFP^-RFP^-), double-positive (GFP^+RFP^+), $FOXP3^+$ (GFP^-RFP^+) and $IL\text{-}10^+$ (GFP^+RFP^-) $CD4^+$ T cells from the lung on day 7 post-infection (gating strategy and post sort purity shown in **Fig 3.3 A & B**). Then mRNA was prepared from each of the FACS-sorted populations, and *Foxp3* and *Il10* mRNA quantified in each population using RT-qPCR. Detectable transcription of both *Foxp3* and *Il10* mRNA was confined to the T cell populations positive for their respective reporters **(Fig 3.3 C)**, thereby validating the reporter system. As a further test of biological specificity, intra-epithelial lymphocytes (IELs) and lamina propria lymphocytes (LPLs) from the small intestine, mesenteric lymph nodes (MLNs), Peyer's patches (PPs), lungs, and spleen from naive dual-reporter mice were also analysed by flow cytometry, as Tr1 cells have been reported in these locations previously [208], [319], [320]. In each of the tissues in the present study there were four populations of $CD4^+$ T cells that could be clearly delineated on the basis of expression of FOXP3 and IL-10 **(Fig 3.4 A & B)**. Consistent with previous reports [319], [320], there were similar numbers of $FOXP3^+$ and $FOXP3^-$ IL-10-producing $CD4^+$ T cells within the gut-associated tissues, with the lamina propria of the small intestine exhibiting the greatest number of $IL\text{-}10^+$ T cells (**Fig 3.4 C**).

3.3 The kinetics of Tr1-like cell generation in IAV infection.

As previously discussed, the cytokine IL-10 has important roles in immune regulation. However, the contribution of different T cell subsets to IL-10 production and the regulation of immune responses following acute infection is poorly understood. To more precisely define the T cells that produce IL-10 in IAV-infected lungs, a detailed examination of the

cellular sources of IL-10 was performed. Previous reports have variously identified $CD8^+$ T cells or $CD4^+$ T cells as the dominant source of T cell-derived IL-10 at the peak of IAV infection [257], [258]. Both of those studies were completed before the availability of the dual-reporter mouse. This mouse provides an advantage as it allows for a much more detailed and sensitive analysis of the different T cell sources of IL-10.

Kinetic analysis of IL-10-secreting T cells in lungs of dual-reporter mice following IAV infection was performed at days 0 (naive), 5, 7, and 10 post-infection, and analysed by flow cytometry (gating strategy shown in **Fig 3.5 A**). Comparing the accumulation of IL-10^+ ($eGFP^+$) T cells in the IAV-infected lungs revealed that, on day 5 post-infection $CD4^-$ $CD8^-$ T cells peaked in cell number and rapidly decreased from day 5 to day 10 post-infection **(Fig 3.5 B)**. These $CD4^-$ $CD8^-$ T cells are most likely either NKT cells, MAIT cells or other innate-like $CD3^+$ T cells [321], [322]. In contrast, conventional $CD4^+$ and $CD8^+$ T cells that expressed IL-10 peaked in frequency in the lung at day 7 post-infection. At this time point, activated $CD3^+$ T cells producing IL-10 were predominately $CD4^+$ rather than $CD8^+$ **(Fig 3.5 B)**. The mean number of IL-10^+ $CD4^+$ T cells was more than double that of the IL-10^+ $CD8^+$ T cells. Furthermore, the majority of the IL-10^+ $CD4^+$ T cells were $FOXP3^-$ **(Fig 3.5 C)**, indicating that conventional Treg cells are not the main IL-10-producing T cell type in the lung at this time. Both the IL-10-producing $CD4^+$ and $CD8^+$ T cell populations declined in number from day 7 to day 10 post-infection **(Fig 3.5 B)**. Together, these data demonstrate that $CD4^+$ T cells are the dominant T cell-derived source of IL-10 in IAV-infected lungs, and that $FOXP3^-$ Tr1-like cells rather than Treg cells are the primary cellular source of IL-10 in the lung during IAV infection.

Four clearly distinct populations of activated $CD4^+$ T cells were identified in the initial kinetic analysis. These populations from the IAV-infected lungs of dual-reporter were defined based on expression of FOXP3 and IL-10. These are i) effector T cells ($FOXP3^-$IL-10^-) ii) Treg cells ($FOXP3^+$IL-10^-) iii) IL-10^+ Treg cells ($FOXP3^+$IL-10^+) and iv) Tr1-like cells ($FOXP3^-$IL-10^+) **(Fig 3.5 C)**. As expected, effector $CD4^+$ T cells were the most abundant population in the lungs over the course of IAV infection **(Fig 3.5 C & D)**. The smallest population by cell number were IL-10^+ Treg cells **(Fig 3.5 C, E, & F)**. Tr1-like and Treg cells (including IL-10^+ Treg cells) were most abundant at day 7 post-infection **(Fig 3.5 C-F)**, validating the initial selection of this time point (Section 3.2) and confirming its utility for further exploration of these $CD4^+$ T cell populations in the IAV model.

Next, to provide an understanding of the kinetics of viral clearance in this model, the level of virus in the IAV infected lungs was assessed after infection. Mice were infected with X-31 IAV and on day 0 (naive), 1, 3, 5, 7, and 10 post-infection whole lungs were harvested and snap frozen for RNA extraction. The mRNA was then processed for RT-

qPCR analysis of viral NP mRNA. IAV NP mRNA peaked in the lungs between days 3 and 5 **(Fig 3.6)**. The viral load significantly decreased by day 7, which coincides with the time point at which Tr1-like cells are observed to peak in cell number in the IAV-infected lungs **(Fig 3.5)**.

Up to this point only female mice had been used for experimentation. In order to maximise the use of dual-reporter mice being generated for this study, it was planned that both male and female mice would be utilised. However, it has been reported that, due to androgen receptor signalling, there are numerous sex-specific differences between males and females in immune responses to IAV infection. For example, in response to stimulation with PR8 IAV, PBMCs from female mice produce less IL-10 compared to PBMCs from male mice [323]. However, other studies have reported no difference in IL-10 production between male and female mice in IAV infection [324]. Of course, these discrepancies could be due to differences in IAV dose, as IL-10 production by Th1 cells is known to increase with increasing antigen stimulation via induction of STAT4 [280]. Therefore, in light of this, it was important to formally establish whether the findings in the present study were similar in both male and female mice. Thus, male mice age-matched to the female mice used in previous experiments were infected with the same dose of X-31 IAV. Similar to female mice, $CD4^+$ T cells were the dominant source of T-cell derived IL-10 in the male IAV-infected lungs **(Fig 3.7 A & B)**. Overall, similar to what was observed in female mice $FOXP3^-$ $IL\text{-}10^+$ $CD4^+$ T cells comprised a small population compared to $FOXP3^-$ $IL\text{-}10^-$ effector $CD4^+$ T cells **(Fig 3.7 C & D)**. Furthermore $IL\text{-}10^+$ Treg cells were less abundant than $IL\text{-}10^-$ Treg cells in the IAV-infected lungs **(Fig 3.7 E)**. In accordance with findings in female mice, the $IL\text{-}10^+$ $CD4^+$ T cells were predominately $FOXP3^-$ Tr1-like cells **(Fig 3.7 C & F)** thereby confirming that the dominant source of T cell-derived IL-10 following IAV infection was a Tr1-like cell type in both male and female mice.

Direct comparison of the cell number between male and female mice indicated there was no significant difference in the total number of live cells recovered from the IAV-infected lungs between male and female mice on day 7 post-infection **(Fig 3.8 A)**. There were no differences in the number of effector T cells or Treg cells between male and female mice **(Fig 3.8 B)**. However, there were statistically significantly more of both $IL\text{-}10^+$ Treg and Tr1-like cells in the IAV-infected lungs of male mice compared to female mice **(Fig 3.8 B)**. Despite these minor differences, the major features and kinetics of the IL-10-secreting T cell response following IAV infection were largely consistent between males and females, so mice from both sexes were subsequently used for experiments to investigate Tr1-like cells in this model.

3.4 A murine model of Tr1-like cell deficiency.

To investigate the function of Tr1-like cells in IAV infection, an adoptive transfer model system with a known deficiency in this cell type was utilised. The *Il27ra*$^{-/-}$ mice were chosen as they reportedly exhibit a defect in generation of IL-10^{+} conventional CD4^{+} T cells without deficiency in IL-10^{+} Treg cells [253]. To detect Tr1-like cells in these mice FOXP3 and IL-10 were identified by intracellular/intranuclear staining. Following IAV infection, *Il27ra*$^{-/-}$ mice lost significantly more weight than littermate *Il27ra*$^{+/+}$ and *Il27ra*$^{+/-}$ control mice **(Fig 3.9 A)**, in agreement with a previous study of *Il27ra*$^{-/-}$ mice in IAV infection [256]. Post-IAV infection there were no statistically significant differences in weight loss and recovery between the *Il27ra*$^{+/+}$ and *Il27ra*$^{+/-}$ littermates **(Fig 3.9 A)**. This led to adoption of a *Il27ra*$^{+/-}$ x *Il27ra*$^{-/-}$ breeding strategy to increase the number of *Il27ra*$^{-/-}$ mice generated for experiments. Furthermore, intranuclear staining demonstrated that both the *Il27ra*$^{+/+}$ and *Il27ra*$^{+/-}$ mice exhibited a greater proportion of FOXP3^{-} IL-10^{+} Tr1-like cells compared to the *Il27ra*$^{-/-}$ mice **(Fig 3.9 B)**.

Comparing the IAV-infected littermates, there was a clear reduction the frequency and number of Tr1-like cells lungs of *Il27ra*$^{-/-}$ mice compared to *Il27ra*$^{+/-}$ mice without any discernible effect on the other three CD4^{+} T cell populations **(Fig 3.9 B-D)**. This is consistent with a previous study of *Il27ra*$^{-/-}$ in a *T.gondii* infection model, which concluded that IL-27 signalling was critical for restricting the effector T cell response to limit cytokine production and tissue damage. However, that study did not specifically identify or assess Tr1-like cells [128]. The increased weight loss observed in IAV-infected *Il27ra*$^{-/-}$ mice in the present study, in line with published findings [128], suggests that Tr1-like cells may regulate ongoing immune responses.

To further investigate the effect of IL-27R deficiency during IAV infection, the BALF was also analysed at day 7 post-infection **(Fig 3.10)**. In *Il27ra*$^{-/-}$ mice there was a statistically significant reduction in Tr1-like cells as a proportion of activated CD4^{+} T cells and total cell number similar to that observed in the lungs **(Fig 3.10 A-C)**. There were no statistically significant differences in the frequency or number of IL-10^{+} Treg cells in the BALF of *Il27ra*$^{-/-}$ mice compared to their *Il27ra*$^{+/-}$ littermates **(Fig 3.10 A-C)**. These data confirmed that within the CD4^{+} T cell compartment Tr1-like cells alone were reduced in both lung tissue and BALF of *Il27ra*$^{-/-}$ mice compared to *Il27ra*$^{+/-}$ littermates following IAV infection.

It is known that IL-10- and IL-27R-deficient mice exhibit an increase in IL-17A production by effector T cells and increased tissue damage in response to IAV infection [258], [325]. Those reports examined CD4^{+} T cell cytokine production in response to infec-

tion but did not address the question of whether Tr1-like cells were present in *Il27ra*$^{-/-}$ mice following IAV infection. As there were a small number of Tr1-like cells detected in *Il27ra*$^{-/-}$ mice in the present study, these cells were assessed for production of IFNγ and IL-17A and compared to Tr1-like cells from the *Il27ra*$^{+/-}$ littermates (gating strategy shown in **Fig 3.11 A**). This determined that Tr1-like cells in the lungs of IAV-infected *Il27ra*$^{-/-}$ mice exhibited a dysregulated phenotype. This was evident as IL-17A was detectable in Tr1-like cells from *Il27ra*$^{-/-}$ mice compared to those from control mice, and displayed a bias towards IL-17A production compared with that of IFNγ **(Fig 3.11 A & B)**. This may indicate that Tr1-like cells are more pro-inflammatory in the absence of IL-27R signalling as they produce more IL-17A.

These data confirm that there is disruption of Tr1-like cell generation in *Il27ra*$^{-/-}$ mice. These mice exhibited increased weight loss and delayed recovery along with a statistically significant reduction in the accumulation of Tr1-like cells compared to littermate control mice following IAV infection. In addition, the phenotype of the small population of Tr1-like cells present in the *Il27ra*$^{-/-}$ was dysregulated compared to littermate controls, with these cells producing less IFNγ and more IL-17A. Collectively, these findings suggest Tr1-like cells may contribute to the regulation of the immune response during IAV infection by exerting control over the magnitude of effector T cell responses in IAV infection. Together, these data indicate that the *Il27ra*$^{-/-}$ mice exhibit a selective deficiency in Tr1-like cells within the lungs following IAV infection and provided a valid model to investigate Tr1 cell function in IAV infection.

3.5 Investigating the function of Tr1-like cells in IAV infection.

In order to conduct adoptive transfer experiments to determine the function of Tr1 cells in IAV, an *in vitro* culture system was developed to provide a source of Tr1 cells. Naive CD4$^+$ T cells were purified from dual-reporter mice and activated in the presence of α-CD3 and α-CD28 antibodies in the presence of combinations of TGFβ1, IL-27, and IL-10 **(Fig 3.12 A-C)**. CD4$^+$ T cells activated in the presence of both IL-27 and TGFβ1 exhibited significant induction of a FOXP3$^-$ IL-10$^+$ population (around 20% of cells had this phenotype) **(Fig 3.12 B & C)**. Exogenous IL-10 did not substantially modify the phenotype of the T cells from these cultures but TGFβ1 and IL-27 in combination generated the highest frequency of Tr1-like cells **(Fig 3.12 B & C)**. After establishing that Tr1-like cells could be derived *in vitro* using published methods [194], [195], how closely these cells resemble previously described Tr1 cells, and the Tr1-like cells characterised in IAV infection in the present study, was investigated. First, the cytokine secretion profile of the *in vitro*-derived Tr1-like cells was examined and compared to Th1, Th2, Th17, and iTreg cell subsets generated *in*

vitro from naive CD4$^+$ T cells cultured under different Th polarising conditions for three days. In contrast to the Th cell populations, iTreg cells did not detectably express IFNγ, IL-4, IL-17A, or IL-10 **(Fig 3.13 A & B)**. Tr1-like cells were more similar to effector Th cell populations than Treg cells as they expressed both IFNγ and IL-10, however, they did not appreciably express IL-17A or IL-4. As expected, Th1 cells expressed the most IFNγ in addition to a small amount of IL-10 **(Fig 3.13 A & B)**. Th2 cells were the only CD4$^+$ T cell population to express any detectable IL-4 **(Fig 3.13 A & B)**, whereas Th17 cells had the greatest expression of IL-17A **(Fig 3.13 A & B)**. As these Th17 cells were generated using TGF-β1 in addition to IL-6, there was also a relatively high level of IL-10 expression detected. This was presumably through activation of the IL-6/STAT-3 pathway as previously described [265]. In summary, *in vitro*-generated Tr1-like cells displayed a similar cytokine signature to that previously described in analogous systems of Tr1-like cell generation [194], [326], [265] and more closely resemble effector T cell populations than iTreg cells.

As already discussed, a critical feature of *bona fide* Tr1 cells is their ability to suppress effector T cell division. An important question thereby arose as to whether the *in vitro*-derived Tr1-like cells met this criterion. Therefore, the *in vitro*-derived Tr1-like cells were assessed for their ability to suppress effector T cell division. To begin this investigation an assay was required to assess the ability of regulatory T cells to inhibit effector T cell division. To do this an *in vitro* suppression assay was developed, based on similar assays reported in the literature [317], [194], [210].

There are several important considerations when establishing a T cell suppression assay. First, a robust method to stimulate effector T cell division is required. This is commonly achieved by culturing on α-CD3-coated plates, or α-CD3-coated beads, or soluble α-CD3. Next, T cell co-stimulation is also required. While this can be provided by α-CD28 antibodies or coated beads, an alternative is the inclusion of APCs which express co-stimulatory factors. The APCs can either be irradiated to render them incapable of changes in expression of co-stimulatory molecules and supplying secreted molecules, or live where they can also contribute to the response via surface and secreted molecules. Live APCs were included in this assay as Tr1 cells can modulate APCs to indirectly alter T cell responses, for example by down-regulating antigen-presentation, co-stimulation, and inflammatory cytokine production. Thus, the assay would allow evaluation of the capacity of Tr1-like cells to suppress T cell proliferation both directly and indirectly. Therefore, CD11c$^+$ DCs isolated via positive selection from SLOs of CD45.2$^+$ mice **(Fig 3.14 A)** were placed into culture first to coat the bottom of the 96-well trays and soluble α-CD3 was added. Next, either *in vitro*-derived Tr1-like cells or Treg cells from naive dual-reporter SLOs were added to the suppression assay with labelled effector T cells. The *in vitro*-derived Tr1-like cells were FACS-sorted from three day cultures for CD4$^+$

FOXP3$^-$ IL-10$^+$ cells. Treg cells were also FACS-sorted for CD4$^+$ FOXP3$^+$ CD25$^+$ cells prior to addition to suppression assay **(Fig 3.14 B)**. Either Treg or Tr1-like cells were used as the suppressor cell in an individual well of the assay. Finally, naive CD3$^+$ T cells were enriched by negative selection from SLOs of CD45.1$^+$ mice, and then CD3$^+$ CD25$^-$ T cells were FACS-sorted and labelled with Efluor670 proliferation dye, before being placed into culture **(Fig 3.14 C)**. Suppression assays were cultured for approximately 72 hours at 37°C and 5% CO_2 and the extent of proliferation of Efluor670-labelled CD45.1 T cells assessed by flow cytometry.

First, the suppression assay was validated by analysis of important controls. As positive controls for the suppression assay, CD25$^+$ FOXP3$^+$ Treg cells were first assessed for their ability to suppress effector T cell division. As expected, Treg cells significantly inhibited the division of effector T cells **(Fig 3.15 A-C)**. In these assays a negative control for suppression was also used. Effector T cells (instead of Treg cells) were added along with effector T cells in the presence of live APCs and soluble α-CD3 as these effector T cells were expected to elicit no suppression. This served to control for a background level of suppression elicited by bystander T cells or due to competition for stimulation and accordingly, negligible suppression was observed (Eff+Eff control). The results of these suppression assays determined that Treg cells were statistically significantly suppressive of effector T cell division even at a ratio of 1:16 (Treg cells:effector T cells) and validated the suitability of the assay for assessment of Tr1-like cell-mediated suppression **(Fig 3.15 A & C)**. Similarly to that observed with Treg cells, the *in vitro*-derived Tr1-like cells were able to significantly suppress effector T cell division at a ratio of 1:16 (Tr1-like cells:effector T cells) **(Fig 3.15 A & C)**. This confirmed that the *in vitro*-derived Tr1-like cells were indeed suppressive and hence, *bona fide* Tr1 cells. The division index (DI) is a measure of the mean number of divisions for a population of cells. Calculation of the DI of effector T cells cultured in the presence or absence of either Treg or Tr1 cells (at a 1:1 ratio), indicated a statistically significant reduction **(Fig 3.15 B)**. In addition, there was no statistically significant difference between Tr1 cells or Treg cells with respect to their ability to suppress effector T cell division **(Fig 3.15 B)**.

To ascertain whether the increased weight loss and delayed recovery from maximum infection-induced weight loss documented in the *Il27ra*$^{-/-}$ mice was dependent on Tr1 cells, an adoptive transfer strategy was implemented. The *in vitro*-generated Tr1 cells were employed to determine whether addition of Tr1 cells could reverse the enhanced weight loss or the increased time to weight recovery observed in IAV-infected *Il27ra*$^{-/-}$ mice. 2x10^5 polyclonal Tr1 cells were FACS-sorted from *in vitro* cultures and labelled with Efluor670 prior to transfer into X-31-OVA$_{323-339}$ IAV-infected *Il27ra*$^{-/-}$ mice on day 5 post-infection (pre- and post-sort purity shown in **Fig 3.16 A)**. Note that X31-OVA$_{323-339}$ IAV was selected for *Il27ra*$^{-/-}$ experiments with the intention of ultimately using an antigen-

specific system as a number of previous studies outline that Tr1 cells depend on antigen specificity to elicit their function [216], [191], [327], [230], [328]. Due to unforeseen delays in acquiring OT-II mice and crossing them to dual-reporter mice this was not achievable within the time constraints of this study. In the present study there was no statistically significant difference in maximum weight loss between the *Il27ra*$^{-/-}$ mice receiving either Tr1 cells or PBS **(Fig 3.16 B)**. However, treatment of *Il27ra*$^{-/-}$ mice with Tr1 cells enhanced recovery from maximum infection-induced weight loss **(Fig 3.16 B)**. More specifically, the *Il27ra*$^{-/-}$ + Tr1 cell-treated group, was statistically significantly different from the *Il27ra*$^{-/-}$ + PBS group at day 8 post-infection and displayed an enhanced rate of recovery from weight loss **(Fig 3.16 B)**. Moreover, compared with the PBS-treated *Il27ra*$^{-/-}$ group, the *Il27ra*$^{-/-}$ + Tr1 cell-treated group was not statistically significantly different from the Tr1-sufficient *Il27ra*$^{+/-}$ group in percentage of initial weight over the course of infection **(Fig3.16 B)**. To verify that the adoptively transferred Tr1 cells reached disease-relevant sites post transfer, the BALF and lungs were interrogated on day 7 post-infection (2 days post-transfer) for the presence of those cells at peak weight loss. Efluor670-labelled transferred cells were detected in the lungs of the *Il27ra*$^{-/-}$ + Tr1 cell-treated group and a subset of Tr1 cells were still producing IL-10 **(Fig 3.16 C)**. These results establish that Tr1-deficient *Il27ra*$^{-/-}$ mice, which lack endogenous Tr1-like cells, exhibited restored recovery from weight loss with transfer of 2x10^5 polyclonal FACS-sorted Tr1 cells **(Fig 3.16)**.

After confirming the suppressive function of the *in vitro*-derived Tr1 cells both *in vitro* and *in vivo* it was also important to identify the mechanisms used by these cells to elicit suppression. Therefore, suppression assays were set up with the addition of an isotype control antibody or a nAB against the IL-10Rα, LAG-3, or both, as IL-10 has previously been implicated in the suppressor function of Tr1 cells and LAG-3 is known to be expressed but the functional relevance has not been shown [191], [194], [210]. A statistically significant reduction in the suppression of effector T cell division was demonstrated by FACS-sorted *in vitro*-derived Tr1 cells in the presence of α-IL-10Rα nAB compared to the isotype control **(Fig 3.17 A)**. The addition of an IL-10Rα nAB did not entirely inhibit the ability of Tr1 cells to suppress effector T cell division, suggesting other molecules and mechanisms are involved in their suppressor function. In addition, α-LAG-3 nABs also inhibited suppression of effector T cell division, indicating that LAG-3 was also contributing to the suppressor function of Tr1 cells. However, the effect of α-LAG-3 nAB was less consistent compared to the IL-10Rα nAB between experiments **(Fig 3.17 B)**. It was postulated that there was some redundancy in the suppressive mechanisms of Tr1 cells such that blocking IL-10 or LAG-3 in isolation would result in the other mechanism to compensating for this. When IL-10Rα and LAG-3 nABs were added to the same suppression assay a statistically significant reduction in suppression of effector T cell division was observed, however, suppression was not completely abrogated **(Fig 3.17 C)**.

This indicates that the *in vitro*-derived Tr1 cells elicit suppression via IL-10 and LAG-3 but there are also other other mechanisms at play.

3.6 Positioning and trafficking of IL-10-producing T cells in IAV-infected lungs.

Experiments described above using *Il27ra*$^{-/-}$ mice demonstrated that Tr1 cells contribute to the resolution of IAV infection. This implies Tr1 cells may engage with virally-infected cells or other leukocytes participating in the response at the site of viral challenge. However, whether Tr1-like cells found in the IAV-infected lung, such as those observed in this study, are within the lung parenchyma and/or at the site of infection is not established. Conceivably, these cells could be found within the microvasculature of the lung and whether there are any differences between the regulatory T cell populations with respect to positioning in the lung parenchyma is also unknown. To address this, intravascular labelling experiments were performed. On day 7 post-IAV infection dual-reporter mice were injected with anti-TCR-β-BV421 antibody intravenously three minutes prior to humane euthanasia. Therefore, T cells found in the vasculature would be labelled with this antibody, while T cells that had infiltrated the parenchyma would not [329]. For these experiments, the peripheral blood was also analysed as a positive control for cells within the vasculature. The gating strategy for these experiments and concatenated representative flow cytometry data for each population is shown in **Fig 3.18 A**. Overall, these experiments revealed that over 85% of Tr1-like cells were within the parenchyma of the IAV-infected lungs **(Fig 3.18 A-C)**. Compared to the effector CD4$^+$ T cells and Treg cells, significantly more IL-10$^+$ Treg and Tr1-like cells were found within the parenchyma compared to the vasculature of the IAV-infected lungs **(Fig 3.18 B-D)**. Thus, these data indicate that IL-10$^+$ CD4$^+$ T cells are present at the site of infection where they may directly contribute to the immune response to IAV. Additionally, as some Tr1-like cells were also observed within the vasculature this implies that at least some of these cells are in circulation prior to migration into the lung. This observation led to an investigation of the chemokine receptors involved in recruitment of IL-10-producing CD4$^+$ T cells.

There is a paucity of information regarding the homing mechanisms used by Tr1-like cells. To address this, mRNA levels of all known chemokine receptors were quantified by RT-qPCR in FACS-sorted CD4$^+$ T cell populations (based on FOXP3 and IL-10 expression) harvested from lungs of day 7 IAV-infected dual-reporter mice and the level of expression calculated relative to the housekeeping gene *Rplp0* **(Fig 3.19 A & B)**. Several chemokine receptor genes were highly expressed by Tr1-like cells. These were *Ccr2*, *Ccr5*, *Cxcr3*, *Cxcr4*, and *Cxcr6* **(Fig 3.19 A & B)**. Of these, *Cxcr6* stood out as it was expressed at a

higher level by Tr1-like cells than the three other $CD4^+$ T cell populations. All of the other expressed chemokine receptors were either expressed at equivalent levels in Tr1-like cells to other T cell populations (*Ccr5* and *Cxcr3* had comparable expression in Tr1-like cells and IL-10^+ Treg cells) or were expressed at lower levels than in other $CD4^+$ T cell populations (*Ccr2* and *Cxcr4* were both expressed at higher levels in Treg cells than in Tr1-like cells). It was also noted that *Ccr7* was expressed at very low levels by IL-10^+ $CD4^+$ T cells (including both Tr1-like and IL-10^+ Treg cells) compared to IL-10^- $CD4^+$ T cell populations **(Fig 3.19 A & B)**.

These data prompted the question of whether expression of CXCR6 while co-staining CCR7 could be used to more specifically identify Tr1-like cells by flow cytometry. In line with the RT-qPCR data, Tr1-like cells expressed high levels of surface CXCR6 and little to no CCR7. Around 90% of Tr1-like cells in the lung displayed a $CXCR6^+$ $CCR7^-$ surface profile. Compared to all other $CD4^+$ T cells in the lung, Tr1-like cells had the highest level of surface CXCR6 expression **(Fig 3.20 A & B)**. However, the $CXCR6^+$ $CCR7^-$ profile did not specifically define a Tr1-like cell surface expression profile, as IL-10^+ Treg cells were also predominantly $CXCR6^+$ $CCR7^-$ **(Fig 3.20 A-C)**. In addition, while effector $CD4^+$ T cells and Treg cells both had substantial populations of $CXCR6^-$ $CCR7^+$ and $CXCR6^-$ $CCR7^-$ cells, in both of these populations a significant fraction (10-15%) were also $CXCR6^+$ $CCR7^-$ **(Fig 3.20 A-C)**. These data indicated that unlike the Treg and effector $CD4^+$ T cells, there was no naive-like T cell population amongst Tr1-like and IL-10^+ Treg cells (**Fig 3.20 A & C**), suggesting that IL-10 expression in $CD4^+$ T cells is associated with a more advanced state of differentiation than is necessarily the case in IL-10^- Treg and effector T cells.

To determine whether CXCR6 was required for the homing of Tr1-like cells to the IAV-infected lungs, *Cxcr6*$^{-/-}$ mice were employed. *Cxcr6*$^{-/-}$ and WT mice were infected with X-31 IAV-i.n. On day 7 post-infection the lungs were harvested for intranuclear/intracellular staining of FOXP3 and IL-10 to identify Tr1-like cells by flow cytometry. Unexpectedly, the *Cxcr6*$^{-/-}$ mice exhibited significantly less weight loss than WT mice post-IAV infection **(Fig 3.21 A)**. Analysis of the IAV-infected lungs by flow cytometry revealed a significant reduction in the percentage of both IL-10^+ Treg cells and Tr1-like cells amongst activated $CD4^+$ T cells in *Cxcr6*$^{-/-}$ mice compared to WT **(Fig 3.21 B & C)**. However, there was no difference in total numbers of these cells **(Fig 3.21 D)**. The reduction in the percentage of Tr1-like cells in the *Cxcr6*$^{-/-}$ mice was likely the result of increased frequencies of other $CD4^+$ T cell populations such that Tr1-like cells make up a smaller percentage of the activated $CD4^+$ T cells overall. These data suggest that although Tr1-like cells express a high level of CXCR6 protein, this chemokine receptor is not essential for their recruitment to the lungs in IAV infection.

3.7 Cytokine and effector molecule production by IL-10-producing T cells during IAV infection.

After establishing the potential role for Tr1-like cells in contributing to the resolution of IAV infection, extensive molecular characterisation of *in vivo*-derived Tr1-like cells compared to other activated CD4$^+$ T cell populations from the IAV-infected lungs was performed. The series of molecules selected for this study were as follows: i) lineage-specific effector cytokines from a range of T cell subsets (IFNγ, IL-17A, IL-4 and IL-21), ii) cytokines in addition to IL-10 which have been associated with Tr1-like cells in other contexts (TNFα, CSF1, and TGFβ), and iii) molecules associated with cytolytic effector function (Perforin, Granzyme B and CD107a).

Critical to the function of T cells is their ability to secrete cytokines and effector molecules. As previously discussed, while Tr1 cells are characterised by a high level of IL-10 production they are also known to produce TGF-β and IFNγ whereas, IL-2 and IL-4 have been demonstrated to be expressed at very low levels or are absent from their cytokine profile in a range of mouse models and in human disease [191], [330], [194]. As expression of IL-10 is not unique to Tr1 cells, other lineage specific cytokines were screened by RT-qPCR to establish whether the Tr1-like cells studied in the IAV model expressed cytokines that define Th1, Th2, or Th17 cells **(Fig 3.22 A)**. RT-qPCR identified that Tr1-like cells expressed significantly more *Ifng* compared to Treg, and IL-10$^+$ Treg, and effector CD4$^+$ T cells from the IAV-infected lungs **(Fig 3.22 A)**. High level expression of *Il10* with low level expression of *Ifng* is one definition previously used for Tr1-like cells in the literature [331], [332], [246]. The Th2-specific cytokine *Il4* and Th17-specific cytokine *Il17a* were not appreciably expressed by any subset of CD4$^+$ T cells examined **(Fig 3.22 A)**. Tr1-like cells have been previously shown to be induced by the cytokine IL-27 [333]. The resulting signalling leads to production of both IL-10 and IL-21. In line with this it was observed that Tr1-like cells expressed significantly higher levels of *Il21* compared to IL-10$^+$ or IL-10$^-$ Treg cells **(Fig 3.22 A)**. All four populations of lung CD4$^+$ T cells examined following IAV infection, including Tr1-like cells, expressed some *Tgfb1* **(Fig 3.22 A)**. TGF-β1 is known to be critical for the induction of regulatory T cells in the periphery [334],[160]. In a previous study *Csf1* was identified as significantly more highly expressed by Tr1-like cells compared to Th0 cells, however, *Csf1* expression was not detected in the present study **(Fig 3.22 A)**. Overall this analysis of cytokine mRNA expression demonstrated that the Tr1-like cells from the IAV-infected lung were largely consistent with what has been previously described for Tr1 cells [217].

Given the RT-qPCR data above and the fact that the Tr1-like cells investigated in this study were induced during IAV infection, the cytokines selected for investigation of

protein expression included the type I cytokines IFNγ and TNFα. Dual-reporter mice were infected with IAV and on day 7 lungs were harvested for analysis of intracellular cytokine production. Amongst the 4 sub-populations, Tr1-like cells exhibited the highest frequency of IFNγ^+ cells **(Fig 3.22 B-D)**. A significant proportion of effector CD4$^+$ T cells also expressed IFNγ compared to the Treg and IL-10$^+$ Treg cells. As expected, CD4$^+$ effector T cells expressed significantly more TNFα than Treg cells **(Fig 3.22 E & F)**. There was no significant difference between the effector CD4$^+$ T cells and the Tr1-like cells with respect to the frequency of TNFα single-positive or IFNγ/TNFα double-positive cells **(Fig 3.22 G & H)**. These data demonstrate that Tr1-like cells from the IAV-infected lungs expressed high levels of IFNγ with some TNFα. They shared a similar profile with effector T cells, whereas a lower proportion of the FOXP3$^+$ Treg populations expressed these inflammatory cytokines overall. This implies that Tr1-like cells from the IAV-infected lungs may be multifunctional including being pro-inflammatory in some contexts.

Effector molecules known to be important for Tr1 cell function include *Prf1* and *Gzmb*. Perforin and granzyme B are known to be important for cytotoxic T cell functions, which in IAV infection are required to directly lyse virally-infected cells. Human Tr1-like cells have also been reported to use perforin and granzyme B to specifically kill myeloid cells [335]. Myeloid cell-specific killing could conceivably contribute to the resolution of the immune response to IAV and a decrease in inflammation-mediated damage. Both perforin and granzyme B were expressed at the level of mRNA in Tr1-like cells induced in the lung following IAV infection. Perforin was highly expressed by all IL-10-producing cells with granzyme B showing a similar trend **(Fig 3.23 A)**. As granzyme B was the most highly expressed effector molecule it was selected for further analysis at the protein level. It was found that the IL-10$^+$ Treg and Tr1-like cell populations contained the highest proportion of cells positive for granzyme B **(Fig 3.23 B, C, & E)**. Effector CD4$^+$ T cells and Treg populations contained a a lower proportion of granzyme B$^+$ cells compared to IL-10$^+$ CD4$^+$ T cells (**Fig 3.23 B, C, & E**). Many different types of T cells produce granzyme B, however, without degranulation granzyme B is not secreted. Thus, CD107a was also analysed to provide a measure of CD4$^+$ T cell degranulation. CD107a is expressed within the membrane of lipid granules which house effector molecules including granzyme and perforin within the cell. When a cell is actively degranulating, the granules move to the cell membrane and begin to fuse to release the effector molecules [336], which means that CD107a can be detected on the surface of the cell membrane if a cell is actively de-granulating. The α-CD107a antibody was added to cells and incubated while re-stimulating with PMA and ionomycin to detect de-granulating cells. Compared to naive CD4$^+$ T cells, each of the CD4$^+$ T cell populations expressed a low level of CD107a (**Fig 3.23 D & F**). IL-10$^+$ Treg cells expressed the highest level of CD107a with the Tr1-like cells, Treg cells and effector CD4$^+$ T cells having similarly low levels of CD107a expression **(Fig 3.23**

D & F). This demonstrates that although granzyme B appears to be highly expressed by Tr1-like cells, there is limited degranulation, suggesting that these cells are not significantly contributing to granzyme B-mediated killing during IAV infection.

Taken together this investigation determined that Tr1-like cells from the IAV-infected lungs express IFNγ with a small population also expressing TNFα. This highlights the potential for these Tr1-like cells to exhibit pro-inflammatory function in addition to being suppressor cells. Tr1-like cells also expressed high levels of granzyme B as assessed by both mRNA and protein expression. However, they did not exhibit complete cytotoxic potential as they displayed limited degranulation.

3.8 The transcription factor landscape of Tr1-like cells from the IAV-infected lungs.

To further understand whether the Tr1-like cells generated during IAV infection are similar to Tr1 cells described in the literature, analysis of transcription factor expression is required to determine the drivers of this phenotype. As previously discussed, there is no widely-accepted consensus on Tr1-specific transcription factor(s). Depending on the disease model, Tr1 cells can be phenotypically diverse and identification of a lineage-specific transcription factor/s has remained elusive. To investigate Tr1-specific transcription factor expression in the IAV-setting, a range of T cell lineage specific transcription factors were assessed across FACS-sorted CD4$^+$ T cell populations from the IAV-infected lungs on day 7 post-infection. This included the lineage specific transcription factors for Th1 (*Tbx21*), Th2 (*Gata3*), and Th17 (*Rorc*). In addition, a range of transcription factors shown to be required for Tr1-like cell development and stability in a variety of models were also assessed. These included *Eomes*, *Prdm1*, *Cmaf*, *Batf*, *Irf4*, *Ahr*. Additionally, *Runx2* and *Id2*, two transcription factors which were recently identified to be among the most highly expressed by Tr1 cells [210], [285], but the function of which in the development and maintenance of the Tr1 phenotype is not understood, were also examined.

RT-qPCR analysis of FACS-sorted CD4$^+$ T cell subsets demonstrated that Tr1-like cells expressed very high levels of *Tbx21* compared to the other CD4$^+$ T cell populations **(Fig 3.24 A & B)**. As expected in a type 1 infection model such as IAV infection, the CD4$^+$ T cells did not express significant levels of the Th17 lineage defining transcription factor, *Rorc*. *Gata3* was most highly expressed by IL-10$^-$ Treg cells. Additionally, *Irf4* was uniformly expressed across all four populations. *Eomes* was only expressed at very low levels by Tr1-like cells, at least at the level of mRNA in this model. *Prdm1* was found to be most highly expressed by IL-10$^+$ Treg cells and *Cmaf* was highly expressed by the

Tr1-like cells as well as the IL-10$^+$ Treg cells. *Batf* was most highly expressed by the Tr1-like cells. The transcription factor *Ahr* was expressed at a low level by all of the CD4$^+$ T cell populations. Together, these observations indicate that Tr1-like cells in IAV infection express a range of transcription factors known to be required for initiation and maintenance of the Tr1-like lineage (*Eomes* [246], *Cmaf* [273],[285], *Batf* [237], [275], *Prdm1* [285],[265], *Irf4* [337], [218], and *AhR* [275], [337], [338]). With respect to *Runx2* and *Id2*, *Runx2* was trending to be most highly expressed by Tr1-like cells and IL-10$^+$ Treg cells, whereas, *Id2* mRNA was expressed at the highest level by Tr1-like cells **(Fig 3.24 A & B)**. These data show that in addition to transcription factors with known roles in Tr1 cell development, Tr1-like cells in the IAV-infected lung express both *Runx2* and *Id2*.

To confirm protein expression of a selection of the transcription factors highly expressed by Tr1-like cells in IAV infection, flow cytometry was used to detect expression of BLIMP-1, RUNX2, and ID2. At day 7 post-IAV infection WT mouse lungs were harvested for analysis of transcription factor protein expression with the pre-gating strategy shown in **(Fig 3.25 A)**. BLIMP-1 was most highly expressed by IL-10$^+$ Treg cells with some expression by Tr1-like cells **(Fig 3.25 B & E)**. RUNX2 was expressed by a select population of CD4$^+$ effector T cells as well as the majority of IL-10$^+$ Treg and Tr1-like cells **(Fig 3.25 C & F)**. ID2 was most highly expressed by IL-10$^+$ Treg and Tr1-like cells at the protein level **(Fig 3.25 D & G)**. The frequency of ID2-expressing CD4$^+$ T cells was significantly higher in the IL-10-producing CD4$^+$ T cell populations. However, as CD4$^+$ effector T cells are the most abundant in number there were significantly more ID2$^+$ cells in that population **(Fig 3.25 D & G)**. This analysis determined that although RUNX2 and ID2 were not singularly specific for Tr1-like cells, these transcription factors were highly expressed in that cell population at the level of both mRNA and protein. In contrast, BLIMP-1 was not highly expressed by Tr1-like cells at the level of protein and instead was found to be more specific for IL-10$^+$ Treg cells.

These data establish that Tr1-like cells from IAV-infected lungs express transcription factors classically associated with IL-10 production including *Prdm1*, *Cmaf*, *Batf*, *Irf4*, and *Ahr*. Additionally the RT-qPCR data confirmed that these are Th1-like cells as they express high levels of *Tbx21* and no *Rorc*. Therefore, the overall transcription factor landscape of Tr1-like cells from the IAV-infected lungs fits with published observations of this regulatory T cell subset [264], [237], [236], [195], [210], [285]. Additionally, it appears that Tr1-like cells from the IAV-infected lungs are more similar transcriptionally to Tr1 cells generated *in vitro* in the presence of IL-27 and TGF-β1 as BLIMP-1 is not highly expressed by these cells compared with those generated in the absence of TGF-β1 [218], [282], [279]. An exploration of novel factors involved in the transcriptional landscape of Tr1-like cells highlighted RUNX2 and ID2 as also being highly expressed by Tr1-like cells in IAV infection.

3.9 There are four distinct populations of Tr1-like cells present in the IAV-infected lungs based on expression of LAG-3 and CD49b.

The surface phenotype of Tr1-like cells is an aspect of Tr1-like biology which requires further investigation. To be useful in some clinical settings, a more reliable way to identify Tr1-like cells rather than using cytokine staining would be advantageous, as IL-10 is a notoriously difficult molecule to stain and requires fixation and permeabilisation of the cell [208]. A RT-qPCR screen was therefore undertaken to assess the level of mRNA for a range of surface molecules expressed by Tr1-like cells following IAV infection. This included adhesion molecules, co-inhibitory molecules and cytokine receptors (**Fig 3.26 A & B**). As co-expression of LAG-3 and CD49b had been claimed to define Tr1 cells previously [194], [210], [218], these markers were also included in the analysis. *Itga2* (CD49b) was not highly expressed at the level of mRNA by any of the $CD4^+$ T cell populations analysed, although Treg cells expressed the highest level of CD49b compared to the other $CD4^+$ T cell populations. In contrast *Cd223* (LAG-3) was highly expressed by both IL-10^+ Treg and Tr1-like cells.

In Tr1-like cells, highly expressed mRNAs included *Cd223* (LAG-3), *Cd152* (CTLA-4), *Cd279* (PD-1), *Tigit*, and *Icos* (**Fig 3.26 A & B**). Although highly expressed, *Cd223* expression was not unique to Tr1-like cells in IAV as it was also expressed by IL-10^+ Treg cells. *Cd152* was expressed by Tr1-like cells and also by IL-10^+ and IL-10^- Treg cells. *Cd279* was highly expressed by all four populations of $CD4^+$ T cells and in line with published findings [284], *Tigit* was tightly associated with T cells producing IL-10. The IL-10^+ Treg cells expressed the highest levels of *Tigit* but this molecule was also expressed by the other $CD4^+$ T cell populations. Other surface receptors investigated included the cytokine receptors *Il27ra* and *Il10r*α. These receptors were expressed by each of the four $CD4^+$ T cell populations. The alpha-chain of the receptor for the cytokine IL-27 (*Il27ra*) was expressed most highly by IL-10^+ $CD4^+$ T cell populations at the level of mRNA. In contrast, the *Il10r*α was most highly expressed by IL-10^+ Treg cells (**Fig 3.26 A & B**).

The two receptors most highly expressed by Tr1-like cells at the level of mRNA that were not more highly expressed by other populations were PD-1 and LAG-3. Another surface receptor TIM-3, previously associated with regulatory T cells [339], was assessed alongside PD-1 by flow cytometry, the gating strategy for which is shown in **Fig 3.27 A & B**. Tr1-like cells were predominately PD-1^+ and exhibited the highest proportion of TIM-3^+ PD-1^+ double-positive cells **(Fig 3.27 B-E)**. IL-10^+ Treg cells similarly exhibited a high level of PD-1 and TIM-3 expression **(Fig 3.27 B-E)**. This established that the majority of Tr1-like cells from the IAV-infected lungs expressed co-inhibitory molecules and therefore, conformed to this criterion for classification as a Tr1 cell [217].

Previous reports have stated that the majority of Tr1-like cells in a parasite infection of the lungs co-express CD49b and LAG-3 [194]. In the present study, a population of FOXP3$^-$ IL-10$^+$ CD4$^+$ T cells co-expressing CD49b and LAG-3 was observed in IAV-infected lungs. In contrast to that which has been published [194], [210], [218], there were also populations of Tr1-like cells expressing either LAG-3 or CD49b in isolation **(Fig 3.28 A)**. Compared to Treg cells, there were greater numbers of Tr1-like cells expressing either CD49b and LAG-3, or LAG-3 alone **(Fig 3.28 A-C)**. LAG-3 and CD49b expressing populations were only a small proportion of the effector CD4$^+$ T cells. Due to the high frequency of effector T cells amongst the total CD4$^+$ T cells in the lungs, there were comparable numbers of CD49b$^+$ LAG-3$^+$ (DP) and LAG-3$^+$ single-positive (LAG-3$^+$) effector T cells to the Tr1-like cells **(Fig 3.28 A-C)**. Based on the literature, this result was unexpected. The reason for the differences in expression of LAG-3 and CD49b was not apparent and as such, this became the subject of further investigation into the function and phenotype of Tr1-like cells that are generated during IAV infection, the results of which are described in the following chapter.

3.10 Chapter 3 Conclusion

Taken together, the data presented in this chapter indicate that Tr1-like cells are generated in response to IAV infection and represent an important source of T cell-derived IL-10 in the IAV-infected lungs. The peak of Tr1-like cell accumulation in the IAV-infected lungs corresponded to a time point after significant viral clearance and the beginning of the resolution of the immune response. IAV-infected *Il27ra*$^{-/-}$ mice exhibited a clear reduction in Tr1-like cell generation in the lungs and BALF without any discernible effect on other CD4$^+$ T cell sub-populations. Following IAV infection, *Il27ra*$^{-/-}$ mice exhibited increased weight loss, with a delayed recovery from weight loss. The small number of Tr1-like cells present in the lungs of IAV-infected *Il27ra*$^{-/-}$ mice displayed dysregualted cytokine production with decreased production of IFNγ and increased IL-17A. Adoptive transfer of Tr1 cells into *Il27ra*$^{-/-}$ mice was able to restore recovery from weight loss similarly to control mice (*Il27ra*$^{+/-}$). This established a role for Tr1-like cells in IAV infection during the resolution of the immune response. Following this finding, the Tr1-like cells from the lungs were extensively characterised which determined that Tr1-like cells expressed IFNγ, low levels of TNFα, and exhibit a phenotype consistent with a moderate capacity for cytotoxicity. Additionally, Tr1-like cells from the IAV-infected lungs expressed a range of transcription factors known to be involved in the induction and maintenance of IL-10 production as well as RUNX2 and ID2, transcription factors not previously directly implicated in Tr1 cell biology. Tr1-like cells were also found to be enriched in expression of co-inhibitory molecules, including PD-1 and TIM-3 confirming specialisation as a

regulatory T cell population. Finally, four populations of Tr1-like cells were identified in the IAV-infected lungs based on differential LAG-3 and CD49b expression. This Tr1-like cell phenotype is unique and may represent distinct populations or discrete stages of Tr1-like differentiation and function. An investigation exploring this will be presented in the following chapter.

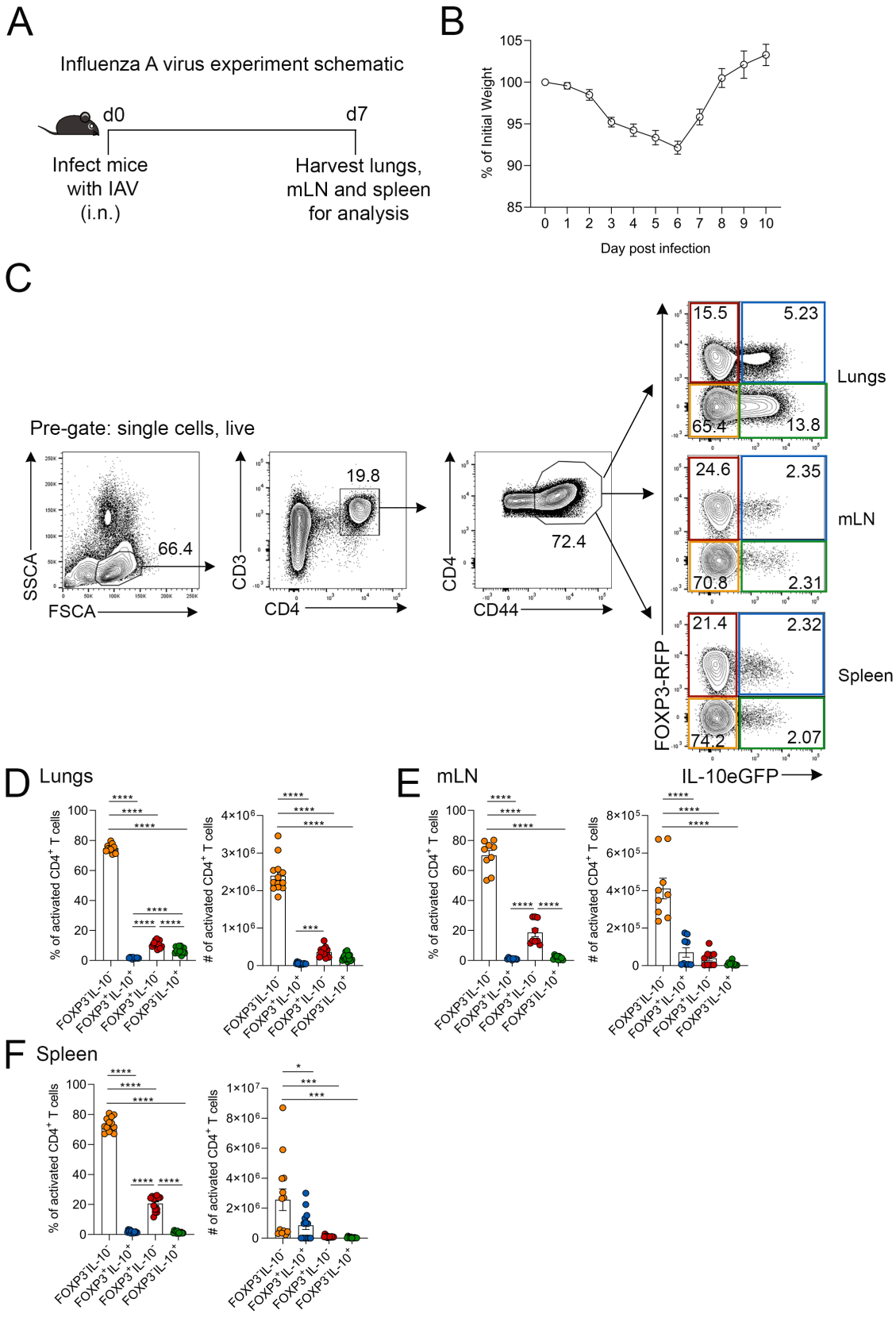
A
Influenza A virus experiment schematic
d0
d7
Infect mice with IAV (i.n.)
Harvest lungs, mLN and spleen for analysis
B
% of Initial Weight
Day post infection
C
Pre-gate: single cells, live
SSCA
FSCA
66.4
CD3
CD4
19.8
CD4
CD44
72.4
FOXP3-RFP
IL-10eGFP
15.5
5.23
65.4
13.8
Lungs
24.6
2.35
70.8
2.31
mLN
21.4
2.32
74.2
2.07
Spleen
D Lungs
% of activated CD4+ T cells
# of activated CD4+ T cells
E mLN
F Spleen
FOXP3-IL-10-
FOXP3+IL-10+
FOXP3+IL-10-
FOXP3-IL-10+

Figure 3.1: Quantitation of Tr1-like cells in IAV infection.
Dual-reporter mice were infected with X-31 IAV-i.n as described (refer to **2.5.1**). On day 7 post-IAV infection mice were humanely killed and lungs, mLN, and spleens were harvested for analysis by flow cytometry. (A) Experimental schematic for IAV infection model. (B) The average percentage of initial weight each day post-IAV infection. (C) Representative gating strategy for identification of activated $CD4^+$ T cell populations expressing FOXP3 and IL-10 in the lungs, mLN, and spleen. Frequency and number of activated $CD4^+$ T cell populations expressing FOXP3 and/or IL-10 from the (D) lungs, (E) mLN, and (F) spleen. (B) Each symbol represents the mean +/- SEM. (D)-(F) Each symbol represents a different biological replicate, shown as mean +/- SEM, n=13 (lungs), 9 (mLN), and 13 (spleens) from 2 independent experiments. Statistical analysis using one-way ANOVA with Bonferroni's post-test (where $^* = p \leq 0.05, ^{***} = p \leq 0.001$, and $^{****} = p \leq 0.0001$).

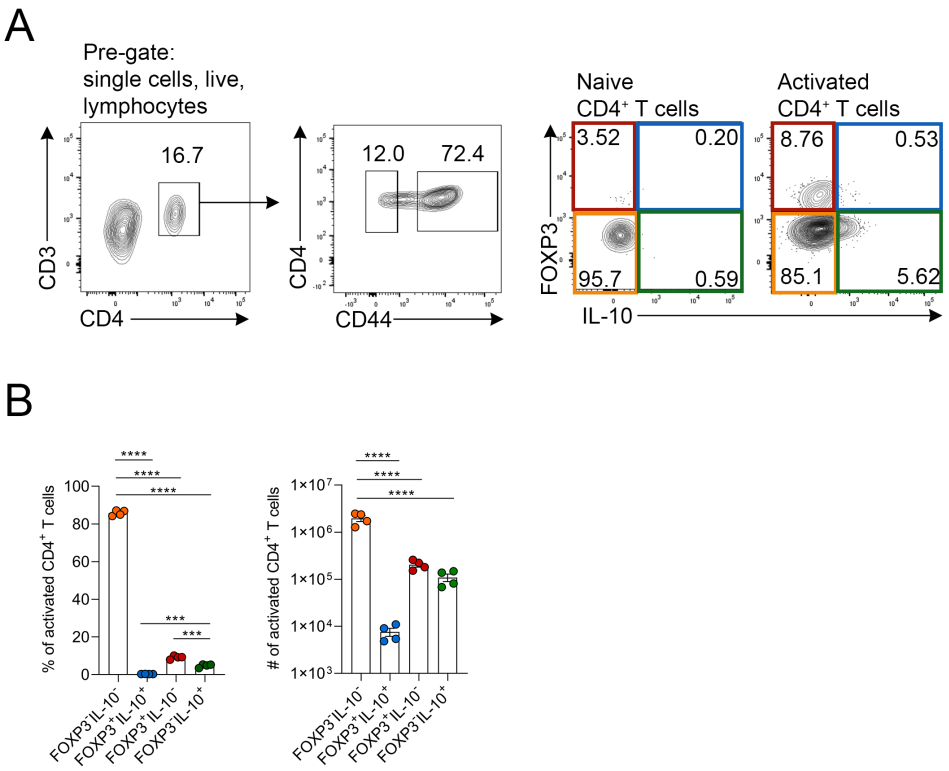

Figure 3.2: Detection of IL-10-secreting cells in IAV-infected lungs.
C57BL/6 mice were infected with X-31 IAV-i.n as described (refer to **2.5.1**). On day 7 post-infection mice were humanely killed and lungs harvested for intranuclear/intracellular staining of FOXP3 and IL-10. (A) Representative, concatenated flow cytometry of activated $CD4^+$ T cells on d7 post-IAV infection. (B) Frequency and number of $CD4^+$ T cell populations based on expression of FOXP3 and IL-10. Each symbol represents a different biological replicate, shown as mean +/- SEM, n=4 total from 2 independent experiments. Statistical analysis using one-way ANOVA with Bonferroni's post-test (where $^{***} = p \leq 0.001$ and $^{****} = p \leq 0.0001$).

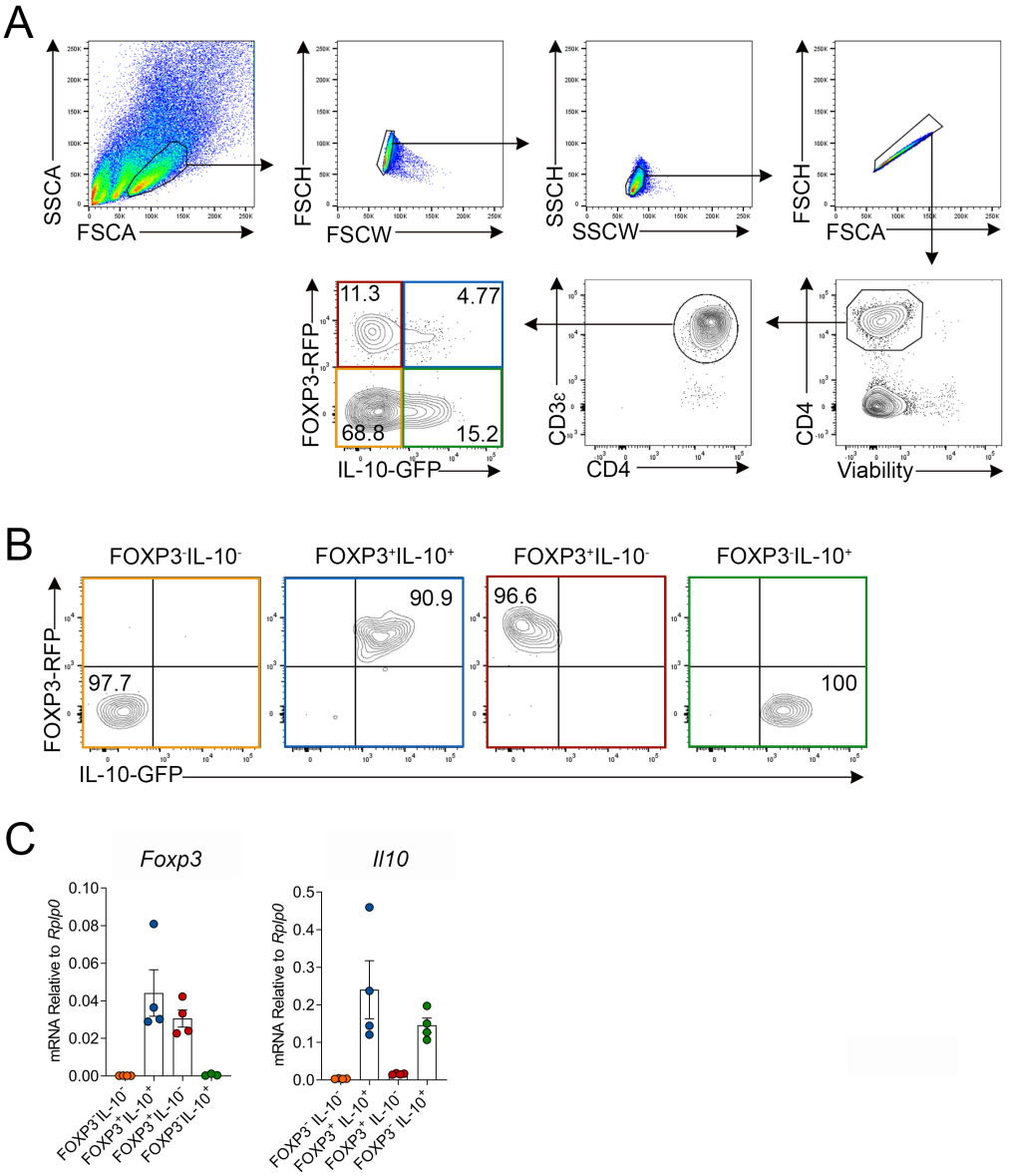

Figure 3.3: Validation of FOXP3^{RFP}IL-10^{eGFP} dual-reporter mice.
Dual-reporter mice were infected with X-31 IAV-i.n as described (refer to **2.5.1**). On day 7 post-infection mice were humanely killed and lungs were harvested for FACS-sorting. (A) Gating strategy for FACS-sorting different populations of CD4$^+$ T cells based on expression of FOXP3 and IL-10. (B) Post- sort purity of CD4$^+$ T cell populations. (C) RT-qPCR of *Foxp3* and *Il10* expression by FACS-sorted populations relative to *Rplp0*. Each symbol represents a different biological replicate, shown as mean +/- SEM, n=4 biological replicates total from 2 independent experiments.

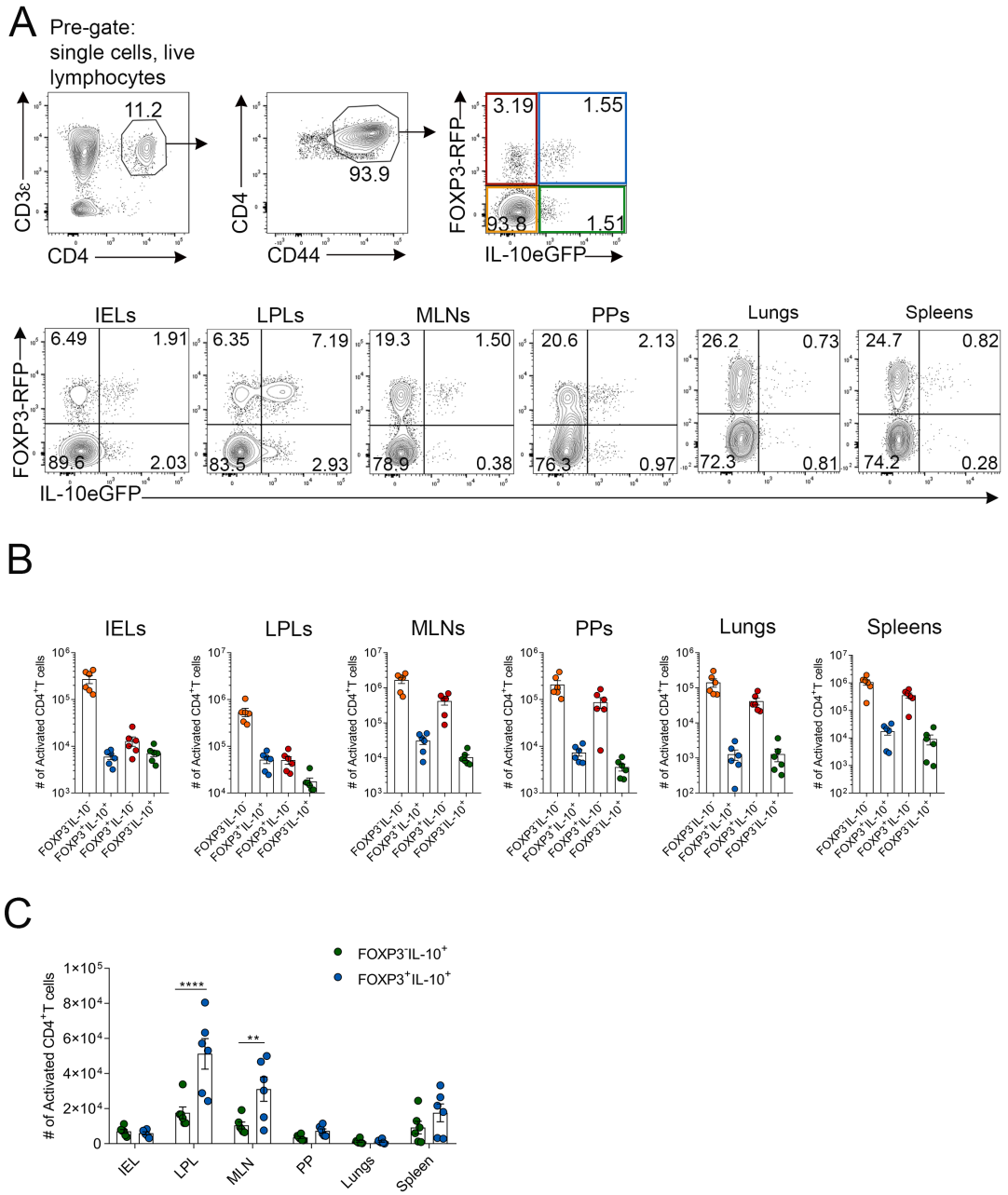

Figure 3.4: Quantitation of Tr1-like cells at homeostasis.
IELs, LPLs, MLNs, PP, lungs, and spleens from dual-reporter mice were analysed for the presence of $CD4^+$ T cell populations (based on expression of FOXP3 and IL-10) by flow cytometry. (A) Representative, concatenated flow cytometry of activated $CD4^+$ T cell populations based on FOXP3 and IL-10 expression. (B) Number of $CD4^+$ T cells expressing FOXP3 and IL-10. (C) Comparison of the number of $FOXP3^+$ and $FOXP3^-$ $IL\text{-}10^+$ $CD4^+$ T cells. Each symbol represents a different biological replicate, shown as mean +/- SEM, n=6 biological replicates total from 2 independent experiments. Statistical analysis using one-way ANOVA with Bonferroni's post-test (where $** = p \leq 0.01$ and $**** = p \leq 0.0001$).

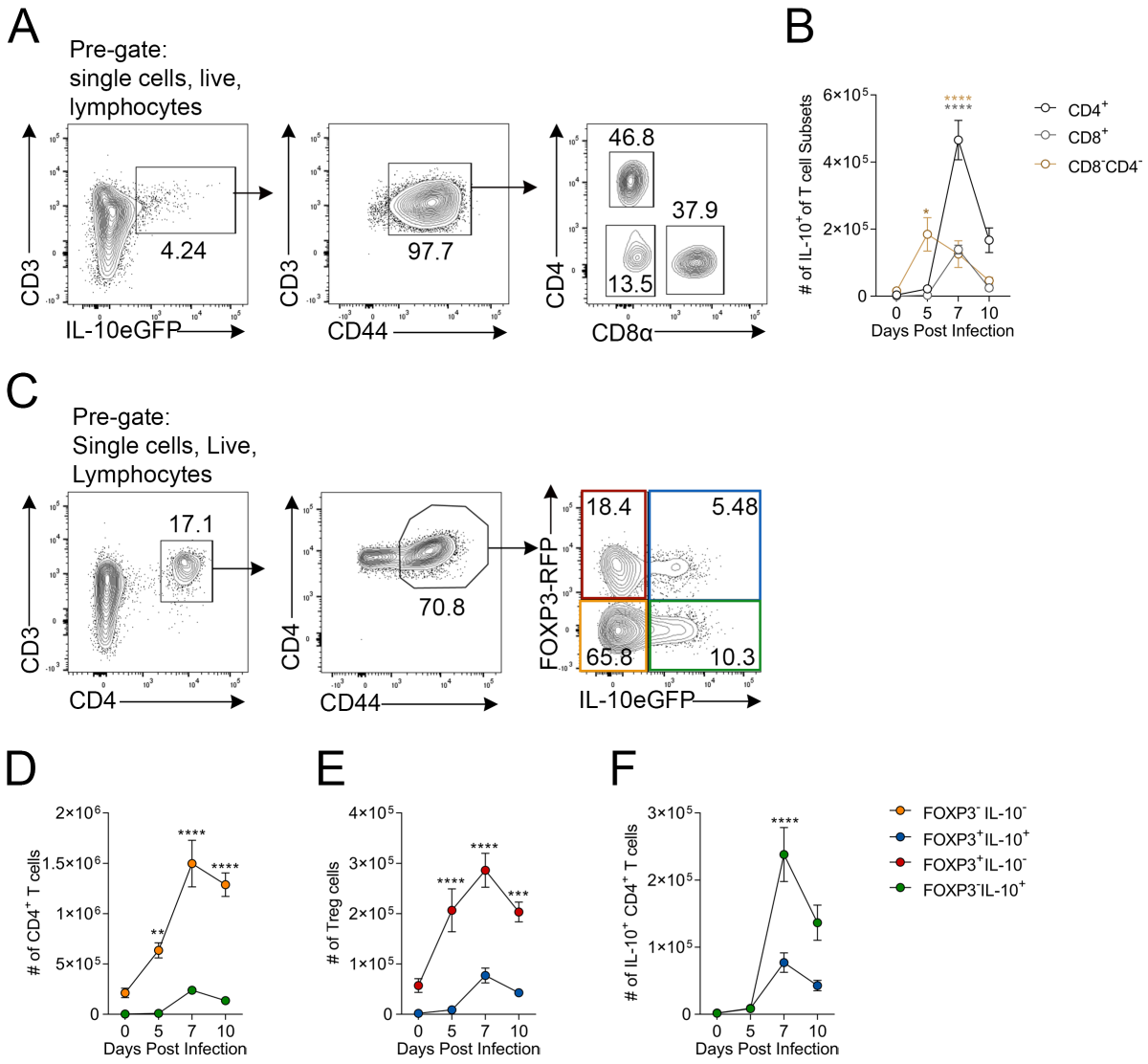

Figure 3.5: Quantitation of cellular sources of T cell-derived IL-10 in the lungs during IAV infection.

Female dual-reporter mice were infected with X-31 IAV-i.n as described (refer to **2.5.1**). Activated $CD4^+$ T cell populations from the lungs were analysed at days 0 (naive), 5, 7, and 10 post-infection. (A) Representative gating strategy for identification of $IL\text{-}10^+$ $CD3^+$ T cell populations from the IAV-infected lungs. (B) Quantitation of the number of $CD8^+$, $CD4^+$, and $CD8^-$ $CD4^-$, $IL\text{-}10^+$ $CD3^+$ T cells. (C) Representative gating strategy for populations of $CD4^+$ T cells based on expression of FOXP3 and IL-10. (D) The number of $CD4^+$ effector T cells and Tr1-like cells over the course of infection. (E) The number of $IL\text{-}10^+$ and $IL\text{-}10^-$ Treg cells over the course of infection. (F) The number of Tr1-like cells and $IL\text{-}10^+$ Treg cells over the course of infection. The symbols represent the mean +/- SEM, n=3-16 biological replicates per time point from 2 independent experiments. Statistical analysis using one-way ANOVA with Bonferroni's post-test (where $^* = p \leq 0.05, ^{**} = p \leq 0.01, ^{***} = p \leq 0.001$, and $^{****} = p \leq 0.0001$).

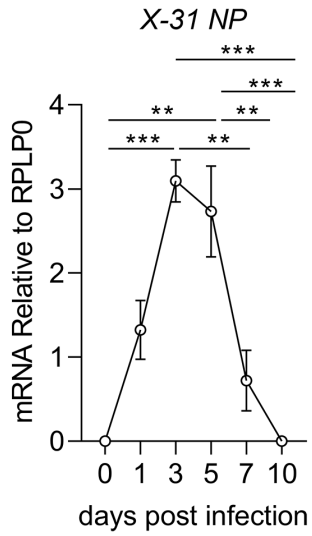

Figure 3.6: Kinetics of viral RNA in whole lungs during IAV infection. C57BL/6 mice were infected with X-31 IAV-i.n as described (refer to **2.5.1**). On days 0 (naive), 1, 3, 5, 7 and 10 post-infection lungs were taken, RNA extracted, and viral load was assessed by RT-qPCR. Figure shows the level of viral RNA in the infected lungs over the course of infection relative to *Rplp0*. The symbols represent the mean +/- SEM, n=3-5 biological replicates total per time point. Statistical analysis using one-way ANOVA with Bonferroni's post-test (where $^{**} = p \leq 0.01$ and $^{***} = p \leq 0.001$).

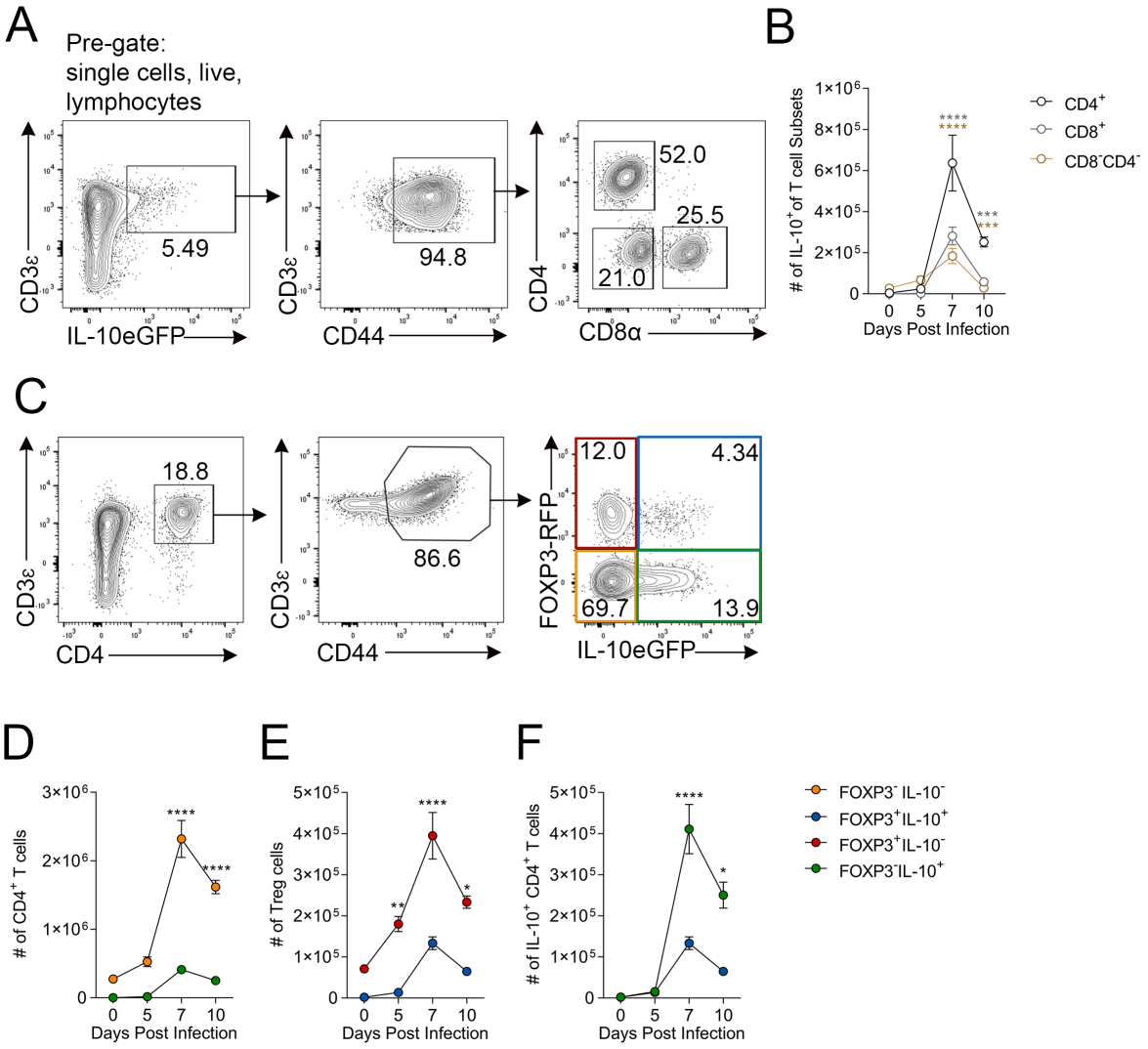

Figure 3.7: Quantitation of cellular sources of T cell-derived IL-10 in the lungs during IAV infection in male mice.

Male dual-reporter mice were infected with X-31 IAV-i.n as described (refer to **2.5.1**). Activated $CD4^+$ T cell populations from the lungs were analysed at days 0 (naive), 5, 7, and 10 post-infection.(A) Representative gating strategy for identification of IL-10^+ $CD3^+$ T cell populations from the IAV-infected lungs. (B) Quantitation of the number of $CD8^+$, $CD4^+$, and $CD8^-$ $CD4^-$, IL-10^+ $CD3^+$ T cells. (C) Representative gating strategy for populations of $CD4^+$ T cells based on expression of FOXP3 and IL-10. (D) The number of $CD4^+$ effector T cells and Tr1-like cells over the course of infection. (E) The number of IL-10^+ and IL-10^- Treg cells over the course of infection. (F) The number of Tr1-like cells and IL-10^+ Treg cells over the course of infection. The symbols represent the mean +/- SEM, n=3-7 biological replicates per time point from 2 independent experiments. Statistical analysis using one-way ANOVA with Bonferroni's post-test (where $^* = p \leq 0.05$, $^{**} = p \leq 0.01$, and $^{****} = p \leq 0.0001$).

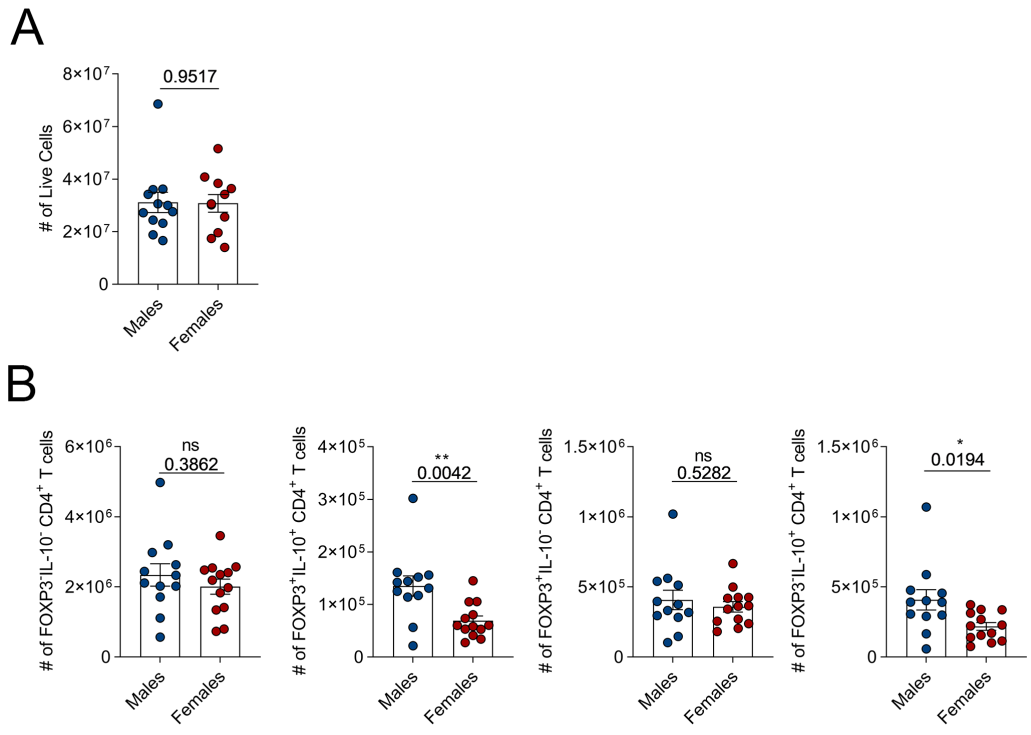

Figure 3.8: Sex-specific differences in the activated CD4$^+$ T cell compartment in the lungs post-IAV infection.

Female and male were infected with X-31 IAV-i.n as described (refer to **2.5.1**) and T cell populations were analysed over the course of infection. On day 7 post-infection the CD4$^+$ T cell populations from the lungs were analysed by flow cytometry. (A) The total number of live cells in the male and female lungs. (B) The number of FOXP3$^-$IL-10$^-$, FOXP3$^+$IL-10$^+$, FOXP3$^+$IL-10$^-$ and FOXP3$^-$IL-10$^+$ CD4$^+$ T cells on day 7 post-infection. Each symbol represents a different biological replicate, shown as mean +/- SEM, n=12 biological replicates total from 2 independent experiments. Statistical analysis completed using unpaired Student's t-tests (where $^* = p \leq 0.05$ and $^{**} = p \leq 0.01$).

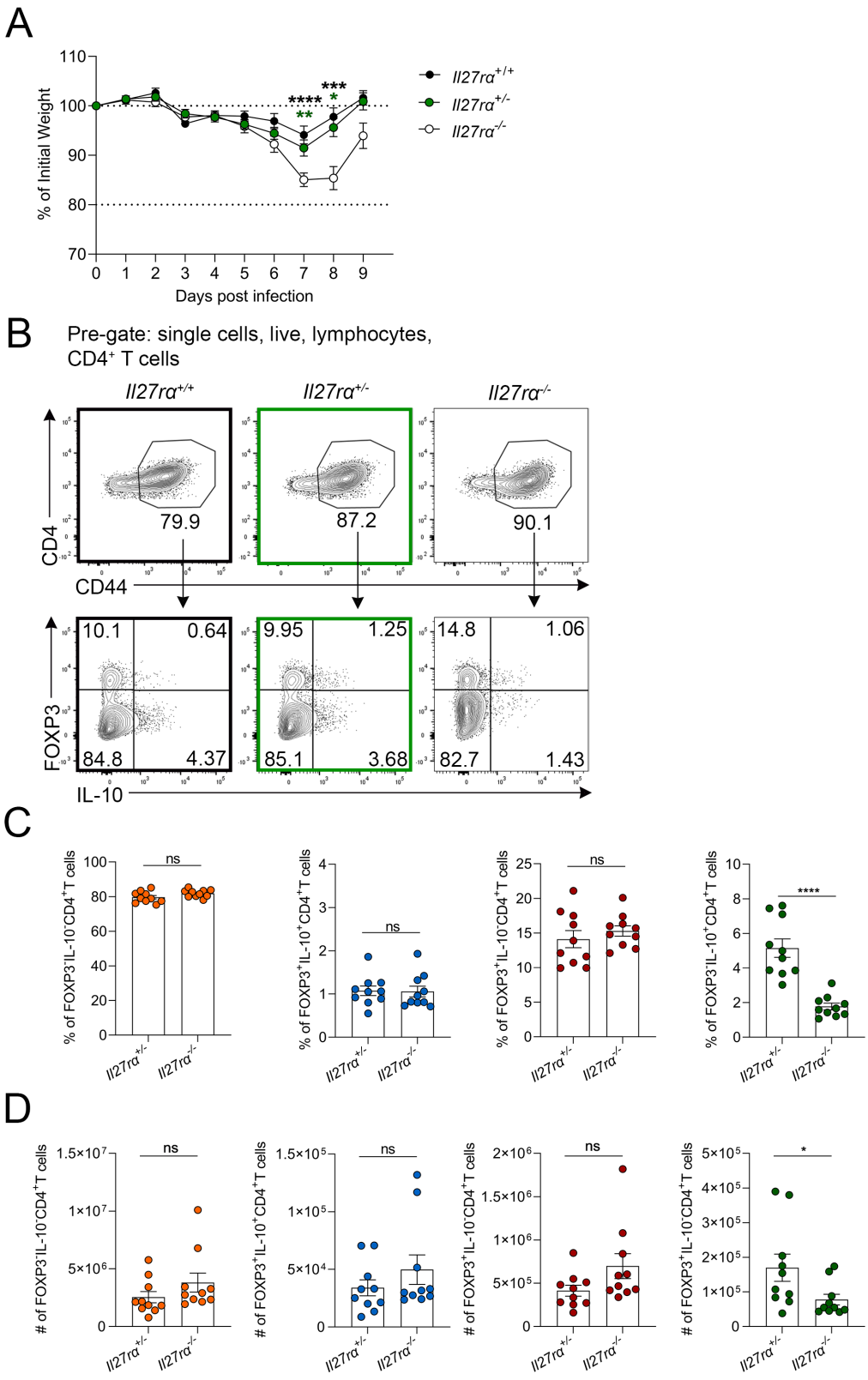
A
% of Initial Weight
Days post infection
Il27rα+/+
Il27rα+/-
Il27rα-/-
B
Pre-gate: single cells, live, lymphocytes, CD4+ T cells
CD4
CD44
FOXP3
IL-10
79.9
87.2
90.1
10.1
0.64
84.8
4.37
9.95
1.25
85.1
3.68
14.8
1.06
82.7
1.43
C
% of FOXP3-IL-10-CD4+T cells
% of FOXP3+IL-10+CD4+T cells
ns
****
D
# of FOXP3-IL-10-CD4+T cells
# of FOXP3+IL-10+CD4+T cells
*

Figure 3.9: The phenotype of activated CD4$^+$ T cells from IAV-infected *Il27ra*$^{-/-}$ lungs.

Il27ra$^{+/+}$, *Il27ra*$^{+/-}$ and *Il27ra*$^{-/-}$ mice were infected with X-31-OVA$_{323\text{-}339}$ IAV-i.n as described (refer to **2.5.1**) and lungs were analysed on day 7 post-infection. (A) The percentage of initial weight over the course of IAV infection. (B) Representative flow cytometry of CD4$^+$ T cells in the lungs at day 7 post-infection. The percentage (C), and number (D) of CD4$^+$ T cell populations in the lungs on day 7 post-infection. (A) The symbols represent the mean +/- SEM. (C-D) Each symbol represents a different biological replicate, shown as mean +/- SEM, n=13 (*Il27ra*$^{+/+}$), 10 (*Il27ra*$^{+/-}$), 10 (*IL-27ra*$^{-/-}$) biological replicates total from 3 independent experiments. Statistical analysis using (A) 2-way ANOVA, (C-D) unpaired Student's T-tests (where $^* = p \leq 0.05, ^{**} = p \leq 0.01$, and $^{***} = p \leq 0.001 ^{****} = p \leq 0.0001$).

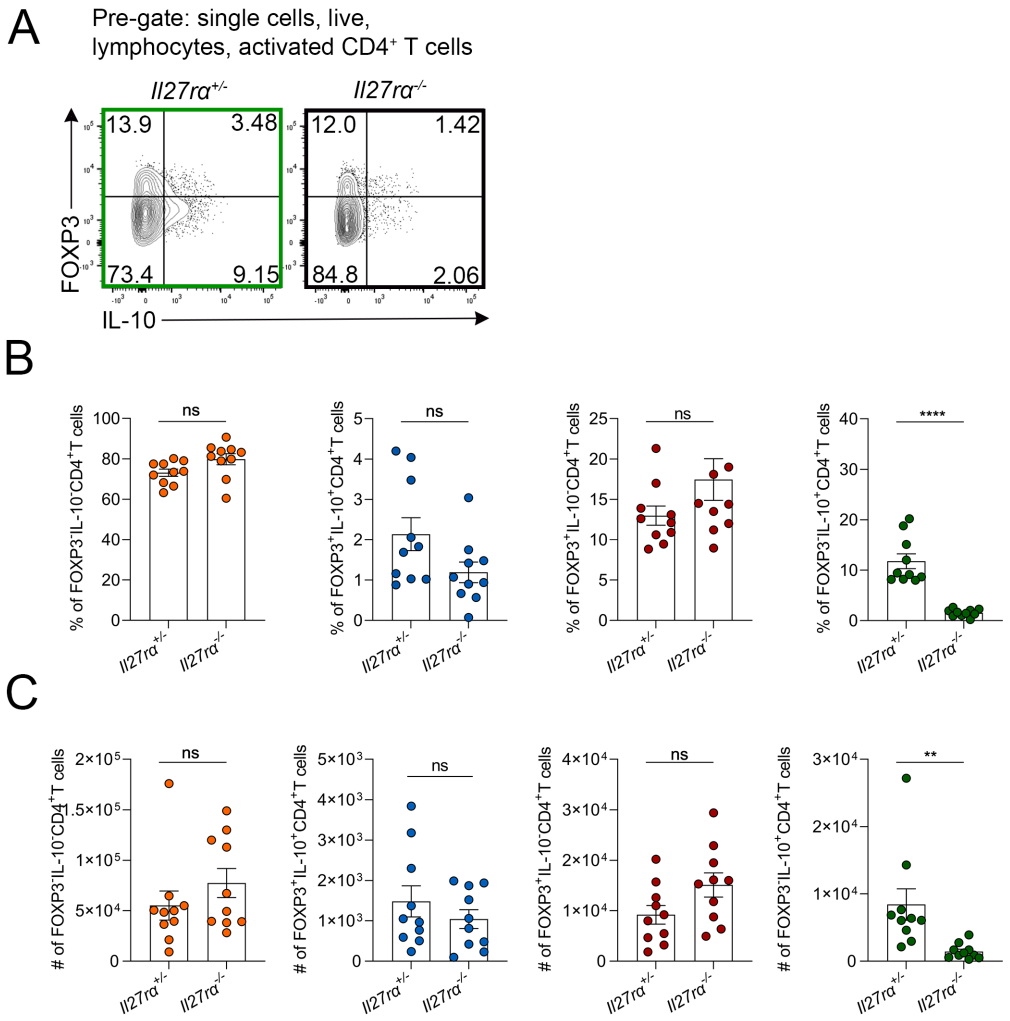

Figure 3.10: The phenotype of activated CD4$^+$ T cells in the BALF of IAV-infected *Il27ra*$^{-/-}$ mice.

Il27ra$^{+/-}$ and *Il27ra*$^{-/-}$ mice were infected with X-31-OVA$_{323\text{-}339}$ IAV-i.n as described (refer to **2.5.1**) and cells washed from the airways were analysed on day 7 post-infection. (A) Concatenated representative flow cytometry depicting activated CD4$^+$ T cell populations in the airways. The percentage (B), and number (C) of activated CD4$^+$ T cell populations in the IAV-infected airways on day 7 post-infection. Each symbol represents a different biological replicate, shown as mean +/- SEM, n=10 (*Il27ra*$^{+/-}$), 10 (*Il27ra*$^{-/-}$) biological replicates total from 3 independent experiments. Statistical analysis completed with unpaired Student's T-tests (where $^{**} = p \leq 0.01$, and $^{****} = p \leq 0.0001$).

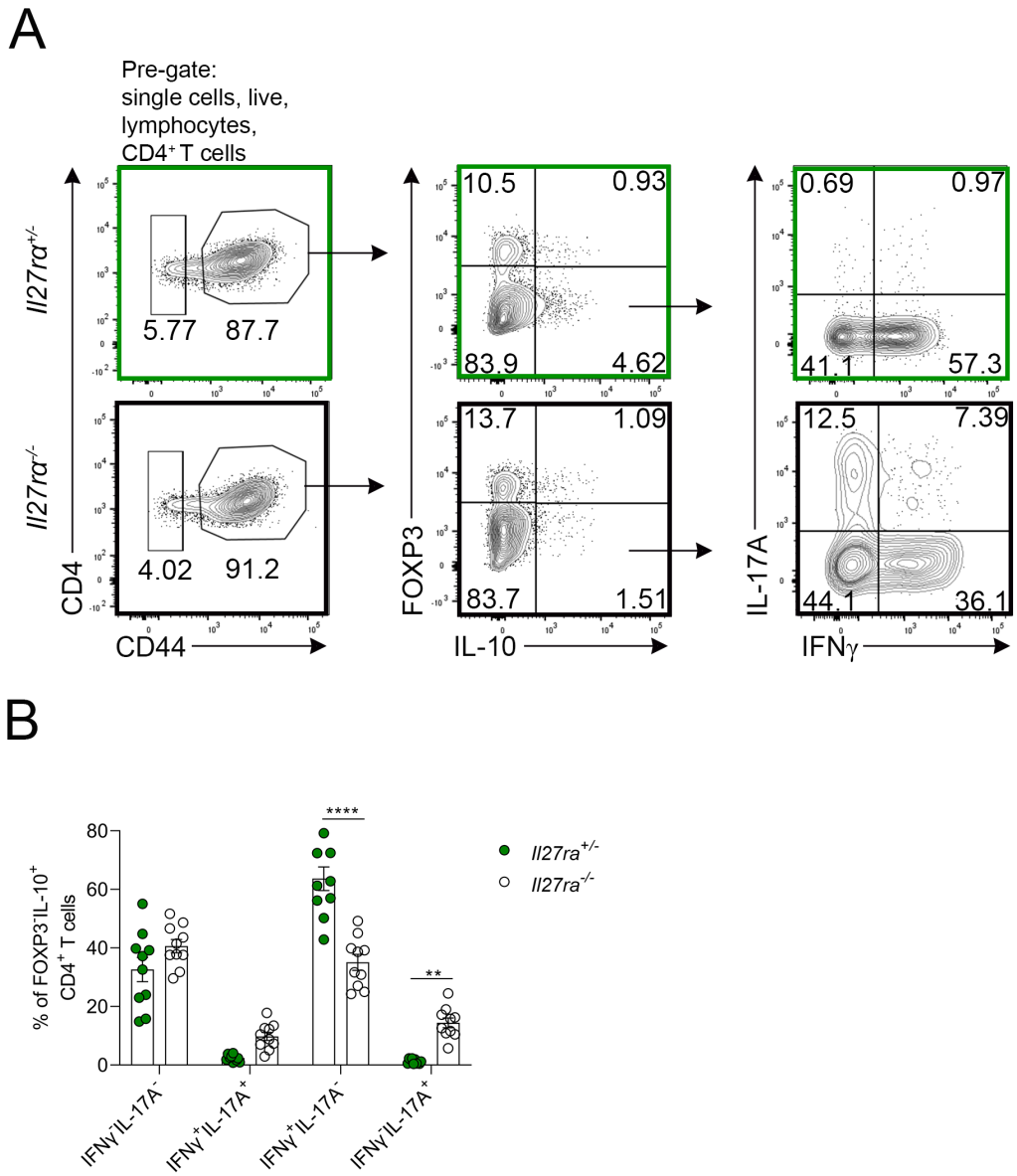

Figure 3.11: The cytokine production of Tr1-like cells in the lungs of IAV-infected *Il27ra*$^{-/-}$ mice.

Il27ra$^{+/-}$ and *Il27rα*$^{-/-}$ mice were infected with X-31-OVA$_{323\text{-}339}$ IAV-i.n as described (refer to **2.5.1**) and lungs were harvested for analysis on day 7 post-infection. (A) Representative flow cytometry from one of three similar experiments showing the gating strategy used for analysis of IFNγ and IL-17A production by Tr1-like cells from the IAV-infected lungs. (B) The percentage of Tr1-like cells that are IFNγ^- IL-17A$^-$, IFNγ^+IL-17A$^+$, IFNγ^+IL-17A$^-$, and IFNγ^-IL-17A$^+$. Each symbol represents a different biological replicate, shown as mean +/- SEM, n=10 (*Il27ra*$^{+/-}$), 10 (*Il27ra*$^{-/-}$) biological replicates total from 3 independent experiments. Statistical analysis using one-way ANOVA with Bonferroni's post-test (where $** = p \leq 0.01$, and $**** = p \leq 0.0001$).

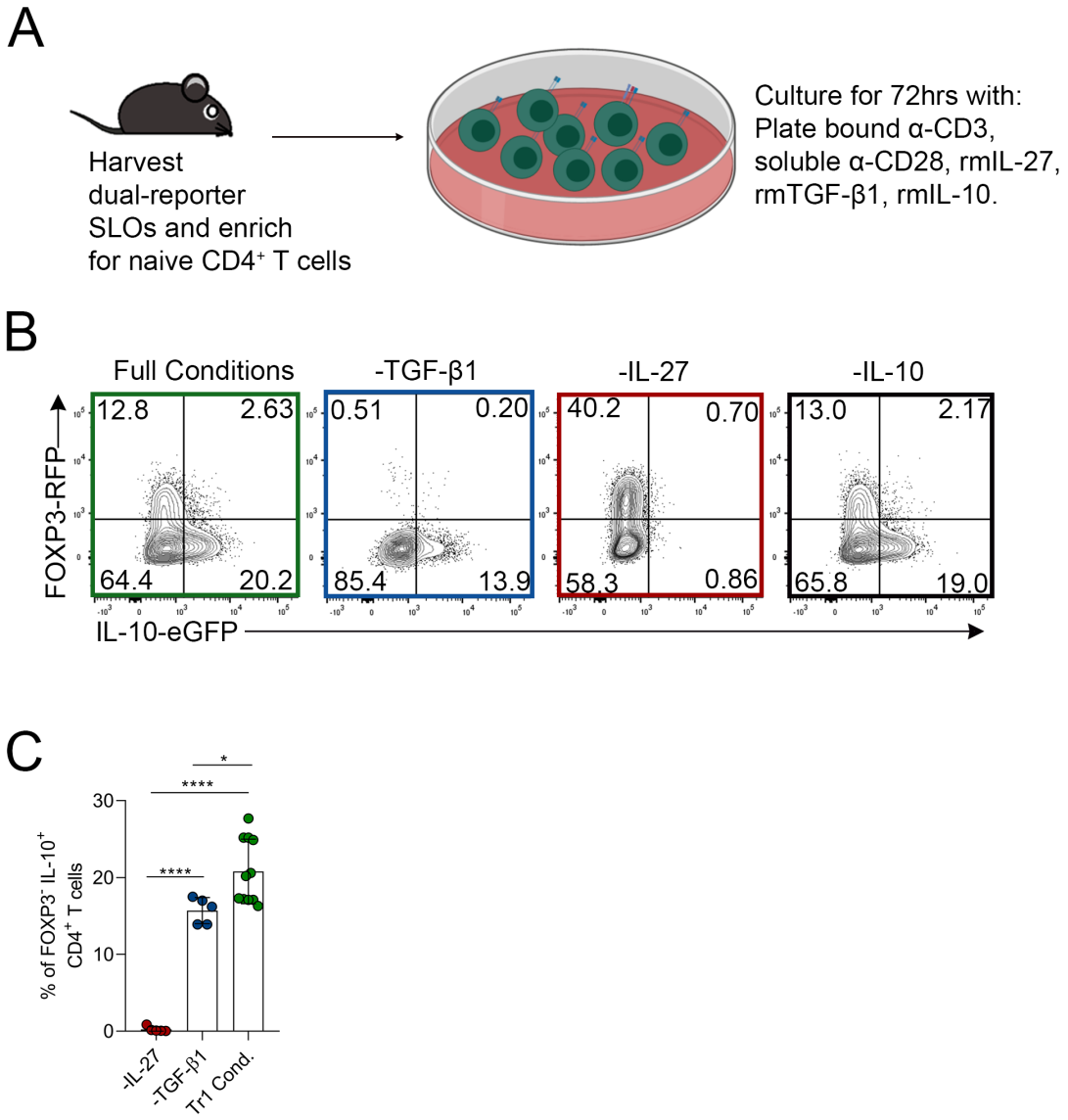

Figure 3.12: *In vitro*-generation of Tr1-like cells from naive CD4$^+$ T cells.

Optimisation of a protocol to generate Tr1-like cells from naive CD4$^+$ T cells. (A) Schematic of culture protocol using dual-reporter mice. (B) Representative flow cytometry showing the effect of culture conditions on FOXP3 and IL-10 protein expression. Each sample was cultured under full cytokine conditions (rmIL-27, rmTGFβ1, and rmIL-10) or under full conditions minus a single cytokine. (C) The percentage of FOXP3$^-$ IL-10$^+$ CD4$^+$ T cells when cultured under each condition. Each symbol represents a different technical replicate, the mean is shown +/- SD, n=11 (Tr1 conditions), 5 (-IL-27), 5 (-TGF-β) technical replicates total, from 4 independent experiments. Statistical analysis completed using one-way ANOVA with Bonferroni's post-test (where $^* = p \leq 0.05$ and $^{****} = p \leq 0.0001$).

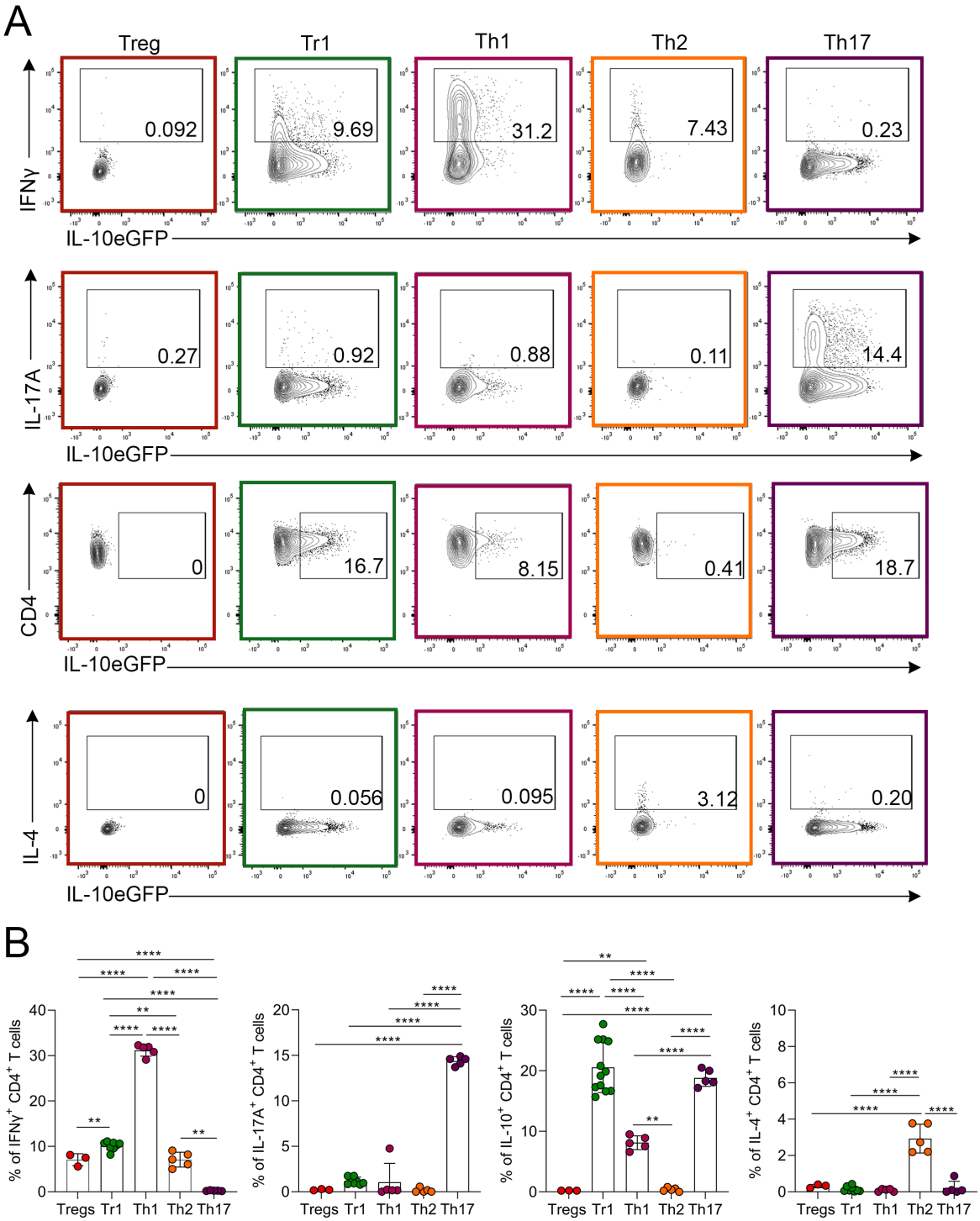
A
Treg
Tr1
Th1
Th2
Th17
IFNγ
IL-10eGFP
0.092
9.69
31.2
7.43
0.23
IL-17A
0.27
0.92
0.88
0.11
14.4
CD4
0
16.7
8.15
0.41
18.7
IL-4
0
0.056
0.095
3.12
0.20
B
% of IFNγ+ CD4+ T cells
% of IL-17A+ CD4+ T cells
% of IL-10+ CD4+ T cells
% of IL-4+ CD4+ T cells
Tregs Tr1 Th1 Th2 Th17

Figure 3.13: Cytokine profile of *in vitro*-generated Tr1-like cells compared to other Th cell lineages.

In vitro Th subset polarising conditions were used to generate Tr1-like, Th1, Th2, Th17, and Treg cells. (A) Concatenated, representative flow cytometry of Th subset-specific cytokine expression by Tr1-like, Th1, Th2, Th17, and iTreg cells. (B) Frequency of IFNγ, IL-17A, IL-10, and IL-4 expressed by each of the *in vitro*-generated Th cell populations. Each symbol represents a different technical replicate, shown as mean +/- SD, n=4 (iTreg), 8 (Tr1-like), 5 (Th1), 5 (Th2), 5 (Th17) technical replicates from 2 independent experiments. Statistical analysis using one-way ANOVA with Bonferroni's post-test (where $^{*} = p \leq 0.05, ^{**} = p \leq 0.01$, and $^{****} = p \leq 0.0001$).

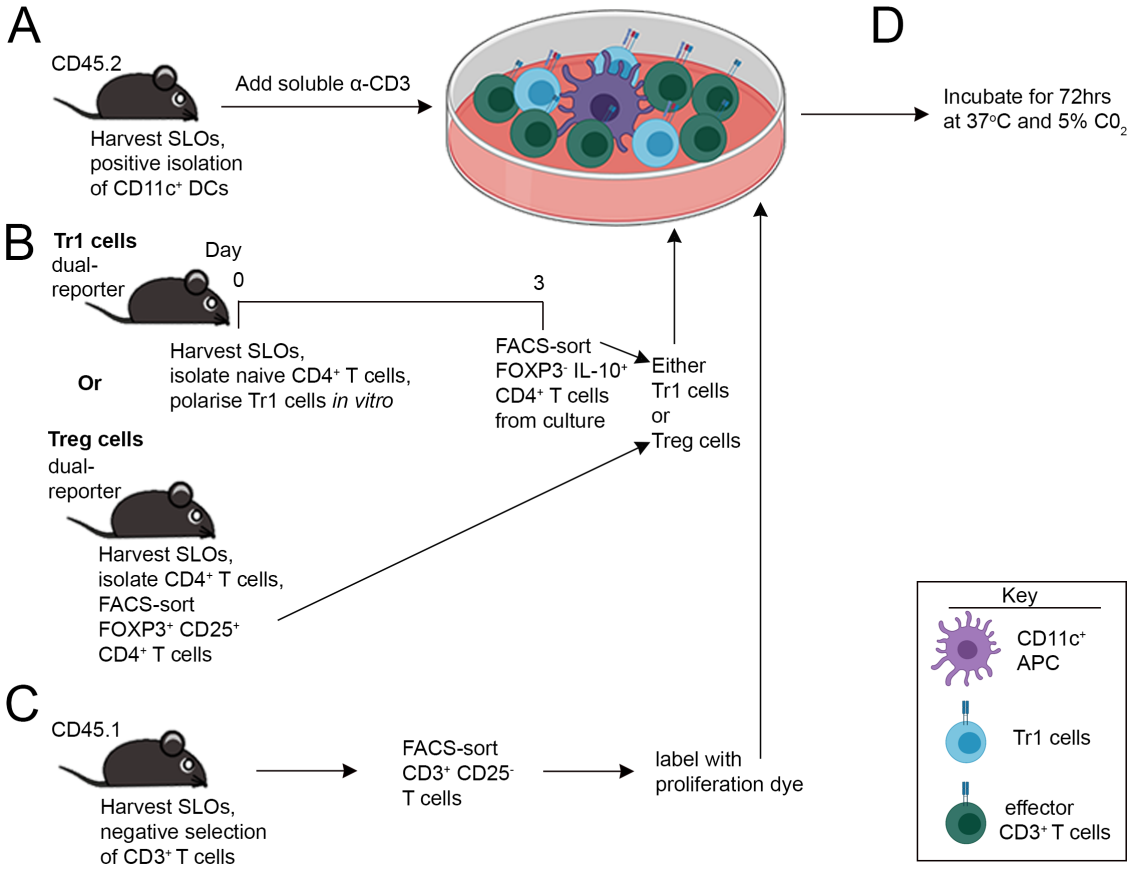

Figure 3.14: Suppression Assay Experimental Schematic.
(A) For suppression assays SLOs were harvested from naive CD45.2 mice, CD11c$^+$ DCs were enriched by positive isolation and 5x10^3 were added to each well of the suppression assay. Next, 1μg/mL α-CD3 (purified 2C11) was added to the APCs. (B) Three days prior to collection of CD11c$^+$ DCs and naive CD3$^+$ T cells, dual-reporter mice SLOs were harvested and naive CD4$^+$ T cells were enriched using negative selection prior to polarisation under Tr1 conditions for 3 days. Either FACS-sorted *in vitro*-derived Tr1-like cells or FOXP3$^+$ CD25$^+$ Treg cells were placed into culture with labelled effector T cells. (C) SLOs were also harvested from CD45.1 mice and CD3$^+$ T cells were enriched by negative selection. CD3$^+$ CD25$^-$ T cells were then sorted by FACS and labelled with Efluor670 proliferation dye. These cells were then added into suppression assays (2x10^4/well). (D) Suppression assays were incubated for approximately 72 hours before analysis using flow cytometry to detect effector T cell proliferation.

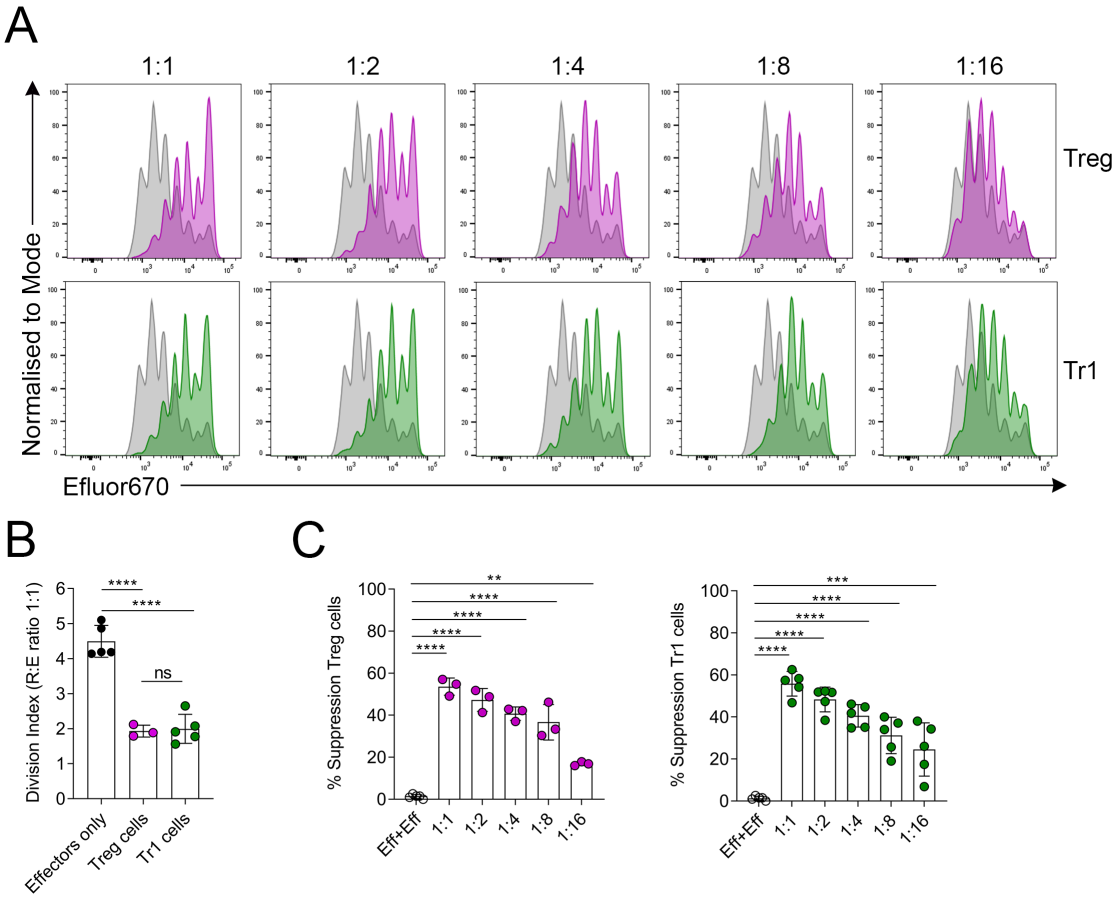

Figure 3.15: Suppression of effector T cell division by *in vitro*-derived Tr1-like cells and Treg cells.

In vitro derived Tr1 cells from dual-reporter mice were co-cultured with Efluor670-labelled effector $CD3^+$ T cells in the presence of $CD11c^+$ APCs and soluble α-CD3. (A) Representative flow cytometry showing the proliferation of Efluor670-labelled $CD3^+$, $CD25^-$ effector T cells alone (grey histogram), or in the presence of *in vitro*-derived Treg cells (purple histogram), or Tr1-like cells (green histogram) at ratios of 1:1, 1:2, 1:4, 1:8 and 1:16 (ratio=regulatory T cells:effector T cells). Where 1:1 ratio= $2x10^4$ regulatory T cells:$2x10^4$ effector T cells. (B) DI of effector T cells cultured alone and with either *in vitro*-derived Treg cells or Tr1-like cells at a 1:1 ratio. (C) The percentage suppression of effector T cell division when cultured with effector T cells (Eff+Eff) or with either Treg cells or Tr1-like cells at each of the ratios. Each symbol represents a different technical replicate, shown as mean +/- SD, n=3-5 technical replicates total from 3 independent experiments. Statistical analysis using (B), (C) one-way ANOVA with Bonferroni's post-test (where $** = p \leq 0.01, *** = p \leq 0.001$, and $**** = p \leq 0.0001$).

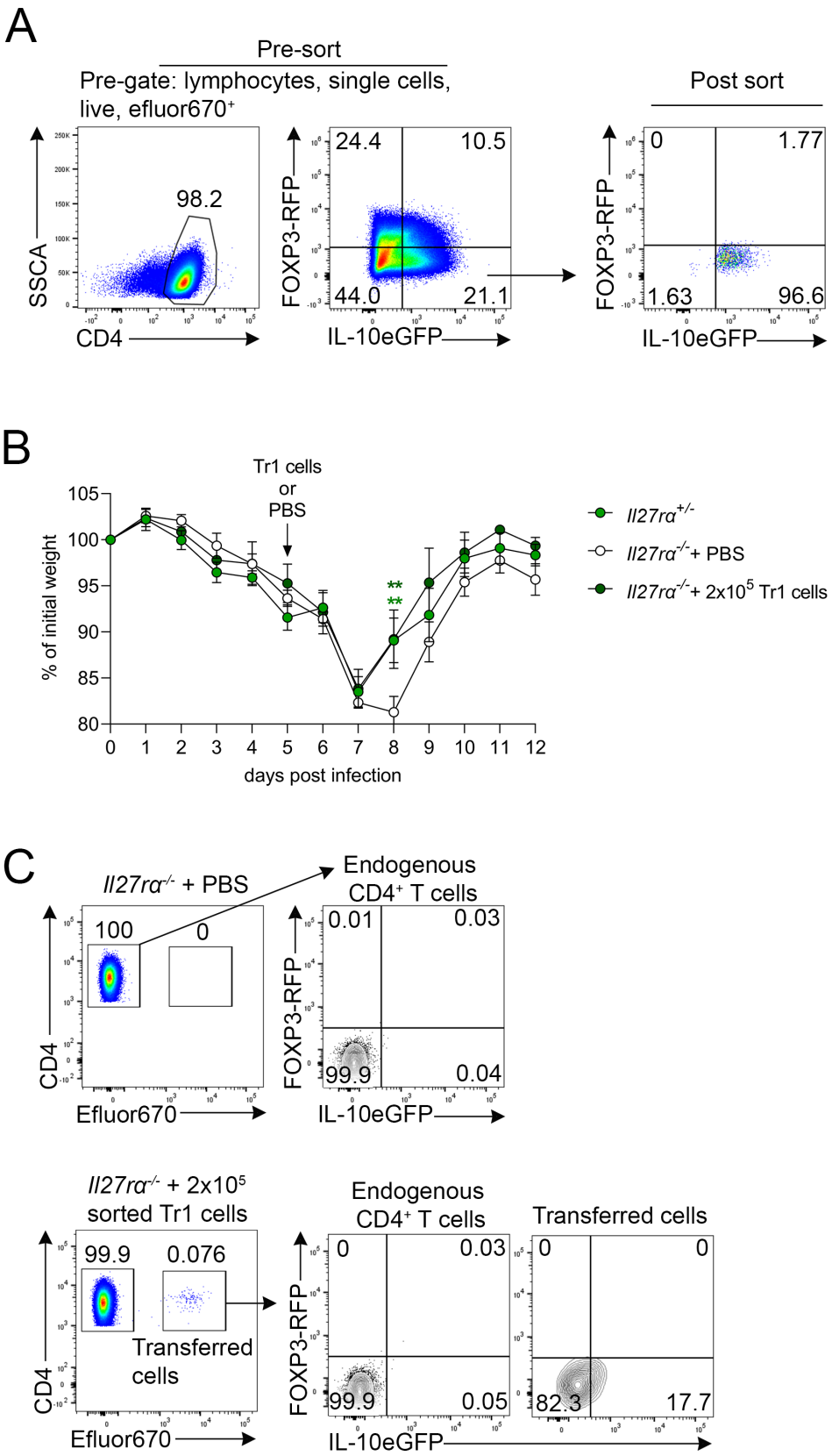
A
Pre-sort
Pre-gate: lymphocytes, single cells, live, efluor670+
Post sort
SSCA
CD4
98.2
FOXP3-RFP
IL-10eGFP
24.4
10.5
44.0
21.1
0
1.77
1.63
96.6
B
Tr1 cells or PBS
% of initial weight
days post infection
Il27rα+/-
Il27rα-/- + PBS
Il27rα-/- + 2x10^5 Tr1 cells
**
**
C
Il27rα-/- + PBS
Endogenous CD4+ T cells
100
0
0.01
0.03
99.9
0.04
Efluor670
Il27rα-/- + 2x10^5 sorted Tr1 cells
Transferred cells
99.9
0.076
0
0.03
0
0
99.9
0.05
82.3
17.7

Figure 3.16: *In-vivo* function of *in vitro*-derived FACS-sorted Tr1 cells during IAV infection.

Il27ra$^{+/-}$ and *Il27ra*$^{-/-}$ littermates were infected with X-31-OVA$_{323-339}$ IAV-i.n as described (refer to **2.5.1**). On day 5 post-infection *Il27ra*$^{-/-}$ mice were administered either PBS or 2x10^5 FACS-sorted *in vitro*-derived polyclonal Tr1 cells. (A) Sorting strategy for *in vitro*-derived polyclonal Tr1 cells and post-sort purity. (B) The percentage of initial weight post-infection comparing *Il27ra*$^{+/-}$, *Il27ra*$^{-/-}$+ PBS, and *Il27ra*$^{-/-}$+ Tr1 cells. (C) Representative flow cytometry of Efluor670-labelled transferred cells in the lungs of *Il27ra*$^{-/-}$ mice on day 7 post-infection compared to PBS control. Each symbol represents the mean +/- SEM. Statistical significance as indicated by asterisks is comparing the *Il27ra*$^{-/-}$ + Tr1 cells and *Il27ra*$^{-/-}$ + PBS (dark green), and *Il27ra*$^{+/-}$ and *Il27ra*$^{-/-}$ + PBS (light green), n=6 (*Il27ra*$^{+/-}$), 7 (*Il27ra*$^{-/-}$ + PBS), 6 (*Il27ra*$^{-/-}$ + Tr1-like cells) total, from 2 independent experiments. Statistical analysis completed using one-way ANOVA with Bonferroni's post-test (where $^{**} = p \leq 0.01$).

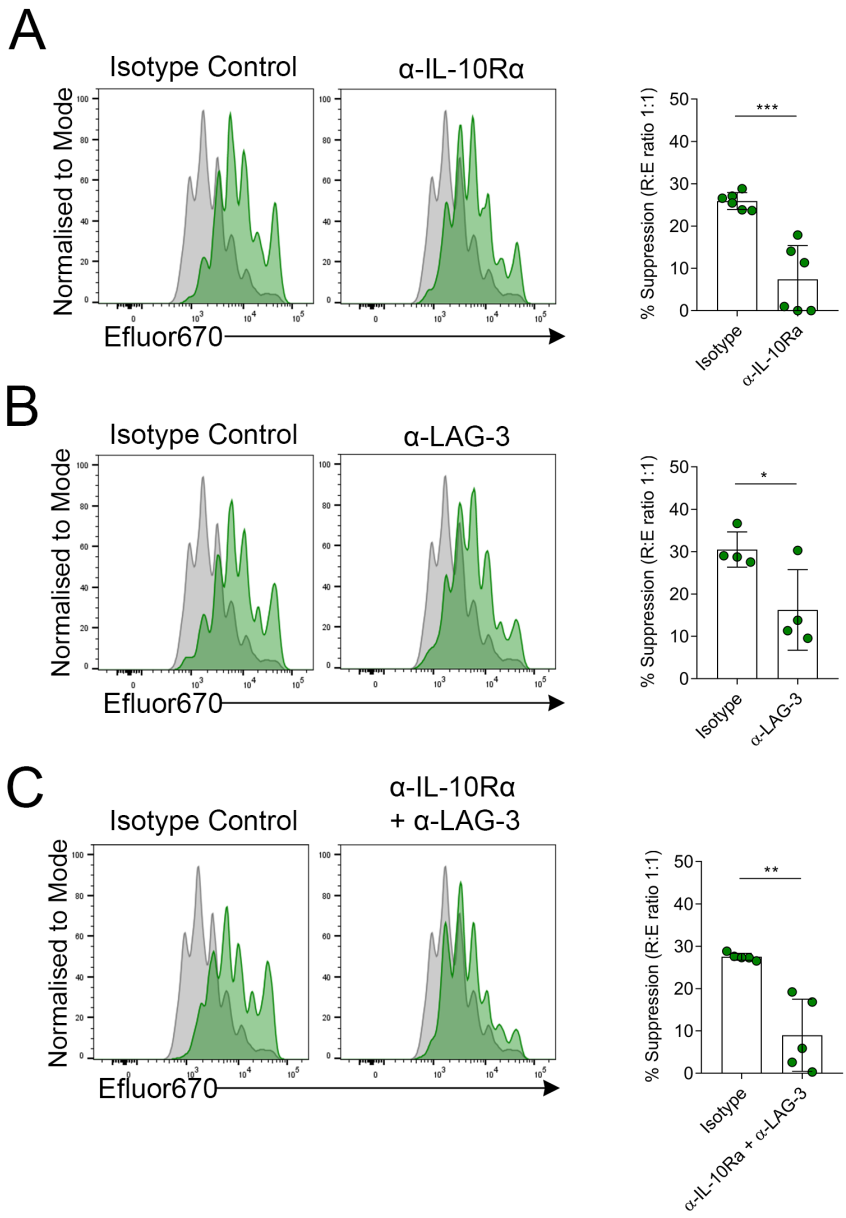

Figure 3.17: Dependence on IL-10 and LAG-3 for suppression by *in vitro* derived Tr1 cells.

(A-C) Histograms depicting the division of labelled effector T cells either alone with APCs and stimulation (grey histogram), or co-cultured with *in vitro*-derived FACS-sorted Tr1 cells (green histograms). For each assay the ratio of regulatory T cells to effector T cells is 1:1 (where 1:1 ratio = $1x10^4$ regulatory T cells:$1x10^4$ effector T cells). Suppression assays were conducted in the presence of an isotype control (A) α-rat IgG, (B) α-armenian hamster IgG, (C) both, or (A) α-IL-10Rα, (B) α-LAG-3, or (C) both nABs. The percentage suppression of effector T cell division is quantified (right) in each comparison. Each symbol represents a different technical replicate, shown as mean +/- SD, n=4-7 technical replicates from 3 independent experiments. Statistical analysis using unpaired Student's T-tests (where $* = p \leq 0.05, ** = p \leq 0.01$, and $*** = p \leq 0.001$).

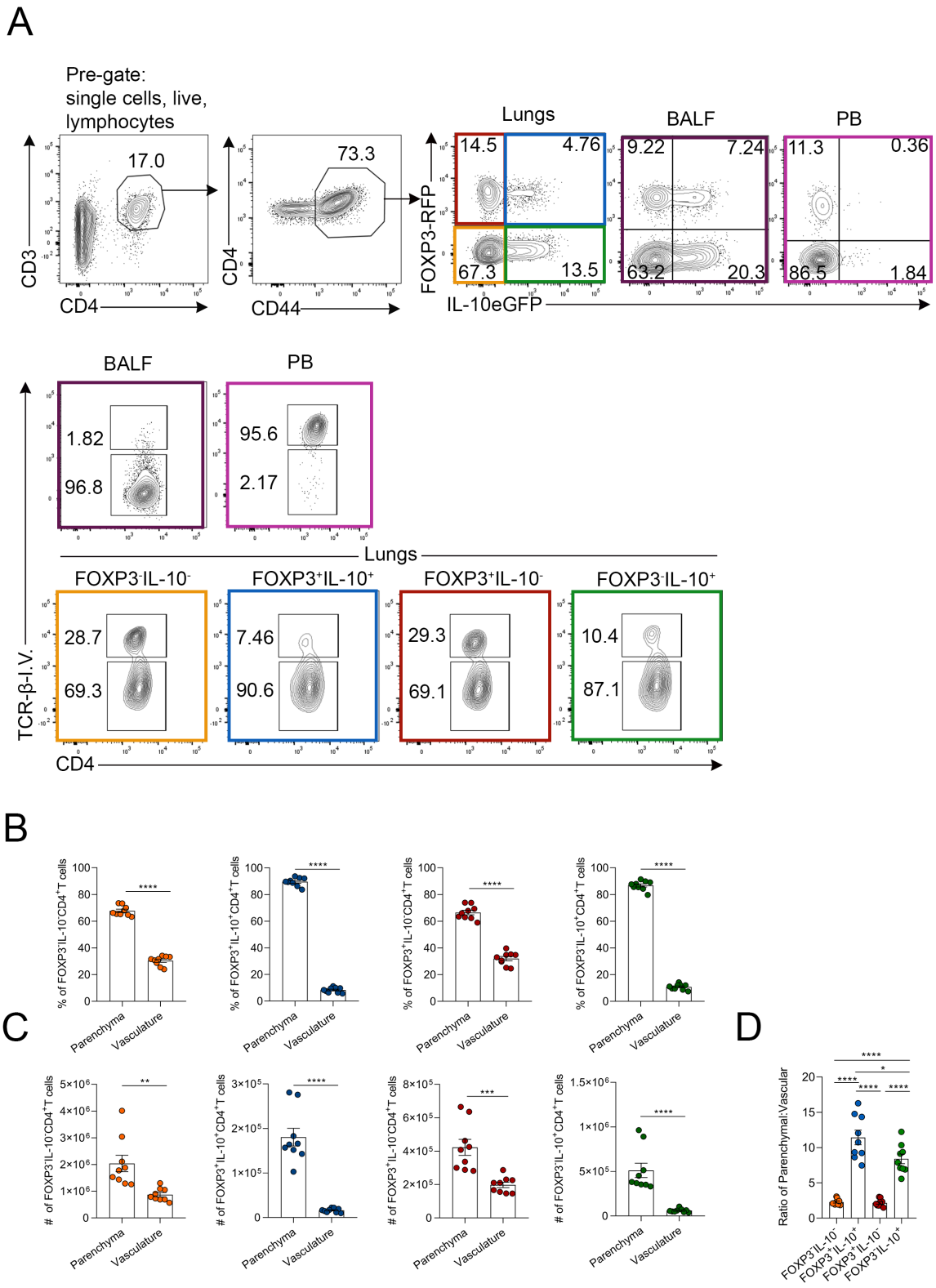
A
Pre-gate:
single cells, live,
lymphocytes
CD3
CD4
17.0
CD4
CD44
73.3
FOXP3-RFP
IL-10eGFP
Lungs
BALF
PB
14.5
4.76
67.3
13.5
9.22
7.24
63.2
20.3
11.3
0.36
86.5
1.84
BALF
PB
1.82
96.8
95.6
2.17
Lungs
FOXP3-IL-10-
FOXP3+IL-10+
FOXP3+IL-10-
FOXP3-IL-10+
TCR-β-I.V.
CD4
28.7
69.3
7.46
90.6
29.3
69.1
10.4
87.1
B
C
D
% of FOXP3-IL-10-CD4+T cells
% of FOXP3+IL-10+CD4+T cells
% of FOXP3+IL-10-CD4+T cells
% of FOXP3-IL-10+CD4+T cells
# of FOXP3-IL-10-CD4+T cells
# of FOXP3+IL-10+CD4+T cells
# of FOXP3+IL-10-CD4+T cells
# of FOXP3-IL-10+CD4+T cells
Parenchyma
Vasculature
Ratio of Parenchymal:Vascular
FOXP3-IL-10-
FOXP3+IL-10+
FOXP3+IL-10-
FOXP3-IL-10+

Figure 3.18: Analysis of CD4$^+$ T cell infiltration into the lung parenchyma on day 7 post-IAV infection.

Dual-reporter mice were infected with X-31 IAV-i.n as described (refer to **2.5.1**). On day 7 post-infection, TCR-β was injected i.v. prior to humane killing for intravascular labelling. (A) Representative flow cytometry gating strategy showing intravascular labelling of CD4$^+$ T cell populations on day 7 post-IAV infection in the lungs, BALF, and PB. The percentage (B), and number (C) of each of the CD4$^+$ T cell populations in the parenchyma and the vasculature of the lungs. (D) The ratio of parenchymal:vasculature-localised cells for each of the CD4$^+$ T cell populations. Each symbol represents a different biological replicate, shown as mean +/- SEM, n=9 biological replicates from 2 independent experiments. Statistical analysis using Student's paired T-tests (B),(C), and one-way ANOVA with Bonferroni's post-test (D) (where $^* = p \leq 0.05, ^{**} = p \leq 0.01, ^{***} = p \leq 0.001$, and $^{****} = p \leq 0.0001$).

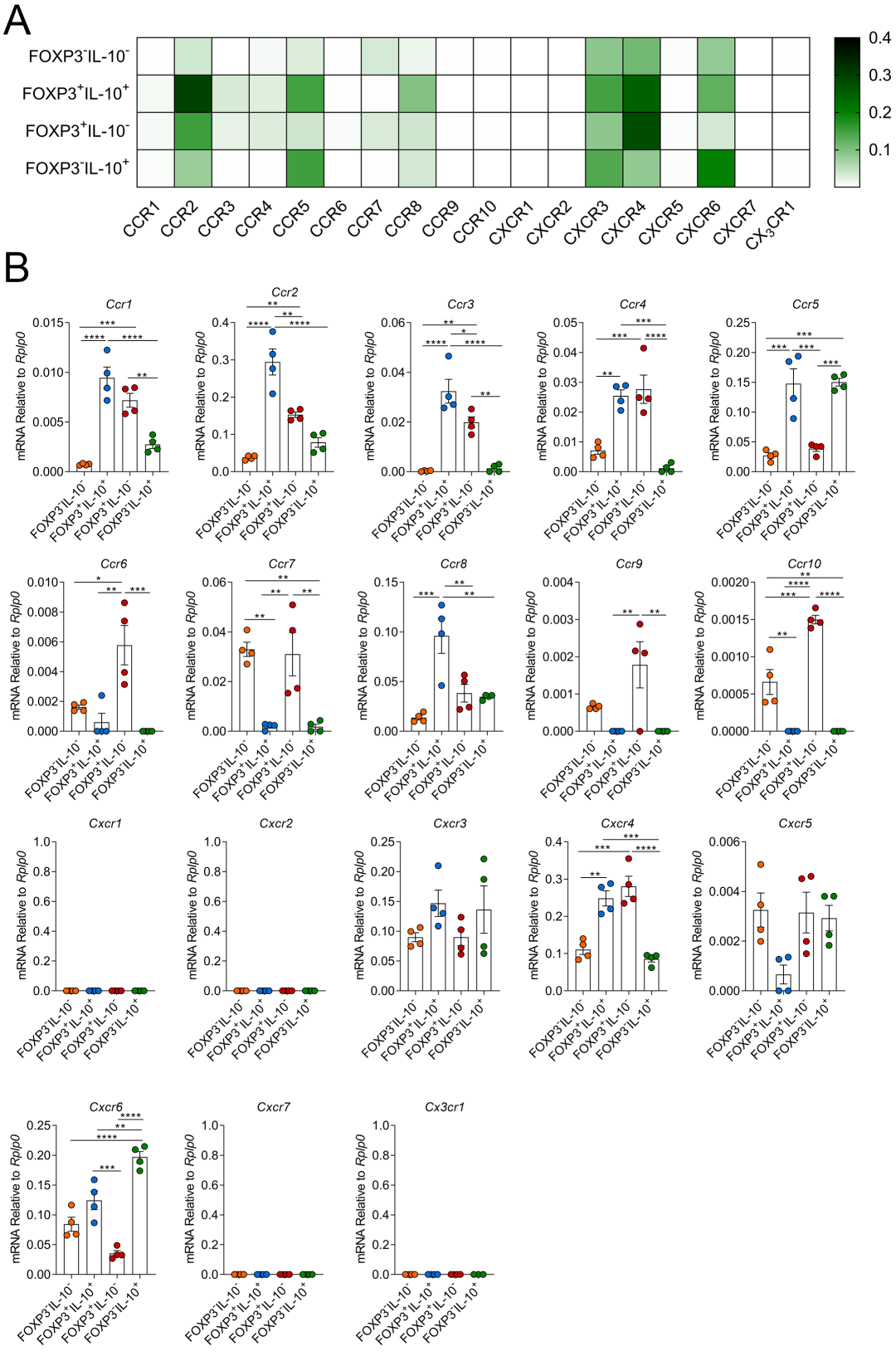
A
FOXP3⁻IL-10⁻
FOXP3⁺IL-10⁺
FOXP3⁺IL-10⁻
FOXP3⁻IL-10⁺
0.4
0.3
0.2
0.1
CCR1
CCR2
CCR3
CCR4
CCR5
CCR6
CCR7
CCR8
CCR9
CCR10
CXCR1
CXCR2
CXCR3
CXCR4
CXCR5
CXCR6
CXCR7
CX3CR1
B
Ccr1
Ccr2
Ccr3
Ccr4
Ccr5
Ccr6
Ccr7
Ccr8
Ccr9
Ccr10
Cxcr1
Cxcr2
Cxcr3
Cxcr4
Cxcr5
Cxcr6
Cxcr7
Cx3cr1
mRNA Relative to Rplp0
FOXP3⁻IL-10⁻
FOXP3⁺IL-10⁺
FOXP3⁺IL-10⁻
FOXP3⁻IL-10⁺

Figure 3.19: Transcriptional analysis of chemokine receptor expression by activated CD4$^+$ T cells from the IAV-infected lungs.
Dual-reporter mice were infected with X-31 IAV-i.n as described (refer to **2.5.1**). On day 7 post-infection effector CD4$^+$ T cells, Treg cells, IL-10$^+$ Treg cells, and Tr1-like cells were FACS-sorted from the lungs. The mRNA from FACS-sorted populations was assessed for chemokine receptor expression using RT-qPCR compared to the housekeeping gene *Rplp0*. (A) Heatmap comparing relative expression of chemokine receptors by each of the four CD4$^+$ T cell populations. (B) Individual chemokine receptor plots showing relative RNA expression by each of the four populations. Each symbol represents a different biological replicate, bars show the mean +/- SEM, n=4 biological replicates total from 2 independent experiments. Statistical analysis using paired T-tests (where $^* = p \leq 0.05, ^{**} = p \leq 0.01, ^{***} = p \leq 0.001$, and $^{****} = p \leq 0.0001$).

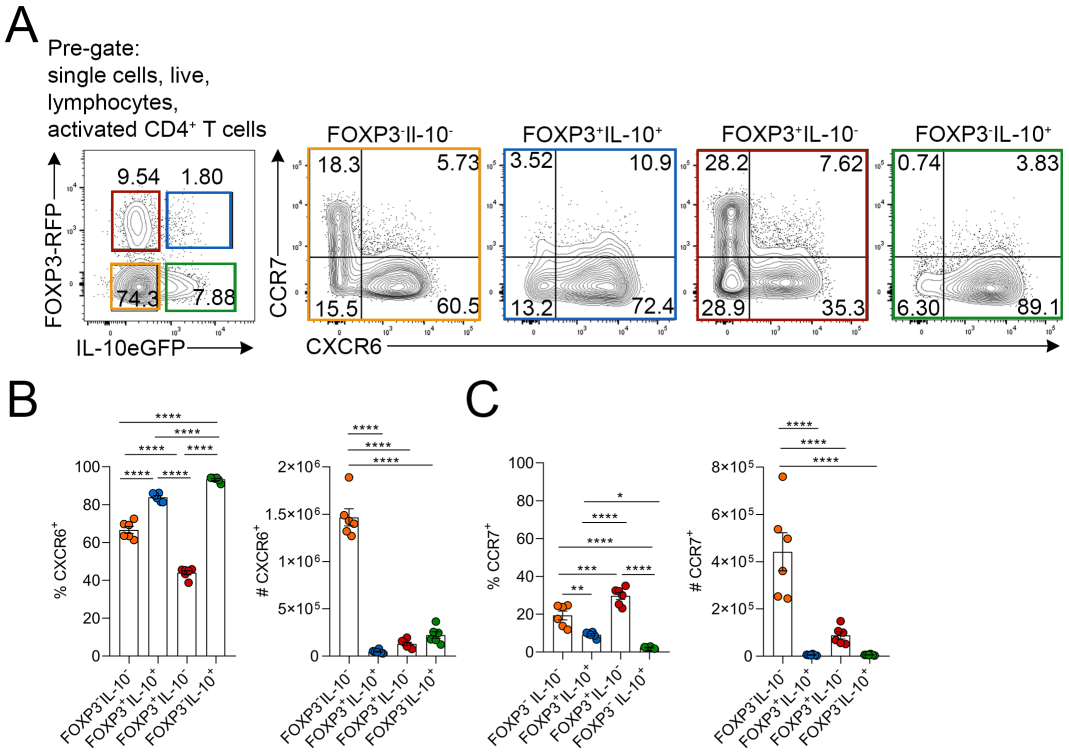

Figure 3.20: Analysis of CXCR6 and CCR7 protein expression by activated CD4$^+$ T cells from the IAV-infected lungs.

Dual-reporter mice were infected with X-31 IAV-i.n as described (refer to **2.5.1**). On day 7 post-infection effector CD4$^+$ T cells, Treg cells, IL-10$^+$ Treg cells, and Tr1-like cells from the lungs were analysed by flow cytometry. (A) Concatenated gating strategy showing expression of CCR7 and CXCR6 by FOXP3 and IL-10 populations. Frequency and number of (B) CXCR6- and (C) CCR7-expressing CD4$^+$ T cell populations determined by flow cytometry. Each symbol represents a different biological replicate, shown as mean +/- SEM, n=6 biological replicates total from 2 independent experiments. Statistical analysis using one-way ANOVA with Bonferroni's post-test (where $^* = p \leq 0.05, ^{**} = p \leq 0.01, ^{***} = p \leq 0.001$, and $^{****} = p \leq 0.0001$).

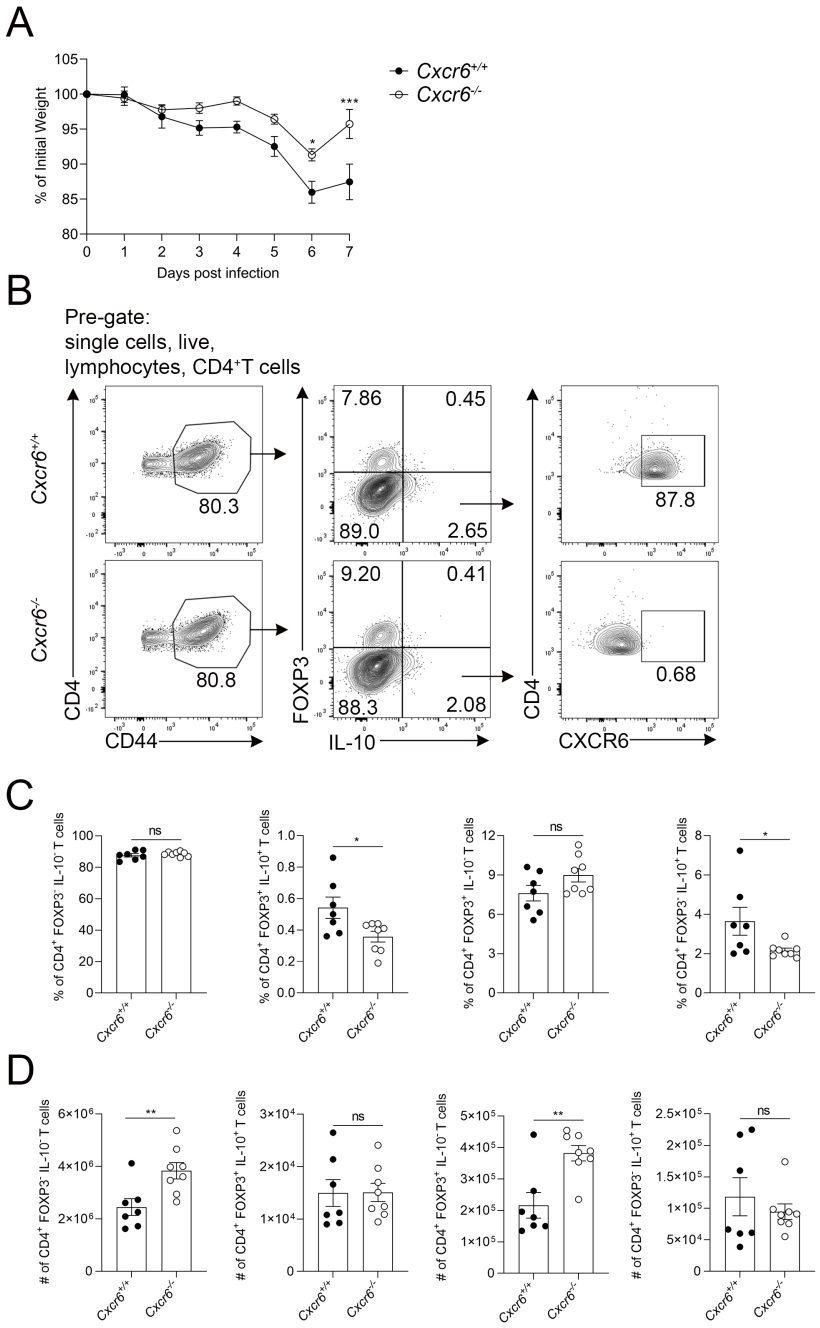

Figure 3.21: Recruitment of CD4$^+$ T cells to the lungs in CXCR6-deficient mice at day 7 post-IAV infection.

CXCR6$^{+/+}$ and CXCR6$^{-/-}$ mice were infected with with X-31 IAV-i.n as described (refer to **2.5.1**). On day 7 post-infection lungs were assessed for the presence of Tr1-like cells by intranuclear/intracellular cytokine staining. (A) Percentage of initial weight during the course of IAV infection. (B) Gating strategy to identify populations of activated CD4$^+$ T cells based on expression of FOXP3 and IL-10. (C) Percentage and (D) number of effector CD4$^+$ T cells, IL-10$^+$ Treg cells, Treg cells, and Tr1-like cells in the lungs. Each symbol represents the mean +/- SEM (A). Each symbol represents a different biological replicate, shown as mean +/- SEM (C), (D), n=7 (CXCR6$^{+/+}$) and 8 (CXCR6$^{-/-}$), from 2 independent experiments. Statistical analysis using one-way ANOVA with Bonferroni's post-test in (A) and unpaired Student's T-tests in (C),(D) (where $^* = p \leq 0.05, ^{**} = p \leq 0.01, ^{***} = p \leq 0.001$, and $^{****} = p \leq 0.0001$).

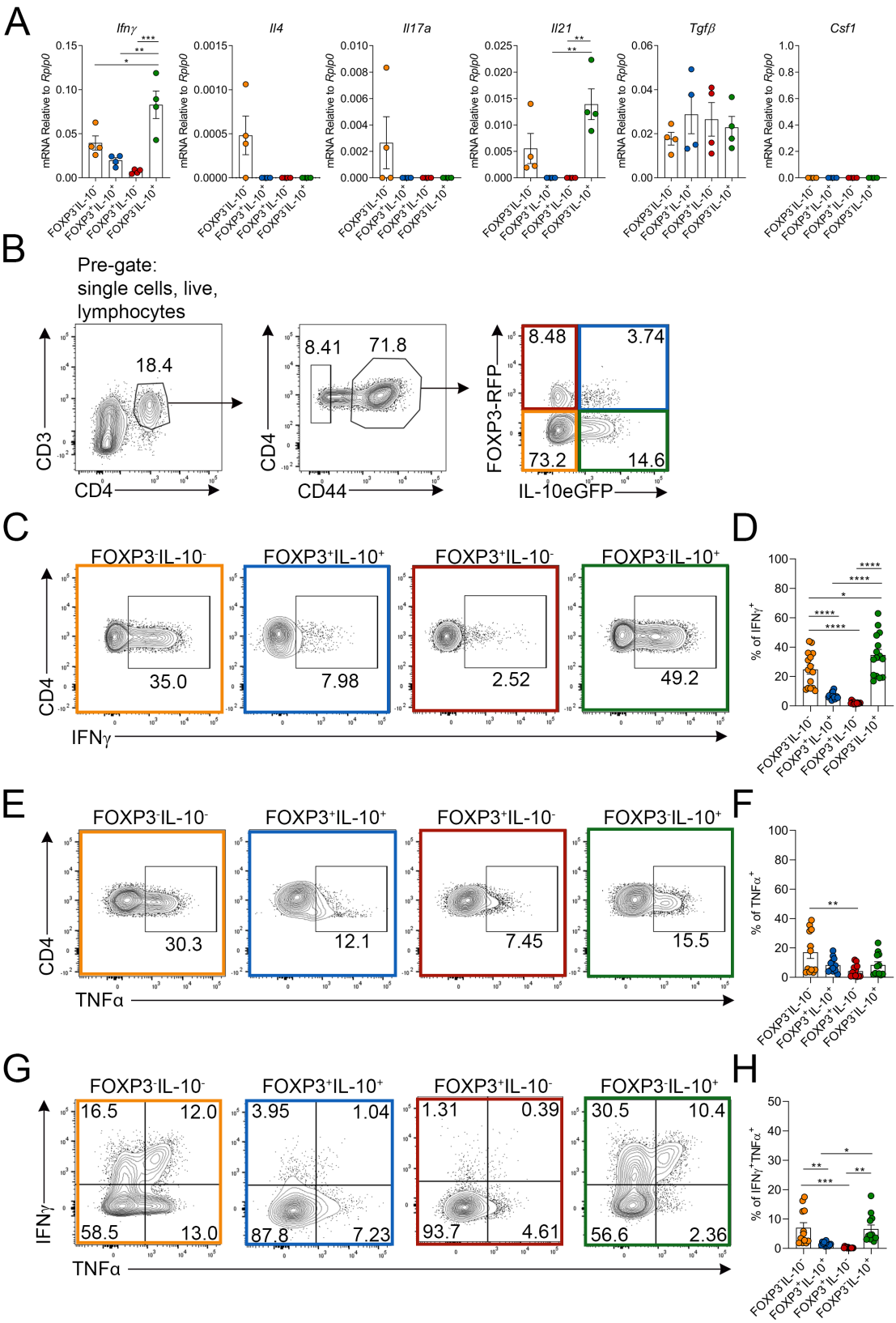
A
Ifnγ
Il4
Il17a
Il21
Tgfβ
Csf1
mRNA Relative to Rplp0
FOXP3-IL-10-
FOXP3+IL-10+
FOXP3+IL-10-
FOXP3-IL-10+
B
Pre-gate:
single cells, live,
lymphocytes
CD3
CD4
18.4
CD4
CD44
8.41
71.8
FOXP3-RFP
IL-10eGFP
8.48
3.74
73.2
14.6
C
FOXP3-IL-10-
FOXP3+IL-10+
FOXP3+IL-10-
FOXP3-IL-10+
CD4
IFNγ
35.0
7.98
2.52
49.2
D
% of IFNγ+
E
FOXP3-IL-10-
FOXP3+IL-10+
FOXP3+IL-10-
FOXP3-IL-10+
CD4
TNFα
30.3
12.1
7.45
15.5
F
% of TNFα+
G
FOXP3-IL-10-
FOXP3+IL-10+
FOXP3+IL-10-
FOXP3-IL-10+
IFNγ
TNFα
16.5
12.0
58.5
13.0
3.95
1.04
87.8
7.23
1.31
0.39
93.7
4.61
30.5
10.4
56.6
2.36
H
% of IFNγ+TNFα+

Figure 3.22: Quantitation of cytokine expression by activated CD4$^+$ T cells from IAV-infected lungs.

Dual-reporter mice were infected with X-31 IAV-i.n as described (refer to **2.5.1**). On day 7 post-infection the four CD4$^+$ T cell populations were FACS-sorted from the lungs and mRNA extracted for RT-qPCR. (A) RT-qPCR analysis of cytokine mRNA. (B) Gating strategy for analysis of activated CD4$^+$ T cell populations from the IAV-infected lung. Representative flow cytometry of (C) IFNγ expression, (E) TNFα expression, and (G) IFNγ TNFα double-positive CD4$^+$ T cell populations. The percentage of (D) IFNγ^+, (F) TNFα^+, (H) IFNγ^+ TNFα^+ of each of the CD4$^+$ T cell populations. Each symbol represents a different biological replicate, shown as mean +/- SEM, n=12-15 total from 3 independent experiments. Statistical analysis using one-way ANOVA with Bonferroni's post-test (where $^* = p \leq 0.05, ^{**} = p \leq 0.01, ^{***} = p \leq 0.001$, and $^{****} = p \leq 0.0001$).

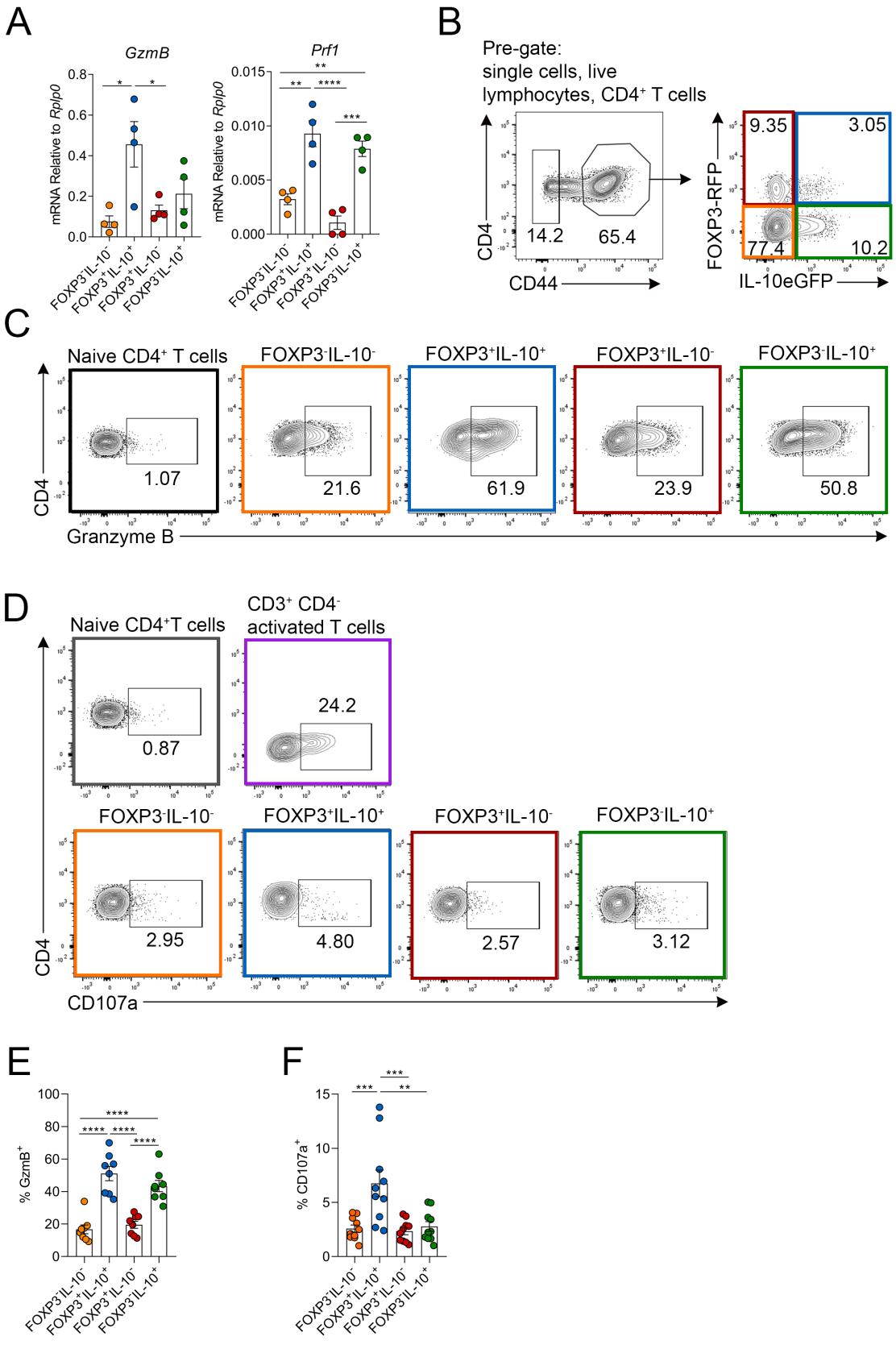
A
GzmB
Prf1
mRNA Relative to Rplp0
FOXP3-IL-10-
FOXP3+IL-10+
FOXP3+IL-10-
FOXP3-IL-10+
B
Pre-gate:
single cells, live
lymphocytes, CD4+ T cells
CD4
CD44
14.2
65.4
FOXP3-RFP
IL-10eGFP
9.35
3.05
77.4
10.2
C
Naive CD4+ T cells
FOXP3-IL-10-
FOXP3+IL-10+
FOXP3+IL-10-
FOXP3-IL-10+
1.07
21.6
61.9
23.9
50.8
CD4
Granzyme B
D
Naive CD4+T cells
CD3+ CD4-
activated T cells
0.87
24.2
2.95
4.80
2.57
3.12
CD4
CD107a
E
% GzmB+
F
% CD107a+

Figure 3.23: Quantitation of cytotoxic molecule expression and degranulation potential by activated CD4$^+$ T cells from the IAV-infected lungs.

Dual-reporter mice were infected with X-31 IAV-i.n as described (refer to **2.5.1**). On day 7 post-infection the four CD4$^+$ T cell populations were sorted from the lungs and mRNA extracted for RT-qPCR. (A) RT-qPCR analysis of the cytotoxic effector molecules perforin and granzyme B mRNA. On day 7 post-infection, activated CD4$^+$ T cells were assessed for protein expression of Granzyme B and CD107a by flow cytometry. (B) Gating strategy for activated CD4$^+$ T cell populations. (C) Flow cytometry of granzyme B expression by naive CD4$^+$ T cells (negative control) and CD4$^+$ T cell populations based on FOXP3 and IL-10. (D) Flow cytometry of CD107a expressed by naive CD4$^+$ T cells (negative control), activated CD3$^+$ CD4$^-$ T cells (positive control), and the four CD4$^+$ T cell populations based on FOXP3 and IL-10. (E) The percentage of activated CD4$^+$ T cells expressing Granzyme B. (F) The percentage of CD4$^+$ T cells expressing CD107a. Each symbol represents a different biological replicate, shown as mean +/- SEM, n=10 biological replicates total from 2 independent experiments. Statistical analysis using one-way ANOVA with Bonferroni's post-test (where $^* = p \leq 0.05, ^{**} = p \leq 0.01, ^{***} = p \leq 0.001$, and $^{****} = p \leq 0.0001$).

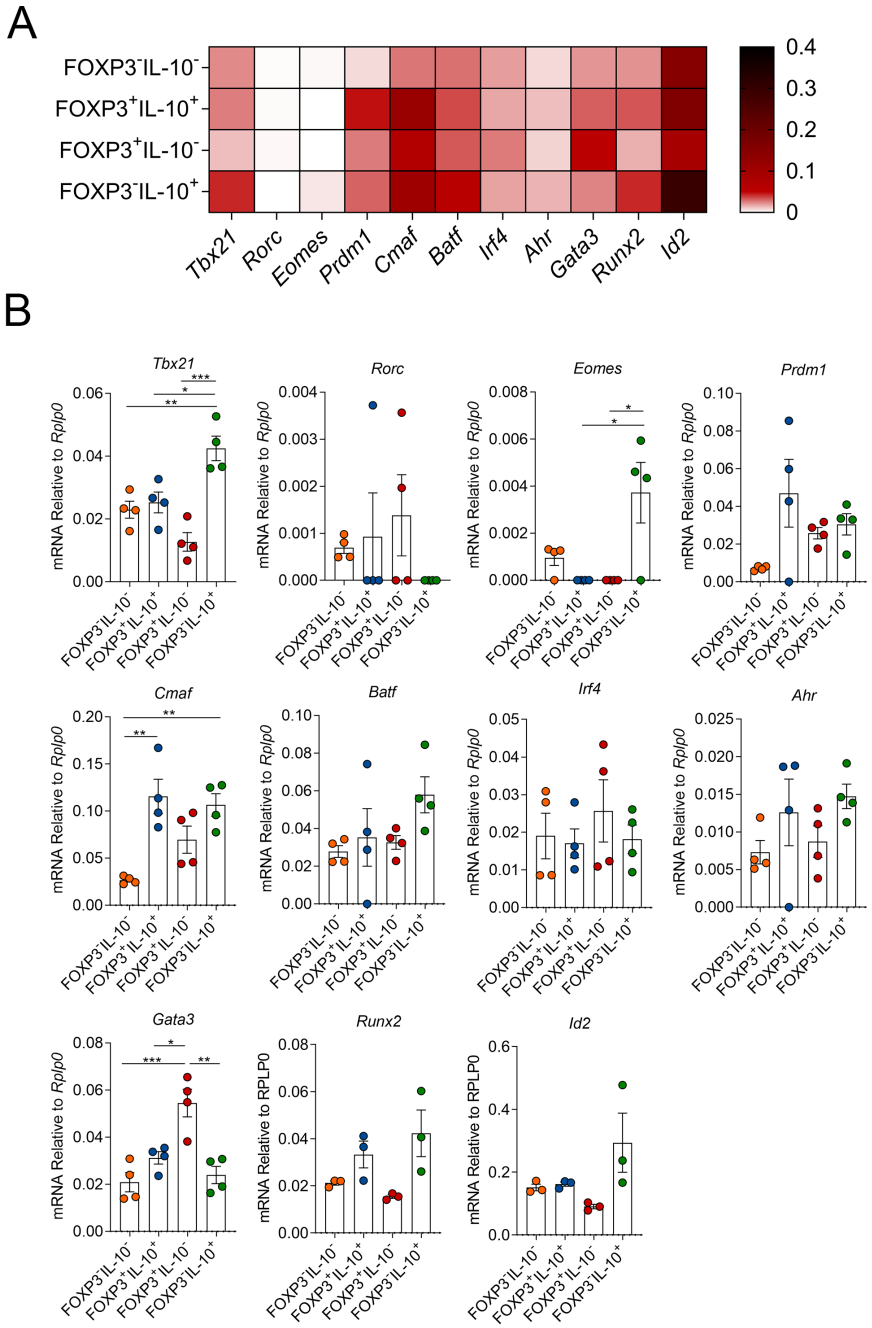

Figure 3.24: The transcriptional profile of activated CD4$^+$ T cell populations from the IAV-infected lungs.

Dual-reporter mice were infected with X-31 IAV-i.n as described (refer to **2.5.1**). On day 7 post-infection the four CD4$^+$ T cell populations were FACS-sorted from the lungs and RNA extracted for RT-qPCR. (A) Heatmap comparing relative expression of transcription factors by each of the four CD4$^+$ T cell populations. (B) Individual RT-qPCR plots displaying the relative level of transcription factor expression for each population. Each symbol represents a different biological replicate, shown as mean +/- SEM, n=3-4 biological replicates from 2 independent experiments. (where $^* = p \leq 0.05, ^{**} = p \leq 0.01$, and $^{***} = p \leq 0.001$).

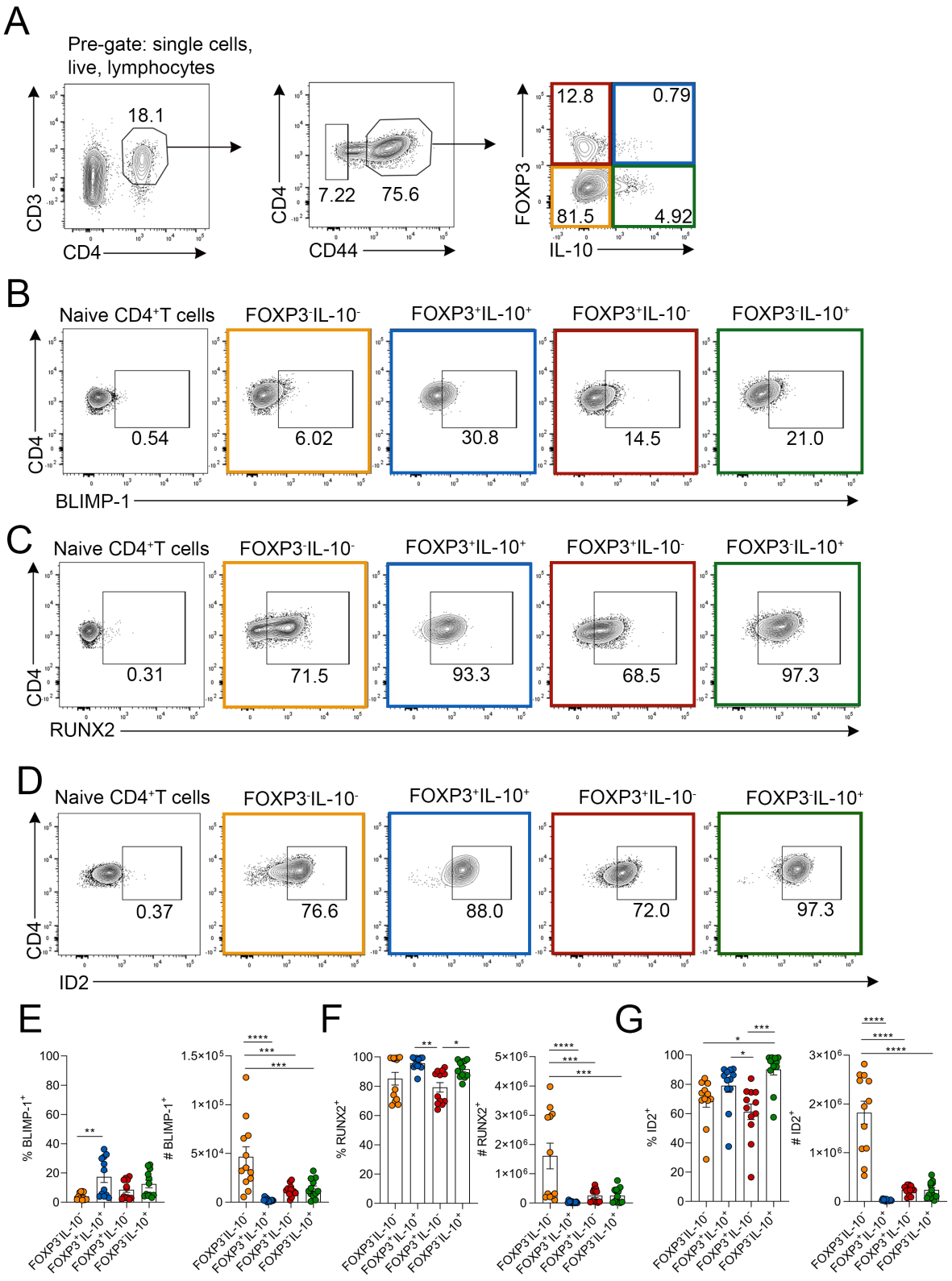
A
Pre-gate: single cells, live, lymphocytes
18.1
CD3
CD4
7.22
75.6
CD4
CD44
12.8
0.79
81.5
4.92
FOXP3
IL-10
B
Naive CD4+T cells
FOXP3-IL-10-
FOXP3+IL-10+
FOXP3+IL-10-
FOXP3-IL-10+
0.54
6.02
30.8
14.5
21.0
CD4
BLIMP-1
C
Naive CD4+T cells
FOXP3-IL-10-
FOXP3+IL-10+
FOXP3+IL-10-
FOXP3-IL-10+
0.31
71.5
93.3
68.5
97.3
CD4
RUNX2
D
Naive CD4+T cells
FOXP3-IL-10-
FOXP3+IL-10+
FOXP3+IL-10-
FOXP3-IL-10+
0.37
76.6
88.0
72.0
97.3
CD4
ID2
E
% BLIMP-1+
# BLIMP-1+
F
% RUNX2+
# RUNX2+
G
% ID2+
# ID2+
FOXP3-IL-10-
FOXP3+IL-10+
FOXP3+IL-10-
FOXP3-IL-10+

Figure 3.25: Expression of BLIMP-1, RUNX2, and ID2 protein by CD4$^+$T cell populations from the IAV-infected lungs.

Dual-reporter mice were infected with X-31 IAV-i.n as described (refer to **2.5.1**). On day 7 post-IAV infection lungs were harvested for analysis of CD4$^+$ T cell expression of transcription factors by flow cytometry. (A) Gating strategy to identify populations of CD4$^+$ T cells. Concatenated, representative flow cytometry displaying expression of (B) BLIMP-1, (C) RUNX2, and (D) ID2 by CD4$^+$ T cell populations compared to naive CD4$^+$ T cells. The frequency and number of each of the CD4$^+$ T cell populations expressing (E) BLIMP-1, (F) RUNX2, and (G) ID2. Each symbol represents a different biological replicate, shown as mean +/- SEM, n=12 from 2 independent experiments. Statistical analysis completed using One-Way ANOVA with Bonferroni's correction (where $^* = p \leq 0.05, ^{**} = p \leq 0.01, ^{***} = p \leq 0.001$, and $^{****} = p \leq 0.0001$).

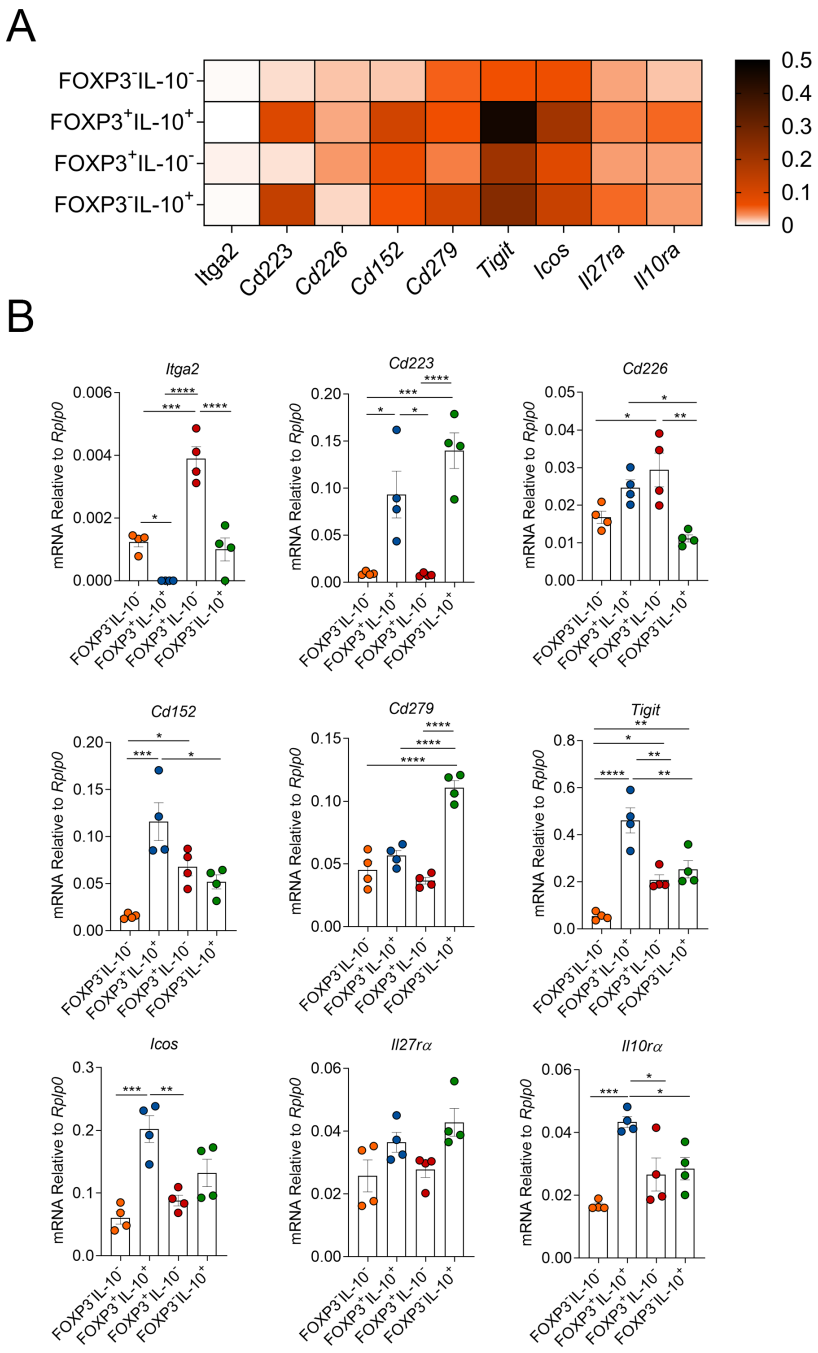

Figure 3.26: Co-inhibitory molecule expression at the level of RNA by CD4$^+$ T cell populations from the IAV-infected lungs.
Dual-reporter mice were infected with X-31 IAV-i.n as described (refer to **2.5.1**). On day 7 post-infection, activated CD4$^+$ T cell populations were FACS-sorted from the lungs for analysis of surface molecule expression by RT-qPCR. (A) Heatmap comparing relative expression of surface molecules by each of the four CD4$^+$ T cell populations. (B) Individual surface molecule plots showing relative RNA expression by each of the four populations. Each symbol represents a different biological replicate, the mean is shown +/- SEM, n=4 total from 2 independent experiments. Statistical analysis using paired T-tests (where $* = p \leq 0.05, ** = p \leq 0.01, *** = p \leq 0.001$, and $**** = p \leq 0.0001$).

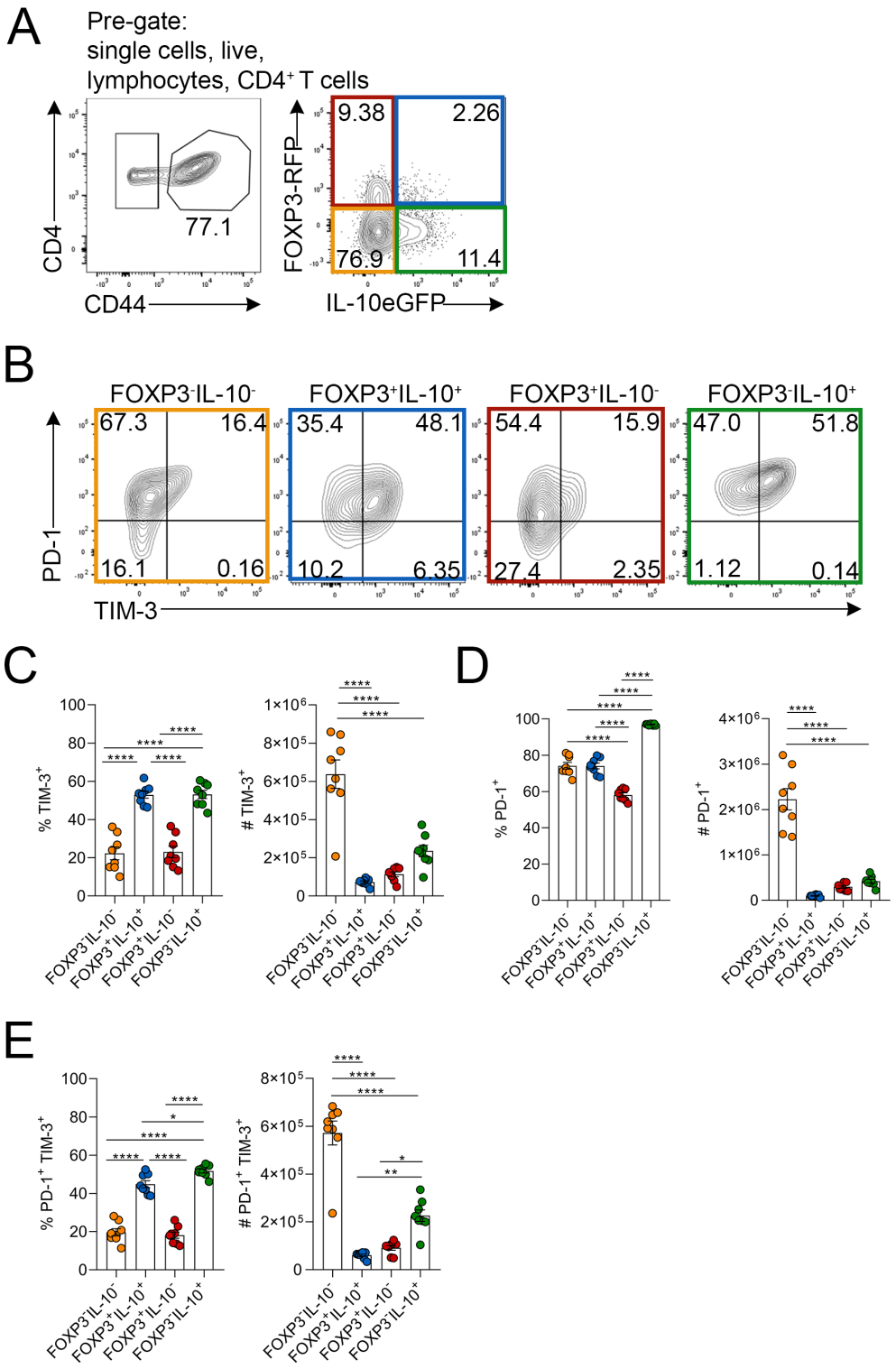
A
Pre-gate:
single cells, live,
lymphocytes, CD4+ T cells
CD4
CD44
77.1
FOXP3-RFP
IL-10eGFP
9.38
2.26
76.9
11.4
B
FOXP3-IL-10-
FOXP3+IL-10+
FOXP3+IL-10-
FOXP3-IL-10+
PD-1
TIM-3
67.3
16.4
16.1
0.16
35.4
48.1
10.2
6.35
54.4
15.9
27.4
2.35
47.0
51.8
1.12
0.14
C
% TIM-3+
# TIM-3+
D
% PD-1+
# PD-1+
E
% PD-1+ TIM-3+
# PD-1+ TIM-3+
FOXP3-IL-10-
FOXP3+IL-10+
FOXP3+IL-10-
FOXP3-IL-10+

Figure 3.27: Quantitation of PD-1 and TIM-3 protein expression by activated CD4$^+$ T cells from the IAV-infected lungs.

Dual-reporter mice were infected with X-31 IAV-i.n as described (refer to **2.5.1**). On day 7 post-infection the lungs were harvested for analysis of co-inhibitory molecule expression by flow cytometry. (A) Gating strategy used to identify activated CD4$^+$ T cell populations expressing FOXP3 and IL-10. (B) Representative concatenated plots depicting PD-1 and TIM-3 protein expression by CD4$^+$ T cell populations. Percentage and number of (C) TIM-3$^+$, (D) PD-1$^+$, and (E) TIM-3$^+$ PD-1$^+$ CD4$^+$ T cells. Each symbol represents a different biological replicate, the mean is shown +/- SEM, n=8 from 2 independent experiments. Statistical analysis completed using One-Way ANOVA with Bonferroni's post-test. $^* = p \leq 0.05, ^{**} = p \leq 0.01$, and $^{****} = p \leq 0.0001$).

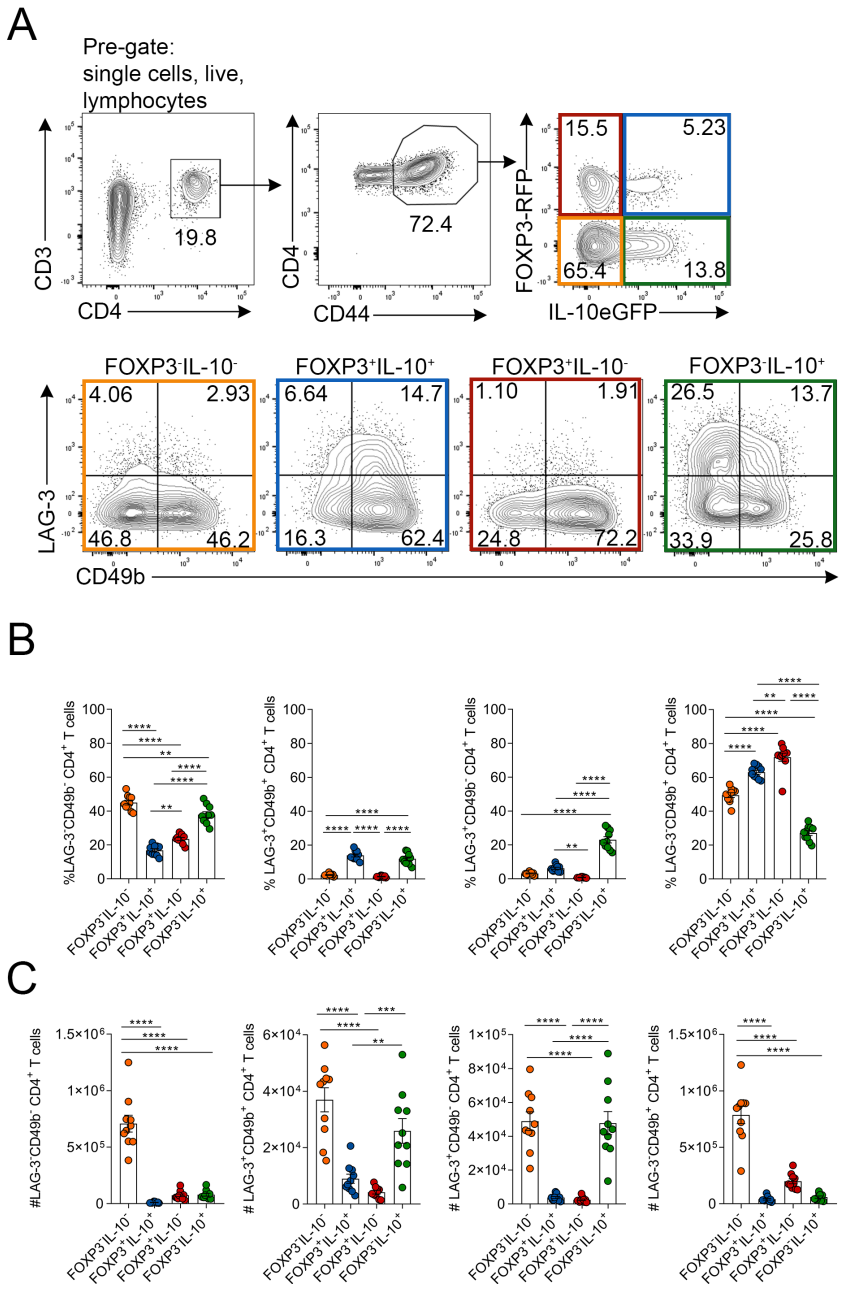

Figure 3.28: Quantitation of LAG-3 and CD49b protein expression by activated CD4$^+$ T cells from the IAV-infected lungs.
Dual-reporter mice were infected with X-31 IAV-i.n as described (refer to **2.5.1**).(A) Concatenated representative flow cytometry depicting the gating strategy for identification of LAG-3 and CD49b-expressing CD4$^+$ T cell populations based on FOXP3 and IL-10 expression on day 7 post-infection. (B) Percentage and (C) number of LAG-3 and CD49b expressing effector CD4$^+$ T cells, Treg cells, IL-10 Treg cells and Tr1-like cells. Each symbol represents a different biological replicate, the mean is shown +/- SEM, n=3-15 total from 3 independent experiments. Statistical analysis completed using One-Way ANOVA with Bonferroni's post-Test. $** = p \leq 0.01$, $*** = p \leq 0.001$, and $**** = p \leq 0.0001$).

Chapter 4: Novel Tr1 populations that arise in IAV infection.

4.1 Introduction

From the results in Chapter 3, it was clear that four distinct populations of Tr1-like cells could be identified in IAV-infected lungs on day 7 post-infection. These included the canonical LAG-3$^+$ CD49b$^+$ (DP) Tr1 cell population, as well as single-positive LAG-3$^-$ CD49b$^+$ (CD49b$^+$), single-positive LAG-3$^+$ CD49b$^-$ (LAG-3$^+$), and the double-negative LAG-3$^-$ CD49b$^-$ (DN) Tr1-like cells. Having characterised the bulk Tr1-like cells in the lung and shown their adherence to the defining functional characteristics of Tr1 cells as summarised in the conclusion section of the previous chapter, the investigation next focused specifically on these novel Tr1-like cell populations. For this investigation, the initial question was whether each of these Tr1-like populations represented distinct independent subsets of Tr1 cells or discrete stages of development within the Tr1 lineage. To address this, extensive analysis of the expressed surface markers, secreted molecules and transcription factors that are known to define Tr1 cells was conducted. In addition, their suppressive capacity was examined and mechanisms of any observed suppression were investigated. Whether these distinct Tr1 cell populations were all *bona fide* Tr1 cells, and in addition, obtaining information on potential roles they may play in acute infection were considered important lines of investigation.

4.2 The kinetics and phenotype of novel Tr1-like cell populations in IAV infection.

Given multiple prior reports that indicated Tr1 cells uniformly exhibit a LAG-3$^+$ CD49b$^+$ phenotype [194], [210], [218], the heterogeneity observed in the present study was surprising and prompted investigation of the significance of these phenotypically distinct Tr1-like cells in IAV infection. Initially, a time course was performed from day 0 (naive mice) to day 10 post IAV infection, the gating strategy for which is shown in **Fig 4.1 A**. Few Tr1-like cells were found in the lungs of mice at day 0 and day 5 post-infection. The Tr1-like cells detected at these time points were predominately DN with some LAG-3$^+$ and CD49b$^+$ cells. In contrast, by day 7 post-infection, the proportion and number of Tr1-like cells markedly increased in the lung **(Fig 4.1 A-C)**. Around 7.5x10^4 DN Tr1-like cells were recovered from lungs of IAV-infected mice on day 7 and these cells continued to increase in number up to day 10 post-infection **(Fig 4.1 C)**. The retention of DN Tr1 cells out to day 10 was in stark contrast to the DP, LAG-3$^+$, and CD49b$^+$ Tr1-like cells as each of these populations were present transiently in highest numbers on day 7 and decreased in number by day 10 post-infection **(Fig 4.1 A-C)**. As stated in Chapter 3, day 7 post-infection corresponds to a time point at which significant viral clearance has occurred

(refer to **Fig 3.6**). Thus, overall the kinetic data generated in these experiments implys that Tr1-like cell responses in IAV infection are tightly controlled and appear to be closely linked to the resolution of inflammation.

The data presented in Chapter 3 indicated that during IAV infection, the bulk population of Tr1-like cells recovered from the lung were predominately located in the lung parenchyma rather than the vasculature (refer to **Fig 3.18**). Therefore, whether each of the four distinct populations of Tr1-like cells found in IAV-infected lungs on day 7 also displayed this distribution or were differentially distributed between lung parenchyma and vasculature was evaluated using intravascular labelling (refer to **Fig 4.2 A** for the flow cytometry gating strategy). These experiments revealed all of the Tr1-like cell populations were more abundant in the parenchyma than in the lung vasculature **(Fig 4.2 A-C)**. However, when analysed as a ratio of parenchymal:vascular, it was observed that DP Tr1-like cells were more abundant within the the lung parenchyma compared to the other three Tr1-like populations **(Fig 4.2 D)**. In fact, the DP Tr1-like cells were found to be around 15-fold more abundant in the parenchyma than the vasculature compared with around 10-fold for the other three populations.

To investigate the distribution of the four subsets of Tr1 cells in more detail during IAV infection, the lung-draining mLN, PB, lungs, and BALF were analysed by flow cytometry to identify these populations of Tr1-like cells at day 7 post-infection (flow cytometry pre-gating strategy and representative concatenated plots are shown in **Fig 4.3 A & B**). The DN and single-positive LAG-3$^+$ Tr1-like cells were determined to be most abundant in the PB **(Fig 4.3 B-D)**. The single-positive LAG-3$^+$ Tr1-like cells were the most abundant population in the mLN and lungs **(Fig 4.3 B-D)**. The DP and single-positive LAG-3$^+$ populations comprised the greatest proportion of Tr1 cells in BALF **(Fig 4.3 B-D)**. The single-positive CD49b$^+$ population was very low in frequency compared to the other populations in each of these organs **(Fig 4.3 B-D)**. These experiments determined that each of the Tr1-like cell populations accumulated to different extents in the tissues (and BALF) relevant to IAV infection. These data, including those indicating differential localisation of subsets in the parenchyma compared with the vasculature, may suggest conversion between the different populations during the immune response and/or differential recruitment of the populations to the effector sites (the lungs and BALF).

The four populations of Tr1-like cells were also assessed for proliferative capacity using Ki67 expression as a measure of actively cycling cells. It was not known if Tr1-like cells in the IAV-infected lungs were proliferative and if there were differences in the extent of active cycling between each of the distinct Tr1-like cell populations. Therefore, this was assessed by flow cytometry (gating strategy shown in **Fig 4.4 A**). There were no significant differences between any of the Tr1 cell populations in terms of Ki67 expression **(Fig 4.4 B**

& C), indicating that each of the Tr1-like cell populations was proliferating to a similar extent.

It was also of interest to determine whether any of the Tr1-like populations expressed higher levels of pro-inflammatory cytokines which could suggest pro-inflammatory function. Data from Chapter 3 suggested a small population of the bulk Tr1-like cells co-expressed IFNγ and TNFα. To examine whether this was restricted to one of the four Tr1-like cell populations intracellular cytokine staining was performed on IAV-infected lungs on day 7 post-infection (gating strategy shown in **Fig 4.5 A**). Firstly, it was found that IL-10 was most highly expressed by the LAG-3$^+$, followed by the DP Tr1 cells by mean fluorescence intensity (MFI) **(Fig 4.5 A)**. There were no significant differences in the proportion of IFNγ^+ cells between each of the populations of Tr1-like cells based on expression of LAG-3 and CD49b **(Fig 4.5 B)**. In contrast TNFα was found to be statistically significantly more highly expressed by the DN Tr1-like cells compared to the LAG-3$^+$ cells **(Fig 4.5 C)**. Examining co-expression of IFNγ and TNFα yielded no significant differences between the four Tr1-like populations, although, there was a trend toward IFNγ and TNFα co-expressing cells coming predominately from the DN or CD49b$^+$ populations rather than the DP and LAG-3$^+$ Tr1-like cells **(Fig 4.5 D)**, suggesting that these two populations may possess pro-inflammatory function in contrast to the other Tr1-like cells. Next, the 4 sub-populations of Tr1-like cells were compared for expression of markers of cytotoxic function (pre-gating strategy shown in **Fig 4.6 A**). Thus, granzyme B expression was analysed by flow cytometry of single cell suspensions prepared from IAV-infected lungs at day 7 post-infection. The Tr1-like populations expressing CD49b had displayed the highest frequency of Granzyme B$^+$ cells **(Fig 4.6 B & C)**. To determine whether Tr1-like cells were actively de-granulating, CD107a expression was assessed. Surface staining for CD107a was performed during PMA ionomycin restimulation, with IL-10$^+$ Treg cells as a biological positive control **(Fig 4.6 D)**. While this staining revealed a similar trend to granzyme B expression, there were no statistically significant differences **(Fig 4.6 D & E)**. The four Tr1-like cell populations all exhibited low surface CD107a expression, indicating that none of the Tr1-like cell populations were actively degranulating to a significant extent.

Also from data shown in Chapter 3, it was known that Tr1-like cells from the IAV-infected lungs express multiple co-inhibitory receptors. These surface receptors have previously been used to mark functional populations of regulatory T cells [210]. To compare the expression of co-inhibitory molecules between the four Tr1-like populations, flow cytometry was used to assess the protein expression of PD-1 and TIM-3 (gating strategy shown in **Fig 4.7 A**). The expression of TIM-3 protein, in terms of proportion of TIM-3$^+$ cells in the population displayed graded levels, ranging from the DP population which had the highest level of expression, to the CD49b$^+$ population, which had the lowest level of

expression **(Fig 4.7 A & B)**. PD-1 was found to be expressed by a high proportion of cells in all four Tr1-like populations **(Fig 4.7 A & C)**. Additionally, co-staining for PD-1 and TIM-3 indicated that the DP Tr1 cells were the most enriched for co-inhibitory molecule expression, followed by the LAG-3$^+$, then CD49b$^+$, and finally the DN population **Fig 4.7 A-D)**. These data imply that the DP population is likely to be the most immunoregulatory Tr1-like cells as the DP cells exhibited the highest proportion of cells expressing these co-inhibitory receptors.

4.3 Determining the suppressive capacity of distinct Tr1-like cell populations.

As already discussed previously, a critical feature of *bona fide* Tr1 cells is their ability to suppress effector T cell division. Therefore, the four FOXP3$^-$ IL-10$^+$ CD4$^+$ T cell populations that differentially co-expressed CD49b and LAG-3 were assessed for their ability in this regard. To do this, the *in vitro* suppression assay was once again employed. This assay was conducted in the presence of live CD11c$^+$ DCs and soluble α-CD3 for co-stimulation and TCR stimulation, respectively **(Fig 4.8 A)**. Efluor670-labelled effector T cells were used to allow measurement of proliferation by flow cytometry **(Fig 4.8 B)**. The difference between the assay in Chapter 3 and the present assay is the Tr1-like cell populations were FACS-sorted from IAV-infected lungs **(Fig 4.8 C)**. CD45.1$^+$ CD3$^+$ T cell division was assessed after incubation for approximately 72hrs **(Fig 4.8 D)**.

The different Tr1-like populations that accumulate in the lungs of IAV-infected mice were next tested to determine their capacity to suppress effector T cell division using the assay optimised in Chapter 3 (**Fig 4.9-DN, Fig 4.10-DP, Fig 4.11-LAG-3$^+$, Fig 4.12-CD49b$^+$**). The gating strategy for sorting Tr1-like cells from the IAV-infected lungs is shown in panel A for each figure (**Fig 4.9 A-DN, Fig 4.10 A-DP, Fig 4.11 A-LAG-3$^+$, Fig 4.12 A-CD49b$^+$**). Each of the distinct Tr1-like populations was capable of significantly suppressing effector T cell division (**Fig 4.9 B & C, Fig 4.10 B & C, Fig 4.11 B & C, Fig 4.12 B & C)** confirming that each of the four populations of FOXP3$^-$ IL-10$^+$ Tr1-like cells expressing different combinations of LAG-3 and CD49b were *bona fide* Tr1 cells. Therefore, from this point on, these populations will be referred to as Tr1 cells. The DN and CD49b$^+$ Tr1 cells exhibited statistically significant suppression at a ratio of 1:4 (Tr1 cells:effector T cells) (**Fig 4.9 B & C and Fig 4.12 B & C**). In comparison the DP and LAG-3$^+$ populations exhibited statistically significant suppression at a ratio of 1:8 (Tr1 cells:effector T cells) (**Fig 4.10 B-C & Fig 4.11 B & C**). Accordingly, each of the four Tr1 cell populations exhibited the ability to statistically significantly reduce the DI of effector T cells in the suppression assays (**Fig 4.9 D, Fig 4.10 D, Fig 4.11 D, 4.12 D**). Overall,

these experiments demonstrated that each of the Tr1 cell populations was able to suppress effector T cell division, with the DP and LAG-3$^+$ displaying the highest level of activity in this regard.

In other models, Tr1 cells have been shown to depend to a significant extent on IL-10 to elicit their suppressive effects [191], [194], [195]. To determine whether IL-10 was essential for the suppressive capacity of IAV-induced Tr1 cell populations, suppression assays were set up and incubated in the presence of an isotype control or IL-10Rα nAB. This assay was slightly different to the previous as 1x10^4 regulatory T cells and effector T cells were added per well to ensure the isotype control and nAB could be assayed within the same biological replicate. In this assay, Treg cells suppressed effector T cell division independently of IL-10 as there was no significant difference between the isotype control and the IL-10Rα nAB **(Fig 4.13 A & B)**. Statistically significant inhibition of suppression by the DP and CD49b$^+$ Tr1 cell populations was observed upon neutralisation of IL-10R **(Fig 4.13 A & B)**. In contrast, neutralisation of IL-10R had no effect on the ability of DN or LAG-3$^+$ Tr1 cells to suppress effector T cell division **(Fig 4.13 A & B)**. Together, these experiments establish that each of the four populations are *bona fide* Tr1 cells as they are capable of suppressing effector T cell division, although the dependence on IL-10 was found to differ between the populations.

4.4 There are transcriptionally distinct populations of Tr1 cells in the IAV-infected lungs.

The differences identified above in kinetics, localisation, tissue distribution, suppressive capacity, and mechanisms of suppression drove further enquiry into these Tr1 cell types. To this end, a bulk RNA sequencing experiment was undertaken to determine the global transcriptional differences between these populations. On day 7 post X-31 IAV infection CD3$^+$ CD4$^+$ CD44$^+$ FOXP3$^-$ IL-10$^+$ Tr1 cells expressing the four combinations of LAG-3 and CD49b were sorted from the lungs (gating strategy and post sort purity check shown in **Fig 4.14 A & B**). The sorted cells were lysed and RNA extracted for library preparation and sequencing. An initial analysis was conducted to determine the library size for each sample. This was consistent between all of the samples with 25-35 million reads per sample (**Fig 4.15 A**), in line with recommendations to ensure sufficient sequencing depth [340]. Next, principal component analysis (PCA) was used to visualise the variation within and between populations. PCA allows for dimensionality reduction of complex data-sets resulting in visualisation of variance in two dimensions (at a time). In the present study these were denoted PC1 and PC2 (**Fig 4.15 B**). Unexpectedly, the DN Tr1 cells varied substantially between biological replicates, but the other populations did not. The variation

within the DN population was so great it would have masked any differences between the other three populations **(Fig 4.15 B)**. The very heterogeneous DN population was therefore excluded from further analysis. After exclusion of the DN population the library sizes were unchanged (**Fig 4.16 A**). However, in the PCA plot there was clear and consistent segregation of the DP, LAG-3$^+$ and CD49b$^+$ populations based on condition (**Fig 4.16 B**). That is, in this analysis PC1 accounted for variation due to the individual mice from which the sample was sourced and PC2 accounted for the variation due to population (called condition for this analysis).

To interrogate the differences between the DN, DP, and LAG-3$^+$ Tr1 cell populations, AnnotationHub was used to align the reads to a reference C57BL/6 genome from the Ensembl Genome Browser (reference genome used was AH69210) [341]. In order to properly weight the variance in this dataset, the variance partition [342] package was used specifically for the duplicate correlations tool. This allowed for computation of a mixed linear model with a single variance component using duplicate correlation analysis. Voom with quality weights was then run, followed by the Limma tool which was used to fit the now more accurately weighted data to a linear model based on the duplicate correlation analysis [343]. At this point genes were able to be ranked by log-fold change (LFC) and p-value ($\leq$0.05). A total of 201 differentially-expressed (DE) genes (where significant differences were defined as having a p-value $\leq$0.05 and a log fold change $\geq$1 or $\leq$-1) were identified in the sequencing results. This was then refined to a list of the top 50 most significantly DE genes expressed by each of the three Tr1 cell populations. To achieve this, DE genes were ranked by p-value and then by LFC ($\geq$1) to list the most significant genes expressed by each of the three populations and the top 50 most significant genes were taken from each list and compiled into heatmaps using the Pheatmap tool [344]. This meant each population had an individual heatmap of most highly DE genes allowing direct comparison of expression with the other two populations (top 50 genes ordered by LFC) **(Fig 4.17)**. This resulted in the heatmaps for DP Tr1 cells **(Fig 4.17 A)**, LAG-3$^+$ Tr1 cells **(Fig 4.17 B)**, and CD49b$^+$ Tr1 cells **(Fig 4.17 C)**. The top 50 heatmaps determined that compared to the CD49b$^+$ population, the LAG-3$^+$ Tr1 cells DE *Lag3*, *Il10*, *Areg*, and *Tox* **(Fig 4.18 B)**. The CD49b$^+$ Tr1 cells DE *Itga2*, *P2rx7*, *Gzmm*, and *Cd226* compared to the LAG-3$^+$ population **(Fig 4.17 C)**, whereas the DP Tr1 cells were observed to express genes shared with both LAG-3$^+$ and CD49b$^+$ populations (eg. *Itga2*, *P2rx7*, *Lag3*, *Areg*, and *Tox*) **(Fig 4.17 A)**. This analysis determined that LAG-3$^+$ and CD49b$^+$ Tr1 cell populations were transcriptionally polarised, whereas the DP Tr1 cells appeared to be intermediate between these two populations.

Next, the most DE genes in each comparison were identified by comparing expression of genes between two populations at a time by using ggplot2 to generate volcano plots [345]. Significant differences were defined as having a p-value $\leq$0.05 and a log-fold change $\geq$1

or ≤-1. In each volcano plot comparison (**Fig 4.18 A**:LAG-3$^+$ v DP, **Fig 4.18 B**:CD49b$^+$ v DP, **Fig 4.18 C**:LAG-3$^+$ v CD49b$^+$) the grey dots depict genes whose expression is unchanged, the blue dots represent genes that are expressed at significantly lower levels and the red dots represent genes that are expressed at significantly higher levels, in each comparison, with the most significant DE genes labelled with gene name. The volcano plots allowed for further refinement of the list of DE genes to a smaller list of a maximum of 30 in each comparison. This resulted in a smaller list of highly DE genes for each comparison and identified different significantly DE genes in each comparison, which together with the heatmaps aided in selecting a list of genes to focus on for validation of the RNA sequencing data. It was determined from analysis of the volcano plots that the genes most DE by the LAG-3$^+$ Tr1 cells included the transcription factors *Eomes* and *Tox*, the chemokine receptor *Cxcr5*, the surface molecule *Sell* which encodes CD62L, and the effector molecule the *Areg* which encodes amphiregulin, a protein with tissue repair function **(Fig 4.18 A & C)**. In contrast, the surface receptor encoding genes *Cd226* (DNAM-1), *Klrg1*, and *P2rx7* were all more highly expressed by the CD49b$^+$ Tr1 cells compared to the DP and LAG-3$^+$ populations **(Fig 4.19 A-C)**. The CD49b$^+$ and DP Tr1 cells were also found to DE the effector molecule *Gzmm* compared to the LAG-3$^+$ Tr1 cells **(Fig 4.18 A & C)**.

Similarly to the outcome of the heatmap analyses, the result of the volcano plot analyses suggests that the LAG-3$^+$ Tr1 cells are earlier in their development as they DE genes including, *Il10*, *Eomes*, and *Sell*. In contrast, the CD49b$^+$ were more effector-like as they DE genes such as *Gzmm*, *Klrg1*, and *Cd226*. The DP Tr1 cells shared DE genes with both LAG-3$^+$ and CD49b$^+$ populations. Together, these data suggest a step-wise development of Tr1 cells from LAG-3$^+$ which converges on an intermediate DP fate before transitioning to the more terminally-differentiated CD49b$^+$ state. The implications of these findings are discussed in more detail in Chapter 5.

To delve deeper into the fundamental differences between the Tr1 cell populations, pathway analysis was conducted using ClusterprofileR [346]. This involved generating dot plots of the most different biological processes between each of the population comparisons [346]. Dot plots display the differentially-regulated pathways in a particular comparison along the Y-axis. The dots increase in size with a larger number of genes associated with that particular pathway. The colour of the dots corresponds to the adjusted p-value with the transition from blue to red representing the scale from less to more significant. This allowed clustering of the DE genes in terms of the pathway/or biological processes they correspond to in each comparison (**Fig 4.19A: LAG-3$^+$ vs DP**, **Fig 4.20A: CD49b$^+$ vs DP**, **Fig 4.21A: LAG-3$^+$ vs CD49b$^+$**). This analysis also generated cnet maps which use nodes representing each significant biological process connected to the genes associated with that pathway [346]. The size of the nodes corresponds to the number of genes associated

with that pathway. In addition, the colour of the node for each gene indicates whether it is expressed by one population compared to another. For example in the LAG-3$^+$ and DP comparison **(Fig 4.19 B)**, genes with red dots represent genes expressed more highly by the LAG-3$^+$ population and green dots correspond to genes expressed by the DP Tr1 cells but less so in the LAG-3$^+$ population. The comparisons are in the following figures **Fig 4.19 [LAG-3$^+$ vs DP], 4.20 [CD49b$^+$ vs DP], 4.21 [LAG-3$^+$ vs CD49b$^+$]**.

Comparing the LAG-3$^+$ and DP Tr1 cells the most differentially-regulated pathways were related to "extracellular space", "regulation of response to external stimulus" and "G-protein coupled receptor signalling pathways and chemotaxis" **(Fig 4.19 A & B)**. These terms suggest that the greatest differences between these Tr1 cell populations lie in their secreted molecule profile, surface receptors, and chemokine receptor expression. This was in agreement with the DE genes identified in the heatmap analysis and refined in the volcano plot analysis including *Il10*, *Gzmm*, *Sell*, *Cxcr5*, and *Ccr4* **(Fig 4.17 A & B, 4.18 A)**. In the CD49b$^+$ and DP comparison the most differentially-regulated pathways involved "extracellular space" and "cell-cell adhesion" **(Fig 4.20 A & B)**. This summarised the differences between the CD49b$^+$ and DP Tr1 cells as the differentially-expressed secreted molecules and surface molecules identified are known to be used for interactions with other cell types. These terms cover the DE genes identified between these populations including; *Cxcl16*, *Areg*, *Lag3*, *Cd226*, *Klrg1*, and *P2rx7* **(Fig 4.17 A & C, 4.18 B)**. The comparison between the LAG-3$^+$ and CD49b$^+$ Tr1 cells yielded the greatest number of differences. The most significantly differentially-regulated pathways included; "regulation of response to external stimulus", processes involved in "cell adhesion" and "chemotaxis" **(Fig 4.21 A & B)**. This was consistent with the DE genes identified in the previous analysis as secreted and surface molecules were highlighted as the most DE within this comparison and included the genes encoding secreted molecules *Ccl3*, *Ccl5*, and *Il10* and the surface molecules *Lag3*, *Itga2*, *Itgb3*, *Sell*, *Cxcr5*, and *Ccr4* **(Fig 4.17 B & C, 4.18 C)**. The pathway analysis determined that although many of the biological pathways active in DP, LAG-3$^+$, and CD49b$^+$ Tr1 cells were shared, there were still important subtle differences in their secreted molecule and surface profiles.

4.5 Validation of DE genes expressed by Tr1 cell populations in the IAV-infected lungs.

The RNA sequencing analysis led to the identification of several DE transcription factors, surface molecules and secreted molecules that required independent validation prior to further in-depth analysis. Validation of genes of interest identified in the RNA-sequencing data-set was prioritised based on potential relevance to Tr1 cell function, the size of

the difference observed in volcano plot comparisons, and the availability of reagents to evaluate protein expression. First, the expression of transcription factors at the level of protein was assessed. Between the three Tr1 cell populations there were similarities in the transcription factor landscape at the level of mRNA. Correlating with published data, Tr1 cells all coordinately expressed a number of transcription factors which are known regulate and maintain the expression of their characteristic cytokine, IL-10. This included *Cmaf*, *Prdm1*, *Irf4*, *Batf*, *Irf1*, *Ahr*, and a low level of *Eomes* (as discussed in Chapter 3, validated with counts per million [cpm] plots with the RNA sequencing data [not shown]).

DE transcription factor protein expression was validated first as small changes in expression could lead to significant alteration of cellular programming. *Eomes* stood out as LAG-3$^+$ Tr1 cells exhibited significantly higher expression compared to the DP population and was one of the greatest differences in expression by LFC (**Fig 4.18 A**). EOMES is a transcription factor that was shown to be critical for the development of Tr1 cells in a mouse model of GvHD [246]. In order to evaluate the expression of EOMES protein by the different Tr1 cell populations, each population was sorted from the lungs on day 7 post IAV infection (gating strategy shown in **Fig 4.22 A**, post-sort purity shown in **Fig 4.22 B**). Intranuclear staining of EOMES for each of the sorted Tr1 cell populations confirmed that the LAG-3$^+$ and DN populations exhibited the highest level of expression, which was restricted to a small population within each subset **(Fig 4.22 C-D)**. The RNAseq data (in counts per million of *Eomes* mRNA) confirmed that the LAG-3$^+$ displayed the highest level of *Eomes* mRNA (note that a comparison with the DN population was not possible). These data suggest the LAG-3$^+$ and DN Tr1 cells are potentially at a similar developmental stage in comparison to the DP and CD49b$^+$ populations. LAG-3$^+$ Tr1 cells were also found to DE *Tox* in the heatmap and volcano plot analyses **(Fig 4.17 A & B, Fig 4.18 A & C)**. The DP population was also found to DE *Tox* compared to the CD49b$^+$ Tr1 cells **(Fig 4.17 A)**. TOX protein expression by Tr1 cells from lungs was assessed at day 7 post-IAV infection by flow cytometry (gating strategy shown in **Fig 4.23 A)**. TOX was generally expressed by all Tr1 cell populations but not naive CD4$^+$ T cells (**Fig 4.23 B**). However, in line with the RNAseq results, there was a greater frequency of TOX$^+$ LAG-3$^+$ Tr1 cells compared to each of the other Tr1 cell populations **(Fig 4.23 B & C)**. The same trend that can be seen from TOX protein expression is observed in the cpm plot for *Tox* mRNA **(Fig 4.23 C & D)**.

Pathway analysis indicated that "extracellular space" was the most significantly differentially regulated biological pathway in the comparisons between the LAG-3$^+$ and DP populations **(Fig 4.19 A & B)** and the CD49b$^+$ and DP populations **(Fig 4.20 A & B)**. This could include production of molecules released into the extracellular space such as cytokines, chemokines, and other secreted effector molecules, or surface bound molecules which signal to other cells in the environment. When comparing the DP or LAG-3$^+$

populations to the CD49b$^+$ population *Areg* (which encodes amphiregulin, AREG) was among the most DE genes in the heatmaps and volcano plot analyses **(Fig 4.17 A & B and Fig 4.18 B & C)**. AREG is known to be produced by Treg cells in acute infection and functions to promote tissue repair [306], however, it was not previously known if Tr1 cells could produce AREG. Flow cytometric analysis of Tr1 cells from the IAV-infected lung indicated there was some expression of AREG by each of the four Tr1 cell populations compared to the unstimulated control (gating strategy and representative concatenated flow cytometry shown in **Fig 4.24 A & B**). It was found that while the CD49b$^+$ population exhibited a greater frequency of AREG$^+$ cells than the DP and LAG-3$^+$ Tr1 cells **(Fig 4.24 B & C)**, the DN Tr1 cells exhibited the greatest frequency of AREG$^+$ cells **(Fig 4.24 B & C)**. This was in contrast to the results from the RNA sequencing where the LAG-3$^+$ Tr1 cells exhibited the highest level of *Areg* mRNA expression **(Fig 4.24D)**. AREG can be in membrane bound form (also known as pro-AREG) and can also be cleaved by ADAM17 to result in the functional, secreted form which can bind to EGFR [347], [348]. One possible explanation for the discrepancy between mRNA and protein is that the CD49b$^+$ population may be in the process of down-regulating *Areg* mRNA transcription as AREG has already accumulated at the surface for possible cleavage and function. Together, these data suggest that Tr1 cells are capable of producing AREG and it does not appear to be confined to a single population.

Next, additional surface receptors that had been highlighted were examined. The heatmaps and volcano plot analyses determined that CD49b$^+$ Tr1 cells DE *Cd226* (DNAM-1) and *P2rx7*, respectively **(Fig 4.17 C** and **Fig 4.18 B & C)**. *Cd226* (DNAM-1) has been linked to Tr1 cell function by facilitating close proximity to APCs baring the ligand CD155 or CD112 [335] which allows release of Tr1 cell effector molecules close to their target cell. DNAM-1 expression is considered a characteristic of Tr1 cells. P2RX7 is a surface purogenic receptor which senses extracellular ATP to induce apoptosis that hasn't previously been implicated in Tr1 cell function. Flow cytometry was employed to interrogate the expression of DNAM-1 and P2RX7 at the protein level (gating strategy shown in **Fig 4.25 A**). DNAM-1 and P2RX7 were not expressed by naive CD4$^+$ T cells **(Fig 4.25 B)**, which were used as a negative control. DNAM-1 was most highly expressed by the CD49b$^+$ population at the level of both RNA and protein **(Fig 4.25 B-D)**, supporting the previous suggestion that CD49b$^+$ Tr1 cells are the most effector-like of the Tr1 cell populations. In keeping with the results from the RNAseq, the CD49b$^+$ Tr1 cell population also expressed the highest level of P2RX7 protein in terms of percent of cells positive **(Fig 4.25 B, E, & F)**. In general, P2RX7 was not highly expressed on the cell surface resulting in only a small number of positive cells from the CD49b$^+$ and DP populations **(Fig 4.25 B & E)**. However, as the CD49b$^+$ Tr1 cells expressed the highest level of P2RX7, this supports the notion that these cells may be up-regulating this death receptor as an end-stage

of Tr1 development.

4.6 Chapter 4 Conclusion

In this chapter, the four novel Tr1 cell populations identified in Chapter 3 based on expression of LAG-3 and CD49b, were extensively investigated. The DN Tr1 cells exhibited distinct kinetics of accumulation in the lungs as they continued to increase up to day 10 post-IAV infection. In comparison, the LAG-3$^+$, DP, and CD49b$^+$ Tr1 cells were transiently present and most abundant at day 7 post-infection. Each population of Tr1 cells exhibited differential distribution in the mLN, PB, lungs, and BALF. The LAG-3$^+$ and DP populations were the most enriched Tr1 cells in the BALF and lungs. Each of the four populations were predominately localised within the parenchyma compared to the vasculature of the IAV-infected lungs. The DP Tr1 cells were significantly more prominent within the parenchyma of the lungs compared to the other three populations. Each of the four populations also expressed TIM-3 and PD-1 with the DP showing the greatest percentage of co-inhibitory molecule expressing cells. In functional assays, each of the Tr1 cell populations sorted from IAV-infected lungs were able to suppress effector T cell division, validating their identity as *bona fide* Tr1 cells. Moreover, the LAG-3$^+$ and DP Tr1 cells suppressed effector T cell division up to a ratio of 1:8 (Tr1 cells:effector T cells). This established the LAG-3$^+$ and DP Tr1 cells as the most suppressive populations. To elicit this suppression the DP and CD49b$^+$ Tr1 cells exhibited some dependency on IL-10 to suppress effector T cell division, unlike DN and LAG-3$^+$ Tr1 cells, which exhibited no difference in suppressive capacity with the addition of α-IL-10Rα nAB to the suppression assay. Overall, this suggests that Tr1 cells from the IAV-infected lungs are not solely dependent on IL-10 to elicit suppression.

After determining differences in kinetics, distribution, co-inhibitory molecule expression, and suppressive function, a bulk RNA sequencing experiment was conducted to further interrogate the differences between the Tr1 cell populations from the IAV-infected lungs. Comparing the transcriptional landscape of Tr1 cells, 201 DE genes were identified between the DP, LAG-3$^+$, and CD49b$^+$ Tr1 cells in this analysis. The LAG-3$^+$ Tr1 cells expressed the highest level of *Eomes* and *Tox* suggesting an early differentiation state for these Tr1 cells. The CD49b$^+$ Tr1 cells exhibited the highest expression of markers associated with an effector-like phenotype such as *Gzmm* and *Cd226*. They also expressed the greatest level of the death receptor *P2rx7* suggesting the CD49b$^+$ population may represent an end-stage for Tr1 differentiation. The DP cells shared characteristics of both the LAG-3$^+$ and CD49b$^+$ Tr1 cells, and may represent the most functional, intermediate, or peak fate for Tr1 cells. Overall, the interrogation of Tr1 cells in IAV infection has resulted

in the first description of what may represent different developmental states of Tr1 cells in an acute infection model.

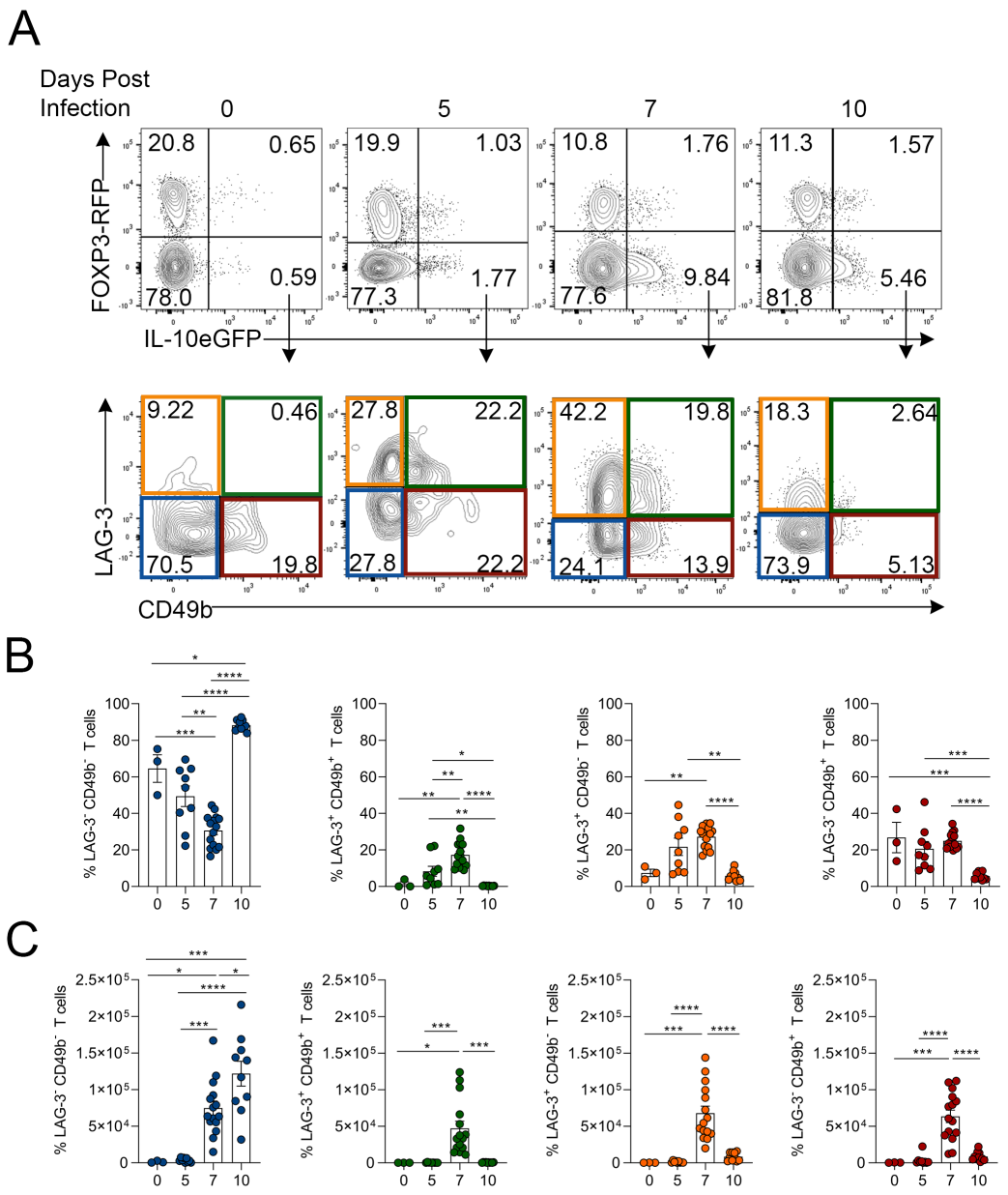

Figure 4.1: Kinetics of Tr1-like cells expressing CD49b and LAG-3 in the IAV-infected lungs.

Dual-reporter mice were infected with X-31 IAV-i.n as described (refer to **2.5.1**). On days 0 (naive), 5, 7, and 10 post-infection mice were humanely killed and lungs were harvested for FACS. (A) Concatenated representative flow cytometry depicting expression of LAG-3 and CD49b by Tr1-like cells. (B) The frequency and (C) number of LAG-3$^-$ CD49b$^-$, LAG-3$^+$ CD49b$^+$, LAG-3$^+$ CD49b$^-$, and LAG-3$^-$ CD49b$^+$ Tr1-like cells post IAV infection. Each symbol represents a different biological replicate, bars show the mean, and error bars depict +/- SEM, n=3-16 biological replicates total per time point from 3 independent experiments. Statistical analysis using One-Way ANOVA with Bonferroni's post-test (where $* = p \leq 0.05, ** = p \leq 0.01, *** = p \leq 0.001$, and $**** = p \leq 0.0001$).

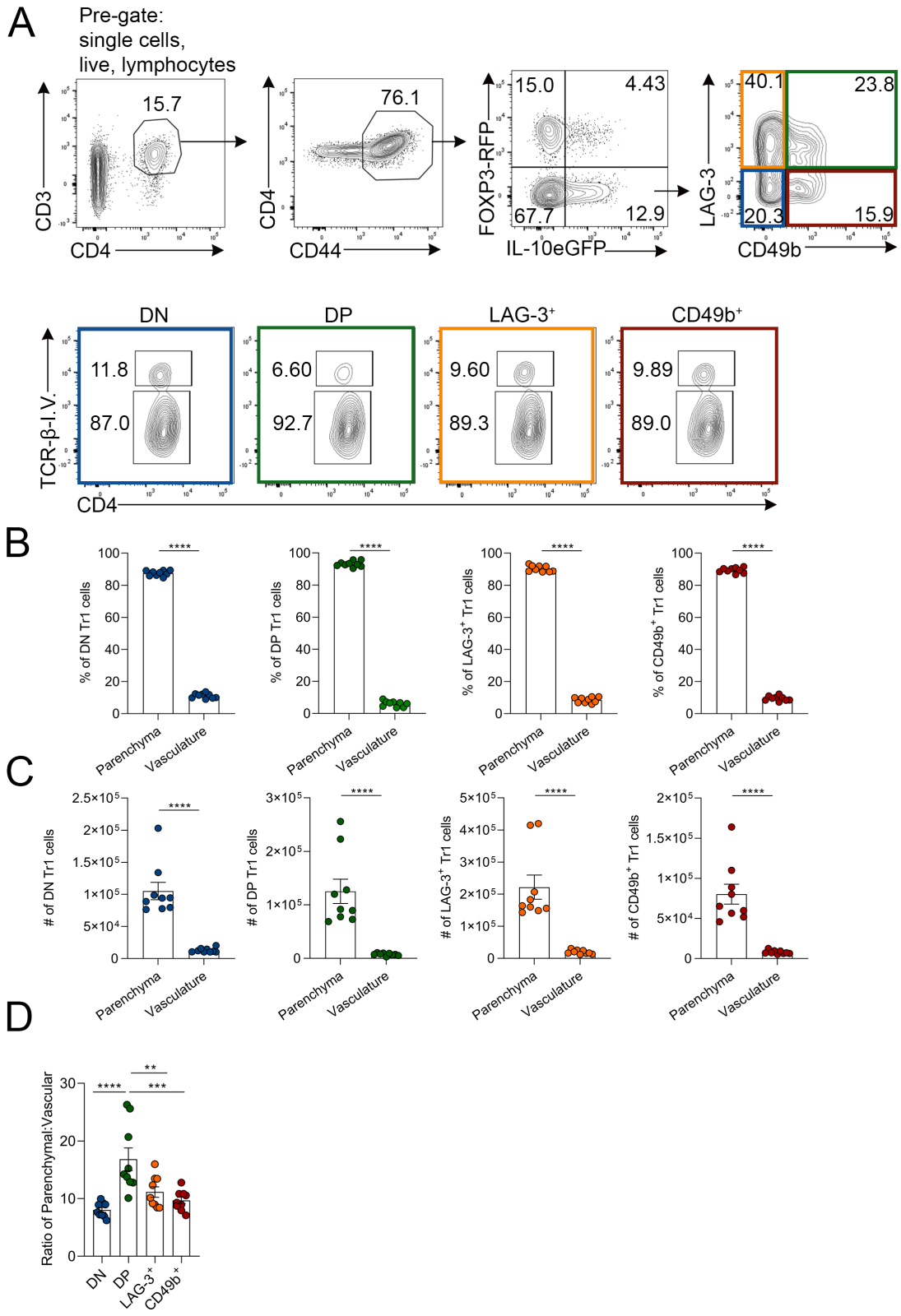
A
Pre-gate:
single cells,
live, lymphocytes
CD3
CD4
15.7
CD4
CD44
76.1
FOXP3-RFP
IL-10eGFP
15.0
4.43
67.7
12.9
LAG-3
CD49b
40.1
23.8
20.3
15.9
DN
DP
LAG-3+
CD49b+
TCR-β-I.V.
CD4
11.8
87.0
6.60
92.7
9.60
89.3
9.89
89.0
B
% of DN Tr1 cells
% of DP Tr1 cells
% of LAG-3+ Tr1 cells
% of CD49b+ Tr1 cells
Parenchyma
Vasculature
****
C
# of DN Tr1 cells
# of DP Tr1 cells
# of LAG-3+ Tr1 cells
# of CD49b+ Tr1 cells
D
Ratio of Parenchymal:Vascular
DN
DP
LAG-3+
CD49b+
**
***

Figure 4.2: Comparing the localisation of Tr1-like cell populations within the parenchyma and vasculature of IAV-infected lungs.
Dual-reporter mice were infected with X-31 IAV-i.n as described (refer to **2.5.1**). On day 7 anti-TCR-β BV421 was injected I.V for intravascular labelling prior to humane killing. (A) Concatenated representative flow cytometry gating strategy for identifying the Tr1-like cell populations based on LAG-3 and CD49b expression located in the vasculature (lower panel, top TCR-β^+ gate) and parenchyma (lower panel, bottom TCR-β^- gate) of the lungs on day 7 post IAV infection. (B) The frequency and (C) number of DN, DP, LAG-3$^+$, and CD49b$^+$ Tr1-like cells in the parenchyma and vasculature of the lungs. (D) The ratio of Tr1-like cells in the parenchyma vs the vasculature. Each symbol represents a different biological replicate, data shown as mean +/- SEM, n=9 biological replicates total from 2 independent experiments. Statistical analysis using an unpaired Student's T-test (B & C), and one-way ANOVA with Bonferroni's post-test (D) (where $^{**} = p \leq 0.01, ^{***} = p \leq 0.001$, and $^{****} = p \leq 0.0001$).

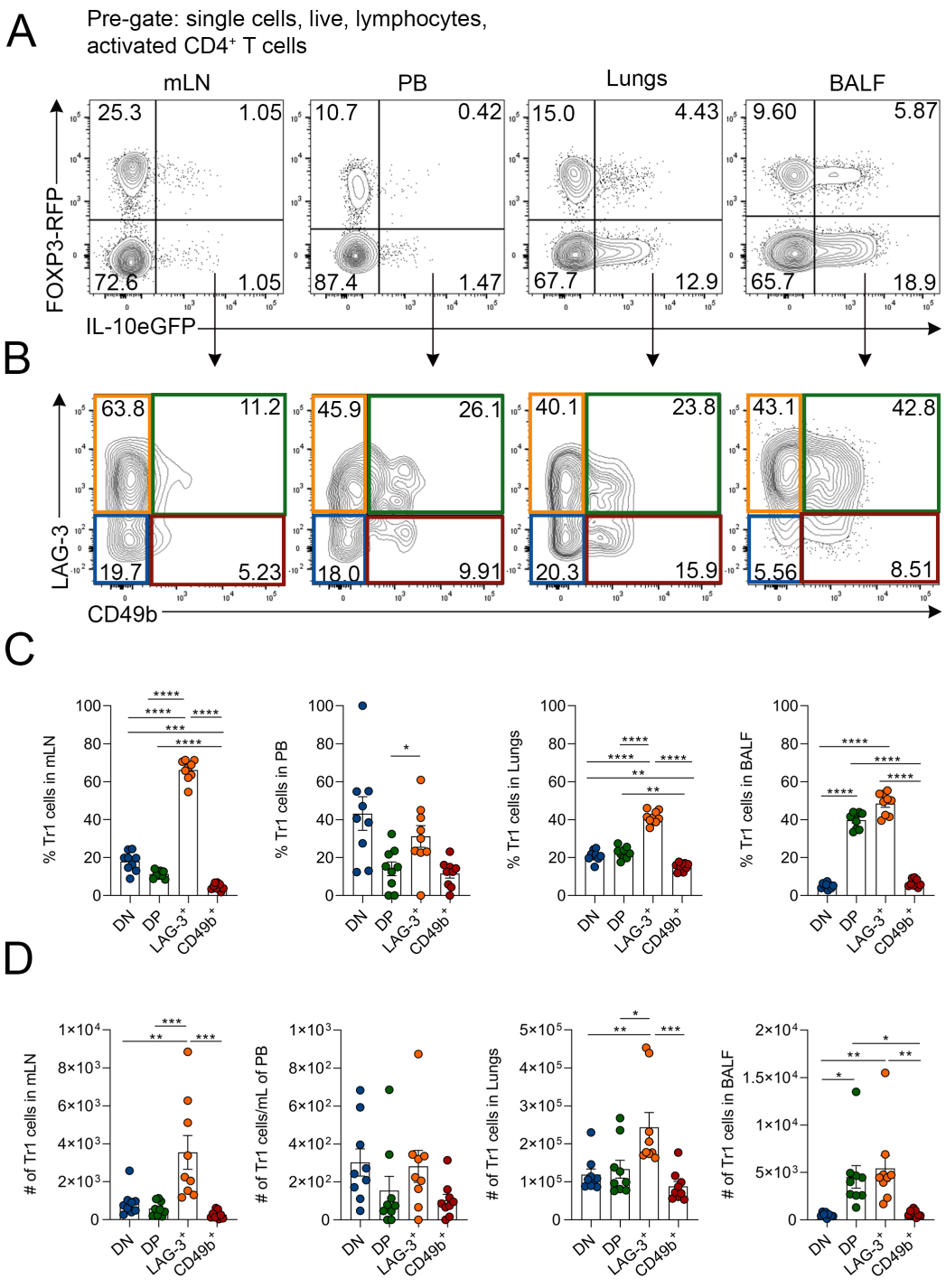
A
Pre-gate: single cells, live, lymphocytes, activated CD4+ T cells
mLN
PB
Lungs
BALF
FOXP3-RFP
IL-10eGFP
25.3
1.05
72.6
1.05
10.7
0.42
87.4
1.47
15.0
4.43
67.7
12.9
9.60
5.87
65.7
18.9
B
LAG-3
CD49b
63.8
11.2
19.7
5.23
45.9
26.1
18.0
9.91
40.1
23.8
20.3
15.9
43.1
42.8
5.56
8.51
C
% Tr1 cells in mLN
% Tr1 cells in PB
% Tr1 cells in Lungs
% Tr1 cells in BALF
DN
DP
LAG-3+
CD49b+
D
# of Tr1 cells in mLN
# of Tr1 cells/mL of PB
# of Tr1 cells in Lungs
# of Tr1 cells in BALF

Figure 4.3: Distribution of Tr1-like cell populations between the mLN, PB, lungs and BALF at day 7 post IAV infection.

Dual-reporter mice were infected with X-31 IAV-i.n as described (refer to **2.5.1**). On day 7 post-infection the mLN, PB, lungs, and BALF were harvested for analysis by flow cytometry. (A) Concatenated representative flow cytometry displaying $CD4^+$ T cell populations expressing FOXP3 and IL-10. (B) Concatenated representative flow cytometry showing LAG-3 and CD49b expression by Tr1-like cells on day 7 post-infection. (C) Frequency and (D) number of DN, DP, $LAG\text{-}3^+$ and $CD49b^+$ Tr1-like cells in the mLN, PB, lungs, and BALF. Each symbol represents a different biological replicate, data shown as mean +/- SEM, n=9 biological replicates total from 2 independent experiments. Statistical analysis using one-way ANOVA with Bonferroni's post-test (where $^* = p \leq 0.05, ^{**} = p \leq 0.01, ^{***} = p \leq 0.001$, and $^{****} = p \leq 0.0001$).

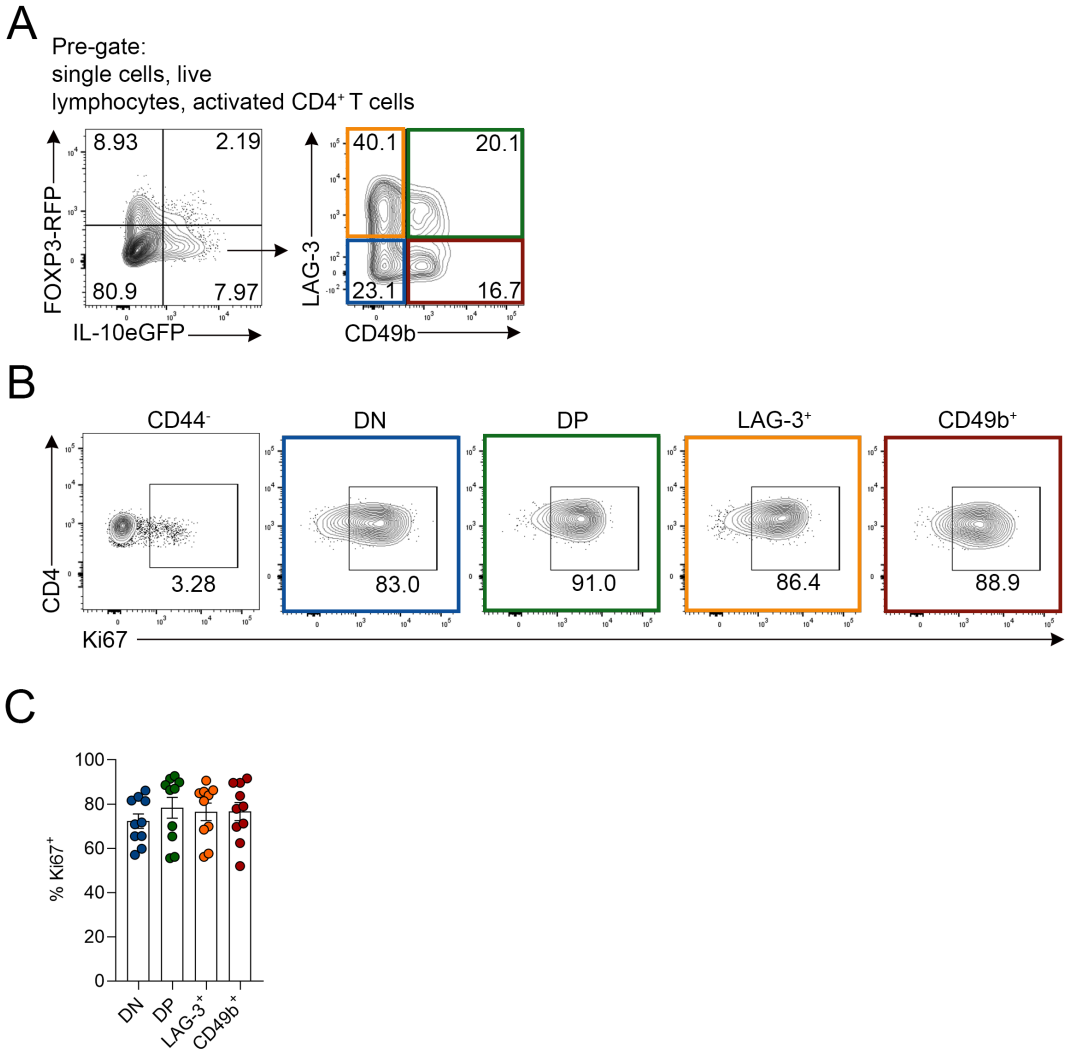

Figure 4.4: The proliferative capacity of Tr1-like populations from the IAV-infected lungs.

Dual-reporter mice were infected with X-31 IAV-i.n as described (refer to **2.5.1**). On day 7 post-infection the lungs were harvested for proliferation analysis by flow cytometry. (A) Concatenated representative flow cytometry gating strategy of the four Tr1-like cell populations in the lungs on day 7 post-infection. (B) Flow cytometry depicting expression of intra-nuclear Ki67 by DN, DP, LAG-3$^+$, and CD49b$^+$ Tr1-like cells. (C) Frequency of Ki67$^+$ of each of the Tr1-like populations. Each symbol is a different biological replicate, data shown as mean +/- SEM, n=10 biological replicates total from 2 independent experiments. Statistical analysis using one-way ANOVA with Bonferroni's post-test (no statistical difference between the four populations).

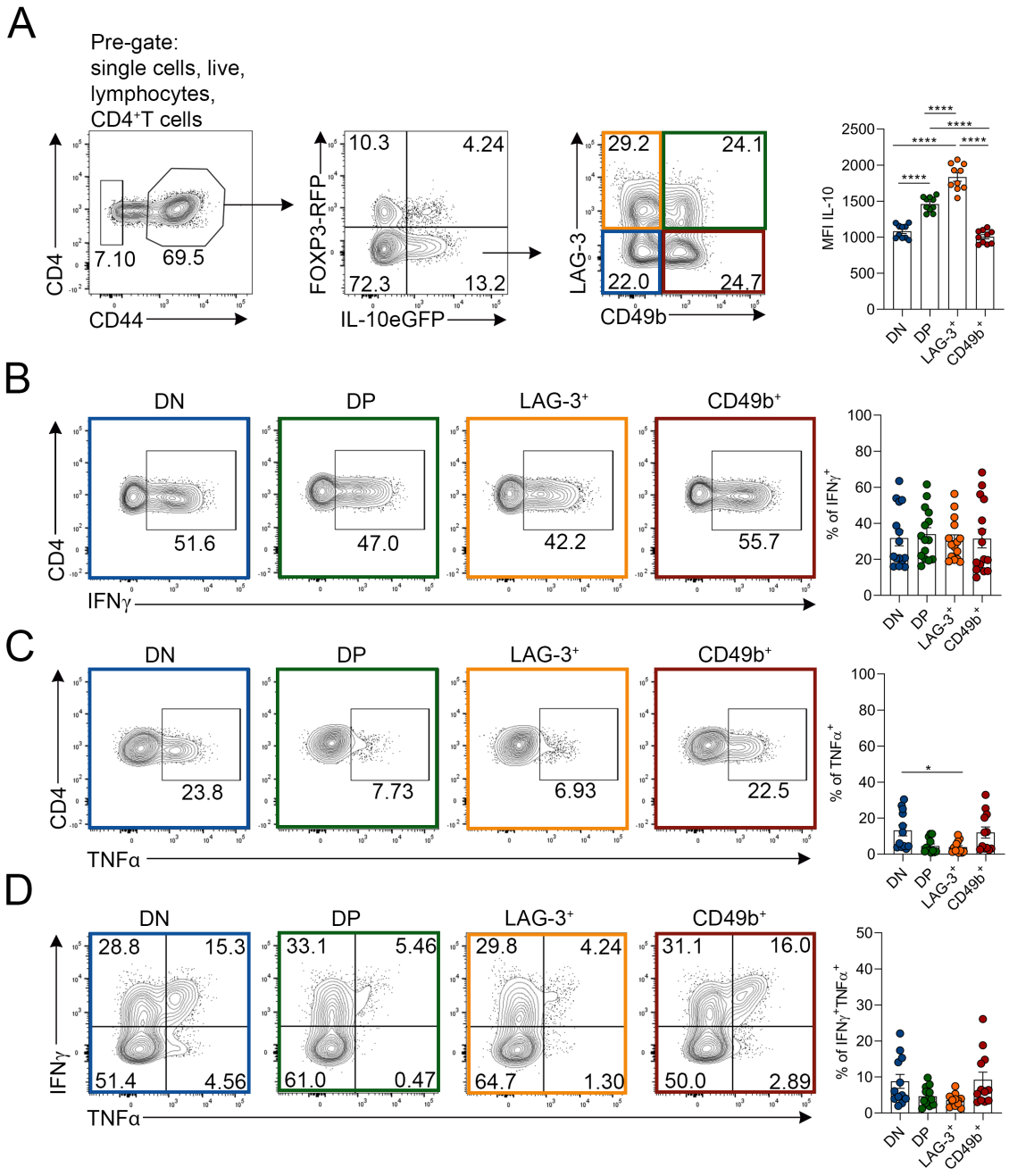

Figure 4.5: Pro-inflammatory cytokine production by Tr1-like populations post IAV infection.

Dual-reporter mice were infected with X-31 IAV-i.n as described (refer to **2.5.1**). On day 7 post-infection the lungs were harvested for analysis by flow cytometry. (A) gating strategy for identification of Tr1-like cell populations defined by LAG-3 and CD49b and quantitation of IL-10 MFI for each population. Representative concatenated flow cytometry of Tr1-like cell populations expressing (B) IFNγ, (C) TNFα, and (D) co-expression of IFNγ and TNFα. Quantitation of the frequency of cytokine$^+$ Tr1-like cells displayed to the right. Each symbol is a different biological replicate, data shown as mean +/- SEM, n=10-15 biological replicates total from 2 independent experiments. Statistical analysis using one-way ANOVA with Bonferroni's post-test (where $^* = p \leq 0.05$ and $^{****} = p \leq 0.0001$).

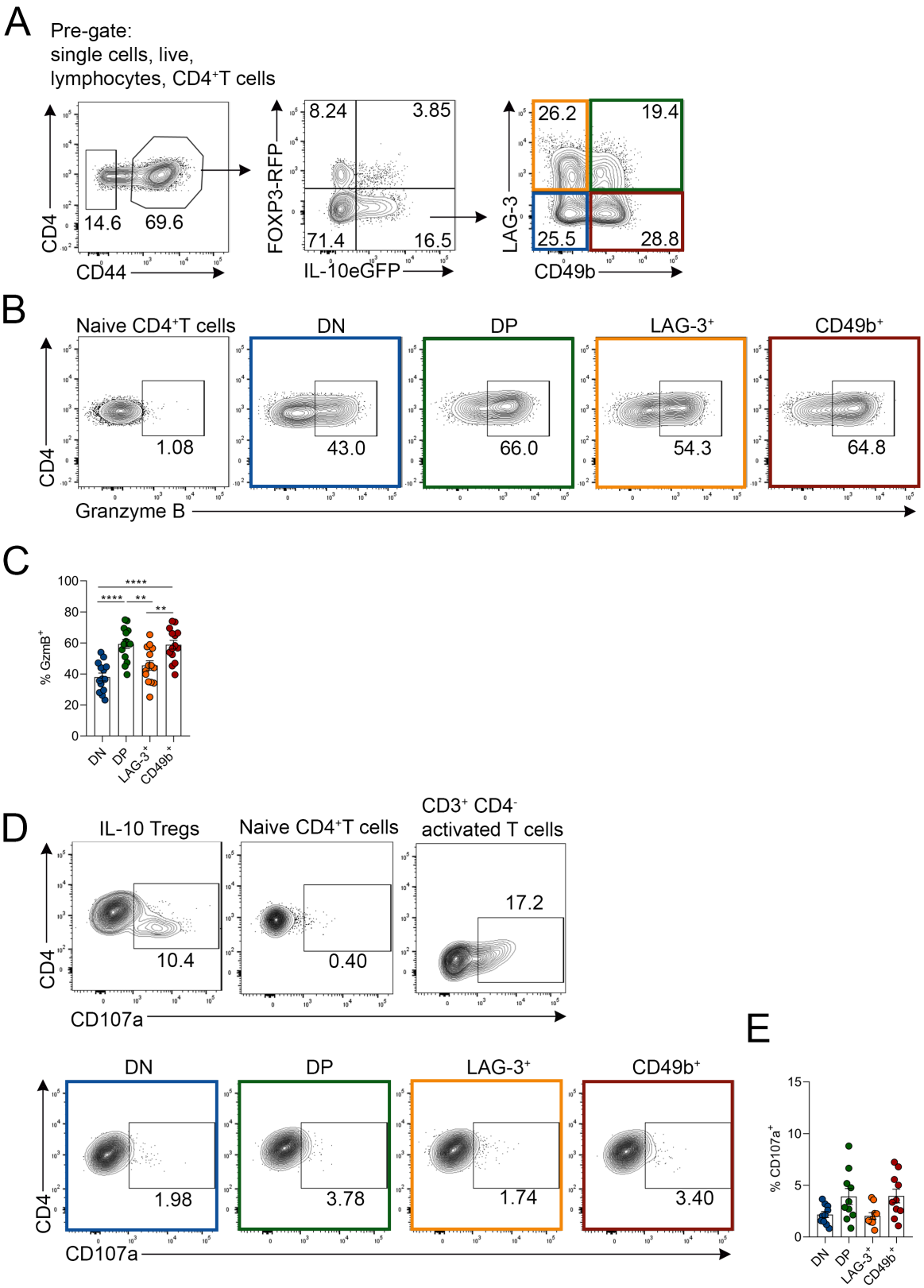
A
Pre-gate:
single cells, live,
lymphocytes, CD4+T cells
CD4
CD44
14.6
69.6
FOXP3-RFP
IL-10eGFP
8.24
3.85
71.4
16.5
LAG-3
CD49b
26.2
19.4
25.5
28.8
B
Naive CD4+T cells
DN
DP
LAG-3+
CD49b+
CD4
Granzyme B
1.08
43.0
66.0
54.3
64.8
C
% GzmB+
DN
DP
LAG-3+
CD49b+
D
IL-10 Tregs
Naive CD4+T cells
CD3+ CD4-
activated T cells
CD4
CD107a
10.4
0.40
17.2
DN
DP
LAG-3+
CD49b+
1.98
3.78
1.74
3.40
E
% CD107a+

Figure 4.6: Granzyme B production and CD107a expression by each of the Tr1-like cell populations.

Dual-reporter mice were infected with X-31 IAV-i.n as described (refer to **2.5.1**). On day 7 post-infection the lungs were harvested for analysis by flow cytometry. (A) Gating strategy used to identify Tr1-like cells from the IAV-infected lungs on day 7 post-infection. (B) Representative, concatenated flow cytometry depicting Granzyme B production by Tr1-like cell populations compared to naive $CD4^+$ T cells. (C) Quantitation of the percentage of Granzyme B producing Tr1-like cells. (D) Positive control (IL-10 Treg cells), negative control (naive $CD4^+$ T cells), and second positive control (activated $CD3^+$ $CD4^-$ T cells) for CD107a expression. Representative, concatenated flow cytometry showing CD107a expression by Tr1-like cells. (E) Frequency of Tr1-like cells expressing CD107a. Each symbol is a different biological replicate, data shown as mean +/- SEM, n=10 biological replicates total from 2 independent experiments. Statistical analysis with one-way ANOVA using Bonferroni's post test (where $^{**} = p \leq 0.01$ and $^{****} = p \leq 0.0001$).

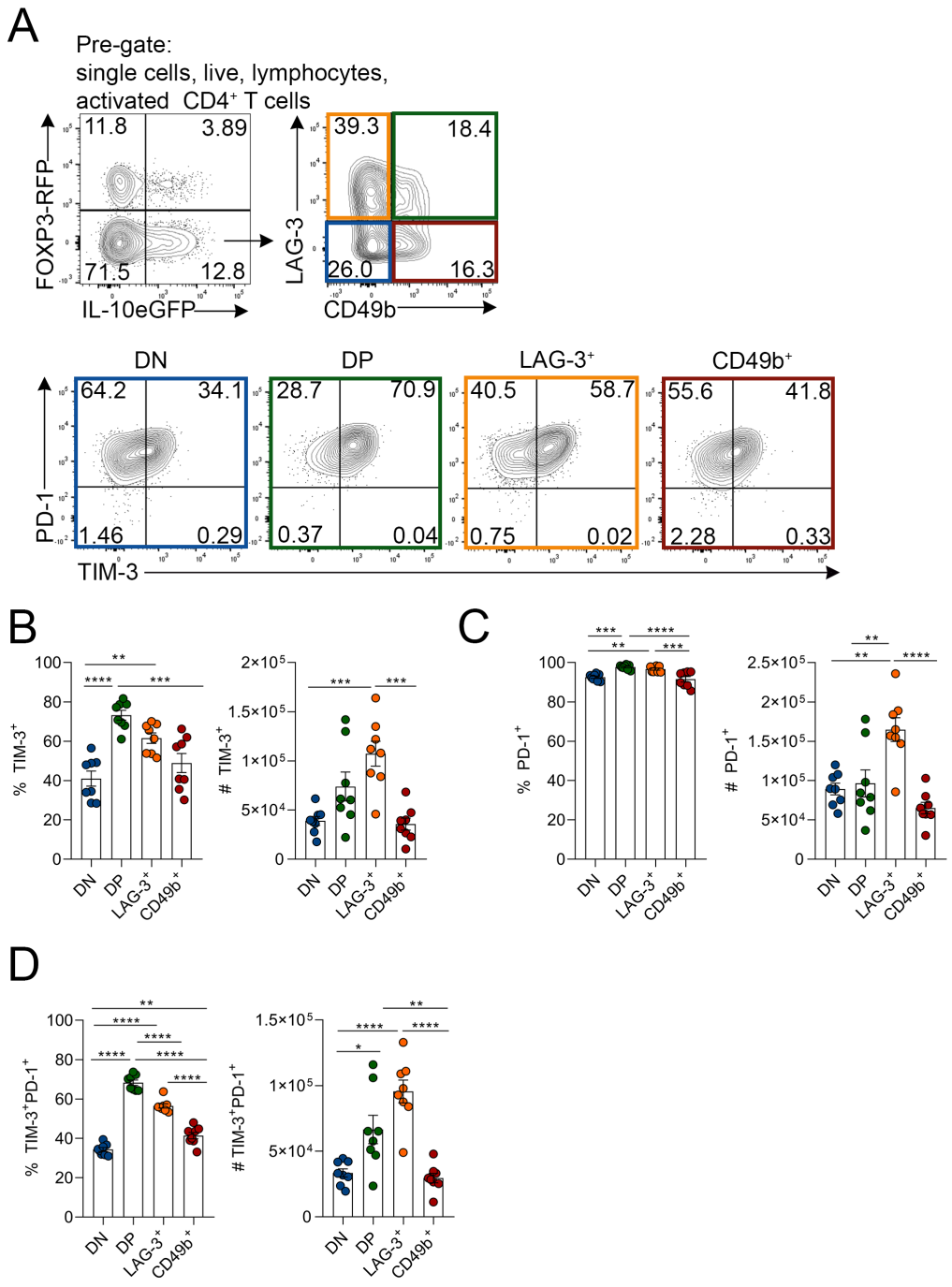

Figure 4.7: Co-inhibitory molecule expression by Tr1-like cells post IAV infection.

Dual-reporter mice were infected with X-31 IAV-i.n as described (refer to **2.5.1**). On day 7 post-infection the lungs were harvested for analysis by flow cytometry. (A) Concatenated flow cytometry showing the gating strategy for Tr1-like cells and expression of the co-inhibitory molecules PD-1 and TIM-3. (B) Frequency and number of TIM-3$^+$ Tr1-like cells. (C) Frequency and number of PD-1$^+$ Tr1-like cells. (D) Frequency and number of TIM-3$^+$ PD-1$^+$ co-expressing Tr1-like cells. Each symbol is a different biological replicate, data shown as mean +/- SEM, n=8 biological replicates total from 2 independent experiments. Statistical analysis using one-way ANOVA with Bonferroni's correction. (where $* = p \leq 0.05, ** = p \leq 0.01, *** = p \leq 0.001$, and $**** = p \leq 0.0001$).

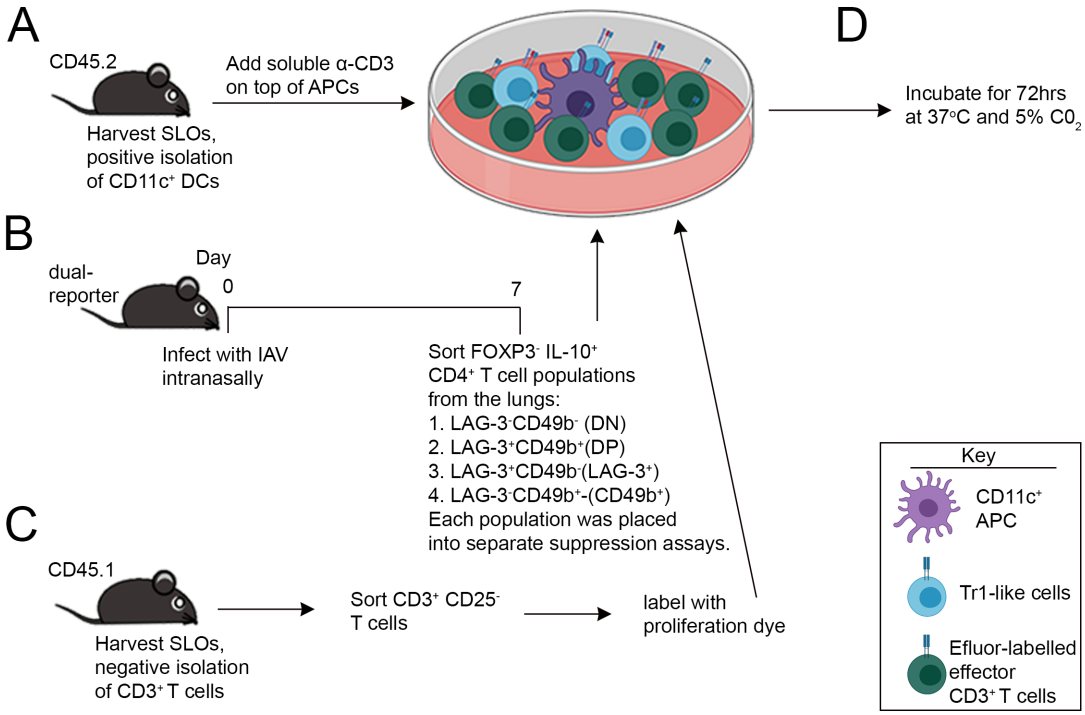

Figure 4.8: Ex-vivo Tr1-like cells suppression assay experimental schematic.

(A) For suppression assays SLOs were harvested from naive CD45.2 mice, CD11c$^+$ DCs were enriched by positive isolation and 5x10^3 were added to each well of the suppression assay. Next, 1μg/mL α-CD3 (purified 2C11) was added on top of APCs. (B) Seven days prior to collection of CD11c$^+$ DCs and naive CD3$^+$ T cells, dual-reporter mice were infected with X-31 IAV-i.n as described (refer to **2.5.1**). On day 7 post-infection the LAG-3 and CD49b-expressing Tr1-like populations were sorted by FACS from the lungs and placed into suppression assays (2x10^4 cells for the 1:1 ratio of regulatory T cells: effector T cells). (C) SLOs were also harvested from CD45.1 mice and CD3$^+$ T cells were enriched by negative selection. CD3$^+$ CD25$^-$ T cells were then sorted by FACS and labelled with Efluor670 proliferation dye. These cells were then added into suppression assays (2x10^4/well). (D) Suppression assays were incubated for approximately 72 hours before analysis using flow cytometry to detect effector T cell proliferation.

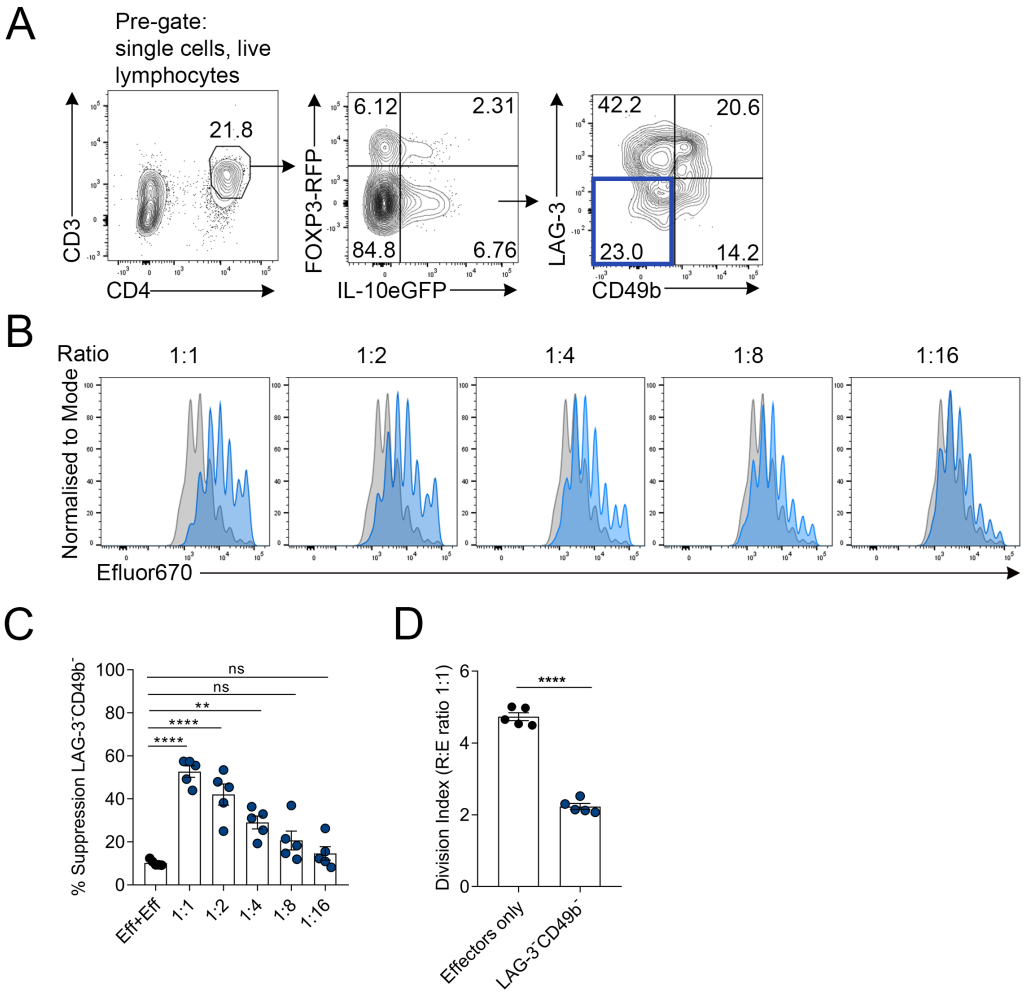

Figure 4.9: Suppressive function of DN Tr1-like cells sorted from IAV-infected lungs on day 7 post-infection.

(A) Dual-reporter mice were infected with X-31 IAV as described (refer to **2.5.1**). Gating strategy for FACS-sorting DN Tr1-like cells from the lungs at day 7 post-infection. (B) Representative flow cytometry showing the proliferation of Efluor670-labelled $CD3^+$ $CD25^-$ effector T cells with APCs and α-CD3 alone (grey histogram) or in the presence of DN Tr1-like cells (blue histogram) at a ratios of 1:1, 1:2, 1:4, 1:8 and 1:16 (Tr1-like cells: effector T cells). Where 1:1 ratio = $2x10^4$ regulatory T cells:$2x10^4$ effector T cells. (C) The percentage suppression of effector T cell division at each ratio of Tr1-like cells:effector T cells compared to effector T cells cultured at a 1:1 ratio with effector T cells (Eff+Eff). (D) DI of effector T cells cultured with APCs and α-CD3 alone or with Tr1-like cells at a 1:1 ratio. Each symbol represents a different biological replicate, data shown as mean +/- SEM, n=5 biological replicates total from 3 independent experiments. Statistical analysis using (C) one-way ANOVA with Bonferroni's post-test and (D) an unpaired Student's T-test (where $** = p \leq 0.01$ and $**** = p \leq 0.0001$).

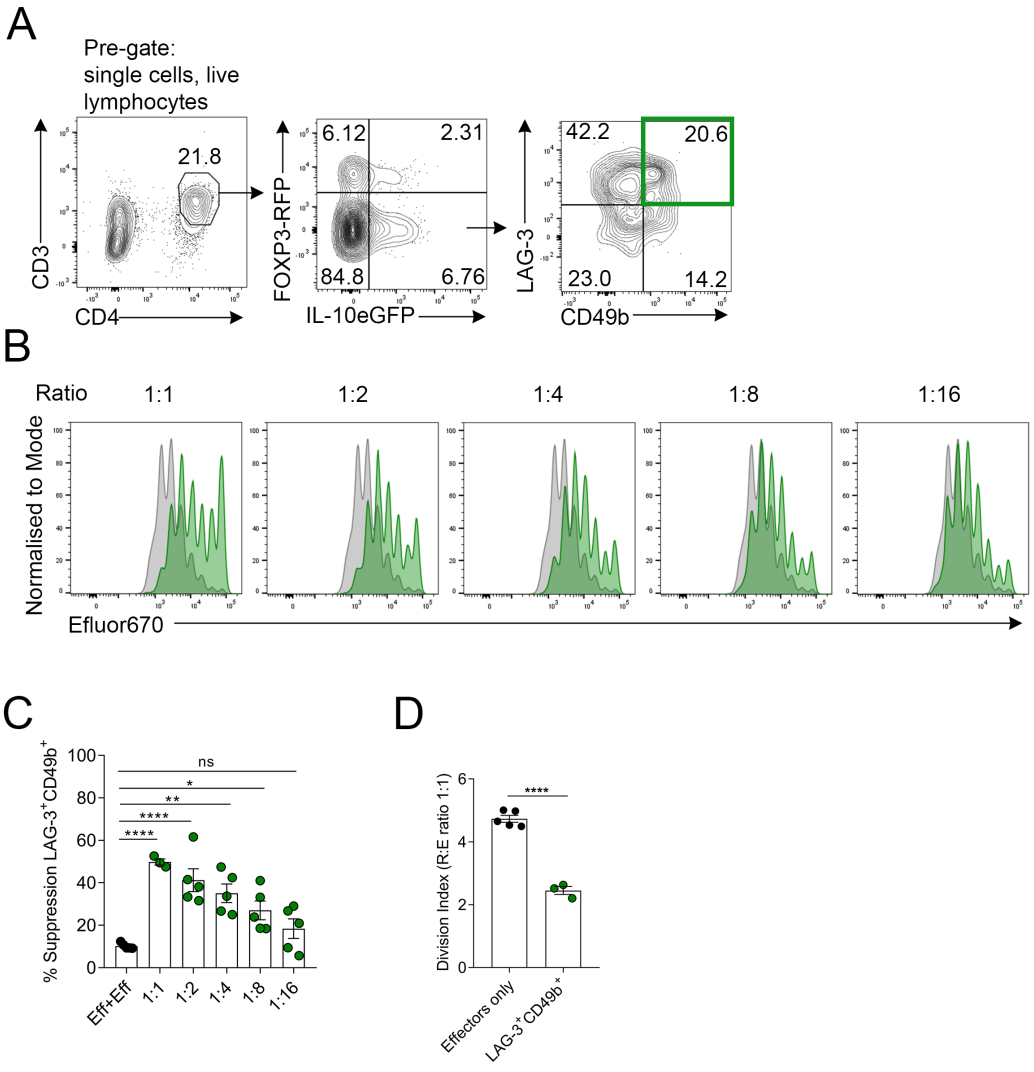

Figure 4.10: Suppressive function of DP Tr1-like cells sorted from IAV-infected lungs on day 7 post-infection.

(A) Dual-reporter mice were infected with X-31 IAV as described (refer to **2.5.1**). Gating strategy for FACS-sorting DP Tr1-like cells from the lungs at day 7 post-infection. (B) Representative flow cytometry showing the proliferation of Efluor670-labelled $CD3^+$ $CD25^-$ effector T cells with APCs and α-CD3 alone (grey histogram) or in the presence of DP Tr1-like cells (green histogram) at a ratios of 1:1, 1:2, 1:4, 1:8 and 1:16 (Tr1-like cells:effector T cells). Where 1:1 ratio = $2x10^4$ regulatory T cells:$2x10^4$ effector T cells. (C) The percentage suppression of effector T cell division at each ratio of Tr1-like cells:effector T cells compared to effector T cells cultured at a 1:1 ratio with effector T cells (Eff+Eff).(D) DI of effector T cells cultured with APCs and α-CD3 alone or with Tr1-like cells at a 1:1 ratio. Each symbol represents a different biological replicate, data shown as mean +/- SEM, n=3-5 biological replicates total from 3 independent experiments. Statistical analysis using (C) one-way ANOVA with Bonferroni's post-test and (D) an unpaired Student's T-test (where $^* = p \leq 0.05, ^{**} = p \leq 0.01$, and $^{****} = p \leq 0.0001$).

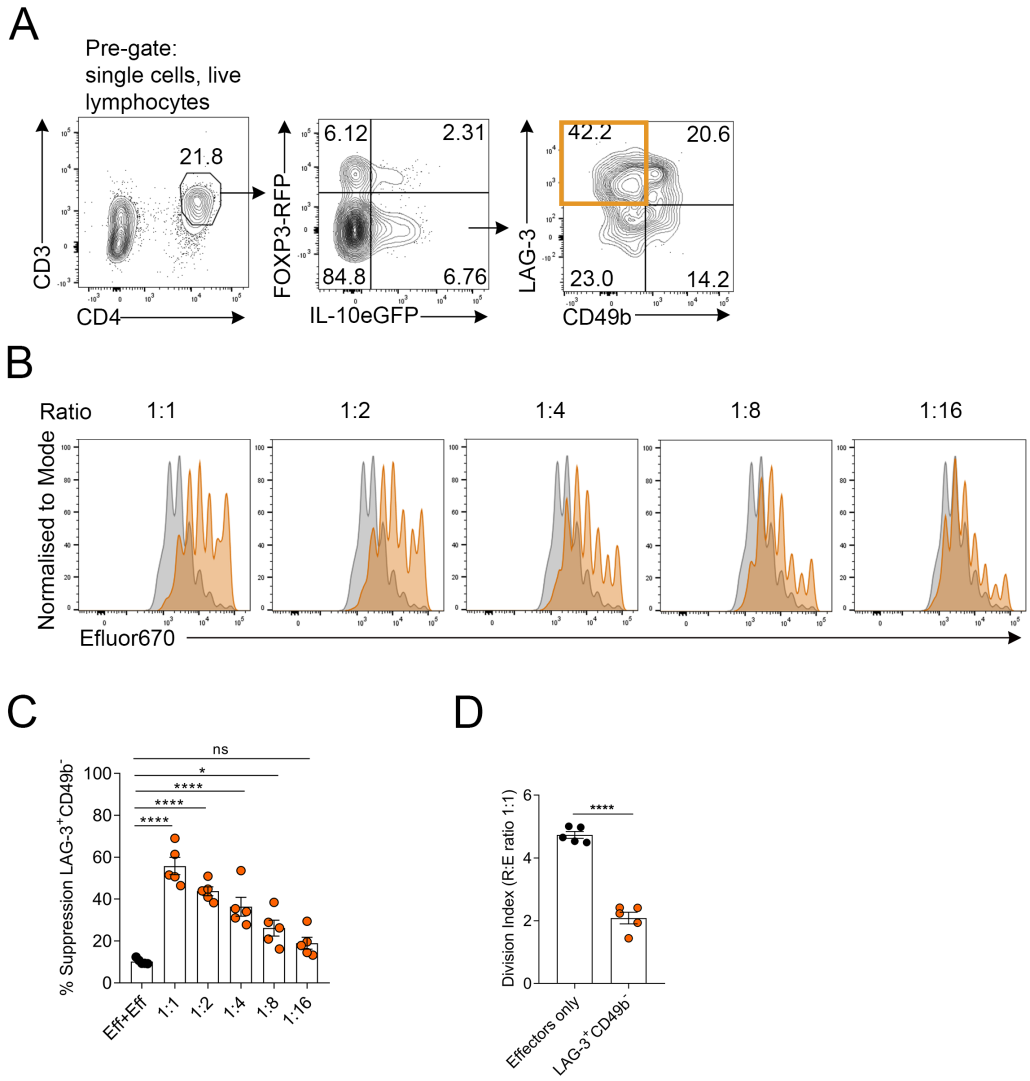

Figure 4.11: Suppressive function of LAG-3$^+$ Tr1-like cells sorted from IAV-infected lungs on day 7 post-infection.

(A) Dual-reporter mice were infected with X-31 IAV as described (refer to **2.5.1**). Gating strategy for FACS-sorting LAG-3$^+$ Tr1-like cells from the lungs at day 7 post-infection. (B) Representative flow cytometry showing the proliferation of Efluor670-labelled CD3$^+$ CD25$^-$ effector T cells with APCs and α-CD3 alone (grey histogram) or in the presence of LAG-3$^+$ Tr1-like cells (orange histogram) at a ratios of 1:1, 1:2, 1:4, 1:8 and 1:16 (Tr1-like cells:effector T cell). Where 1:1 ratio = 2x10^4 regulatory T cells:2x10^4 effector T cells. (C) The percentage suppression of effector T cell division at each ratio of Tr1-like cells:effector T cells compared to effector cells cultured at a 1:1 ratio with effector T cells (Eff+Eff). (D) DI of effector T cells cultured with APCs and α-CD3 alone or with Tr1-like cells at a 1:1 ratio. Each symbol represents a different biological replicate, data shown as mean +/- SEM, n=5 biological replicates total from 3 independent experiments. Statistical analysis using (C) one-way ANOVA with Bonferroni's post-test and (D) an unpaired Student's T-test (where $^* = p \leq 0.05$ and $^{****} = p \leq 0.0001$).

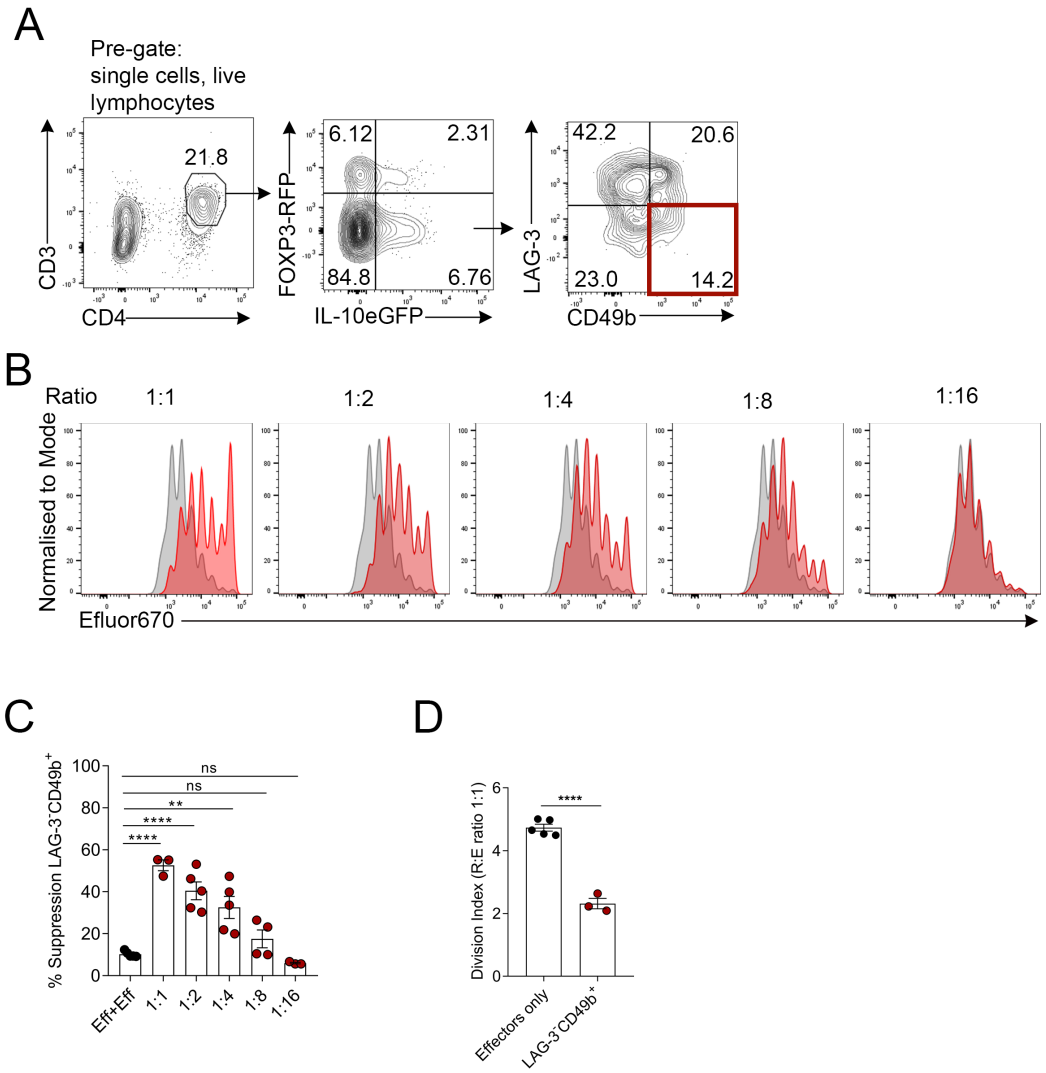

Figure 4.12: Suppressive function of CD49b$^+$ Tr1-like cells sorted from IAV-infected lungs on day 7 post-infection.

(A) Dual-reporter mice were infected with X-31 IAV as described (refer to **2.5.1**). Gating strategy for FACS-sorting CD49b$^+$ Tr1-like cells from the lungs at day 7 post-infection. (B) Representative flow cytometry showing the proliferation of Efluor670-labelled CD3$^+$ CD25$^-$ effector T cells with APCs and α-CD3 alone (grey histogram) or in the presence of CD49b$^+$ Tr1-like cells (red histogram) at a ratios of 1:1, 1:2, 1:4, 1:8 and 1:16 (Tr1-like cells:effector T cell). Where 1:1 ratio = 2x10^4 regulatory T cells:2x10^4 effector T cells. (C) The percentage suppression of effector T cell division at each ratio of Tr1-like cells:effector T cells compared to effector T cells cultured at a 1:1 ratio with effector T cells (Eff+Eff). (D) DI of effector T cells cultured with APCs and α-CD3 alone or with Tr1-like cells at a 1:1 ratio. Each symbol represents a different biological replicate, data shown as mean +/- SEM, n=3-5 biological replicates total from 3 independent experiments. Statistical analysis using (C) one-way ANOVA with Bonferroni's post-test and (D) an unpaired Student's T-test (where $** = p \leq 0.01$ and $**** = p \leq 0.0001$).

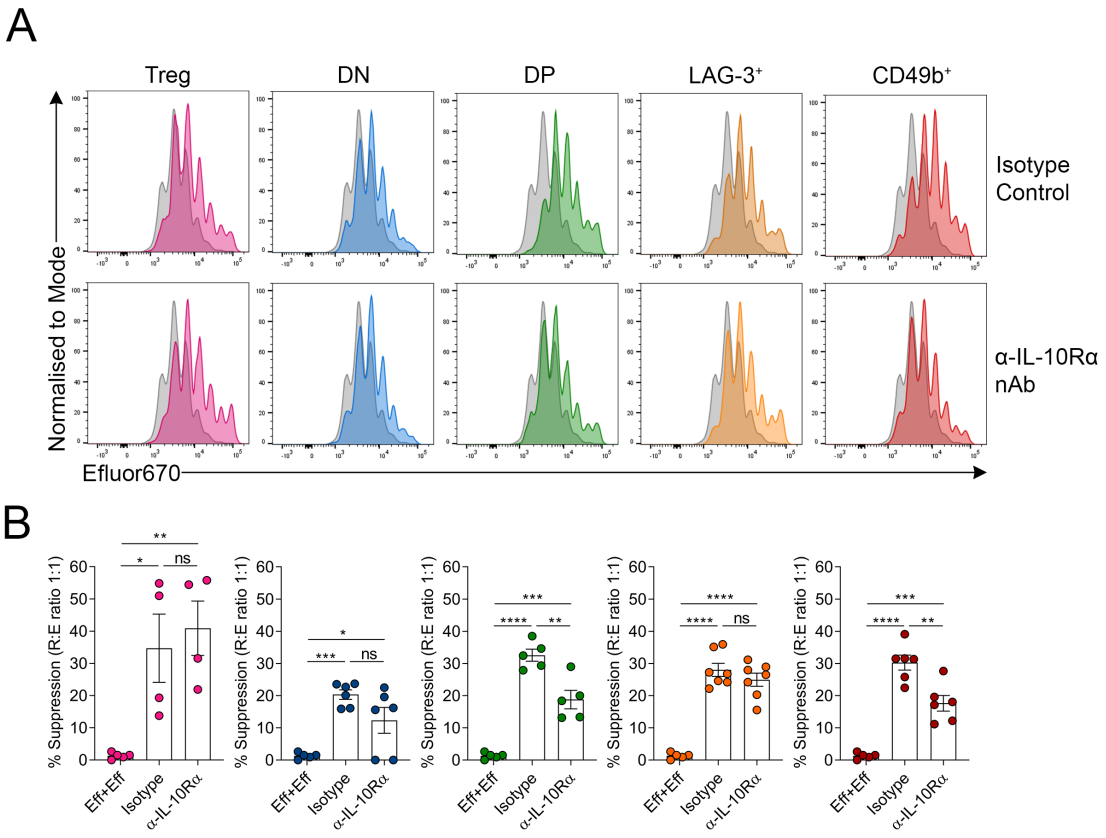

Figure 4.13: Dependence of Tr1 cell populations on IL-10 to elicit Suppression of effector T cell division.

(A) Representative flow cytometry depicting division of labelled effector T cells either with APCs and α-CD3 alone depicted as grey histograms, or co-cultured with Treg cells (FACS-sorted from naive dual-reporter SLOs) or each of the Tr1 cell populations (FACS-sorted on day 7 post IAV-infection from the lungs) depicted in coloured histograms. The ratio used was 1:1 (where 1:1 ratio = $1x10^4$ regulatory T cells:$1x10^4$ effector T cells). Suppression assay was conducted in the presence of an isotype control (α-rat IgG) or α-IL-10Rα nAB. Data are shown as mean +/- SEM, n=4-7 technical replicates from 3 independent experiments. Statistical analysis using one-way ANOVA with Bonferroni's post-test (where $* = p \leq 0.05, ** = p \leq 0.01, *** = p \leq 0.001$, and $**** = p \leq 0.0001$).

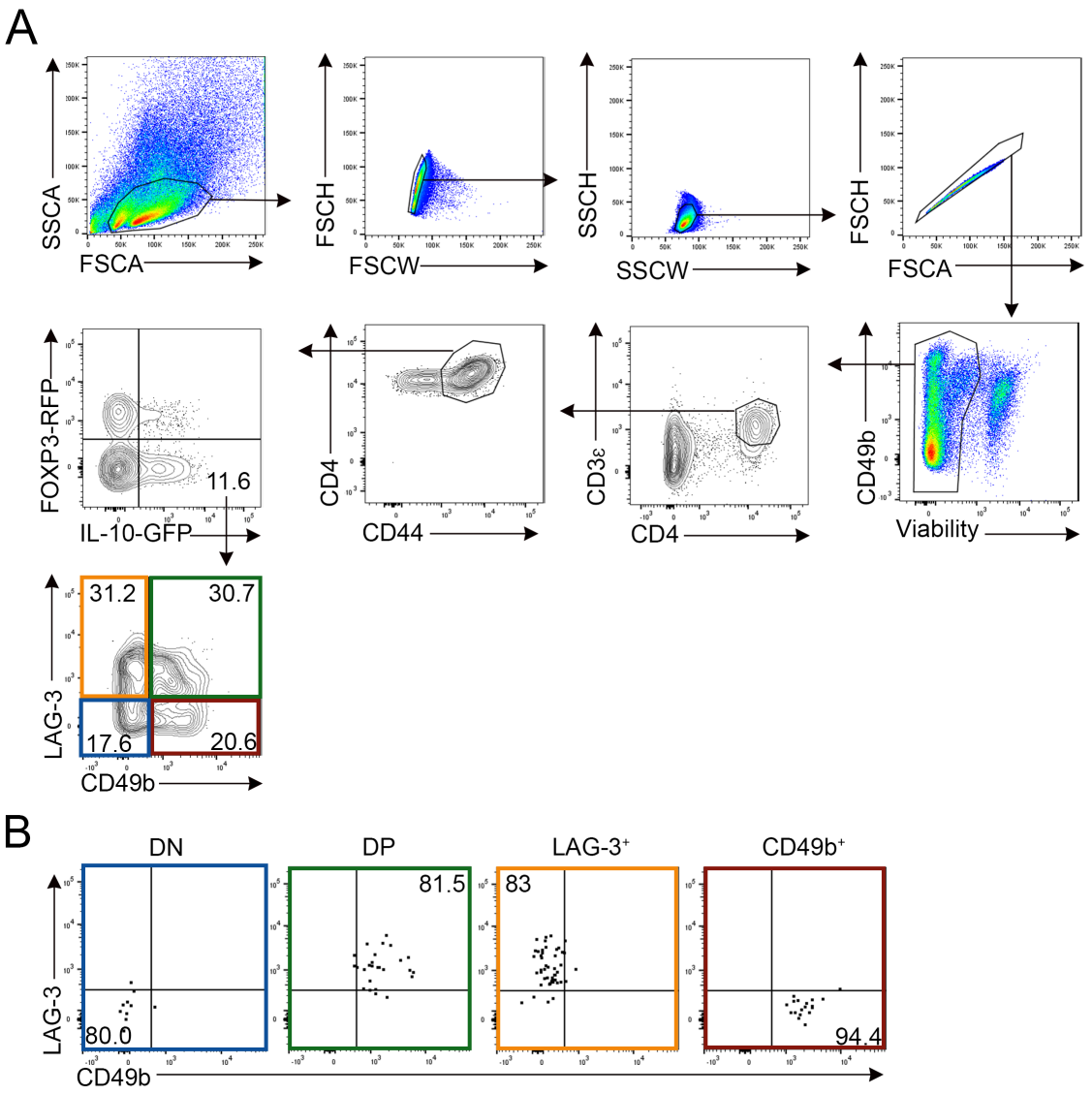

Figure 4.14: FACS-sort of Tr1 cell populations from the IAV-infected lungs for RNA Sequencing.

Dual-reporter mice were infected with X-31 IAV as described (refer to **2.5.1**). (A) Representative flow cytometry gating strategy for FACS-sorting FOXP3^{-} IL-10^{+} CD4^{+} DN, DP, LAG-3^{+}, and CD49b^{+} Tr1 cell populations for RNA-sequencing. (B) Representative plots showing purity of the populations post sorting. Initially, the four Tr1 cell populations were sorted from n=6 biological replicates, in 2 independent experiments, after RNA preparation and QC analysis was conducted by Novogene two biological replicates were excluded due to lower RNA quality. This narrowed the biological replicates to 4 samples per population for RNA sequencing.

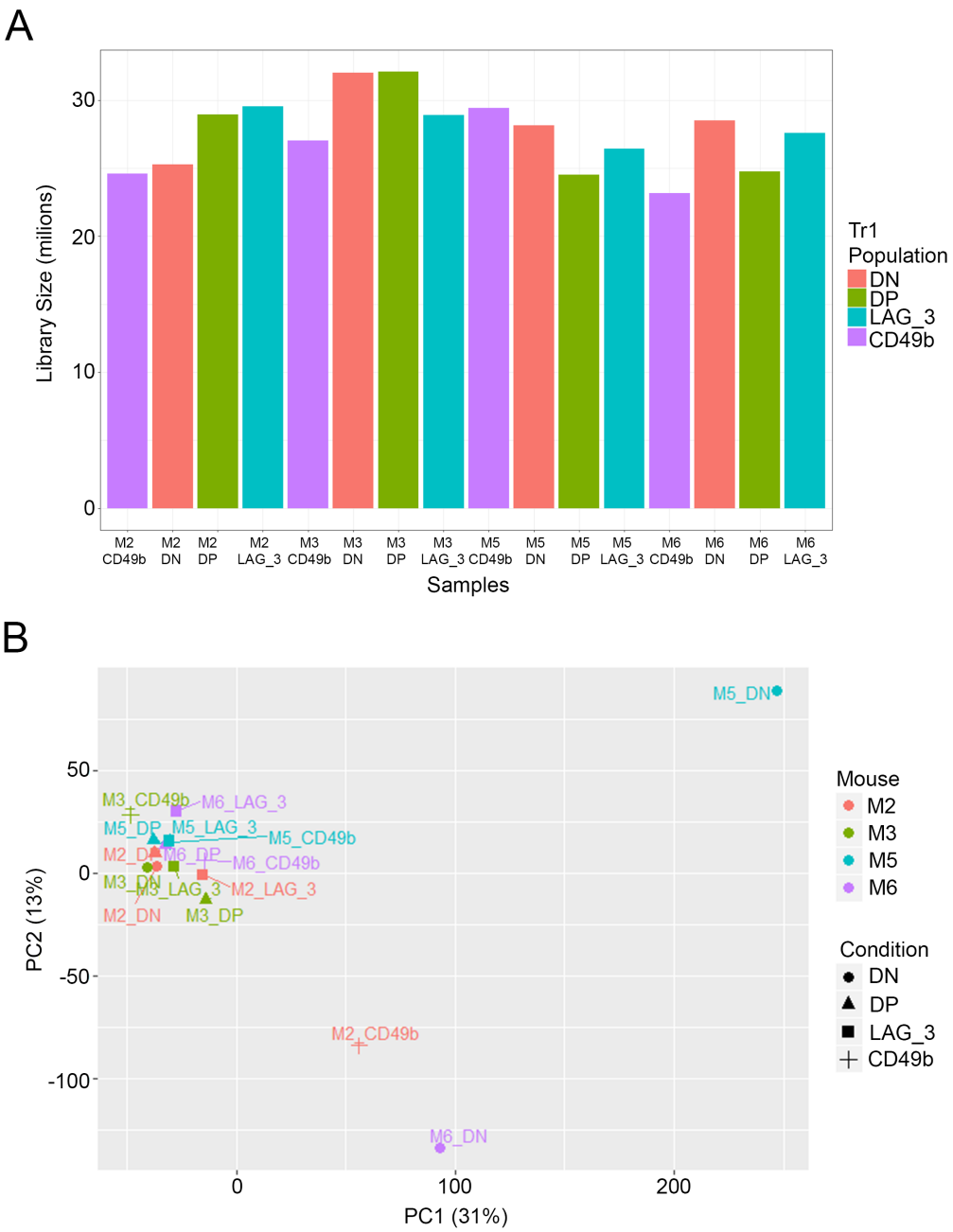

Figure 4.15: Measurement of library size and principal component analysis of variance.

(A) Library sizes for each of the four biological replicates of the four Tr1 cell populations (in counts per million, per sample). (B) Principal component analysis (PCA) representing the sources of variation between individual samples. For the PCA an individual mouse is represented by a shape and each Tr1 population is represented by a colour to visualise variance based on population and biological replicate, n=4 biological replicates total for each population.

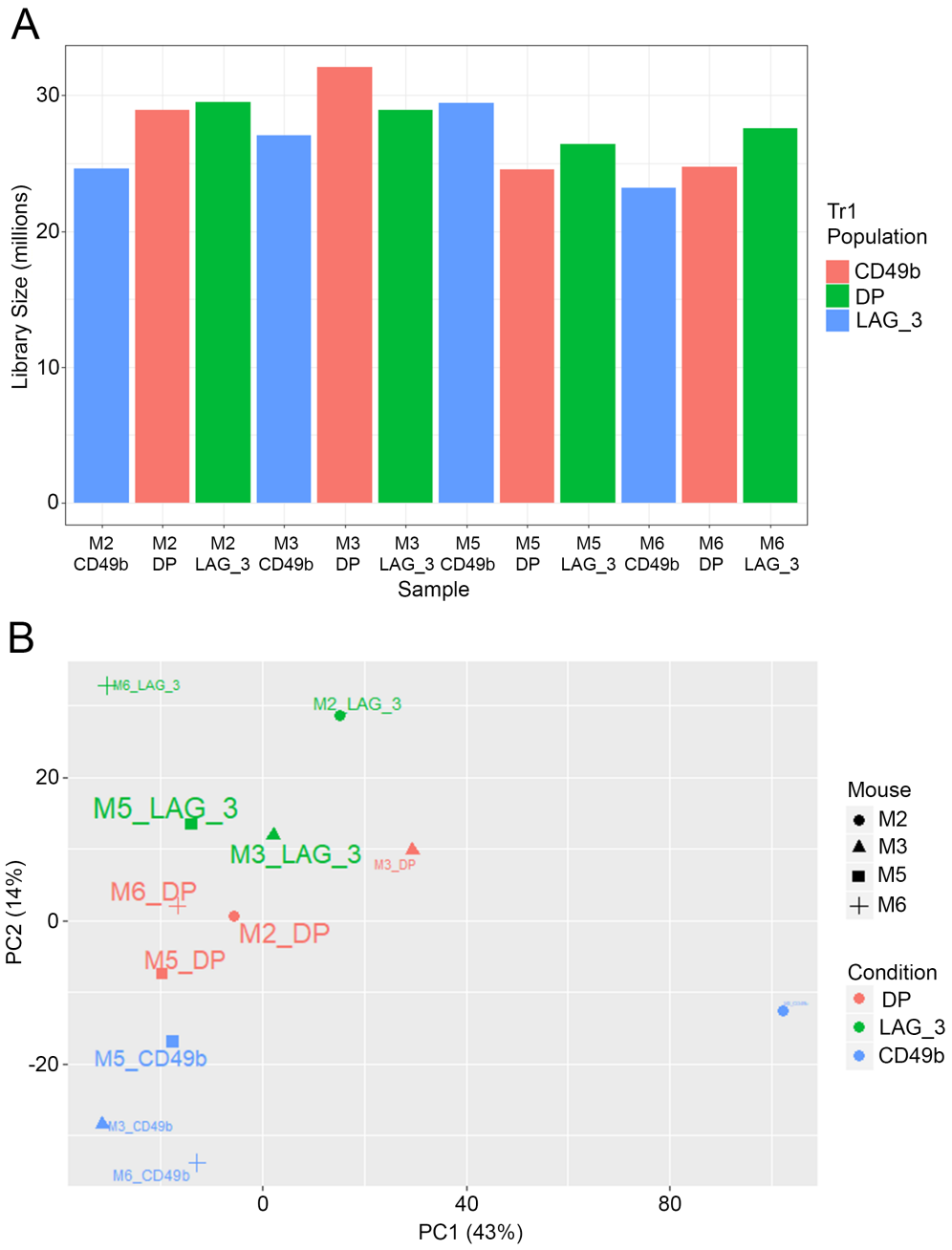

Figure 4.16: Measurement of library size and principal component analysis of variance after removal of DN population.
(A) Library sizes for each of the four biological replicates of the three Tr1 cell populations after excluding the DN population in counts per million (CPM), per sample. (B) PCA plot representing the sources of variation between individual samples (PC1= mouse, PC2= condition), n=4 biological replicates total for each population.

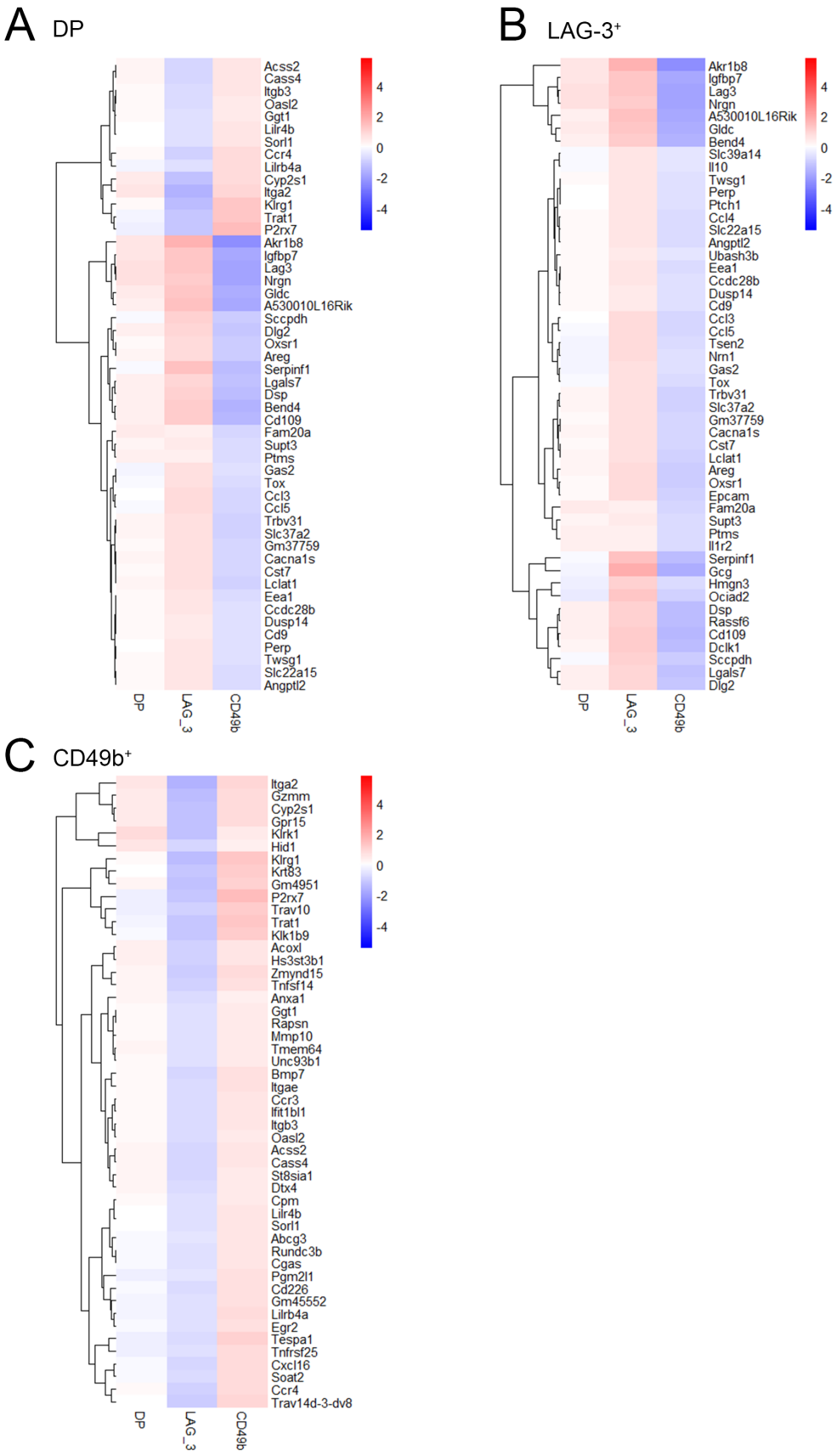
A DP
Acss2
Cass4
Itgb3
Oasl2
Ggt1
Lilr4b
Sorl1
Ccr4
Lilrb4a
Cyp2s1
Itga2
Klrg1
Trat1
P2rx7
Akr1b8
Igfbp7
Lag3
Nrgn
Gldc
A530010L16Rik
Sccpdh
Dlg2
Oxsr1
Areg
Serpinf1
Lgals7
Dsp
Bend4
Cd109
Fam20a
Supt3
Ptms
Gas2
Tox
Ccl3
Ccl5
Trbv31
Slc37a2
Gm37759
Cacna1s
Cst7
Lclat1
Eea1
Ccdc28b
Dusp14
Cd9
Perp
Twsg1
Slc22a15
Angptl2
4
2
0
-2
-4
DP
LAG_3
CD49b
B LAG-3+
Akr1b8
Igfbp7
Lag3
Nrgn
A530010L16Rik
Gldc
Bend4
Slc39a14
Il10
Twsg1
Perp
Ptch1
Ccl4
Slc22a15
Angptl2
Ubash3b
Eea1
Ccdc28b
Dusp14
Cd9
Ccl3
Ccl5
Tsen2
Nrn1
Gas2
Tox
Trbv31
Slc37a2
Gm37759
Cacna1s
Cst7
Lclat1
Areg
Oxsr1
Epcam
Fam20a
Supt3
Ptms
Il1r2
Serpinf1
Gcg
Hmgn3
Ociad2
Dsp
Rassf6
Cd109
Dclk1
Sccpdh
Lgals7
Dlg2
4
2
0
-2
-4
DP
LAG_3
CD49b
C CD49b+
Itga2
Gzmm
Cyp2s1
Gpr15
Klrk1
Hid1
Klrg1
Krt83
Gm4951
P2rx7
Trav10
Trat1
Klk1b9
Acoxl
Hs3st3b1
Zmynd15
Tnfsf14
Anxa1
Ggt1
Rapsn
Mmp10
Tmem64
Unc93b1
Bmp7
Itgae
Ccr3
Ifit1bl1
Itgb3
Oasl2
Acss2
Cass4
St8sia1
Dtx4
Cpm
Lilr4b
Sorl1
Abcg3
Rundc3b
Cgas
Pgm2l1
Cd226
Gm45552
Lilrb4a
Egr2
Tespa1
Tnfrsf25
Cxcl16
Soat2
Ccr4
Trav14d-3-dv8
4
2
0
-2
-4
DP
LAG_3
CD49b

Figure 4.17: Heatmaps of the top 50 DE genes expressed by each of the three Tr1 cell populations.

Heatmaps generated in R studio using the pheatmap tool from DE genes list ordered by p-value ($p \leq 0.05$) and LFC (on the basis of LFC ≥ 1). Based on these parameters, heatmaps are presented as DE genes expressed by the (A) DP Tr1 cells, (B) LAG-3^+ Tr1 cells, and (C) $CD49b^+$ Tr1 cells from the IAV-infected lungs compared to each of the other populations. For each population the top 50 DE genes were plotted in an individual heatmap.

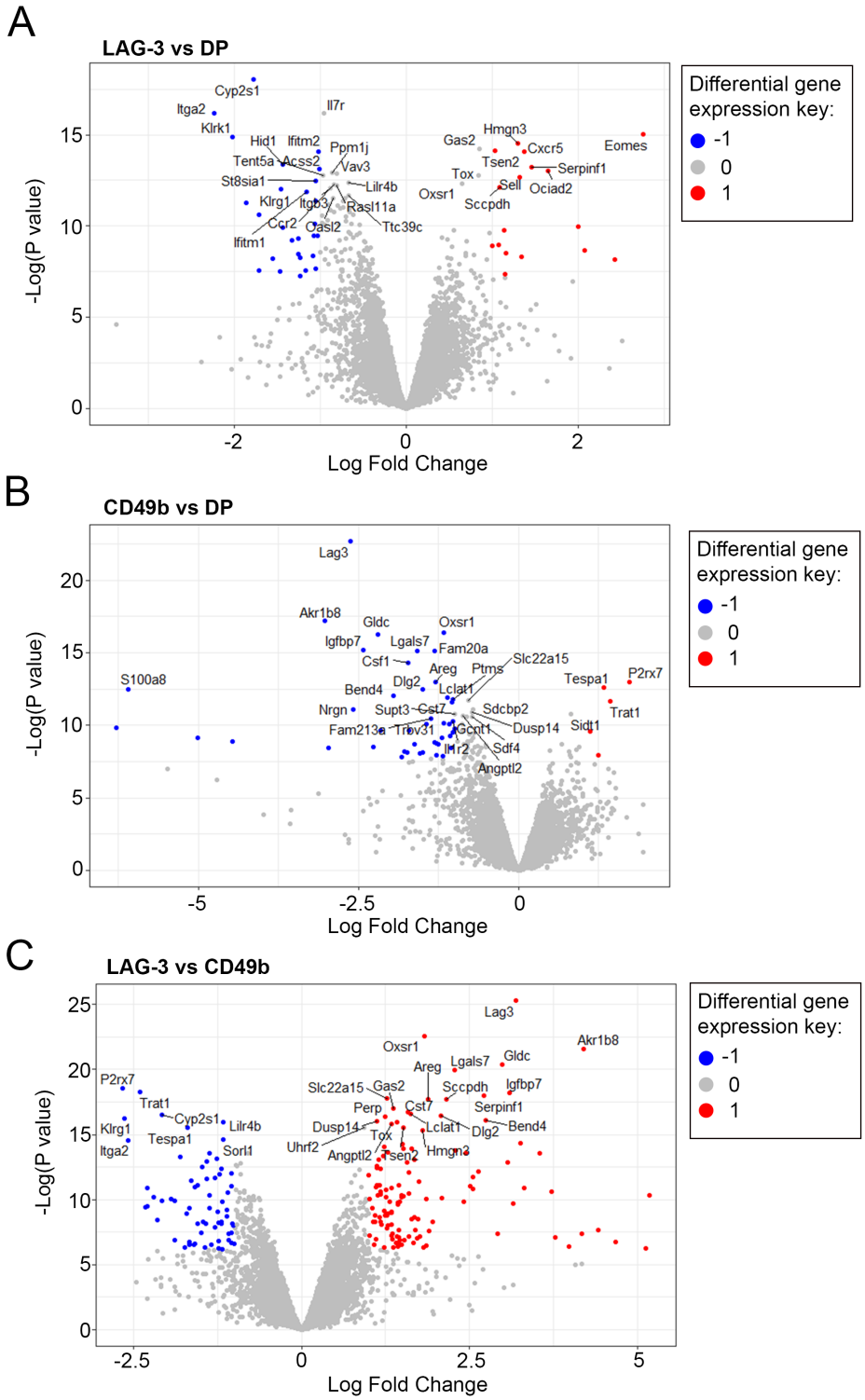

Figure 4.18: Volcano plots displaying the most DE genes between each comparison of the Tr1 cell populations.

Volcano plots identifying the most DE genes in each comparison of the three populations. These were generated using the ggplot2 tool which used DE gene lists ranked by significance based on p-value and LFC. Comparisons between (A) LAG-3$^+$ and DP, (B) CD49b$^+$ and DP and (C) LAG-3$^+$ and CD49b$^+$ populations. The criteria for significant differences were p$\leq$0.05 and a logfc of $\leq$ -1 or $\geq$ 1.

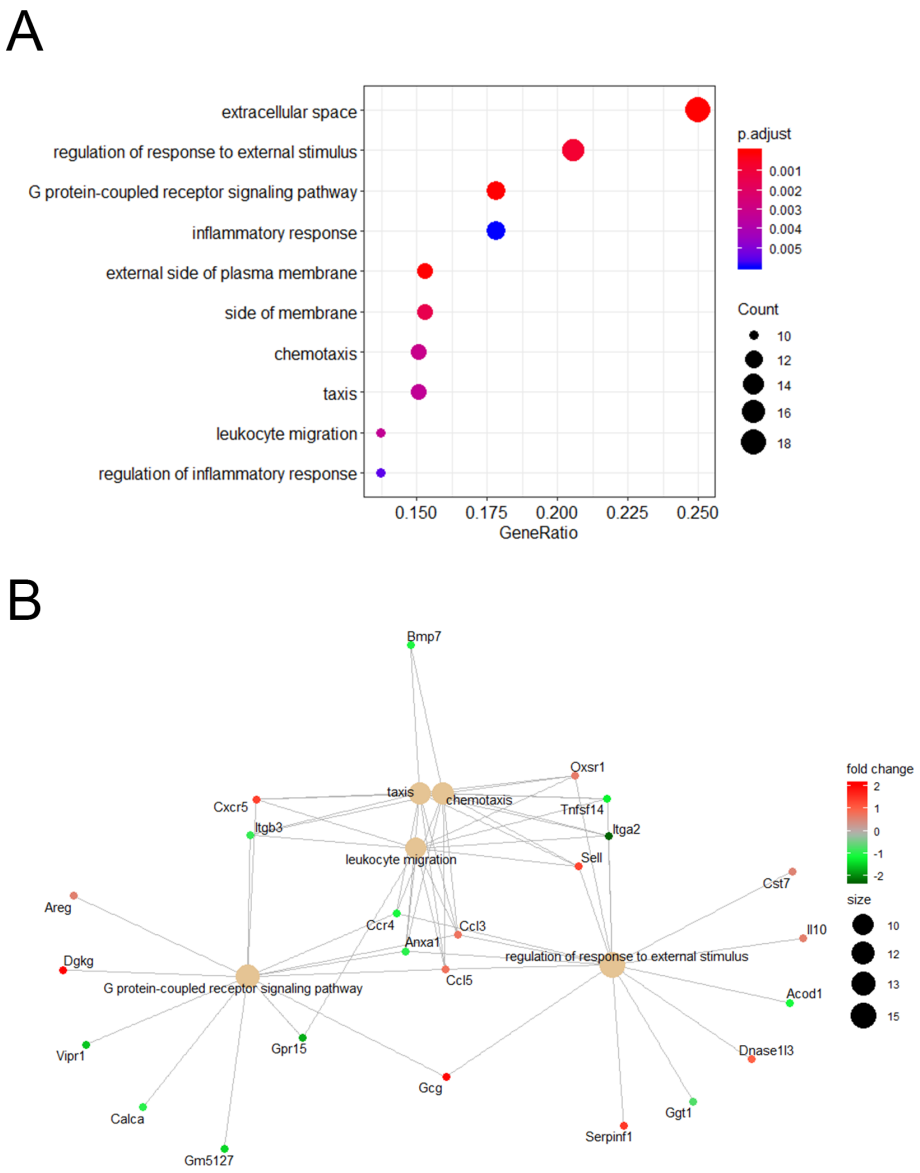

Figure 4.19: Pathway analysis comparing the LAG-3$^+$ and DP Tr1 cell populations.
(A) Dot plot identifying groups of genes most highly expressed by the LAG-3$^+$ population compared to the DP population. (B) Cnet plot identifying clusters of genes highly expressed by the LAG-3$^+$ population compared to the DP population are shown in red. Genes not highly expressed by the LAG-3$^+$ population that are expressed by the DP are depicted in green. Pathway analysis was generated in R studio using the ClusterProfileR package using a p-value cut off ≤ 0.01.

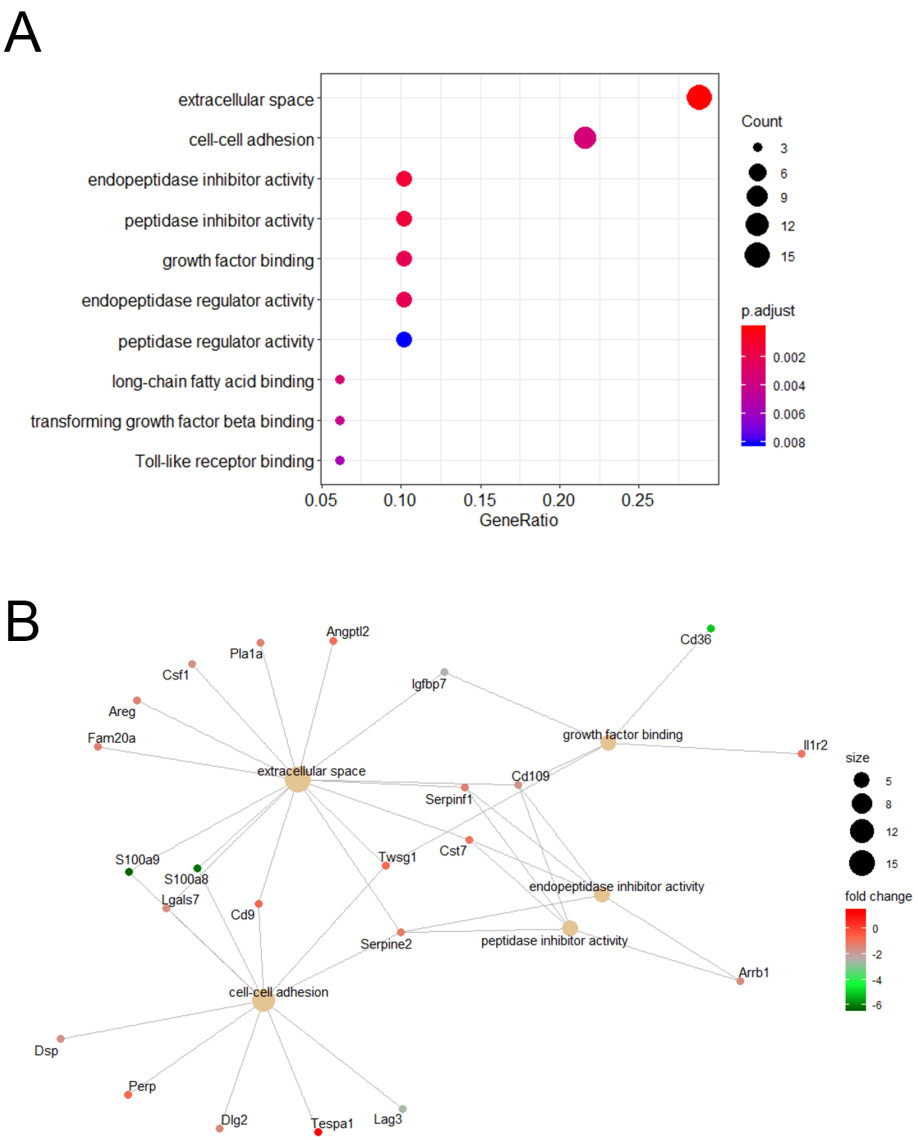

Figure 4.20: Pathway analysis comparing the CD49b$^+$ and DP Tr1 cell populations.

(A) Dotplot identifying groups of genes most highly expressed by the CD49b$^+$ population compared to the DP population. (B) Cnet plot identifying clusters of genes highly expressed by the CD49b$^+$ population compared to the DP population are shown in red. Genes not highly expressed by the CD49b$^+$ population that are expressed by the DP are depicted in green. Pathway analysis was generated in R studio using the ClusterProfileR package using a p-value cut off ≤ 0.01.

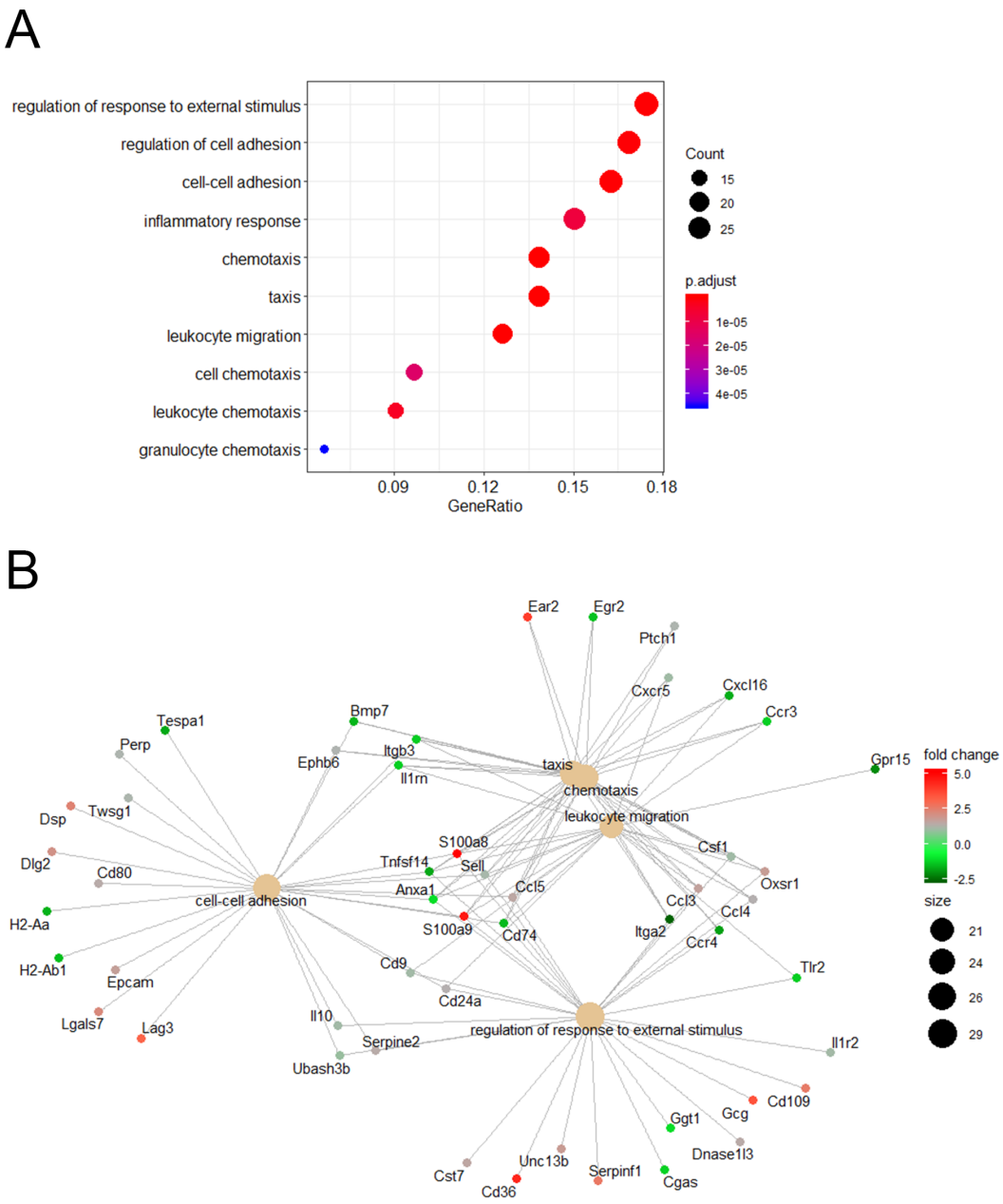

Figure 4.21: Pathway analysis comparing the LAG-3$^+$ and CD49b$^+$ Tr1 cell populations.

(A) Dotplot identifying groups of genes most highly expressed by the LAG-3$^+$ population compared to the CD49b$^+$ population. (B) Cnet plot identifying clusters of genes highly expressed by the LAG-3$^+$ population compared to the CD49b$^+$ population are shown in red. Genes not highly expressed by the LAG-3$^+$ population that are expressed by the CD49b$^+$ are depicted in green. Pathway analysis was generated in R studio using the ClusterProfileR package using a p-value cut off ≤ 0.01.

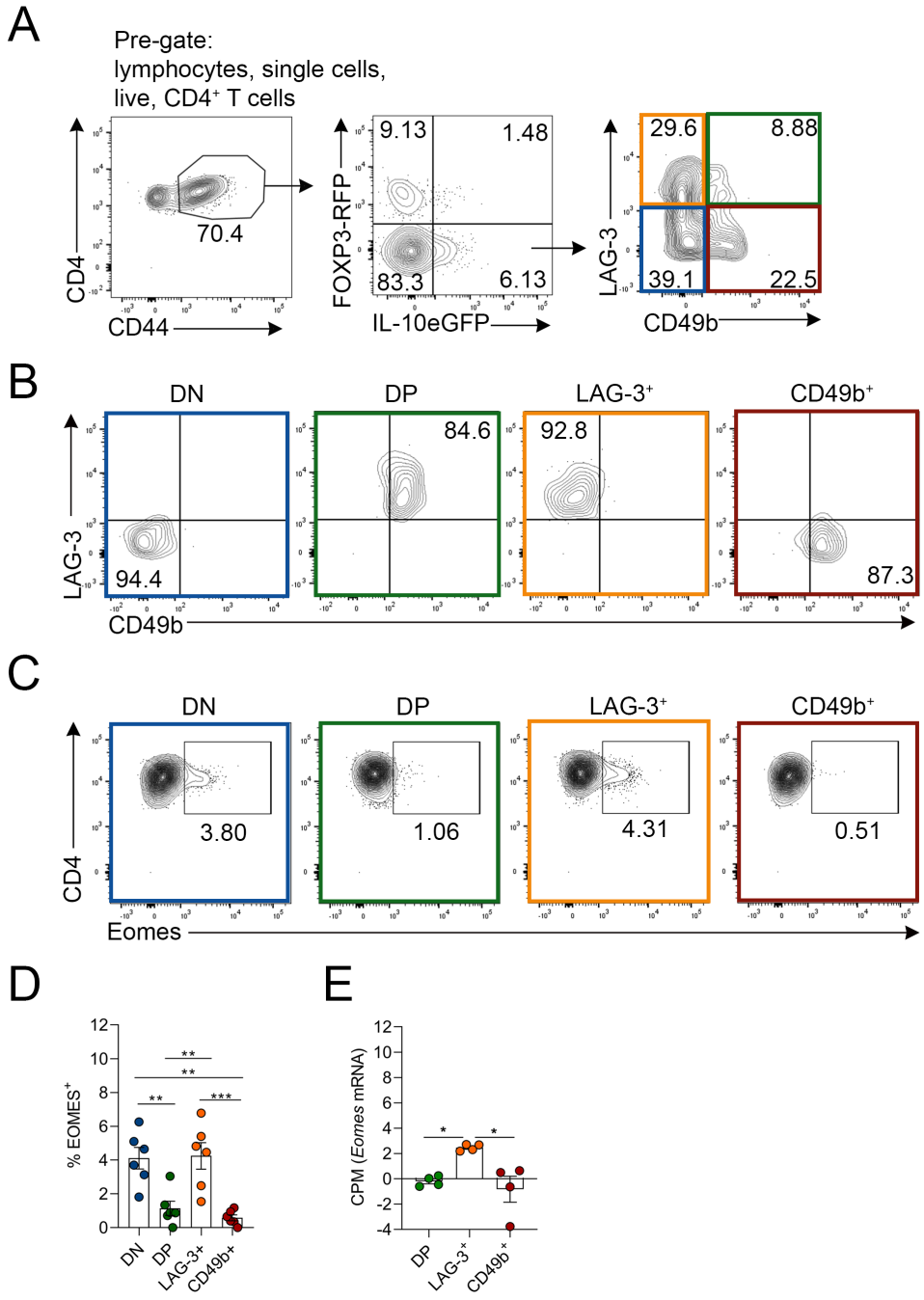
A
Pre-gate:
lymphocytes, single cells,
live, CD4+ T cells
CD4
CD44
70.4
FOXP3-RFP
IL-10eGFP
9.13
1.48
83.3
6.13
LAG-3
CD49b
29.6
8.88
39.1
22.5
B
DN
DP
LAG-3+
CD49b+
LAG-3
CD49b
94.4
84.6
92.8
87.3
C
CD4
Eomes
3.80
1.06
4.31
0.51
D
% EOMES+
DN
DP
LAG-3+
CD49b+
E
CPM (Eomes mRNA)
DP
LAG-3+
CD49b+

Figure 4.22: Validation of Eomes expression by Tr1 cells post IAV infection.

Dual-reporter mice were infected with X-31 IAV-i.n as described (refer to **??**). (A) Gating strategy for sorting of Tr1 cell populations based on LAG-3 and CD49b expression. (B) Post-sort purity was assessed before intranuclear staining of each sample individually, for the transcription factor EOMES. (C) Concatenated representative flow cytometry displaying intranuclear staining of EOMES for each of the Tr1 cell populations. (D) The percentage of $EOMES^+$ Tr1 cells. (E) *Eomes* mRNA in counts per million (CPM) from the RNA sequencing experiment. Each symbol is a different biological replicate, data shown as mean +/- SEM, n=6 biological replicates total from 2 independent experiments (A-D). N=4 biological replicates total from 2 independent experiments (E). Statistical analysis using one-way ANOVA with Bonferroni's post-test (where $^* = p \leq 0.05, ^{**} = p \leq 0.01, ^{***} = p \leq 0.001$, and $^{****} = p \leq 0.0001$).

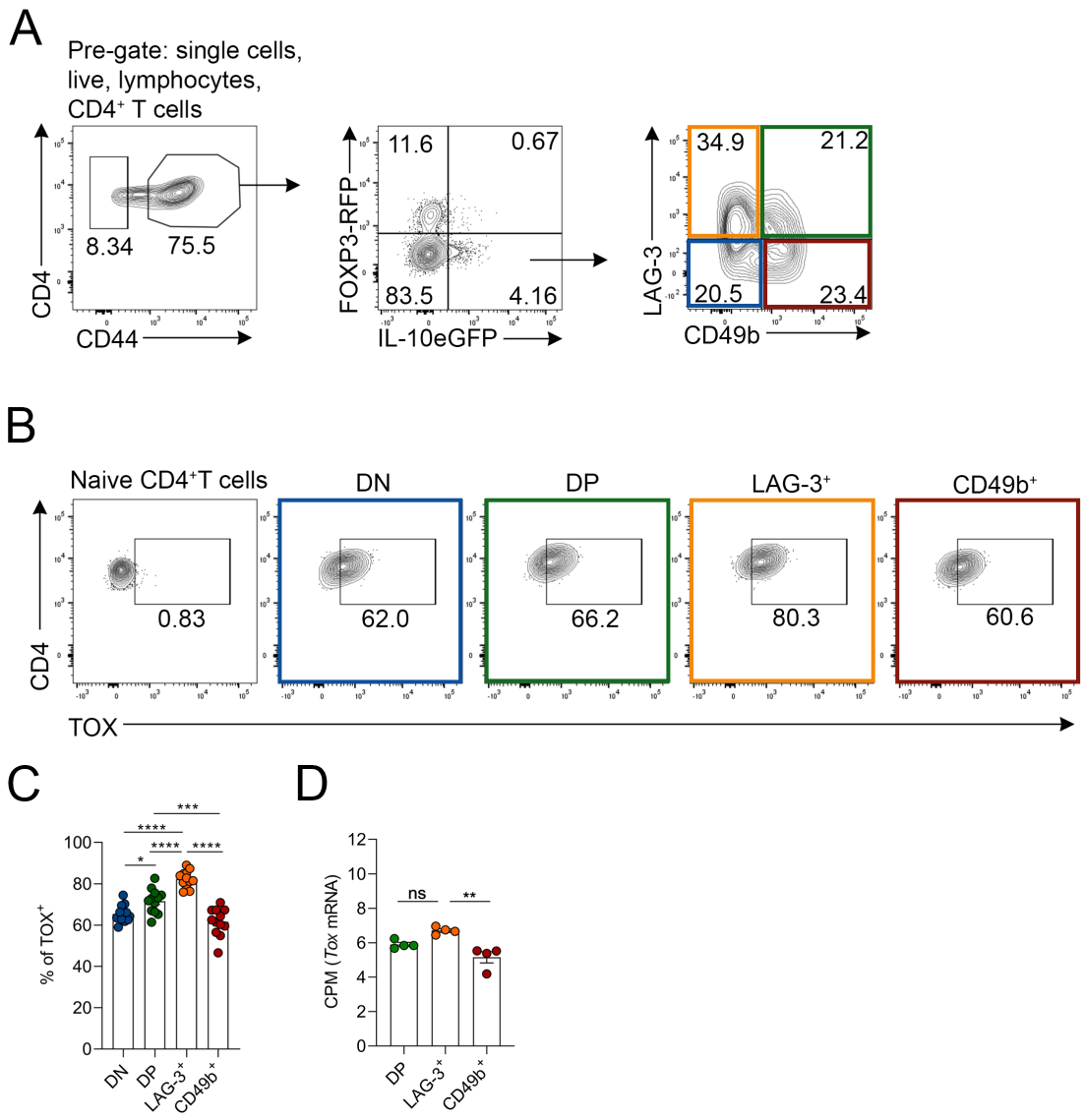

Figure 4.23: Validation of TOX expression by Tr1 cell populations post IAV Infection.

Dual-reporter mice were infected with X-31 IAV-i.n as described (refer to **??**). On day 7 post-infection the lungs were harvested for analysis by flow cytometry. (A) gating strategy for identification of Tr1 cell populations defined by LAG-3 and CD49b. (B) Representative concatenated flow cytometry of TOX expression by Tr1 cell populations compared to naive T cells. (C) Quantitation of the percentage of TOX-expressing Tr1 cells. (D) *Tox* mRNA in counts per million (CPM) from the RNA sequencing experiment. Each symbol is a different biological replicate, data shown as mean +/- SEM, n=11-12 biological replicates total from 2 independent experiments (A-C). N=4 biological replicates total from 2 independent experiments (D). Statistical analysis using one-way ANOVA with Bonferroni's post-test (where $^{*} = p \leq 0.05, ^{**} = p \leq 0.01, ^{***} = p \leq 0.001$, and $^{****} = p \leq 0.0001$).

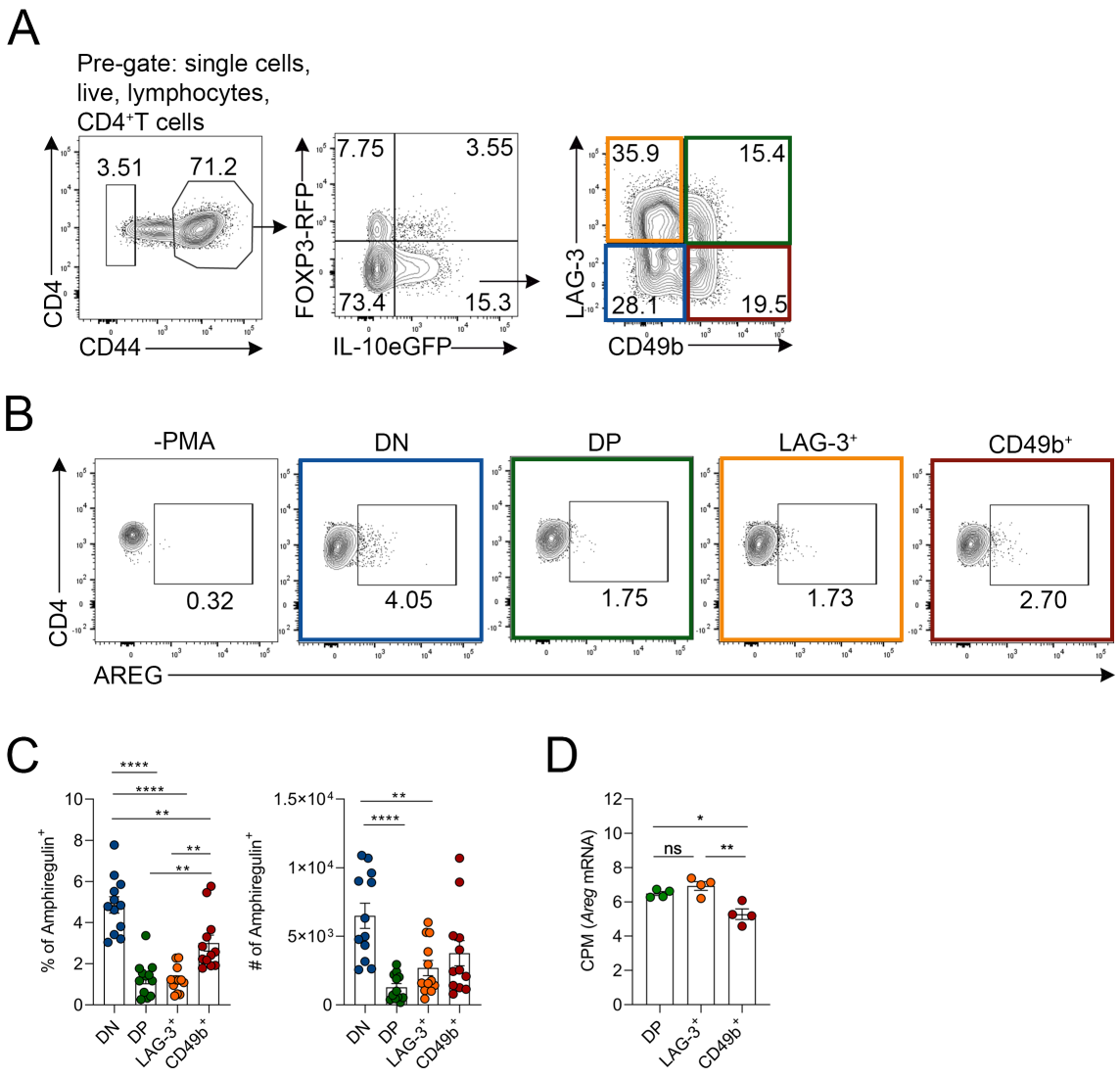

Figure 4.24: Validation of amphiregulin production by Tr1 cells post IAV infection.

Dual-reporter mice were infected with X-31 IAV-i.n as described (refer to **??**). On day 7 post-infection the lungs were harvested for analysis by flow cytometry. (A) gating strategy for identification of Tr1 cell populations defined by LAG-3 and CD49b. (B) Representative concatenated flow cytometry of AREG expression by Tr1 cell populations compared to unstimulated CD4$^+$T cells. (C) Quantitation of the percentage and number of AREG-expressing Tr1 cells. (D) *Areg* mRNA in counts per million (CPM) from the RNA sequencing experiment. Each symbol is a different biological replicate, data shown as mean +/- SEM, n=11-12 biological replicates total from 2 independent experiments (A-C). N=4 biological replicates total from 2 independent experiments (D). Statistical analysis using one-way ANOVA with Bonferroni's post-test (where $^* = p \leq 0.05, ^{**} = p \leq 0.01$, and $^{****} = p \leq 0.0001$).

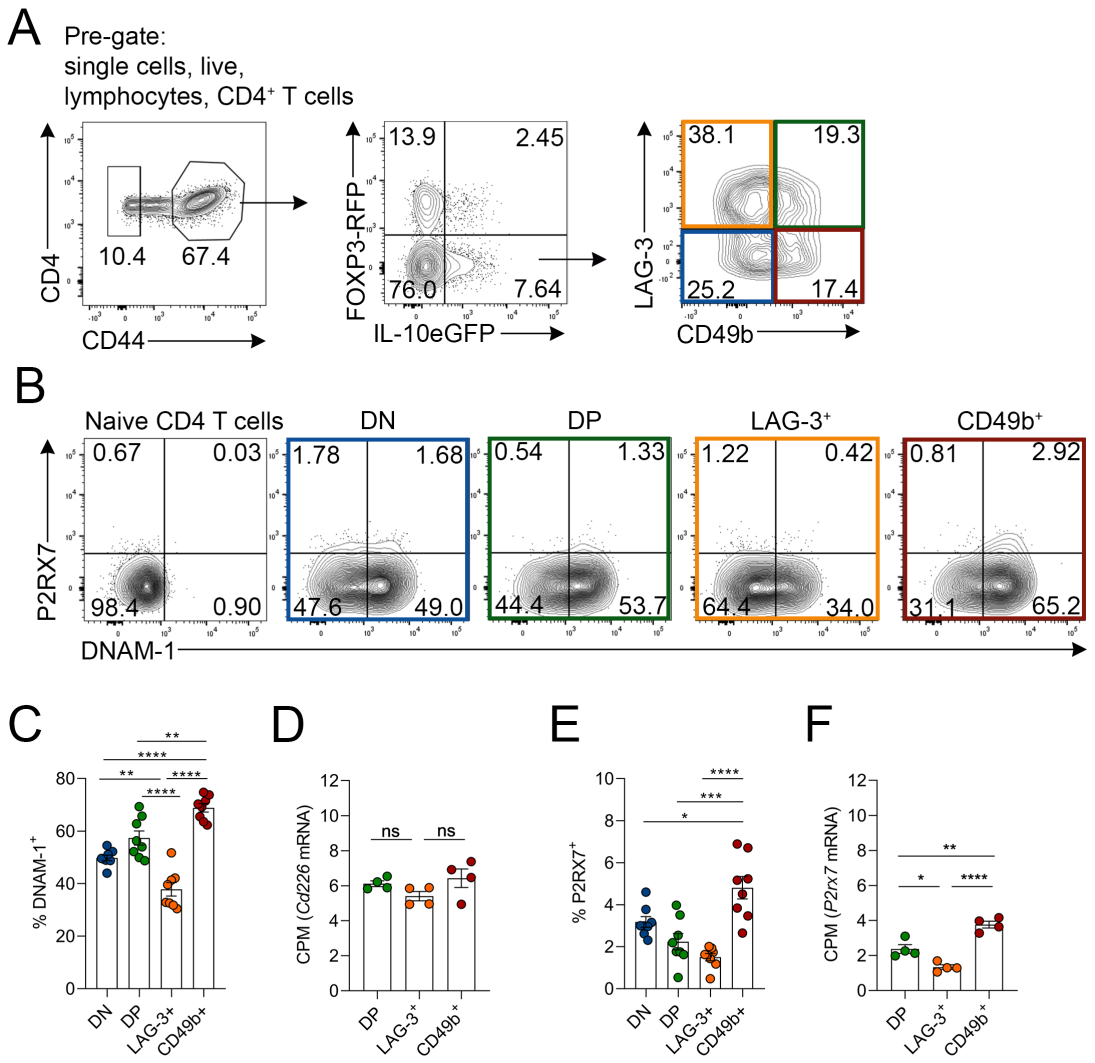

Figure 4.25: Validation of DNAM-1 and P2RX7 expression by Tr1 cell populations post IAV infection.

Dual-reporter mice were infected with X-31 IAV-i.n as described (refer to **2.5.1**). On day 7 post-infection the lungs were harvested for analysis by flow cytometry. (A) gating strategy for identification of Tr1 cell populations defined by LAG-3 and CD49b. (B) Representative concatenated flow cytometry of P2RX7 and DNAM-1 expression by Tr1 cell populations compared to naive CD4$^+$ T cells. (C), (E) Quantitation of the percentage of (C) DNAM-1- and (E) P2RX7-expressing Tr1 cells. (D)*Cd226* and (F) *P2rx7* mRNA in counts per million (CPM) from the RNA sequencing experiment. Each symbol is a different biological replicate, data shown as mean +/- SEM, n=8 biological replicates total from 2 independent experiments. (D), (F) N=4 biological replicates total from 2 independent experiments. Statistical analysis using one-way ANOVA with Bonferroni's post-test (where $^* = p \leq 0.05, ^{**} = p \leq 0.01$, and $^{****} = p \leq 0.0001$).

Chapter 5: Discussion

5.1 Introduction

Understanding the web of cellular and molecular interactions that coordinate the suppression of tissue-damaging effector responses during the resolution of acute inflammation is a major challenge. There are a number of cell types and molecules that have been shown to contribute to the resolution of inflammation. The best studied cells are FOXP3^{+} Treg, which will be discussed in comparison to Tr1 cells in subsequent sections. In terms of molecules that regulate the resolution of inflammation, IL-10 has been ascribed a prominent role. Although studies have investigated the role of IL-10 in globally-deficient mice, the role of specific subsets of IL-10-secreting cells has not been thoroughly addressed with respect to the resolution of acute inflammation. More targeted approaches than those previously used were therefore required to unravel the specific role of Tr1 cells in the regulation of acute infection. One approach used in the present study was a FOXP3/IL-10 reporter mouse that allowed high resolution detection of Tr1-like cells, and this coupled with *Il27ra*$^{-/-}$ mice which exhibit a deficiency in Tr1-like cells allowed a detailed exploration of the phenotype and function of Tr1-like cells in acute infection. The results of the present study have shown that FOXP3^{-} IL-10^{+} CD4^{+} T cells (Tr1 cells) from IAV-infected lungs are capable of suppressing effector T cell division and revealed a Tr1 cell-dependent regulation of recovery from IAV-induced weight loss. These findings substantially advance the understanding of the function of Tr1 cells in the resolution of acute infection. Furthermore, this study has also uncovered multiple novel aspects regarding the biology of Tr1 cells in acute infection with respect to their phenotype, function, mechanisms of recruitment, and dependence on antigen-specificity for immune suppression. In the remainder of this chapter, important aspects of Tr1 cell biology will be explored including the role of Tr1 cells in resolution of acute infection, the defining phenotypic features of Tr1 cells, the mechanisms of Tr1 cell-mediated suppression, the importance of migration for Tr1 function, the development of Tr1 cells, and whether Tr1 cell biology could be manipulated therapeutically to promote the resolution of inflammation in clinical settings.

5.2 The function of Tr1 cells in acute infection.

The role of regulatory populations of T cells during immune responses following viral infection is complex, and highly context-dependent temporally and spatially. For example, in response to viral challenge, Treg cells can proliferate, and promote the initiation of the anti-viral immune response [311], [298]. Depletion of Treg in studies of mucosal herpes virus infection (HSV) and respiratory syncytial virus (RSV) using FOXP3-DTR mice or α-CD25 depleting antibody, has been shown to delay the arrival of anti-viral effector

T cells and DCs at the infection site, and led to a higher viral load, and increased the severity of disease [298], [299]. Other studies exploring depletion of Treg cells (also via FOXP3-DTR mice or with administration of α-CD25 depleting antibody) during infection have elucidated that these cells are critical for limiting the magnitude of anti-viral immune responses to prevent exacerbated tissue pathology and clinical severity post-infection [299], [300], [301], [302], [303], [304], [305]. In contrast, Treg cells are also known to contribute tissue repair following damage due to acute infection [306].

$CD4^+$ T cells are known to be required during the primary challenge for survival and memory formation of anti-viral $CD8^+$ T cell responses [349], [350], [351], [352], [353], however, in the absence of Tregs conventional $CD4^+$ T cells are not essential [354]. Instead, it was demonstrated that conventional $CD4^+$ T cells expressing CD40L (CD154) interact with CD40-expressing DCs to overcome Treg-mediated suppression of $CD8^+$ T cell responses to viral infection. This is a critical concept in immune regulation as both potent effector and regulatory T cell responses require fine-tuning. Treg-mediated suppression of immune responses has been well established in models of viral infection [307], [308], [309], [301], [298], [299], [302]. However, the contribution of Tr1 cells to these regulatory processes following acute infection remains to be fully elucidated, with the major challenge being the availability of reagents which allow the specific study of these cells. Unlike Treg, which are critically reliant on FOXP3, Tr1 cells lack a single lineage-specific transcription factor [217]. Although recent studies have shown BLIMP-1 and cMAF are critical for Tr1 generation and suppressive function [273], [275], [285], these, and other transcription factors are also necessary and sufficient to induce IL-10 production in all effector T cell subsets. While this lack of a single lineage-specific transcription factor lends support to a model in which Tr1 cells are not a separate T cell lineage, it also means that specific depletion of Tr1 cells cannot be achieved thus far, by targeting transcription factors, as has been achieved for the majority of other $CD4^+$ T cell subsets. Therefore, most previous approaches to studying Tr1 cell deficiency have involved using a global or T cell-specific knockout of IL-10, and those models are not sufficiently specific for studying Tr1 cells as many other cell types produce IL-10, including Treg cells.

The present study investigated the T cell-derived sources of IL-10 during IAV infection using a FOXP3/IL-10 dual-reporter mouse. The dual-reporter mouse was generated by crossing the IL-10-tiger mouse [208] to the FOXP3-RFP mouse [209]. Both of these reporters are bi-cistronic reporter systems with an IRES-reporter gene knocked into the endogenous gene locus to retain normal expression levels of FOXP3 and IL-10 alongside reporter expression. Since the generation of the dual-reporter mouse in 2006, this mouse has been used to identify Treg cells and Tr1-like cells in murine models of *N.brasiliensis* infection [194], small intestinal inflammation [194], [210], EAE [236], type I diabetes [230], colitis [210], [210], GvHD [246], and viral infection [218].

In the present study, experiments using the dual-reporter mouse determined that Tr1 cells represent the major T-cell derived source of IL-10 in the IAV-infected lungs, and that they peak in number at a time-point immediately prior to recovery from infection-induced weight loss and after significant viral clearance. The kinetics of accumulation of DP, LAG-3$^+$, and CD49b$^+$ Tr1 cell population in the IAV-infected lungs was transient and peaked at day 7 post-IAV infection. This was similar to the kinetics of FOXP3$^+$ IL-10$^+$ Tregs, although these cells were fewer in number. Tbet$^+$ Tregs have previously been reported to exhibit similar kinetics in IAV infection, and it is likely these Tbet$^+$ Tregs are IFNγ^+ and that there is a small population of IL-10$^+$ Tregs [355]. This suggests that regulatory T cells producing IL-10 exhibit transient accumulation. This is distinct from IL-10$^-$ Tregs which were found to accumulate post-IAV infection and are abundant between days 5 and 10 in the infected lungs. This could suggest that day 7 is a timepoint which specifically requires regulation mediated by IL-10-producing T cells. However, the reasons behind the transiency of the Tr1 response require further investigation. The observation that Tr1 cells are the major source of T cell-derived IL-10 in acute IAV infection, is discordant with some published research. For instance, in contrast to the findings presented here, which align with those of McKinstry *et al.* 2009 [258], who also showed that FOXP3$^-$ CD4$^+$ T cells were the major producers of IL-10 following IAV infection, previous studies have also indicated that CD8$^+$ T cells were the major source of T cell-derived IL-10 [257], [224]. While the reasons for the discrepancy remains to be resolved it should be noted that these two studies differed in a number of important parameters including strain and dose of IAV, background and age of the mice used, and the time-points examined. Nevertheless, while the present study has unequivocally shown that IL-10 production by CD4$^+$ T cells is largely restricted to suppressive populations of *bona fide* Tr1 cells and that these cells are responsible for the majority of IL-10 produced by T cells in the lungs, further investigation in a wider range of scenarios is required to establish the whether these cells are the dominant provider of T cell-derived IL-10 in immune responses other than acute viral infection.

In the present study the issue of Tr1 cell depletion was addressed using *Il27ra*$^{-/-}$ mice, which exhibit a highly selective deficiency in Tr1 cells [258], [356], [256], with the rest of the CD4$^+$ T cell compartment remaining intact [253], thereby allowing critical assessment of the role of Tr1 cells. The *Il27ra*$^{-/-}$ mouse was generated in 2001 by Yoshida and colleagues [295]. In that initial report, there were no significant differences observed in hematopoietic or lymphoid cell development between *Il27ra*$^{-/-}$ and *Il27ra*$^{+/+}$ mice. However, it was noted that *Il27ra*$^{-/-}$ T cells were more proliferative, and *Il27ra*$^{-/-}$ Th1 cells produced less IFNγ compared to *Il27ra*$^{+/+}$ cells [295]. The *Il27ra*$^{-/-}$ mouse is also known to exhibit more robust effector T cell responses and overproduction of inflammatory cytokines in *T. gondii*, *T. cruzi*, and *L. major* infection leading various groups to postulate that there was a general IL-27R-dependent lack of control over inflammatory T cell responses in these contexts

[128], [357], [358]. These results are similar to those reported in the absence or blockade of IL-10 as there are more robust effector T cell responses following CL13 (chronic) LCMV infection [359]. In addition, the cytokine IL-27 is known to induce IL-10 in a number of T cell subsets including Tr1 cells [264], [297], [360], [361] [265]. Of interest, although deficient in Tr1 cells, overall levels of IL-10 have been shown to be intact in the *Il27ra*$^{-/-}$ mouse [357]. Furthermore, one previous study has shown a reduction in IL-10-producing FOXP3^{-} but not FOXP3^{+} CD4^{+} T cells in *Il27ra*$^{-/-}$ mice compared to *Il27ra*$^{+/+}$ [253]. Given these findings, and that data in the present study indicated that all FOXP3^{-} IL-10^{+} CD4^{+} T cells in IAV-infected lungs were *bona fide* Tr1 cells, *Il27ra*$^{-/-}$ mice were selected as a model of Tr1 deficiency for this project.

Consistent with previous findings, *Il27ra*$^{-/-}$ mice displayed a highly selective loss of Tr1 cells in acute infection in the present study. Additionally, *Il27ra*$^{-/-}$ mice exhibited enhanced weight loss and delayed recovery from IAV infection compared to littermate controls. This indicates that like Treg cells, Tr1 cells contribute either to limiting the effector response and the level of inflammation resulting from that response and/or the resolution of inflammation. This was unequivocally proven in experiments showing that transfer of purified *in vitro*-derived Tr1 cells enhanced recovery from infection-induced weight loss in into *Il27ra*$^{-/-}$ host mice. However, it should be noted that in addition to the deficiency in Tr1 cells in IAV-infected *Il27ra*$^{-/-}$ mice, effector T cells also displayed reduced IFNγ and increased IL-17A production compared to those in control mice (data not shown), which is similar to the phenotype of Tr1-like cells in these mice. This is suggestive of a dysregulated T cell phenotype in IAV-infected *Il27ra*$^{-/-}$ mice and potentially indicative of reduced control over inflammatory effector T cell responses, although whether this altered phenotype is due to a lack of Tr1 cells, or reflects the loss of IL-27 signalling in effector T cells is currently unknown. Irrespective of this, a number of important questions now arise from this study. Principally it is of interest to determine the mechanisms by which Tr1 cells regulate recovery from maximum weight loss in this model. This could be evaluated by determining the effect of transfer of Tr1 cells on inflammatory cytokine levels in the lung and BALF or transferring *in vitro*-derived Tr1 cells with specific gene deficiencies. Also, more detailed investigation of the transfer model is warranted in terms of i) the timing of administration of Tr1 cells to more specifically address the phase of the response at which Tr1 cells operate; ii) the requirement for Tr1 cell antigen specificity; iii) the quantity of Tr1 cells required to elicit suppression; and iv) more detailed inquiry into the ability of Tr1 cells to accumulate in infected lungs. Several of these are discussed in more detail below.

A previous study [256] examining the effect of IL-27 administration in IAV provides potential insight into the effect of transfer of Tr1 cells in this study. In the study by Liu and colleagues [256], treatment of WT mice with IL-27 from days 5-10 post-IAV infec-

tion resulted in decreased weight loss, increased survival and reduced lung pathology, and although production of Tr1 cells in response to IL-27 treatment was not assessed in that study, it would be expected that those cells are generated under such conditions [264], [297], [253], [273], [272], [237], [285]. The timing of the IL-27 treatment provides further insight as while there was no effect on viral load when treating from days 5-10 post-infection, if treatment was administered from days 1-7 post-infection there was reduced weight loss but also impaired viral clearance [256]. Together, these observations suggest that initial generation of Tr1 cells while limiting infection-induced weight loss, also attenuate the effector response. In the present study, Tr1 cells appeared at the effector site between days 5 and 7, suggesting that, as has been reported for Treg cells [299], [300], [301], [302], [303], [304], [305], they may play a role in attenuating effector responses to limit pathology. With respect to the adoptive transfer model, when Tr1 cells were transferred into *Il27ra*$^{-/-}$ mice on day 5 post-infection, weight loss was reversed which indicates that under these conditions Tr1 cells have the ability to reduce IAV-induced pathology. However, whether this is by reducing effector cell mediated damage or reversing the pathology, or both was not investigated and would be an important avenue of investigation in future studies. The transferred Tr1 cells could be influencing a number of events during the response to IAV. They could be limiting effector cell expansion, thereby limiting effector cell-induced damage/pathology (as read out by weight loss), they could be enhancing contraction, also limiting damage and weight loss. To more precisely determine whether Tr1 cells can regulate expansion and/or contraction, further experiments could be conducted involving transfer of Tr1 cells into *Il27ra*$^{-/-}$ mice at additional time points during IAV infection. Transfer of Tr1 cells earlier (day 1-3 post-IAV infection) would demonstrate if these cells can reduce maximum weight loss if administered earlier. The effect of these transfers on additional parameters should also be assessed including viral load, cellular studies to assess the number and phenotype (e.g.: activation and cytokine status, division, apoptosis) of IAV-specific $CD4^+$ and $CD8^+$ T cells in the lung. The ability of adoptively transferred Tr1 cells to suppress effector T cell division in the IAV-infected lungs could also be investigated using BrdU as a marker of proliferation. Together the proposed experiments could further elucidate the precise timing and mechanisms of Tr1 function in the resolution of inflammation during IAV infection.

It is clear from the present study that both Treg and Tr1 cells are present in the lung during IAV infection, which raises the question as to why are both types required when they ostensibly perform similar functions. While a simple answer lies in the fact that the adaptive immune system has a plethora of in-built redundancies and that this is yet another example, there are additional possibilities. While it is possible that Tr1 cells may function during the early phase of IAV infection, like has been reported for Treg cells [299], [300], [304], it is also important to note that Tr1 cells were not detected in statistically significant numbers in the lungs of IAV-infected mice until day 7 post-infection, with

a small increase above background being detected on day 5 post-IAV infection. This contrasted with IL-10^{-} Treg cells (FOXP3^{+}IL-10^{-}) which were detected at relatively high levels on day 5 post-infection. Together, these observations suggest, but do not prove that Treg cells play an important protective role by controlling the extent of effector responses early in IAV infection, whereas Tr1 cells are more involved in recovery, perhaps by limiting the extent of damage, promoting effector phase contraction and/or promoting tissue repair.

Another important question that arises from the results of this study is that of antigen-specific Tr1-mediated suppression. Numerous previous studies have indicated that antigen specific activation of Tr1 cells, presumably via interactions with APCs is necessary for Tr1 cell-mediated suppression of effector T cell division both *in vitro* and *in vivo* [216], [191], [160], [327], [230], [328]. However, in the present study both *in vitro*-derived polyclonal (α-CD3 and α-CD28 activated) and *ex-vivo*-derived IAV-generated polyclonal (IAV antigen-specific) Tr1 cells were found to suppress effector T cell division in suppression assays with polyclonal effector T cells with likely mismatched TCR specificity, clearly indicating that once activated, Tr1 cells can suppress effector T cell division. A previous study demonstrated that OVA-specific Tr1 cells were able to suppress the development of colitis induced by transfer of effector T cells but only when mice were fed with OVA-peptide [191]. That requirement for antigen, in contrast to that observed in the present study suggests that there may be a context-dependent requirement for antigen-specificity for Tr1 cell function in *in vivo*. In the case of acute viral infection with IAV, *in vitro*-derived polyclonal Tr1 cells infiltrated the infected lungs where they were able to proliferate and may exert bystander suppression of effector T cells and APCs via secretion of IL-10 or contact-dependent co-inhibitory molecule mechanisms without a requirement to engage antigen. In the case of endogenous Tr1 cells generated during IAV infection, Tr1 cells could also interact with APCs via antigen-dependent mechanisms. In other scenarios, such as colitis, it is possible that antigen receptor signals are required to concentrate circulating Tr1 cells to the appropriate tissue microenvironment where they can mediate suppression. Notably, in the present study, transferred polyclonal Tr1 cells were abundantly detectable in the lung of IAV-infected hosts. It was intended in the current study to directly test whether antigen-specificity would enhance Tr1-mediated suppression in the IAV-model using OT-II Tr1 cells and OVA-transgenic IAV virus, but delays in obtaining animals and the time required for crossing multiple transgenic lines put this beyond the time available in this study. Future work is warranted in the IAV model to determine whether antigen-specificity will enhance Tr1 cell mediated suppression.

5.3 What constitutes a Tr1 cell?

Current classification of Tr1 cells dictates that they are $CD4^+$ T cells that express IL-10 but not FOXP3. However, not all cells with this profile exhibit regulatory function and some clearly display features of other Th lineages with co-expression of IL-10, and can be pro-inflammatory. Th lineages known to produce IL-10 include Th1, Th2, Th9, Th17, and Treg cells [264], [362], [363], [297], [360], [361], [265]. The results of these previous studies led to a designation of Tr1 cell status requiring exclusion of cells from these other lineages alongside the following characteristics: FOXP3 must not be expressed, IL-10 must be more highly expressed than IL-4 and IL-17A at the mRNA or protein level, and the cells must exhibit suppressive function [216], [191], [194], [217]. Thus, to be classified as a Tr1 cell, it is essential that $FOXP3^-$ $IL\text{-}10^+$ $CD4^+$ T cells exhibit suppressor function and must be capable of suppressing effector T cell division [191], [211], [212], [213], [214], [215], [194], [195], [162], [192], [193], [217]. To aid in their identification, co-expression of the surface molecules LAG-3 and CD49b has been shown to identify functionally suppressive Tr1 cells in a range of contexts [194], [210], [218]. However, this evidently does not apply to every scenario [224], [246], [225], including in the present study which found four distinct populations of Tr1 cells based on LAG-3 and CD49b co-expression, all of which exhibited suppressive function. Apart from this observation, the use of LAG-3 and CD49b co-expression as a means to identify Tr1 cells is further complicated by the fact that they are not always unique to Tr1 cells as these molecules have been shown to mark other IL-10-producing T cells including $FOXP3^-$ $CD4^+$ T cells, $CD4^+$ Treg cells, and $CD8^+$ T cells [224], [225]. More recently enrichment for co-inhibitory receptor expression has also been shown to be a surrogate strategy for identification of potently suppressive Tr1 cells [210]. In the present study Tr1 cells met each of the above criteria as they were $FOXP3^-$ $IL\text{-}10^+$ $CD4^+$ T cells with suppressive function, they expressed LAG-3 (i.e. the $LAG\text{-}3^+$ and DP populations), PD-1 and TIM-3, and expressed *Cd223*, *Tigit*, *Cd152*, *Cd279*, and *Hvarc2* mRNAs. In addition to the parameters described above, each of the four Tr1 populations identified in the current study based on LAG-3 and CD49b expressed IFNγ with negligible expression of IL-4 and IL-17A. Together, these observations determined that Tr1 cells in this study were *bona fide* Tr1 cells, enriched for co-inhibitory molecules which reinforces their suppressive phenotype [210].

Thus, the present study has extensively characterised and assessed each of the criteria necessary for classification of Tr1 cells [217], and determined that Tr1 cells from the IAV infected lungs express a range of co-inhibitory molecules at both mRNA and protein levels, and exhibit suppressor function. while it is clear that to study these cells, the above criteria are essential to designate cells as *bona fide* Tr1 cells, in contrast with the findings of previous studies [194], [218], it was determined that LAG-3 and CD49b co-expression did

not identify all *bona fide* Tr1 cells. Instead the population from the IAV-infected lungs aligned more clearly with the more recent criterion enriching for Tr1 cells using expression of a range of co-inhibitory receptors [210].

5.4 Molecular mechanisms of Tr1 cell-mediated suppression.

As discussed above, T cell suppressive function is one of the most important defining features of Tr1 cells, yet historically, assessment of suppressive capacity has not been conducted in many studies purporting to study Tr1 cells or investigating IL-10$^+$ CD4$^+$ T cells. This has hindered development in the field as it is not clear which studies have interrogated *bona fide* Tr1 cells. As discussed previously, this is important as not all IL-10$^+$ CD4$^+$ T cells have suppressive function, in some contexts IL-10 can be pro-inflammatory [210], [181], [101]. Critically, there are also studies which have appropriately assessed the suppressive capacity of Tr1 cells leading to discovery of different mechanisms of suppression and these will be discussed in detail in the context of the results from the present study.

In vitro assays measuring the suppressive capacity of mouse and human Tr1 cells have established that IL-10 and TGF-β are required to mediate suppression of effector T cell division, IFNγ production, and activation in a range of different contexts [191], [211], [212], [213], [214], [215]. While both IL-10 and TGF-β have been consistently implicated in mouse and human Tr1-mediated suppression during *in vitro* suppression assays [191], [192], the mechanisms of Tr1 suppression in T cell transfer colitis models have been shown to be predominantly dependent on IL-10 [193], [195]. Although it has been reported that *in vitro*-derived Tr1 cells inhibit the proliferation of effector T cells in response to α-CD3 and α-CD28, the addition of IL-10R and TGF-β nABs did not completely abrogate this suppression and a cell-contact mediated mechanism of suppression via PD-1 and CTLA-4 was also apparent [162], [192], [213]. A more recent study found that post α-CD3 treatment, small intestinal FOXP3$^-$ IL-10$^+$ CD4$^+$ T cells were enriched for expression of co-inhibitory molecules and potently suppressed effector T cell proliferation *in vitro*, whereas splenic FOXP3$^-$ IL-10$^+$ CD4$^+$ T cells express low levels of co-inhibitory molecules and were not as suppressive, providing further evidence of the role of contact-dependent mechanisms via expression of co-inhibitory molecules [210]. However, blocking TIM-3, LAG-3, or IL-10Rα alone did not inhibit suppressive capacity of the small intestinal Tr1 cells and while those previous data suggest the importance of co-inhibitory molecule expression in the suppressor function of Tr1 cells, this is clearly a complex issue that is not yet completely understood. Most *in vitro* suppression assays use irradiated APCs, which removes the ability of the APC to respond to the Tr1 cells. In the study mentioned

above, there was no statistically significant effect on Tr1 cell-mediated suppression of effector T cell division in the presence of nAB against co-inhibitory receptors. However, the suppression assays conducted in that study used inactivated APCs which would not be able to respond to co-inhibitory molecule interactions with Tr1 cells. This identifies a need to investigate the suppressive function of co-inhibitory molecules expressed by Tr1 cells in assays which allow for assessment of both direct and indirect mechanisms of suppression by using live APCs. Suppression assays conducted in the present study, were designed to determine the suppressor function of Tr1-like cells via both direct and indirect mechanisms through the inclusion of live APCs in the assays. Thus, including these cells creates a system capable of more comprehensive assessment of the potential mechanisms of Tr1-mediated suppression. There were several unequivocal outcomes from these assays. First, they established that each of the four Tr1-like populations isolated from the lungs of IAV-infected mice, as well as the *in vitro*-derived Tr1-like cells, were suppressive and hence, *bona fide* Tr1 cells. Second, it was clear from the *ex vivo*-derived Tr1 suppression assays that LAG-3-expressing Tr1 cell populations (LAG-3$^+$ and DP) were the most potently suppressive cells. Third, it was striking that the CD49b-expressing Tr1 cells (DP and CD49b$^+$ populations) were the only populations to be dependant on IL-10 to mediate suppression. Fourth, the *in vitro*-derived Tr1 cells were found to use both IL-10 and LAG-3 to elicit suppression, however, blocking both of these molecules did not completely abrogate suppression suggesting other mechanisms are also involved. Future investigation could interrogate whether any of the four populations are dependent on TGF-β to elicit suppression of effector T cell division. This could be done by completing suppression assays in the presence of an isotype control or TGF-β nAB.

The ability of regulatory T cells to mediate suppression of T cell responses via effects on APCs has been investigated extensively. Using *in vitro* culture systems, IL-10 has been shown to act on APCs to inhibit expression of MHC-II, co-stimulatory molecules, and pro-inflammatory cytokines [187], [188], [182], [189], [184]. These effects on APCs are known to result in reduced proliferation and pro-inflammatory cytokine production by effector T cells [190], [183], [184]. In terms of effects on MHC-II expression, analysis of a number of publications implicates a ubiquitination event [364], [365], [366], [185], [186], [367], as a possible mechanism whereby IL-10 from Tr1 cells could be suppressing APC activity. MHC-II in immature DCs is ubiquitinated by MARCH-1 and as a result is predominately sequestered in intracellular vesicles where it has a short half-life as it is targeted for degradation. MARCH-1 expression and the ubiquitination event is inhibited upon DC maturation allowing stable expression of MHC-II at the surface [367], [366], [365]. In the present study CD49b-expressing, but not LAG-3$^+$ or DN Tr1 cells, showed a degree of dependence on IL-10 for suppression during *in vitro* assays. To explore the mechanisms underlying the suppression observed in the present study, each of the Tr1 populations

could be further interrogated by using congenically mismatched or dye-labelled APCs in suppression assays to allow analysis of MHC-II and co-stimulatory molecule expression by these cells in combination with assessment of effector T cell proliferation by flow cytometry at the endpoint of the assay. As the CD49b-expressing Tr1 cell populations relied on IL-10 to an extent to mediate suppression, it is possible that IL-10 is signalling in APCs to up-regulate MARCH-1, which in turn down-regulates MHC-II and co-stimulatory molecule expression, thereby indirectly suppressing effector T cell proliferation.

Even in the Tr1 populations that exhibited a reduction in suppressive capacity in the presence of α-IL-10Rα nAB, suppression was not completely abrogated suggesting other mechanisms and molecules are potentially involved. This supports the notion that, although IL-10 is essential in the classification of Tr1 cells, it is not the sole contributor to Tr1-mediated suppression. From this and other studies [210], [191], [327], [368], [338], [162] it is clear that there are a number of different suppression mechanisms, involving either secreted or surface molecules used by Tr1 cells that are independent of IL-10. There are a number of mechanisms Tr1 cells can exploit to elicit suppression. It appears that there are differences in the suppressive mechanisms used by Tr1 cells from different disease models and localised in different organs. For example Tr1 cells from the small intestine are dependent on IL-10 to elicit suppression [194], [195]. In parasite infection, Tr1 cell-derived IL-10 was shown to inhibit TNFα-mediated tissue pathology [369]. Tr1 cells generated *in vitro* from mouse naive $CD4^+$ T cells using vitamin D3 and dexamethasone were able to suppress T cell division, however, this suppression was determined to be independent of IL-10 and instead dependent on PD-1 and CTLA-4 [162]. Additionally, human Tr1 polarised cells have been shown to elicit suppression of T cell division via PD-1 and CTLA-4 in addition to IL-10 [370]. In the current study, the differential dependence of the Tr1 cell populations on IL-10 to mediate suppression could indicate that there are more highly functional states for Tr1 cells, or that there are additional mechanisms at play. The reason for the heterogeneity in function could be to ensure suppression can occur if one particular mechanism is ineffective. Understanding the cellular interactions made by distinct subsets of Tr1 cells during respiratory infection could inform which mechanisms of suppression were likely the most relevant in this context. This would indicate which co-inhibitory molecules or cytokines would be critical to investigate further.

As discussed above other molecules which could be involved include secreted molecules such as TGF-β as well as co-inhibitory molecules which confer suppressive capacity for Tr1 cells such as CTLA-4 and PD-1 which have been shown to be partially responsible for the suppression of effector T cell division mediated by Tr1 cells in published studies [192],[213]. An additional candidate is LAG-3, which is expressed by Tr1 cells and has been implicated in their suppressor activity. However, a previous study investigating the mechanisms used by Tr1 cells to suppress effector T cell division determined that

co-inhibitory receptor enriched Tr1 cells exhibited no difference in their ability to directly suppress effector T cells in the presence of neutralising α-LAG-3 antibody [210]. In contrast, in the present study, *in vitro*-derived Tr1 cells required LAG-3 to elicit maximum suppression potentially indicating that this mechanism is involved via live APCs. Regardless of this, it is clear that further investigation is required to fully elucidate the mechanisms of Tr1-mediated suppression and the *in vitro* suppression assay developed in the present study will prove very useful in this respect. For example, to better define the mechanisms of Tr1 cell-mediated suppression a range of co-inhibitory molecule- and cytokine-deficient mice (eg. mice lacking TGF-β1, PD-1, CTLA-4, TIGIT) could be crossed to the dual-reporter background to allow for isolation of Tr1 cells deficient in specific molecules previously associated with suppressive function. In addition, the *Il27ra*$^{-/-}$ Tr1 transfer model could be used to assess the function of *in vitro*-derived Tr1 cells by administering nAB and antagonists of different cytokines and co-inhibitory molecules, or generating Tr1 cells *in vitro* from dual-reporter crossed to specific suppressor function molecule-deficient mice to determine the molecular requirements for Tr1 cell-mediated restoration of recovery from IAV infection-induced weight loss.

5.5 The migratory capacity of Tr1 cells

As stated in Chapter 1, the immune system relies on the coordinated spatiotemporal localisation of immune cells in order to elicit or suppress a response to antigen. The chemokine system is exploited by T cells, to traffic to priming sites within SLOs and subsequently to migrate to effector sites where a response is required. There is limited knowledge about the migratory axes used by Tr1 cells most likely due to the rare nature of this subset in a range of models and the difficulty in identifying and isolating this subset.

In the present study Tr1-like cells were observed in the blood, spleen, mLN, lung parenchyma, and airways of IAV-infected mice. The identification of Tr1-like cells in the SLOs and circulation suggests firstly, that Tr1 cells can be generated at priming sites and secondly, that they rely on migration to some extent in an acute infection setting. Due to the scarcity of information regarding the chemokine receptors used by Tr1 cells, an extensive investigation was conducted and their expression profile was compared to Treg, IL-10^{+} Treg, and effector T cells. These comparisons were conducted to determine whether any chemokine receptors were uniquely or more robustly expressed by Tr1 cells in the IAV-infected lungs in the hope that a specific Tr1 profile may have been observed. The most highly expressed receptor by Tr1 cells was CXCR6. This receptor is synonymous with resident memory T cells [371] and lymphocytes of a type I lineage [116], and may represent populations of terminally-differentiated effector T cells [372]. Although *in vitro*-derived

Tr1-like cells have been shown to express CXCR6 previously [292], expression of CXCR6 by Tr1 cells *in vivo* has not previously been reported. Therefore, this is the first report of CXCR6 expression by endogenous *bona fide* Tr1 cells *in vivo*. Tr1 cells were also found to exhibit an almost uniform CCR7$^-$ CXCR6$^+$ profile suggesting that there was no naive-like sub-population within the Tr1 population. This pattern of chemokine receptor expression was mirrored in IL-10$^+$ Treg cells. Furthermore, this profile suggests that Tr1 cells likely constituted a highly activated population of T cells. Subsequent experimentation in the present study found that CXCR6 was dispensable for Tr1 cell homing to the IAV-infected lungs. Although not required for trafficking to the lungs, CXCR6 is potentially important for positioning of Tr1 cells within a specific niche in the lung parenchyma as it has been suggested that CXCR6 is only a weak mediator of chemotaxis and may instead be required for subtle T cell positioning within tissues for activation and expression of effector function [373], [374]. For instance, in a recent published study, CXCR6 was shown to be required for co-localisation of CD8$^+$ T cells with activated DCs in mouse solid tumour models [374]. Given more time to investigate this, immunofluorescence imaging of lungs from IAV-infected *Cxcr6*$^{gfp/gfp}$ mice compared to *Cxcr6*$^{gfp/+}$ littermate controls could be undertaken. For a cell-intrinsic system, *in vitro*-derived *Cxcr6*$^{gfp/gfp}$ or *Cxcr6*$^{gfp/+}$ Tr1 cells could be transferred into IAV-infected, congenically mis-matched mice. The lungs could then be processed for immunofluorescence imaging to determine the localisation of CXCR6-sufficient and -deficient Tr1 cells. This would allow for interrogation of the cell types with which Tr1 cells are interacting, potentially DCs or other APCs in the lungs, and provide novel insight into the micro-environmental localisation of Tr1 cells. In addition, there is potential to resolve the likely *in vivo* functions of Tr1 cells and determine whether CXCR6 is required for these processes. However, there are a number of challenges to these experiments. Firstly, accurate immunofluorescence imaging of FOXP3 and IL-10 and other molecules of interest in the lung may require tissue clearing because the lung is a difficult tissue to image, and this technique is complex. Additionally, a surrogate sorting strategy for Tr1 cells from the IAV-infected lungs or *in vitro* cultures to replace the requirement for the dual-reporter mice is also desirable as it would negate the necessity to cross dual-reporter mice onto every chemokine receptor knockout mouse of interest for transfer experiments. This is especially pertinent for the *CXCR6*$^{gfp/gfp}$ mice as it would not be beneficial to cross to the dual-reporter mice that also express GFP. From the results of this study, possible strategies include co-staining TIM-3, LAG-3, and PD-1 to enrich for Tr1 cells (although this strategy would exclude LAG-3$^-$ Tr1 cells identified in this study). Alternatively co-expression of CXCR6 and PD-1 was also found to enrich for Tr1 cells within activated CD4$^+$ T cells in the present study and could be potentially used to enrich for Tr1 cells. These approaches would need to be extensively tested alongside dual-reporter mice to ensure that these markers successfully enriched Tr1 cells to enable these experiments. Another alternative would be to generate chemokine receptor gene KO

Tr1 cells on the reporter background by culturing Tr1 cells and including CRISPR-Cas9 and sgRNA-encoding retroviruses to target specific chemokine receptors.

Other chemokine receptors have been previously associated with Tr1 cells. In the NOD mouse model of T1D, islet antigen-specific Tr1 cells from the intestine were injected intra-rectally and their migration assessed. Transferred Tr1 cells were found in the spleen, lymph nodes, small intestine, colon, and the pancreas. These Tr1 cells expressed CCR4, CCR5, CCR7 and CCR9 [230]. Other receptors found to be expressed by Tr1 cells in the present study within the IAV-infected lungs at the level of mRNA included *Ccr2*, *Ccr5*, *Cxcr3*, and *Cxcr4*. CXCR3 protein expression was not assessed on lung Tr1 cells as CXCR3 detection is impaired following collagenase digestion of the lungs. To circumvent this, CXCR3-CIBER mice which report on CXCR3 via GFP expression could be used in future experiments [375]. *Ccr2* was most highly expressed by Treg cells, however, Tr1 cells and effector T cells exhibited the lowest mRNA levels so protein expression was not assessed in this study. *Ccr5* was found to be expressed by both Tr1 and IL-10^{+} Treg cells. It is also known that human Tr1 cells isolated from the small intestine co-express PD-1 and CCR5 [241]. Although CCR5 staining was not observed on Tr1 cells in the lungs in the present study, at the level of mRNA Tr1 cells expressed both CCR5 and PD-1. This could indicate a technical issue with the CCR5 staining on cells from the lungs which would need to be addressed. Different clones of CCR5 should be sourced and tested for efficacy post-collagenase digestion of tissues.

The present study has progressed the current understanding of the migratory axes used by Tr1 cells in acute infection. However, it is clear that there is still much to interrogate to understand the chemokine receptors required for accumulation in the parenchyma of the IAV-infected lungs. Overall, further characterisation of the migratory axes employed by Tr1 cells is required to unravel their trafficking capacity and understand their localisation in homeostasis and disease.

5.6 The development and phenotype of Tr1 cells.

Two important questions remain regarding Tr1 biology that will be discussed. 1) Do Tr1 cells develop from naive precursors or transdifferentiate under inflammatory conditions as a means of emergency regulation? 2) Are Tr1 cells are a homogeneous T cell subset or do they differ in phenotype and function as a population? It is not known whether Tr1 cells represent a distinct lineage that arise directly from naive precursors in SLOs or if they develop from activated effector T cells at the site of inflammation, an aspect of Tr1 biology that has only been specifically addressed in chronic infection to date [236].

In that study Tr1 cells were found to develop from ex-Th17 cells during the resolution of inflammation in EAE after administration of α-CD3 antibody and in *N.brasiliensis* infection [236]. Initially Tr1 cells had been proposed to develop from naive T cells when supplied with chronic TCR stimulation in the presence of IL-10 [191], [376], [377]. Subsequent studies indicated that IL-10 is not essential for Tr1 cell development in gut associated lymphoid tissue and instead described IL-27 as critical for Tr1 cell generation [378]. Indeed, multiple publications now show that TCR activation of naive mouse T cells in the presence of IL-27 results in the development of Tr1 cells both *in vitro* and *in vivo* [273], [253], [379], [380], [297], [265], [264], [246], [218]. However, the developmental pathway of Tr1 cells in acute infection remains to be resolved in terms of generation from naive precursors and/or transdifferentiation from activated effector T cells as a means of self-regulation [363], [381]. Furthermore, whether Tr1 cells are a homogeneous population of $CD4^+$ T cells in acute infection required thorough investigation.

In the present study Tr1 cells were identified in SLOs and in the circulation during IAV infection, suggesting but not proving these cells may be derived from naive precursors *in vivo*. Additionally, *in vitro*-derived Tr1 cells were able to be generated from naive $CD4^+$ T cell precursors in the presence of α-CD3, α-CD28, IL-27, TGF-β, and IL-10 further supporting the suggestion of development from naive precursors. As the alternative method of Tr1 cell generation relies on conversion of effector T cells, it is difficult to exclude transdifferentiation, which would be required to assess the development of Tr1 cells from naive precursors in isolation. To instead address the questions surrounding the potential for transdifferentiation, activated $FOXP3^-$ $IL\text{-}10^-$ $CD4^+$ effector T cells could be FACS-sorted from IAV-infected dual-reporter lungs on day 5 post infection, prior to the time point at which Tr1 cells are observed to peak in cell number in the lungs. FACS-sorted Tr1 cells could then be transferred into congenically mismatched, infection-matched hosts. The transferred cells could then be interrogated at various time points post-transfer to determine if Tr1 cells are able to develop from activated effector T cell precursors during IAV infection. Together these findings have the potential to reveal intricacies concerning the development of Tr1 cells in acute infection.

As discussed above, based on previous publications, *bona fide* Tr1 cells were expected to conform to one specific phenotype (LAG-3^+ $CD49b^+$-DP) [194], [210], [218]. However, in this study four populations of *bona fide* Tr1 cells were identified on the basis of these markers prompting investigation into the phenotype and function of these cells which arise in IAV-infection *in vivo*. This observation is the first time distinct populations have been described for *bona fide* Tr1 cells and it raises an important question regarding the developmental relationship between these four populations: do they arise independently or is there a step-wise progression from naive $CD4^+$ T cells? Experiments using the *in vitro* culture system provide some insight into this issue. *In vitro*-derived Tr1 cells were

predominately LAG-3$^+$. In this system, 3 day cultures without TGF-β resulted in an increased frequency of LAG-3$^+$ and DP Tr1 cells, with the increase in the frequency of LAG-3$^+$ Tr1 cells likely resulting from a decrease in DN (refer to appendix **Fig A.4**). while this observation demonstrates the role of TGF-β in maintenance of a DN phenotype, to achieve higher proportions of LAG-3$^+$ and increased frequencies of DP Tr1 cells *in vitro* it was important to omit TGF-β (refer to appendix **Fig A.4 B-E**). The *in vitro* culture system also showed that restimulation of FACS-sorted LAG-3$^+$ cells leads to the generation of DP Tr1 cells which suggests a transitional relationship between those two Tr1 populations (refer to appendix **Fig A.5**). Data from the RNAseq experiments conducted in the present study go further and indicate that the developmental relationship *in vivo* may be LAG3$^+$, then DP, then CD49b$^+$. For example, the greatest number of DE genes were identified between the LAG-3$^+$ and CD49b$^+$ populations, whereas the DP Tr1 population appeared to share signatures of both LAG-3$^+$ and CD49b$^+$ Tr1 cells. In addition, the DP Tr1 cells were the most co-inhibitory receptor-enriched and along with the LAG-3$^+$ population, the most suppressive, identifying these two populations as the most regulatory of the Tr1 cell populations. Assuming that the DP and CD49b$^+$ cells are later stage Tr1 cells, the observation that both these CD49b-expressing populations were dependent on IL-10 to suppress effector T cell division, suggests that this mechanism may be a characteristic of more mature Tr1 cell populations. Further evidence that the CD49b$^+$ may be the most differentiated Tr1 population is that these cells expressed molecules associated with late-stage effector T cell differentiation such as DNAM-1, and P2RX7.

DNAM-1 has previously been found to be expressed by functionally suppressive Tr1 cells [194], [382], and in the present study the CD49b$^+$ Tr1 cells had the highest percentage of DNAM-1$^+$ cells. This suggested that CD49b$^+$ Tr1 cells could be the most regulatory of the four populations. However, contrary to those reports, the CD49b$^+$ Tr1 cells were not the most suppressive population in the present study. The purinergic receptor P2RX7 was one of the most significant DE genes in the CD49b$^+$ Tr1 cells. This receptor is known to sense extracellular ATP and NAD$^+$ and resulting signalling can lead to metabolic adaption and also cell death via apoptosis [383], [384]. This provides further support for the concept that CD49b$^+$ Tr1 cells are the most differentiated population and a proportion of these are potentially pre-apoptotic. Alternatively, the CD49b$^+$ Tr1 cells could be the least differentiated and exhausted/functional as they express the fewest co-inhibitory molecules and appear more effector-like. A previous study established that P2RX7 is important for memory CD8$^+$ T cell metabolic fitness and can promote the survival of these cells [385]. There is potential that the P2RX7$^+$ CD49b$^+$ Tr1 cells could exhibit enhanced metabolic fitness and may persist (even if they down-regulate IL-10 production). The role of P2RX7 on CD49b$^+$ Tr1 cells would need to be established to comment on whether it was promoting survival or death. To address this, CD49b$^+$ Tr1 cells could be efluor670-labelled

and transferred into congenically mis-matched IAV-infected recipients and tracked 2-7 days post transfer. A competitive inhibitor of P2RX7 or mock treatment could be administered and proliferation (efluor670) and death (annexin V and 7AAD) could be assessed with and without P2RX7 inhibition.

Egr2 was more highly expressed by the LAG-3$^+$ Tr1 cells compared to the CD49b$^+$ population. Egr2 and Egr3 have been shown to negatively regulate T cell activation and promote anergy [386]. The transcription factor NFAT (nuclear factor of activated T cells) is activated upon TCR ligation and with appropriate activation signals cooperates with AP-1 to result in T cell activation. In the absence of appropriate activation signals NFAT activates EGR2 leading to 'exhaustion' [387]. This could suggest that the LAG-3$^+$ Tr1 cells are in an earlier phase of development within this regulatory lineage as EGR2 may be degraded as activation overrides inhibition. Alternatively, Erg2 may be up-regulated in an 'exhausted' or anergic LAG-3$^+$ Tr1 cell population as a means of negative feedback and would result with induction of co-inhibitory molecule expression, including PD-1 and TIM-3 [387]. This would suggest that the Tr1 cell populations are anergic or 'exhausted' Th1 cells diverted toward an end-stage regulatory phenotype. This identifies that exploration into the role of EGR2 in Tr1 cells is required. An approach to address this would be to generate CRISPR/Cas9 *Egr2* KO and mock Tr1 cells in vitro to determine if their function is altered when transferred into IAV-infected hosts. *In vitro* suppression assays could also be performed to establish any functional differences in Tr1 cells in the absence of *Egr2*.

More detailed investigation examining how the Tr1 cell response develops, functions, and resolves in a physiological model of acute respiratory infection should lead to better understanding of the heterogeneity observed during acute infection. To investigate plasticity within and between Tr1 populations an experiment in which each of the four Tr1 populations are FACS-sorted from IAV-infected lungs and dye-labelled prior to transfer into separate infection-matched hosts could be conducted. Each population could then be interrogated to determine which populations it can give rise to. Additionally, to confirm if the CD49b$^+$ population is terminally differentiated and pre-apoptotic compared to the other populations annexin V staining could be conducted on Tr1 cells from IAV-infected lungs to assess each of the four populations for signs of apoptosis. These experiments would extend the findings of the present study and elucidate important questions that remain with respect to Tr1 cell development and biology during IAV infection.

5.7 Can Tr1 cell biology be manipulated to promote the resolution of inflammation in clinical settings?

An important question surrounds the potential utility of Tr1 cells as a cell-based therapy to inhibit excessive inflammation in clinical settings such as autoimmunity, GvHD or acute respiratory distress syndrome (ARDS). Indeed, Tr1 cell-based therapies have been adopted for clinical trials in the prevention of GvHD in patients with haematological malignancies receiving HSCT and the treatment of refractory Crohn's Disease [388], [243]. The present study, which shows that adoptive transfer of Tr1 cells restored recovery from maximum infection-induced weight loss compared to the littermate PBS recipients, supports a potential application for Tr1 cells in the treatment of acute inflammation caused by respiratory viral infection. Of further potential utility, the findings generated in this study showed that antigen-specificity was not necessary for this action of Tr1 cells which greatly simplifies the manufacturing of such a therapy.

Tr1 cells have been shown to promote tolerance to transplantation in a number of studies including pre-clinical models [200], [191], [229], [214], [389], [390], [246], [230]. The ALT-TEN trial is a clinical trial using Tr1 cells to treat transplant recipients to prevent GvHD. This clinical trial was proposed as a strategy to treat high risk patients with advanced stage haematological malignancies. The treatment in this trial consisted of a haploidentical T cell-depleted HSCT from a healthy donor. This was combined with donor-derived T cells pre-treated with IL-10 *in vitro* after HSCT. Post-IL-10 treatment, approximately 5% of transferred donor T cells were Tr1 cells [243]. It has been shown that activation of alloantigen specific Tr1 cells results in IL-10 production and tolerance [215], [199]. In total 12 patients were treated with this therapy and four exhibited stable chimerism, were in disease remission, and free from immunosuppression between 6 and 8 years post-HSCT. Of the remaining eight patients, three died early post-HSCT from infections, four died from failed transplants, and one patient developed GvHD which did not respond to treatment [243]. It is promising that this therapy in its early stage of development promoted stable engraftment in four patients especially when taking in account the low percentage of Tr1 cells generated in the protocol employed. The dose of anergised T cells used for that study was $1x10^5$ $CD3^+$ T cells/kg. This is much lower than the doses usually required for cellular therapies such as CAR-T therapy (approximately $1x10^6$ CAR-T cells/kg), but similar to the transfer experiments in the present study that required only small doses for a beneficial effect to the host. The result from that trial is also promising as the protocol could be enhanced to increase Tr1 generation by adding IL-27 and TGF-β into the T cell cultures prior to transfer to further drive Tr1 differentiation. Additionally, as mentioned previously, if surrogate markers can be identified for Tr1 cells this could be used

to enrich Tr1 cells in the population for transfer into transplant recipients. A second trial aiming to treat haematological malignancies with a Tr1 cell therapy is the T-allo-10 trial (ClinicalTrials.gov identifier: NCT03198234). This trial involves mismatched HSCT from healthy donors along with a T-allo-10 preparation of cells from the same healthy donor. The T-allo-10 preparation consists of T cells activated in the presence of IL-10 *in vitro* to drive Tr1 generation. The resulting cultured T cells contain Tr1 cells. This trial differs from the previous as T-allo-10 cells will be supplied to the recipient prior to transplant (early in comparison to other trials) to ensure Tr1 cells within the transferred T cells can act as soon as the transplant occurs. This trial aims to prevent GvHD and promote stable engraftment. Similar to the first trial the T-allo-10 trial could be improved by enhancing the Tr1 polarisation conditions to increase generation of these cells for transfer.

Another trial for clinical use of Tr1 cells is the CATS1 study aiming to treat refractory Crohn's Disease [388]. Twenty patients were selected for the trial and given a first dose of OVA-Treg cells which were made from the patient's own blood by isolating PBMCs and culturing them in the presence of ovalbumin (as OVA- is a common food antigen) supplemented with IL-2 and IL-4. When the phenotype of these cells was assessed a substantial proportion produced IL-10, approximately 40% expressed FOXP3, low levels of IL-4, and moderate levels of IFNγ suggestive of a type I profile for these regulatory T cells [388]. The treatment in this trial was not specifically Tr1 cells, although there was a high proportion of IL-10$^+$ cells, and the polarisation conditions would result in both Treg and Tr1 cells. This highlights a potentially useful strategy to combine both Tr1 and Treg cells depending on the disease requiring treatment. For instance, in autoimmune disease, treatment with different types of regulatory T cells (both Treg and Tr1 cells) would be beneficial to quench the detrimental inflammation in the intestine. Even within the present study focused on acute infection, Treg and Tr1 cells appear to regulate different and overlapping phases of the immune response. The treatment administered in the CATS1 trial was well tolerated and deemed safe in patients and 40% of patients in this trial exhibited significant clinical improvement, an effect that continued up to 5 weeks post-treatment after which the efficacy declined [388]. This suggests a window of action for OVA-Treg cells which is consistent with the transfer experiments in the present study, and also the Tr1 cell kinetics in acute infection revealed a transient window for Tr1 cell function. These results suggest a finite window of opportunity for OVA-Treg function analogous to previous studies investigating the role of regulatory T cells in a variety of challenges [298], [299], [300], [304]. This temporally restricted regulatory function, as discussed, is exemplified during acute infection as regulation is required at defined time points to regulate the anti-viral immune response and promote recovery and repair once the virus is cleared. This is also consistent with the present study as Tr1 cells were only transiently present in the IAV-infected lungs and transfer experiments indicated that they elicit their regulatory function between day 5

and day 8 at which point recovery from infection-induced weight loss is observed.

A temporally restricted window of transfer with respect to optimal efficacy of T cell therapy would be well-suited to the treatment of acute respiratory inflammation. This would require a burst of regulatory protection to prevent lethal pulmonary inflammation and promote tissue repair. One specific application for such a therapy would be ARDS which can develop from acute respiratory infections including IAV and SARS-COV-2 [391], [392], [393], as well as sepsis and major traumatic injury to the spine, head, or chest [394], [392]. ARDS is caused by excessive innate immune activation that results in pulmonary oedema that prevents gas exchange in alveoli, which can result in multi-organ failure and often is fatal. Currently treatment options are extremely limited. As mentioned above, Tr1 cell based therapies are in early stages of development and have shown success in preventing GvHD and treating refractory Crohn's Disease. It is conceivable that Tr1 cell based therapies could be developed for ARDS patients in future. It would require 3 days to polarise Tr1 cells from patient blood and deliver them to the patient. With many ARDS patients requiring months to recover with oxygen as the main treatment, cell therapy could be an option to promote recovery and tissue repair. In the present study polyclonal Tr1 cells were able to restore recovery from infection-induced weight loss in Tr1 cell-deficient mice. While many questions remain before testing such strategies in human ARDS patients, the results of this study suggest that Tr1 cell-based therapy may be an option for providing rapid suppression of inflammation and could provide the necessary control over potentially-lethal inflammatory responses in ARDS.

5.8 Limitations of this study.

This study was conducted using mouse models of IAV-infection with mouse-adapted virus strains. To assess the relevance of the Tr1 cell phenotypes for human disease IAV-infected human patient BALF washes could be interrogated for Tr1 cell presence and phenotype. The *Il27ra*$^{-/-}$ mouse was used as a model of Tr1 deficiency. This was accurate, however, as this is a broad knockout other cell populations could also be affected. There is now a CD4conv$^{iCreERT2\text{-}hCD2}$ mouse [395] which could be crossed with an *Il10*$^{fl/fl}$ mouse[277] to delete IL-10 on FOXP3^{-} conventional CD4^{+} T cells. Additionally, adoptive transfer of Tr1 cells was able to rescue recovery from maximum infection-induced weight loss however, it remains to be determined if Tr1 cell transfer can rescue recovery in WT mice infected with a high dose of IAV. To further elucidate the extent of Tr1 contributions to regulation of immune responses other viruses and infection models should be investigated.

5.9 Conclusion

The overall hypothesis for this study was that Tr1 cells contribute to the regulation of the immune response during acute infection. To address this Tr1-like cell accumulation was investigated in IAV infection and it was established that Tr1-like cells contribute to recovery from infection. Further investigation into the phenotype and function of these cells identified a number of chemokine receptors, cytokines, and co-inhibitory molecules expressed by these populations. Moreover, four novel populations of Tr1 cells based on expression of LAG-3 and CD49b were defined in this study. Each of these populations were classified as *bona fide* Tr1 cells as they were able to suppress effector T cell division in *ex vivo* suppression assays (refer to **Fig 5.1**). Further interrogation of these populations revealed distinct differences at the level of mRNA and protein. Overall, this study has shown that *bona fide* Tr1 cells have an important role in recovery from maximum infection-induced weight loss in IAV-infection, and together the results present the potential for clinical application of Tr1-based cell therapies in ARDS.

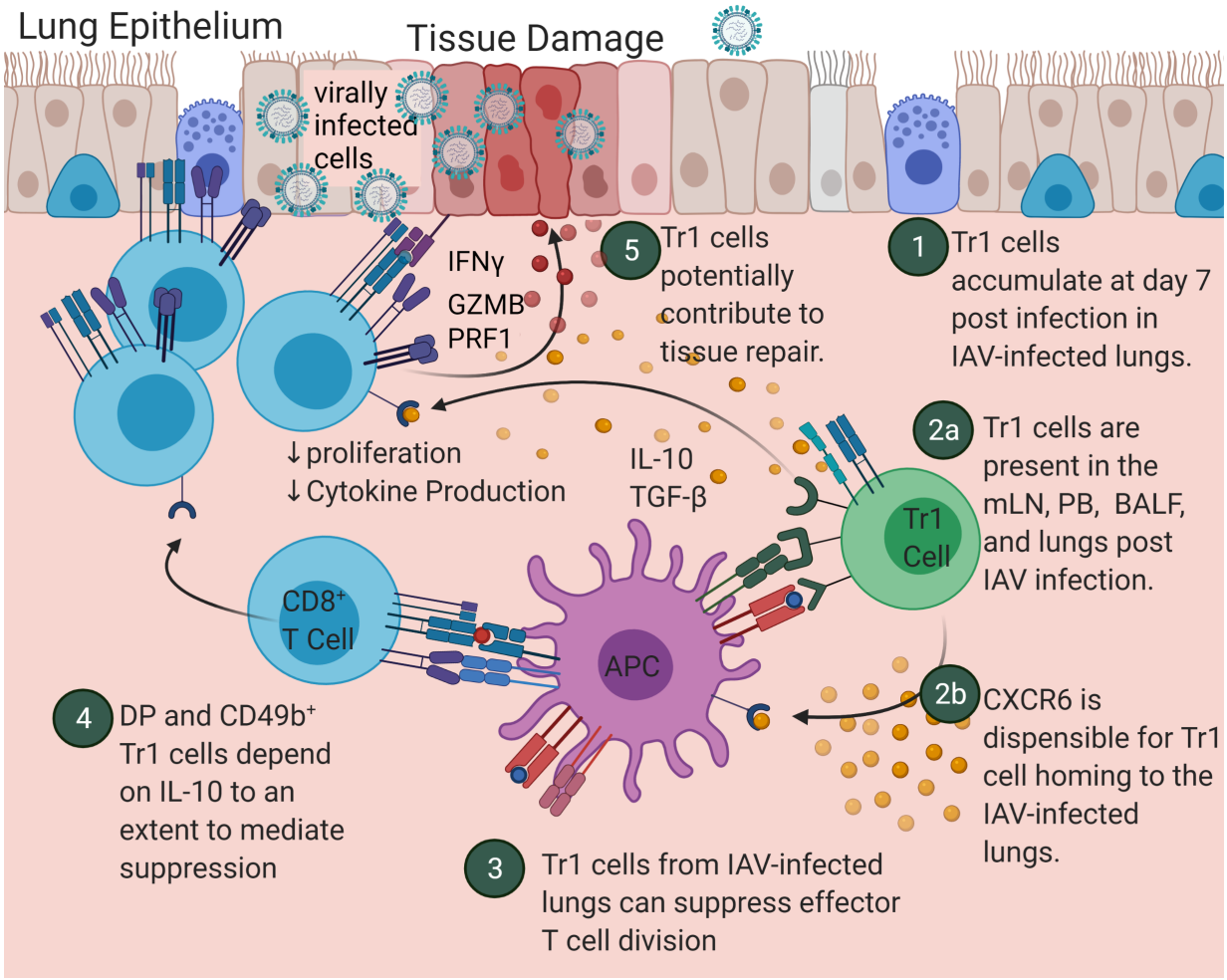
Lung Epithelium
Tissue Damage
virally infected cells
IFNγ
GZMB
PRF1
5 Tr1 cells potentially contribute to tissue repair.
1 Tr1 cells accumulate at day 7 post infection in IAV-infected lungs.
↓proliferation
↓Cytokine Production
IL-10
TGF-β
2a Tr1 cells are present in the mLN, PB, BALF, and lungs post IAV infection.
Tr1 Cell
CD8+ T Cell
APC
2b CXCR6 is dispensible for Tr1 cell homing to the IAV-infected lungs.
4 DP and CD49b+ Tr1 cells depend on IL-10 to an extent to mediate suppression
3 Tr1 cells from IAV-infected lungs can suppress effector T cell division

Figure 5.1: Tr1 cell contributions to the regulation of the anti-IAV immune response.

The contributions of Tr1 cells to the regulation of the immune response during acute infection were investigated in this study. The questions guiding this investigation were addressed as (1) The extent of Tr1 cell accumulation was assessed. (2a) Tr1 cells were detected in the mLN, PB, BALF and lungs of IAV infected mice, suggesting the importance of migration to reach these sites. (2a) CXCR6 however, was not required for Tr1 cells to accumulate in the IAV-infected lungs. (3) Tr1-like cells suppressive in the context of acute infection and therefore,were classified as *bona fide* Tr1 cells. (4) Each of the four populations was found to suppress effector T cell division with the DP and CD49b^{+} Tr1 cells depending somewhat on IL-10 to mediate suppression. (5) Additionally Tr1 cells were determined to produce AREG and therefore, exhibit the potential to contribute to tissue repair. (Created with BioRender.com)

Appendix A: Appendix

A.1 Supplementary Figures

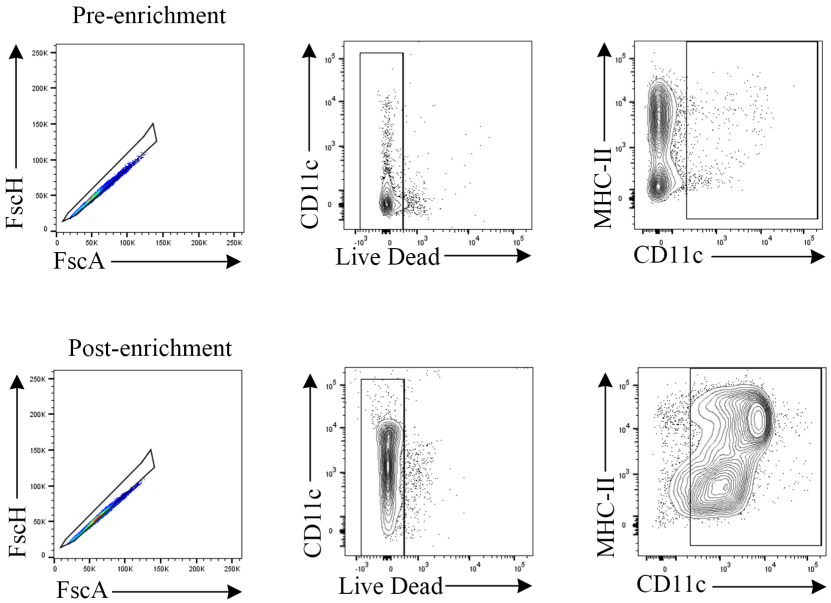

Figure A.1: Purification of CD11c$^+$ APCs for Suppression Assays.
CD11c$^+$ APCs were enriched from CD45.2 naive mouse spleens. The Stem Cell CD11c$^+$ positive isolation kit was used to enrich for these APCs. Post enrichment CD11c and MHC-II expression was analysed immediately after processing.

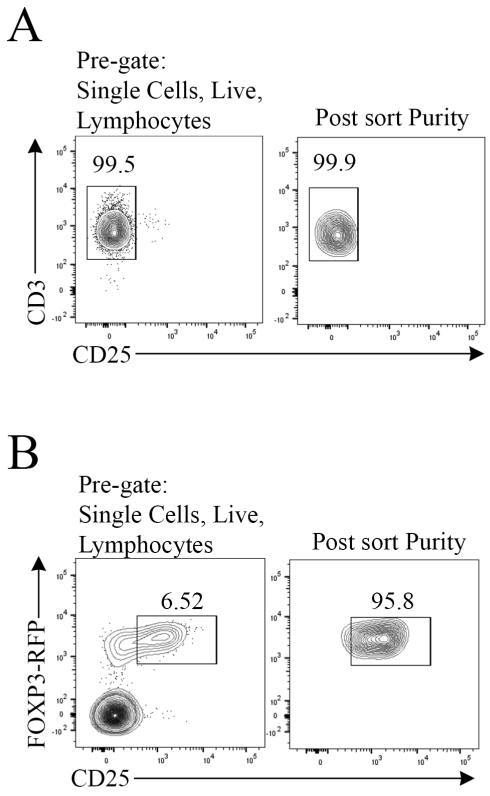

Figure A.2: Sorting Effector T Cells and Tregs from naive SLOs for Suppression Assays.

(A) Effector T cells for suppression assays were isolated from naive Ly5.1 spleens and inguinal lymph nodes. The stem cell pan naive T cell negative isolation kit was used to isolate $CD3^{+}$T cells. These were then FACS-sorted to ensure $CD25^{-}CD3^{+}$ effector T cells had been through the same process as regulatory T cells. (B) Tregs for a positive control for suppression were isolated from naive $FOXP3^{RFP}IL\text{-}10^{eGFP}$ reporter $CD45.2^{+}$ spleens. The Stem Cell CD4 T cell negative isolation kit was used to enrich for $CD4^{+}$T cells. Enriched CD4s were then FACS sorted for $FOXP3^{+}CD25^{+}$Tregs.

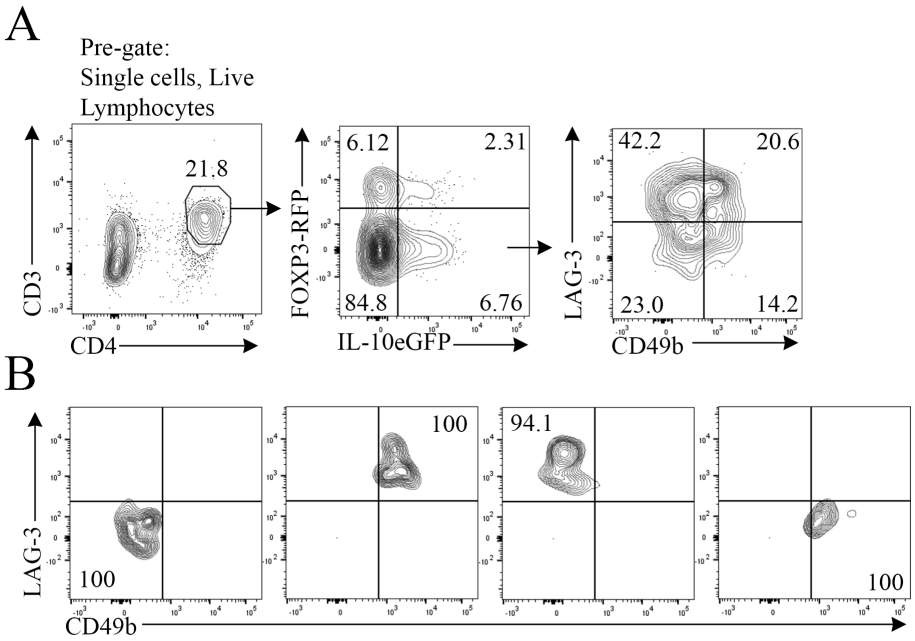

Figure A.3: Sorting Tr1s from the Influenza Infected Lungs for Suppression Assays.

(A) To isolate Tr1s for suppression assays FOXP3^{RFP}IL-10^{eGFP} mice were infected with X-31 IAV. On day 7 post infection the FOXP3^{-}IL-10^{+} Tr1s were sorted from the infected lungs based on expression of CD49b and LAG-3. (B) Representative flow cytometry of purity checks for the Tr1 populations.

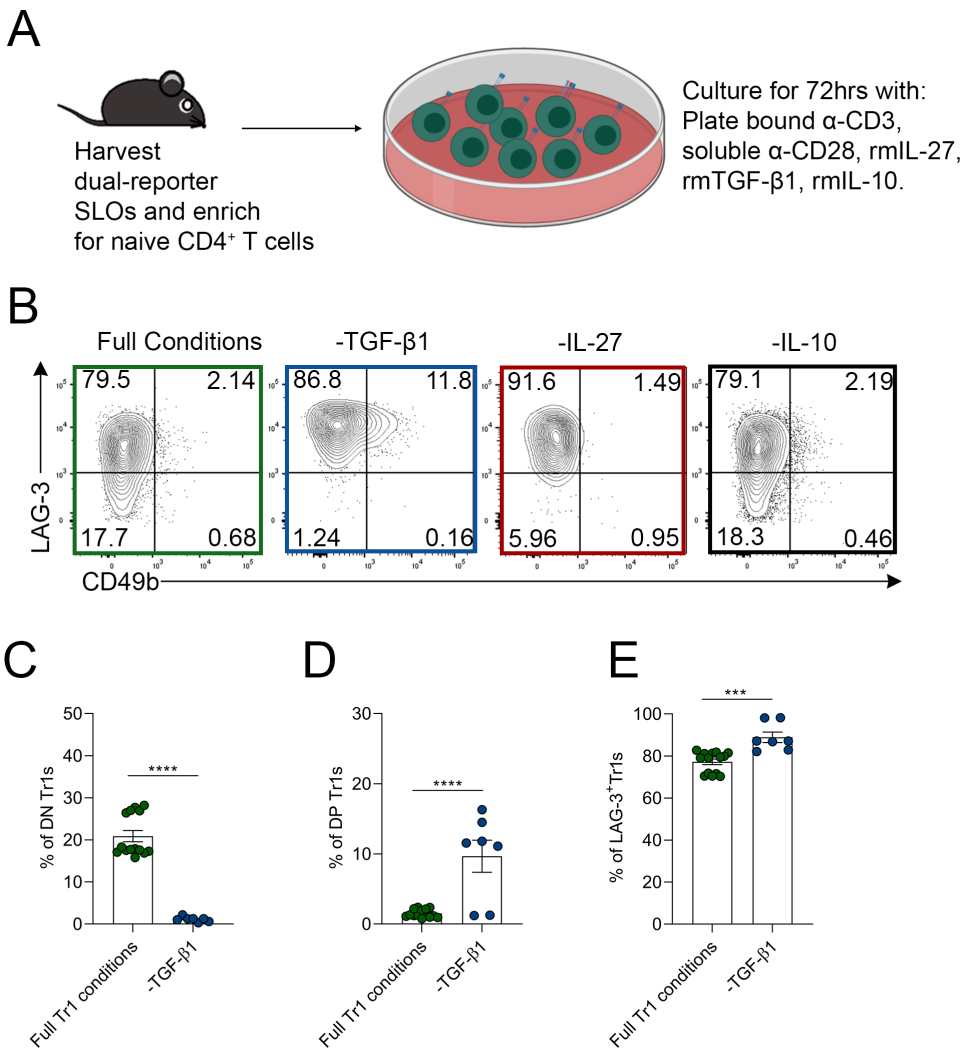
A
Harvest
dual-reporter
SLOs and enrich
for naive CD4⁺ T cells
Culture for 72hrs with:
Plate bound α-CD3,
soluble α-CD28, rmIL-27,
rmTGF-β1, rmIL-10.
B
Full Conditions
-TGF-β1
-IL-27
-IL-10
LAG-3
CD49b
79.5
2.14
17.7
0.68
86.8
11.8
1.24
0.16
91.6
1.49
5.96
0.95
79.1
2.19
18.3
0.46
C
% of DN Tr1s
****
Full Tr1 conditions
-TGF-β1
D
% of DP Tr1s
****
Full Tr1 conditions
-TGF-β1
E
% of LAG-3⁺Tr1s
***
Full Tr1 conditions
-TGF-β1

Figure A.4: *In vitro*-generated Tr1 cell LAG-3 and CD49b expression.

(A) Schematic of cultures for *in vitro* generation of Tr1 cells from naive $CD4^+$ T cells. (B) Representative flow cytometry of *in vitro*-generated Tr1 cell expression of LAG-3 and CD49b under full Tr1 conditions (rmIL-27, rmTGFβ1, and rmIL-10), - TGFβ1 (full Tr1 conditions - TGFβ1), -IL-27 (full Tr1 conditions - IL-27), or -IL-10 (full Tr1 conditions - IL-10), each condition included plate bound α-CD3 antibody and soluble α-CD28 antibody. Frequency of DN (C), DP (D), and LAG-3^+ (E) Tr1 cells cultured under full Tr1 conditions or - TGFβ1. Each symbol represents a different technical replicate, the mean is shown +/- SEM, n=13 (Tr1 conditions), 7 (-TGF-β), 5 (-IL-27), 3 (-IL-10), from 4 independent experiments. Statistical analysis completed using one-way ANOVA with Bonferroni's post-test (where $^{***} = p \leq 0.001, and ^{****} = p \leq 0.0001$).

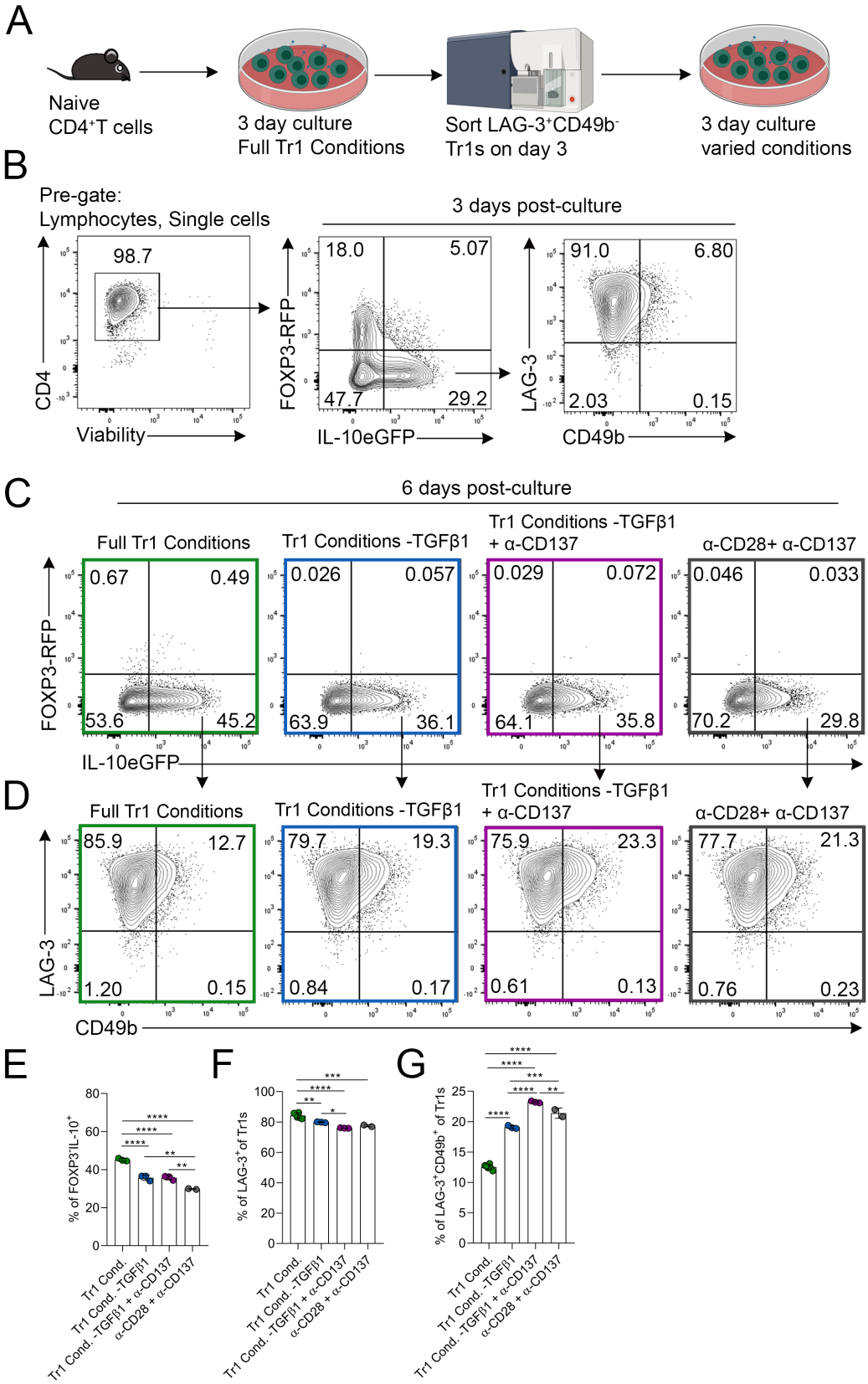
A
Naive
CD4+T cells
3 day culture
Full Tr1 Conditions
Sort LAG-3+CD49b-
Tr1s on day 3
3 day culture
varied conditions
B
Pre-gate:
Lymphocytes, Single cells
3 days post-culture
98.7
CD4
Viability
18.0
5.07
47.7
29.2
FOXP3-RFP
IL-10eGFP
91.0
6.80
2.03
0.15
LAG-3
CD49b
C
6 days post-culture
Full Tr1 Conditions
Tr1 Conditions -TGFβ1
Tr1 Conditions -TGFβ1
+ α-CD137
α-CD28+ α-CD137
0.67
0.49
53.6
45.2
0.026
0.057
63.9
36.1
0.029
0.072
64.1
35.8
0.046
0.033
70.2
29.8
FOXP3-RFP
IL-10eGFP
D
Full Tr1 Conditions
Tr1 Conditions -TGFβ1
Tr1 Conditions -TGFβ1
+ α-CD137
α-CD28+ α-CD137
85.9
12.7
1.20
0.15
79.7
19.3
0.84
0.17
75.9
23.3
0.61
0.13
77.7
21.3
0.76
0.23
LAG-3
CD49b
E
% of FOXP3+IL-10+
Tr1 Cond.
Tr1 Cond. -TGFβ1
Tr1 Cond. -TGFβ1 + α-CD137
Tr1 Cond. -TGFβ1 + α-CD28 + α-CD137
F
% of LAG-3+of Tr1s
Tr1 Cond.
Tr1 Cond. -TGFβ1
Tr1 Cond. -TGFβ1 + α-CD137
α-CD28 + α-CD137
G
% of LAG-3+CD49b+ of Tr1s
Tr1 Cond.
Tr1 Cond. -TGFβ1
Tr1 Cond. -TGFβ1 + α-CD137
Tr1 Cond. -TGFβ1 + α-CD28 + α-CD137

Figure A.5: Plasticity of *in vitro*-derived LAG-3$^+$Tr1 cells

(A) Schematic of experiment: dual-reporter mouse SLOs were used to generate *in vitro*-derived Tr1 cells. FOXP3$^-$, IL-10$^+$, LAG-3$^+$, CD49b$^-$ Tr1 cells were FACS-sorted after 3 days of culture. Post sort LAG-3$^+$ Tr1 cells were placed back into culture with plate bound α-CD3 antibody under Tr1 conditions, or Tr1 conditions without TGF-β1, or Tr1 conditions without TGF-β1 with added α-CD137, or with co-stimulation alone.(B) gating strategy for identifying LAG-3$^+$ Tr1 cells on day 3 post culture. (C), (D) Flow cytometry displaying the expression of (C) FOXP3 and IL-10 and (D) LAG-3 and CD49b by sorted LAG-3$^+$ Tr1 cells after a further 3 days of culture (6 days of culture total) in the conditions stated. (E) The percentage of FOXP3$^-$ IL-10$^+$ Tr1 cells after 6 days of culture. (F) The frequency of LAG-3$^+$ Tr1 cells after 6 days of culture. (G) The percentage of DP Tr1 cells after 6 days of culture. Each symbol represents a different technical replicate, shown as mean +/- SD, n=2-6 technical replicates from 2 independent experiments. Statistical analysis using a one-way ANOVA with Bonferroni's post-test (where
$^* = p \leq 0.05, ^{**} = p \leq 0.01, ^{***} = p \leq 0.001, and ^{****} = p \leq 0.0001$).

Appendix B: RNA Sequencing Code

```
#install packages
install.packages("BiocManager")
install.packages("devtools")
install.packages("tidyverse")
install.packages("magrittr")
BiocManager::install("limma")
BiocManager::install("edgeR")
BiocManager::install("ggrepel")
BiocManager::install("AnnotationHub")
BiocManager::install("ensembldb")
BiocManager::install("RColorBrewer")
install.packages("ggplot2")
install.packages("pheatmap")
install.packages("plotly")
install.packages("RColorBrewer")
BiocManager::install("clusterProfiler")
BiocManager::install("org.Mm.eg.db")
BiocManager::install("variancePartition")
BiocManager::install("KEGG.db")
install.packages("statmod")

setwd("C:/Users/caitlin/Desktop/Tr1␣RNA␣seq")
library(tidyverse)
library(magrittr)
library(limma)
library(edgeR)
library(ggrepel)
library(ggplot2)
library(pheatmap)
library(AnnotationHub)
library(ensembldb)
library(plotly)
library(RColorBrewer)
library(clusterProfiler)
library(org.Mm.eg.db)
library(variancePartition)

file <- "Caitlin_genes.out"
counts <- read.delim(file, comment = "#")
head(counts)
```

```
#Converting counts data into a readable list called dgelist

dgeList <- counts %>%
  dplyr::select(Geneid, ends_with("bam")) %>%
  as.data.frame() %>%
  column_to_rownames("Geneid") %>%
  as.matrix() %>%
  DGEList()
dgeList$counts

dgeList

#change sample names

colnames(dgeList) <- basename(gsub("X.data.biohub.20190819_
   McColl_RNASeq.Caitlin.2_alignedData.bams.", "", colnames(
   dgeList)))
colnames(dgeList) <- basename(gsub("Aligned.sortedByCoord.out.
   bam", "", colnames(dgeList)))

dgeList$counts[,c(2,3,4,5,6,7,8,9,12,13,14,15)] -> dgeList$
   counts
dgeList$samples
dgeList$samples <- dgeList$samples[c(2,3,4,5,6,7,8,9,12,13,14,15
   ),]


#Normfactors based on library size condition is from sample
   names

dgeList <- calcNormFactors(dgeList, method = c("TMM"))
dgeList$samples$condition <- gsub("M2_|M3_|M5_|M6_", "",
   rownames(dgeList$samples)) #add column to show populations
dgeList$samples$condition <- factor(dgeList$samples$condition,
                                    levels= c("DP", "LAG_3", "CD
                                       49b"))
dgeList$samples$mouse <- str_extract(colnames(dgeList), "M[0-9]"
   )
dgeList$samples
```

```
#Library size for each sample

dgeList$samples %>%
  rownames_to_column("Sample") %>%
  mutate(CellType = dgeList$samples$condition) %>%
  ggplot(aes(x = Sample, y = lib.size / 1e6, fill = CellType)) +
  geom_bar(stat = "identity") +
  labs(y = "Library Size (millions)") +
  theme_bw()

#MDS plot

#mds <- plotMDS(dgeList[,], col = as.integer(dgeList$samples$
   condition))

#Filter out unnecessary genes

logcount <- cpm(dgeList, log = TRUE)
plotDensities(logcount)
genes2keep <- rowSums(logcount > 1) >3 #>1million reads in at
   least 3 samples
summary(genes2keep)
plotDensities(logcount[genes2keep, ])
dgeFilt <- dgeList[genes2keep, , keep.lib.sizes = FALSE]
dgeFilt

# PCA and filter out DN samples

pca <- dgeFilt %>%
  # .[,!grepl("DN", colnames(.))] %>%
  cpm(log = TRUE) %>%
  t() %>%
  prcomp()

x <- "PC1"
y <- "PC2"
dgeFilt$samples %>%
  rownames_to_column("Sample") %>%
  #dplyr::filter(!str_detect(Sample, "DN")) %>%
  mutate(Mouse = str_extract(Sample, "M[0-9]")) %>%
  as_tibble() %>%
```

```
  dplyr::filter(condition != "DN") %>%
  cbind(pca$x[.$Sample,]) %>%
  ggplot(aes_string(x, y, shape = "Mouse", colour = "condition")
     ) +
  geom_point(size = 3) +
  geom_text_repel(aes(label = Sample), show.legend =FALSE) +
  labs(
    x = paste0(x, " (", scales::percent(summary(pca)$importance[
       2, x]), ")"),
    y = paste0(y, " (", scales::percent(summary(pca)$importance[
       2, y]), ")")
  )

#Annotating

Ah <- AnnotationHub()
#{Find which genome we used}
unique(Ah$dataprovider)
subset(Ah, dataprovider == "Ensembl") %>%  #In Ensembl databse
  subset(species == "Mus musculus") %>%  #under Mouse
  subset(rdataclass == "EnsDb")
ensDb <- Ah[["AH69210"]] #This is the genome I used for the
   sequencing
genes <- genes(ensDb) %>% #extract the genes
  subset(seqnames %in% c(1:19, "MT", "X", "Y")) %>%
  keepStandardChromosomes()
seqlevels(genes) <- str_sort(seqlevels(genes), numeric = TRUE) #
   order it by numeric
genes
dgeFilt$genes <- genes[rownames(dgeFilt),]
dgeFilt$genes

#vooming

design <- model.matrix(~0 + condition, data = dgeFilt$samples)
colnames(design) <- str_remove(colnames(design), "condition")
v = voomWithQualityWeights(dgeFilt, design = matrix(1, nrow =
   ncol(dgeFilt)), plot = TRUE)


#PCA plot
```

```
mds$cmdscale.out %>%
  as.data.frame() %>%
  set_colnames(c("Dim1", "Dim2")) %>%
  rownames_to_column("sample") %>%
  cbind(v$targets[.$sample,]) %>%
  dplyr::rename(w = sample.weights) %>%
  ggplot(aes(Dim1, Dim2, colour = condition, label = sample)) +
  geom_point(aes(size = w)) +
  geom_text_repel() +
  labs(x = "Leading␣logFC␣dim␣1",
       y = "Leading␣logFC␣dim␣2",
       size = "Sample\nweight",
       colour = "Cell␣Type") +
  theme_bw(pca <- v$E) %>%
  #.[,!grepl("DN", colnames(.))] %>%
  cpm(log = TRUE) %>%
  t() %>%
  prcomp()

x <- "PC1"
y <- "PC2"
v$targets %>%
  rownames_to_column("Sample") %>%
  #dplyr::filter(!str_detect(Sample, "DN")) %>%
  mutate(Mouse = str_extract(Sample, "M[0-9]")) %>%
  as_tibble() %>%
  dplyr::filter(condition != "DN") %>%
  cbind(pca$x[.$Sample,]) %>%
  ggplot(aes_string(x, y, shape = "Mouse", colour = "condition",
      size = "sample.weights")) +
  geom_point(size = 3) +
  geom_text_repel(aes(label = Sample), show.legend =FALSE) +
  labs(
    x = paste0(x, "␣(", scales::percent(summary(pca)$importance[
       2, x]), ")"),
    y = paste0(y, "␣(", scales::percent(summary(pca)$importance[
       2, y]), ")")
  )

v$targets %>%
```

```
  ggplot(aes(condition, sample.weights, fill = mouse)) +
  geom_bar(stat = "identity") +
  geom_hline(yintercept = 1, linetype = 2) +
  facet_wrap(~mouse)

#Calculate correlations

#{apply duplicateCorrelation in two rounds}
tmp <- voom(dgeFilt, design, plot=FALSE)
dupcor <- duplicateCorrelation(tmp, design, block=dgeFilt$
   samples$mouse)

#run voom considering the duplicateCorrelation results in order
   to compute more accurate precision weights

v = voomWithQualityWeights(
  counts = dgeFilt,
  design = matrix(1, nrow = ncol(dgeFilt)),
  plot=FALSE,
  block=dgeFilt$samples$mouse,
  correlation=dupcor$consensus
)

#Estimate linear mixed model with a single variance component.
   Fit the model for each gene

dupcor <- duplicateCorrelation(v, design, block=dgeFilt$samples$
   mouse)

#But this step uses only the genome-wide average for the random
   effect
#fitDupCor <- lmFit(vobj, design, block=metadata$Individual,
   correlation=dupcor$consensus)

cont.matrix <- makeContrasts(
  LAG3vCD49b = LAG_3 - CD49b,
  CD49bvDP = CD49b - DP,
  LAG3vDP = LAG_3 - DP,
  levels = design)

#Limma
```

```
fit <- lmFit(v, design = design, block = v$targets$mouse,
   correlation = dupcor$consensus)
fit.cont <-  contrasts.fit(fit, cont.matrix) %>%
  eBayes()

summa.fit <- decideTests(fit.cont, lfc = 1)
summary(summa.fit)
plotSA(fit.cont)

#Make Tables

topTable(fit.cont, coef = "LAG3vDP", number = Inf, sort.by = "p"
   , p.value = 0.05, lfc = 1) -> LAG3vDP
LAG3vDP %>% select(ID.gene_id, ID.gene_name, logFC, AveExpr, P.
   Value, adj.P.Val) -> FiltLAG3DP

topTable(fit.cont, coef = "CD49bvDP", number = Inf, sort.by = "p
   ", p.value = 0.05, lfc = 1) -> CD49bvDP
CD49bvDP %>% select(ID.gene_id, ID.gene_name, logFC, AveExpr, P.
   Value, adj.P.Val) -> FiltCD49bDP

topTable(fit.cont, coef = "LAG3vCD49b", number = Inf, sort.by =
   "p", p.value = 0.05, lfc = 1) -> LAG3vCD49b
LAG3vCD49b %>% select(ID.gene_id, ID.gene_name, logFC, AveExpr,
   P.Value, adj.P.Val) -> FiltLAG3CD49b

#Table with all three comparisons

allCont <- colnames(fit.cont)
Comparisons <- lapply(allCont, function(x){
  topTable(fit.cont, coef = x, number = nrow(fit)) %>%
    rownames_to_column("Gene") %>%
    as_tibble()
}) %>%
  set_names(allCont)

#volcano plot for each comparison

currentComp <- "LAG3vCD49b"
Comparisons[[currentComp]] %>%
```

```
  dplyr::rename(fdr = adj.P.Val,
                Name = ID.gene_name) %>%
  mutate(DE = abs(logFC) >1 & fdr < 0.05,
         DE = sign(logFC) * DE,
         DE = as.factor(DE)) %>%
  arrange(desc(P.Value)) %>%
  ggplot(aes(logFC, -log(P.Value), label = Name, fdr = fdr)) +
  geom_point(aes(colour = DE)) +
  ggtitle(currentComp) +
  geom_text_repel(data = . %>% tail(20)) +
  scale_color_manual(values = c("blue", "grey", "red")) +
  theme_bw()

currentComp <- "CD49bvDP"
Comparisons[[currentComp]] %>%
  dplyr::rename(fdr = adj.P.Val,
                Name = ID.gene_name) %>%
  mutate(DE = abs(logFC) >1 & fdr < 0.05,
         DE = sign(logFC) * DE,
         DE = as.factor(DE)) %>%
  arrange(desc(P.Value)) %>%
  ggplot(aes(logFC, -log(P.Value), label = Name, fdr = fdr)) +
  geom_point(aes(colour = DE)) +
  ggtitle(currentComp) +
  geom_text_repel(data = . %>% tail(20)) +
  scale_color_manual(values = c("blue", "grey", "red")) +
  theme_bw()

currentComp <- "LAG3vDP"
Comparisons[[currentComp]] %>%
  dplyr::rename(fdr = adj.P.Val,
                Name = ID.gene_name) %>%
  mutate(DE = abs(logFC) >1 & fdr < 0.05,
         DE = sign(logFC) * DE,
         DE = as.factor(DE)) %>%
  arrange(desc(P.Value)) %>%
  ggplot(aes(logFC, -log(P.Value), label = Name, fdr = fdr)) +
  geom_point(aes(colour = DE)) +
  ggtitle(currentComp) +
  geom_text_repel(data = . %>% tail(20)) +
  scale_color_manual(values = c("blue", "grey", "red")) +
```

```
  theme_bw()

#Average expression versus LoGFC plots

plotly::ggplotly(
  data_frame(Gene = rownames(fit.cont),
             Name = fit.cont$genes$gene_name,
             logFC = fit.cont$coefficients[,currentComp],
             AveExpr = fit.cont$Amean,
             p = Comparisons[[currentComp]]$P.Value,
             fdr = Comparisons[[currentComp]]$adj.P.Val,
             DE = abs(logFC) > 1) %>%
    mutate(DE = sign(logFC)*DE,
           DE = as.factor(DE),
           fdr = round(fdr, 4),
           logFC= round(logFC, 3),
           AveExpr= round(AveExpr, 3)) %>%
    arrange(desc(p)) %>%
    ggplot(aes(AveExpr, logFC, label = Name, fdr = fdr)) +
    geom_point(aes(colour = DE)) +
    guides(colour = FALSE) +
    scale_colour_manual(values = c("blue", "grey", "red")) +
    ggtitle(currentComp) +
    theme_bw() +
    theme(legend.position = "none",
          plot.title = element_text(hjust = 0.5))
)

#High confidence table

highConfTable <- lapply(allCont, function(x){
  topTable(fit.cont, coef = x, number = nrow(fit), sort.by = "p"
     , p.value = 0.05, lfc = 1) %>%
    rownames_to_column("Gene") %>%
    as_tibble()
}) %>%
  set_names(allCont)

HighConfGenes <- highConfTable%>%
  lapply(extract2, "Gene") %>%   #isolate ensembl IDs
  unlist() %>%  #merge everything into one list
```

```
  unique() #retrieve only unique ensembl IDs
length(HighConfGenes)

#only extract the confident genes from the highConfGenes list
   without the LFC

highConfTable <- sapply(allCont, function(x){
  topTable(fit.cont, coef = x, number = Inf, p.value = 0.05) %>%
    rownames_to_column("Gene") %>%
    as_tibble() %>%
    dplyr::filter(Gene %in% HighConfGenes)
}, simplify = FALSE)
highConfTable$genes <- genes[HighConfGenes,] #table containing
   our high confidence genes

#New table with all the highConfGenes in it regardless of P or
   logFC

alltable <- topTable(fit.cont, coef = "LAG3vCD49b", number = Inf
   ) %>%
  rownames_to_column("Gene") %>%
  dplyr::filter(Gene %in% HighConfGenes) %>%
  select(Gene, ID.gene_name, logFC, adj.P.Val, ID.entrezid)

#Heatmap

mat_col <- data.frame(group = v$design)
mat_colours <- list(group = brewer.pal(4, "Set1"))
names(mat_colours$group) <- unique(mat_col)
valueRange <- fit.cont$coefficients[HighConfGenes,] %>%
  subtract(rowMeans(.)) %>%
  range()
myPalette <- colorRampPalette(c("blue", "white", "red"))(101)
myBreaks <- c(seq(min(valueRange), 0, length.out = 51),
              seq(max(valueRange) / 101, max(valueRange), length
                 .out = 50))


#c("LAG3", "CD49b", "DP") -> hello

pheatmap(mat = fit$coefficients[HeatmapGenes$gene_id,] %>%
```

```
    subtract(rowMeans(.)),
          color = myPalette,
          breaks = myBreaks,
          border_color = NA,
          # show_colnames = FALSE,
          show_rownames = TRUE,
          cluster_cols = FALSE,
          scale = "none",
          #labels_col = hello,
          labels_row = HeatmapGenes$gene_name,
          #cutree_rows = 3,
          drop_levels = TRUE,
          fontsize = 11)

# Making isolated heatmaps for genes upregulated in the three
    populations

highConfTable$LAG3vCD49b %>%
  select(Gene, ID.gene_name, logFC, adj.P.Val) %>%
  arrange(logFC) -> FCLAG3CD49b
highConfTable$CD49bvDP %>%
  select(Gene, ID.gene_name, logFC, adj.P.Val) %>%
  arrange(logFC) -> FCCD49bDP
highConfTable$LAG3vDP %>%
  select(Gene, ID.gene_name, logFC, adj.P.Val)  %>%
  arrange(logFC)-> FCLAG3DP

subset(FCCD49bDP, logFC >=0.1) %>% select(Gene) -> UPonCD49b
c(subset(FCLAG3CD49b, logFC<=0.1) %>% select(Gene), UPonCD49b)
    -> UPonCD49b
UPonCD49b %>% unlist() %>% unique() -> UPonCD49b
dplyr::filter(alltable, Gene %in% UPonCD49b) -> CD49bnames

subset(FCCD49bDP, logFC<=1) %>% select(Gene) -> UPonDP
c(subset(FCLAG3DP, logFC<=1) %>% select(Gene), UPonDP) -> UPonDP
UPonDP %>% unlist() %>% unique() -> UPonDP
dplyr::filter(alltable, Gene %in% UPonDP) -> DPnames

subset(FCLAG3CD49b, logFC >=0.1) %>% select(Gene) -> UPonLAG3
c(subset(FCLAG3DP, logFC>=0.1) %>% select(Gene), UPonLag3) ->
    UPonLAG3
```

```
UPonLAG3 %>% unlist() %>% unique() -> UPonLAG3
dplyr::filter(alltable, Gene %in% UPonLAG3) -> LAG3names

pheatmap(mat = fit$coefficients[LAG3names$Gene [1:50],] %>%
           subtract(rowMeans(.)),
         color = myPalette,
         breaks = myBreaks,
         border_color = NA,
         # show_colnames = FALSE,
         show_rownames = TRUE,
         cluster_cols = FALSE,
         scale = "none",
         labels_row = LAG3names$ID.gene_name [1:50],
         #cutree_rows = 3,
         drop_levels = TRUE,
         fontsize = 11)

#cpm plots with pretty colours, mean for each population
cpm(dgeList, log = TRUE)["ENSMUSG00000046186",] %>%
  as.data.frame() %>%
  set_colnames("CPM") %>%
  rownames_to_column("Sample") %>%
  left_join(rownames_to_column(dgeFilt$samples, "Sample")) %>%
  #filter(condition != "DN") %>%
  droplevels() %>%
  arrange(Sample) %>%
  group_by(condition) %>%
  summarise(CPM = mean(CPM)) %>%
  ggplot(aes(condition, CPM, fill = condition)) +
  scale_fill_manual(values = c("#228B22", "#FFA500", "#B22222")
     ) +
  ylim(-1, 15) +
  geom_bar(stat = "identity") +
  #scale_y_continuous(breaks = seq(0, 12, by = 2,)) +
  theme_bw() +
  theme(axis.text.x = element_text(angle = 90, hjust = 1, vjust
     = 0.5))


#cpm plots with pretty colours, each sample and population, to
   get mean CPM for each population remove #before summarise
```

```
   line and change Sample on ggplot line with condition
cpm(dgeList, log = TRUE)["ENSMUSG00000041272",] %>%
  as.data.frame() %>%
  set_colnames("CPM") %>%
  rownames_to_column("Sample") %>%
  left_join(rownames_to_column(dgeFilt$samples, "Sample")) %>%
  #filter(condition != "DN") %>%
  droplevels() %>%
  arrange(sample) %>%
  group_by(condition) %>%
  #summarise(CPM = mean(CPM)) %>%
  ggplot(aes(Sample, CPM, fill = condition)) +
  scale_fill_manual(values = c("#228B22", "#FFA500", "#B22222")
     ) +
  ylim(-1, 12) +
  geom_bar(stat = "identity") +
  #scale_y_continuous(breaks = seq(0, 12, by = 2,)) +
  theme_bw() +
  theme(axis.text.x = element_text(angle = 90, hjust = 1, vjust
     = 0.5))

#Tables for top 50 genes according to adj.P.Val

Top50LAG3vCD49b <- highConfTable$LAG3vCD49b %>%
  arrange(adj.P.Val) %>%
  select(ID.gene_id, ID.gene_name, P.Value, adj.P.Val, logFC,
     AveExpr)
Top50LAG3vCD49b <- Top50LAG3vCD49b[1:50,]

Top50LAG3vDP <- highConfTable$LAG3vDP %>%
  arrange(adj.P.Val) %>%
  select(ID.gene_id, ID.gene_name, P.Value, adj.P.Val, logFC,
     AveExpr)
Top50LAG3vDP <- Top50LAG3vDP[1:50,]

Top50CD49bvDP <- highConfTable$CD49bvDP %>%
  arrange(adj.P.Val) %>%
  select(ID.gene_id, ID.gene_name, P.Value, adj.P.Val, logFC,
     AveExpr)
Top50CD49bvDP <- Top50CD49bvDP[1:50,]
```

```
Top50ALL <- c(Top50CD49bvDP$ID.gene_id, Top50LAG3vCD49b$ID.gene_
   id, Top50LAG3vDP$ID.gene_id) %>%
  unlist() %>%
  unique()

Top50heatmap <- dplyr::filter(alltable, Gene %in% Top50ALL) %>%
   arrange(logFC)


#heatmap of the genes from the top 50 most significant genes

pheatmap(mat = fit$coefficients[Top50heatmap[1:50],] %>%
           subtract(rowMeans(.)),
         color = myPalette,
         breaks = myBreaks,
         border_color = NA,
         # show_colnames = FALSE,
         show_rownames = TRUE,
         cluster_cols = FALSE,
         scale = "none",
         labels_row = Top50heatmap$ID.gene_name[1:50],
         #cutree_rows = 3,
         drop_levels = TRUE,
         fontsize = 11)


#Pathway analysis
#Define universe for go terms (Use dgefilt for all gene ID)

universe <- dgeFilt$genes$entrezid %>%
  unlist() %>%
  extract(!is.na(.)) %>% #keep non NA gene
  unique() %>%
  as.character()

#get the EnterezID from each contrast

DELAG3vCD49b <- highConfTable$LAG3vCD49b %>%
  dplyr::filter(adj.P.Val < 0.05) %>%
  dplyr::select(Gene, ID.gene_name, ID.entrezid)
```

```
DE49vDP <- highConfTable$CD49bvDP %>%
  dplyr::filter(adj.P.Val < 0.05) %>%
  dplyr::select(Gene, ID.gene_name, ID.entrezid)

DELag3vDP <- highConfTable$LAG3vDP %>%
  dplyr::filter(adj.P.Val < 0.05) %>%
  dplyr::select(Gene, ID.gene_name, ID.entrezid)

#ClusteredprofileR LAG-3vDP

clusterLag3vDP <- enrichGO(gene = DELag3vDP$ID.entrezid,
                           universe = universe,
                           OrgDb = org.Mm.eg.db,
                           ont = "ALL",
                           keyType = "ENTREZID",
                           pAdjustMethod = "bonferroni",
                           pvalueCutoff = 0.01,
                           qvalueCutoff = 0.05,
                           readable = TRUE)

FCLAG3DP <- structure(highConfTable$LAG3vDP$logFC, names =
   highConfTable$LAG3vDP$ID.entrezid %>%
                            vapply(function(x){as.character(x)[[
                               1]]}, character(1))) #grab the
                               fold change and make it into a
                               character
FCLAG3DP <- FCLAG3DP[!is.na(names(FCLAG3DP))]

#make the cluster into a dataframe for easy readability
dLAG3vDP <- as.data.frame(clusterLag3vDP)
head(summary(LAG3vDP))
dotplot(clusterLag3vDP, showCategory = 10)
cnetplot(clusterLag3vDP, node_label = "all", foldChange = FCLAG3
   DP)
emapplot(clusterLag3vDP)


#ClusteredprofileR LAG-3 v CD49b

clusterLag3vCD49b <- enrichGO(gene = DELAG3vCD49b$ID.entrezid,
                           universe = universe,
```

```
                              OrgDb = org.Mm.eg.db,
                              ont = "ALL",
                              keyType = "ENTREZID",
                              pAdjustMethod = "bonferroni",
                              pvalueCutoff = 0.01,
                              qvalueCutoff = 0.05,
                              readable = TRUE)

FCLAG3CD49b <- structure(highConfTable$LAG3vCD49b$logFC, names =
    highConfTable$LAG3vCD49b$ID.entrezid %>%
                           vapply(function(x){as.character(x)[[1
                              ]]}, character(1))) #grab the fold
                              change and make it into a character
FCLAG3CD49b <- FCLAG3CD49b[!is.na(names(FCLAG3CD49b))]



#make the cluster into a dataframe for easy readability
dCD49vLag3 <- as.data.frame(cluster49vLag3)
head(summary(dCP49vLag3))
dotplot(clusterLag3vCD49b, showCategory = 10)
cnetplot(clusterLag3vCD49b, node_label = "all", foldChange =
   FCLAG3CD49b)
emapplot(clusterLag3vDP)


#CLusterProfileR CD49b v DP

clusterCD49bvDP <- enrichGO(gene = DE49vDP$ID.entrezid,
                            universe = universe,
                            OrgDb = org.Mm.eg.db,
                            ont = "ALL",
                            keyType = "ENTREZID",
                            pAdjustMethod = "bonferroni",
                            pvalueCutoff = 0.01,
                            qvalueCutoff = 0.05,
                            readable = TRUE)

FC49bvDP <- structure(highConfTable$CD49bvDP$logFC, names =
   highConfTable$CD49bvDP$ID.entrezid %>%
                            vapply(function(x){as.character(x)[[1
```

```
                                ]]}, character(1))) #grab the fold
                                 change and make it into a
                                character
FC49bvDP <- FC49bvDP[!is.na(names(FC49bvDP))]


#make the cluster into a dataframe for easy readability
dCD49bvDP <- as.data.frame(clusterCD49bvDP)
head(summary(dCD49bvDP))
dotplot(clusterCD49bvDP, showCategory = 10)
cnetplot(clusterCD49bvDP, node_label = "all", foldChange = FC49
   bvDP)
```

Bibliography

1. Paget, J. *et al.* Global mortality associated with seasonal influenza epidemics: New burden estimates and predictors from the GLaMOR Project. *J Glob Health* **9,** 020421 (Dec. 2019).
2. Shao, W., Li, X., Goraya, M. U., Wang, S. & Chen, J. L. Evolution of Influenza A Virus by Mutation and Re-Assortment. *Int J Mol Sci* **18** (Aug. 2017).
3. Kuiken, T. & Taubenberger, J. K. Pathology of human influenza revisited. *Vaccine* **26 Suppl 4,** 59–66 (Sept. 2008).
4. Short, K. R., Kroeze, E. J. B. V., Fouchier, R. A. M. & Kuiken, T. Pathogenesis of influenza-induced acute respiratory distress syndrome. *Lancet Infect Dis* **14,** 57–69 (Jan. 2014).
5. Couceiro, J. N., Paulson, J. C. & Baum, L. G. Influenza virus strains selectively recognize sialyloligosaccharides on human respiratory epithelium; the role of the host cell in selection of hemagglutinin receptor specificity. *Virus Res* **29,** 155–165 (Aug. 1993).
6. Button, B. *et al.* A periciliary brush promotes the lung health by separating the mucus layer from airway epithelia. *Science* **337,** 937–941 (Aug. 2012).
7. Kim, K. C. Role of epithelial mucins during airway infection. *Pulm Pharmacol Ther* **25,** 415–419 (Dec. 2012).
8. Le Goffic, R. *et al.* Cutting Edge: Influenza A virus activates TLR3-dependent inflammatory and RIG-I-dependent antiviral responses in human lung epithelial cells. *J Immunol* **178,** 3368–3372 (Mar. 2007).
9. Shornick, L. P. *et al.* Airway epithelial versus immune cell Stat1 function for innate defense against respiratory viral infection. *J Immunol* **180,** 3319–3328 (Mar. 2008).
10. Lambrecht, B. N. & Hammad, H. The airway epithelium in asthma. *Nat Med* **18,** 684–692 (May 2012).
11. Rudolph, D. *et al.* Severe liver degeneration and lack of NF-kappaB activation in NEMO/IKKgamma-deficient mice. *Genes Dev* **14,** 854–862 (Apr. 2000).

12. Chu, W. M. *et al.* JNK2 and IKKbeta are required for activating the innate response to viral infection. *Immunity* **11,** 721–731 (Dec. 1999).

13. Schoggins, J. W. Interferon-Stimulated Genes: What Do They All Do? *Annu Rev Virol* **6,** 567–584 (Sept. 2019).

14. Kärre, K., Ljunggren, H. G., Piontek, G. & Kiessling, R. Selective rejection of H-2-deficient lymphoma variants suggests alternative immune defence strategy. *Nature* **319,** 675–678 (1986).

15. Perussia, B. *et al.* The Fc receptor for IgG on human natural killer cells: phenotypic, functional, and comparative studies with monoclonal antibodies. *J Immunol* **133,** 180–189 (July 1984).

16. Trinchieri, G., Bauman, P., De Marchi, M. & Tökés, Z. Antibody-dependent cell-mediated cytotoxicity in humans. I. Characterization of the effector cell. *J Immunol* **115,** 249–255 (July 1975).

17. Kägi, D. *et al.* Cytotoxicity mediated by T cells and natural killer cells is greatly impaired in perforin-deficient mice. *Nature* **369,** 31–37 (May 1994).

18. Voskoboinik, I., Smyth, M. J. & Trapani, J. A. Perforin-mediated target-cell death and immune homeostasis. *Nat Rev Immunol* **6,** 940–952 (Dec. 2006).

19. Karlhofer, F. M., Ribaudo, R. K. & Yokoyama, W. M. MHC class I alloantigen specificity of Ly-49+ IL-2-activated natural killer cells. *Nature* **358,** 66–70 (July 1992).

20. Wagtmann, N., Rajagopalan, S., Winter, C. C., Peruzzi, M. & Long, E. O. Killer cell inhibitory receptors specific for HLA-C and HLA-B identified by direct binding and by functional transfer. *Immunity* **3,** 801–809 (Dec. 1995).

21. Hwang, I. *et al.* Activation mechanisms of natural killer cells during influenza virus infection. *PLoS One* **7,** e51858 (2012).

22. Schnare, M. *et al.* Toll-like receptors control activation of adaptive immune responses. *Nat Immunol* **2,** 947–950 (Oct. 2001).

23. Medzhitov, R., Preston-Hurlburt, P. & Janeway, C. A. A human homologue of the Drosophila Toll protein signals activation of adaptive immunity. *Nature* **388,** 394–397 (July 1997).

24. Krappmann, D. *et al.* The IkappaB kinase complex and NF-kappaB act as master regulators of lipopolysaccharide-induced gene expression and control subordinate activation of AP-1. *Mol Cell Biol* **24,** 6488–6500 (July 2004).

25. Lam, J. H. & Baumgarth, N. The Multifaceted B Cell Response to Influenza Virus. *J Immunol* **202,** 351–359 (Jan. 2019).

26. Bennett, S. R., Carbone, F. R., Karamalis, F., Miller, J. F. & Heath, W. R. Induction of a CD8+ cytotoxic T lymphocyte response by cross-priming requires cognate CD4+ T cell help. *J Exp Med* **186,** 65–70 (July 1997).

27. Schoenberger, S. P., Toes, R. E., van der Voort, E. I., Offringa, R. & Melief, C. J. T-cell help for cytotoxic T lymphocytes is mediated by CD40-CD40L interactions. *Nature* **393,** 480–483 (June 1998).

28. Bennett, S. R. *et al.* Help for cytotoxic-T-cell responses is mediated by CD40 signalling. *Nature* **393,** 478–480 (June 1998).

29. Ridge, J. P., Di Rosa, F. & Matzinger, P. A conditioned dendritic cell can be a temporal bridge between a CD4+ T-helper and a T-killer cell. *Nature* **393,** 474–478 (June 1998).

30. Halle, S., Halle, O. & Förster, R. Mechanisms and Dynamics of T Cell-Mediated Cytotoxicity In Vivo. *Trends Immunol* **38,** 432–443 (June 2017).

31. Pace, J. L., Russell, S. W., Torres, B. A., Johnson, H. M. & Gray, P. W. Recombinant mouse gamma interferon induces the priming step in macrophage activation for tumor cell killing. *J Immunol* **130,** 2011–2013 (May 1983).

32. Nathan, C. F., Murray, H. W., Wiebe, M. E. & Rubin, B. Y. Identification of interferon-gamma as the lymphokine that activates human macrophage oxidative metabolism and antimicrobial activity. *J Exp Med* **158,** 670–689 (Sept. 1983).

33. Jurkovich, G. J., Mileski, W. J., Maier, R. V., Winn, R. K. & Rice, C. L. Interferon gamma increases sensitivity to endotoxin. *J Surg Res* **51,** 197–203 (Sept. 1991).

34. Kamijo, R. *et al.* Mice that lack the interferon-gamma receptor have profoundly altered responses to infection with Bacillus Calmette-Guérin and subsequent challenge with lipopolysaccharide. *J Exp Med* **178,** 1435–1440 (Oct. 1993).

35. Lorsbach, R. B., Murphy, W. J., Lowenstein, C. J., Snyder, S. H. & Russell, S. W. Expression of the nitric oxide synthase gene in mouse macrophages activated for tumor cell killing. Molecular basis for the synergy between interferon-gamma and lipopolysaccharide. *J Biol Chem* **268,** 1908–1913 (Jan. 1993).

36. Wu, C. *et al.* IFN- primes macrophage activation by increasing phosphatase and tensin homolog via downregulation of miR-3473b. *J Immunol* **193,** 3036–3044 (Sept. 2014).

37. King, D. P. & Jones, P. P. Induction of Ia and H-2 antigens on a macrophage cell line by immune interferon. *J Immunol* **131,** 315–318 (July 1983).

38. Wong, G. H., Clark-Lewis, I., McKimm-Breschkin, L., Harris, A. W. & Schrader, J. W. Interferon-gamma induces enhanced expression of Ia and H-2 antigens on B lymphoid, macrophage, and myeloid cell lines. *J Immunol* **131,** 788–793 (Aug. 1983).

39. Zinkernagel, R. M. & Doherty, P. C. Restriction of in vitro T cell-mediated cytotoxicity in lymphocytic choriomeningitis within a syngeneic or semiallogeneic system. *Nature* **248,** 701–702 (Apr. 1974).

40. August, A. & Dupont, B. Activation of src family kinase lck following CD28 crosslinking in the Jurkat leukemic cell line. *Biochem Biophys Res Commun* **199,** 1466–1473 (Mar. 1994).

41. Pagès, F. *et al.* Two distinct intracytoplasmic regions of the T-cell adhesion molecule CD28 participate in phosphatidylinositol 3-kinase association. *J Biol Chem* **271,** 9403–9409 (Apr. 1996).

42. Truitt, K. E., Hicks, C. M. & Imboden, J. B. Stimulation of CD28 triggers an association between CD28 and phosphatidylinositol 3-kinase in Jurkat T cells. *J Exp Med* **179,** 1071–1076 (Mar. 1994).

43. Curtsinger, J. M. *et al.* Inflammatory cytokines provide a third signal for activation of naive CD4+ and CD8+ T cells. *J Immunol* **162,** 3256–3262 (Mar. 1999).

44. Curtsinger, J. M., Lins, D. C. & Mescher, M. F. Signal 3 determines tolerance versus full activation of naive CD8 T cells: dissociating proliferation and development of effector function. *J Exp Med* **197,** 1141–1151 (May 2003).

45. Curtsinger, J. M., Valenzuela, J. O., Agarwal, P., Lins, D. & Mescher, M. F. Type I IFNs provide a third signal to CD8 T cells to stimulate clonal expansion and differentiation. *J Immunol* **174,** 4465–4469 (Apr. 2005).

46. Mosmann, T. R., Cherwinski, H., Bond, M. W., Giedlin, M. A. & Coffman, R. L. Two types of murine helper T cell clone. I. Definition according to profiles of lymphokine activities and secreted proteins. *J Immunol* **136,** 2348–2357 (Apr. 1986).

47. Chen, J. & Liu, X. The role of interferon gamma in regulation of CD4+ T-cells and its clinical implications. *Cell Immunol* **254,** 85–90 (2009).

48. Martín-Fontecha, A. *et al.* Induced recruitment of NK cells to lymph nodes provides IFN-gamma for T(H)1 priming. *Nat Immunol* **5,** 1260–1265 (Dec. 2004).

49. Morandi, B., Bougras, G., Muller, W. A., Ferlazzo, G. & Münz, C. NK cells of human secondary lymphoid tissues enhance T cell polarization via IFN-gamma secretion. *Eur J Immunol* **36,** 2394–2400 (Sept. 2006).

50. Afkarian, M. *et al.* T-bet is a STAT1-induced regulator of IL-12R expression in naïve CD4+ T cells. *Nat Immunol* **3,** 549–557 (June 2002).

51. Szabo, S. J. *et al.* A novel transcription factor, T-bet, directs Th1 lineage commitment. *Cell* **100,** 655–669 (Mar. 2000).

52. Mullen, A. C. *et al.* Role of T-bet in commitment of TH1 cells before IL-12-dependent selection. *Science* **292,** 1907–1910 (June 2001).

53. Szabo, S. J. *et al.* Distinct effects of T-bet in TH1 lineage commitment and IFN-gamma production in CD4 and CD8 T cells. *Science* **295,** 338–342 (Jan. 2002).

54. Finotto, S. *et al.* Development of spontaneous airway changes consistent with human asthma in mice lacking T-bet. *Science* **295,** 336–338 (Jan. 2002).

55. Kaplan, M. H., Sun, Y. L., Hoey, T. & Grusby, M. J. Impaired IL-12 responses and enhanced development of Th2 cells in Stat4-deficient mice. *Nature* **382,** 174–177 (July 1996).

56. Thierfelder, W. E. *et al.* Requirement for Stat4 in interleukin-12-mediated responses of natural killer and T cells. *Nature* **382,** 171–174 (July 1996).

57. Snapper, C. M. & Paul, W. E. Interferon-gamma and B cell stimulatory factor-1 reciprocally regulate Ig isotype production. *Science* **236,** 944–947 (May 1987).

58. Stevens, T. L. *et al.* Regulation of antibody isotype secretion by subsets of antigen-specific helper T cells. *Nature* **334,** 255–258 (July 1988).

59. Coutelier, J. P., van der Logt, J. T., Heessen, F. W., Warnier, G. & Van Snick, J. IgG2a restriction of murine antibodies elicited by viral infections. *J Exp Med* **165,** 64–69 (Jan. 1987).

60. Zheng, W. & Flavell, R. A. The transcription factor GATA-3 is necessary and sufficient for Th2 cytokine gene expression in CD4 T cells. *Cell* **89,** 587–596 (May 1997).

61. Zhang, D. H., Cohn, L., Ray, P., Bottomly, K. & Ray, A. Transcription factor GATA-3 is differentially expressed in murine Th1 and Th2 cells and controls Th2-specific expression of the interleukin-5 gene. *J Biol Chem* **272,** 21597–21603 (Aug. 1997).

62. Zhu, J. *et al.* Conditional deletion of Gata3 shows its essential function in T(H)1-T(H)2 responses. *Nat Immunol* **5,** 1157–1165 (Nov. 2004).

63. Pai, S. Y., Truitt, M. L. & Ho, I. C. GATA-3 deficiency abrogates the development and maintenance of T helper type 2 cells. *Proc Natl Acad Sci U S A* **101,** 1993–1998 (Feb. 2004).

64. Zhu, J., Yamane, H., Cote-Sierra, J., Guo, L. & Paul, W. E. GATA-3 promotes Th2 responses through three different mechanisms: induction of Th2 cytokine production, selective growth of Th2 cells and inhibition of Th1 cell-specific factors. *Cell Res* **16,** 3–10 (Jan. 2006).

65. Swain, S. L., Weinberg, A. D., English, M. & Huston, G. IL-4 directs the development of Th2-like helper effectors. *J Immunol* **145,** 3796–3806 (Dec. 1990).

66. Takeda, K. *et al.* Essential role of Stat6 in IL-4 signalling. *Nature* **380,** 627–630 (Apr. 1996).

67. Jankovic, D. *et al.* Single cell analysis reveals that IL-4 receptor/Stat6 signaling is not required for the in vivo or in vitro development of CD4+ lymphocytes with a Th2 cytokine profile. *J Immunol* **164,** 3047–3055 (Mar. 2000).

68. Finkelman, F. D. *et al.* Stat6 regulation of in vivo IL-4 responses. *J Immunol* **164,** 2303–2310 (Mar. 2000).

69. Voehringer, D., Shinkai, K. & Locksley, R. M. Type 2 immunity reflects orchestrated recruitment of cells committed to IL-4 production. *Immunity* **20,** 267–277 (Mar. 2004).

70. Van Panhuys, N. *et al.* In vivo studies fail to reveal a role for IL-4 or STAT6 signaling in Th2 lymphocyte differentiation. *Proc Natl Acad Sci U S A* **105,** 12423–12428 (Aug. 2008).

71. Zhu, J., Cote-Sierra, J., Guo, L. & Paul, W. E. Stat5 activation plays a critical role in Th2 differentiation. *Immunity* **19,** 739–748 (Nov. 2003).

72. Cote-Sierra, J. *et al.* Interleukin 2 plays a central role in Th2 differentiation. *Proc Natl Acad Sci U S A* **101,** 3880–3885 (Mar. 2004).

73. Kagami, S. *et al.* Stat5a regulates T helper cell differentiation by several distinct mechanisms. *Blood* **97,** 2358–2365 (Apr. 2001).

74. Kanhere, A. *et al.* T-bet and GATA3 orchestrate Th1 and Th2 differentiation through lineage-specific targeting of distal regulatory elements. *Nat Commun* **3,** 1268 (2012).

75. Voehringer, D., Reese, T. A., Huang, X., Shinkai, K. & Locksley, R. M. Type 2 immunity is controlled by IL-4/IL-13 expression in hematopoietic non-eosinophil cells of the innate immune system. *J Exp Med* **203,** 1435–1446 (June 2006).

76. Van der Werf, N., Redpath, S. A., Azuma, M., Yagita, H. & Taylor, M. D. Th2 cell-intrinsic hypo-responsiveness determines susceptibility to helminth infection. *PLoS Pathog* **9,** e1003215 (Mar. 2013).

77. Okoye, I. S. *et al.* Transcriptomics identified a critical role for Th2 cell-intrinsic miR-155 in mediating allergy and antihelminth immunity. *Proc Natl Acad Sci U S A* **111,** E3081–3090 (July 2014).

78. Oliphant, C. J. *et al.* MHCII-mediated dialog between group 2 innate lymphoid cells and CD4(+) T cells potentiates type 2 immunity and promotes parasitic helminth expulsion. *Immunity* **41,** 283–295 (Aug. 2014).

79. Chen, F. *et al.* An essential role for TH2-type responses in limiting acute tissue damage during experimental helminth infection. *Nat Med* **18,** 260–266 (Jan. 2012).

80. Liang, S. C. *et al.* An IL-17F/A heterodimer protein is produced by mouse Th17 cells and induces airway neutrophil recruitment. *J Immunol* **179,** 7791–7799 (Dec. 2007).

81. Pelletier, M. *et al.* Evidence for a cross-talk between human neutrophils and Th17 cells. *Blood* **115,** 335–343 (Jan. 2010).

82. Ivanov, I. I. *et al.* The orphan nuclear receptor RORgammat directs the differentiation program of proinflammatory IL-17+ T helper cells. *Cell* **126,** 1121–1133 (Sept. 2006).

83. Yang, X. O. *et al.* T helper 17 lineage differentiation is programmed by orphan nuclear receptors ROR alpha and ROR gamma. *Immunity* **28,** 29–39 (Jan. 2008).

84. McGeachy, M. J. *et al.* TGF-beta and IL-6 drive the production of IL-17 and IL-10 by T cells and restrain T(H)-17 cell-mediated pathology. *Nat Immunol* **8,** 1390–1397 (Dec. 2007).

85. Mangan, P. R. *et al.* Transforming growth factor-beta induces development of the T(H)17 lineage. *Nature* **441,** 231–234 (May 2006).

86. Veldhoen, M., Hocking, R. J., Atkins, C. J., Locksley, R. M. & Stockinger, B. TGFbeta in the context of an inflammatory cytokine milieu supports de novo differentiation of IL-17-producing T cells. *Immunity* **24,** 179–189 (Feb. 2006).

87. Langrish, C. L. *et al.* IL-23 drives a pathogenic T cell population that induces autoimmune inflammation. *J Exp Med* **201,** 233–240 (Jan. 2005).

88. Liang, S. C. *et al.* Interleukin (IL)-22 and IL-17 are coexpressed by Th17 cells and cooperatively enhance expression of antimicrobial peptides. *J Exp Med* **203,** 2271–2279 (Oct. 2006).

89. McGeachy, M. J. *et al.* The interleukin 23 receptor is essential for the terminal differentiation of interleukin 17-producing effector T helper cells in vivo. *Nat Immunol* **10,** 314–324 (Mar. 2009).

90. Ghoreschi, K. *et al.* Generation of pathogenic T(H)17 cells in the absence of TGF-signalling. *Nature* **467,** 967–971 (Oct. 2010).

91. Lee, Y. *et al.* Induction and molecular signature of pathogenic TH17 cells. *Nat Immunol* **13,** 991–999 (Oct. 2012).

92. El-Behi, M. *et al.* The encephalitogenicity of T(H)17 cells is dependent on IL-1- and IL-23-induced production of the cytokine GM-CSF. *Nat Immunol* **12,** 568–575 (June 2011).

93. Codarri, L. *et al.* RORt drives production of the cytokine GM-CSF in helper T cells, which is essential for the effector phase of autoimmune neuroinflammation. *Nat Immunol* **12,** 560–567 (June 2011).

94. Chen, Z. *et al.* Selective regulatory function of Socs3 in the formation of IL-17-secreting T cells. *Proc Natl Acad Sci U S A* **103,** 8137–8142 (May 2006).

95. Laurence, A. *et al.* Interleukin-2 signaling via STAT5 constrains T helper 17 cell generation. *Immunity* **26,** 371–381 (Mar. 2007).

96. Yang, G., Xu, Y., Chen, X. & Hu, G. IFITM1 plays an essential role in the antiproliferative action of interferon-gamma. *Oncogene* **26,** 594–603 (Jan. 2007).

97. Purwar, R. *et al.* Robust tumor immunity to melanoma mediated by interleukin-9-producing T cells. *Nat Med* **18,** 1248–1253 (Aug. 2012).

98. Lu, Y. *et al.* Th9 cells promote antitumor immune responses in vivo. *J Clin Invest* **122,** 4160–4171 (Nov. 2012).

99. Veldhoen, M. *et al.* Transforming growth factor-beta 'reprograms' the differentiation of T helper 2 cells and promotes an interleukin 9-producing subset. *Nat Immunol* **9,** 1341–1346 (Dec. 2008).

100. Chang, H. C. *et al.* The transcription factor PU.1 is required for the development of IL-9-producing T cells and allergic inflammation. *Nat Immunol* **11,** 527–534 (June 2010).

101. Dardalhon, V. *et al.* IL-4 inhibits TGF-beta-induced Foxp3+ T cells and, together with TGF-beta, generates IL-9+ IL-10+ Foxp3(-) effector T cells. *Nat Immunol* **9,** 1347–1355 (Dec. 2008).

102. Goswami, R. *et al.* STAT6-dependent regulation of Th9 development. *J Immunol* **188,** 968–975 (Feb. 2012).

103. Staudt, V. *et al.* Interferon-regulatory factor 4 is essential for the developmental program of T helper 9 cells. *Immunity* **33,** 192–202 (Aug. 2010).

104. Wolk, K. *et al.* IL-22 increases the innate immunity of tissues. *Immunity* **21,** 241–254 (Aug. 2004).

105. Aujla, S. J. *et al.* IL-22 mediates mucosal host defense against Gram-negative bacterial pneumonia. *Nat Med* **14,** 275–281 (Mar. 2008).

106. Wolk, K. *et al.* IL-22 regulates the expression of genes responsible for antimicrobial defense, cellular differentiation, and mobility in keratinocytes: a potential role in psoriasis. *Eur J Immunol* **36,** 1309–1323 (May 2006).

107. Zheng, Y. *et al.* Interleukin-22 mediates early host defense against attaching and effacing bacterial pathogens. *Nat Med* **14,** 282–289 (Mar. 2008).

108. Basu, R. *et al.* Th22 cells are an important source of IL-22 for host protection against enteropathogenic bacteria. *Immunity* **37,** 1061–1075 (Dec. 2012).

109. Duhen, T., Geiger, R., Jarrossay, D., Lanzavecchia, A. & Sallusto, F. Production of interleukin 22 but not interleukin 17 by a subset of human skin-homing memory T cells. *Nat Immunol* **10,** 857–863 (Aug. 2009).

110. Trifari, S., Kaplan, C. D., Tran, E. H., Crellin, N. K. & Spits, H. Identification of a human helper T cell population that has abundant production of interleukin 22 and is distinct from T(H)-17, T(H)1 and T(H)2 cells. *Nat Immunol* **10,** 864–871 (Aug. 2009).

111. Rutz, S. *et al.* Transcription factor c-Maf mediates the TGF--dependent suppression of IL-22 production in T(H)17 cells. *Nat Immunol* **12,** 1238–1245 (Oct. 2011).

112. Zheng, Y. *et al.* Interleukin-22, a T(H)17 cytokine, mediates IL-23-induced dermal inflammation and acanthosis. *Nature* **445,** 648–651 (Feb. 2007).

113. Backert, I. *et al.* STAT3 activation in Th17 and Th22 cells controls IL-22-mediated epithelial host defense during infectious colitis. *J Immunol* **193,** 3779–3791 (Oct. 2014).

114. Schaerli, P. *et al.* CXC chemokine receptor 5 expression defines follicular homing T cells with B cell helper function. *J. Exp. Med.* **192,** 1553–1562 (Dec. 2000).

115. Breitfeld, D. *et al.* Follicular B helper T cells express CXC chemokine receptor 5, localize to B cell follicles, and support immunoglobulin production. *J. Exp. Med.* **192,** 1545–1552 (Dec. 2000).

116. Kim, C. H. *et al.* Subspecialization of CXCR5+ T cells: B helper activity is focused in a germinal center-localized subset of CXCR5+ T cells. *J Exp Med* **193,** 1373–1381 (June 2001).

117. Ansel, K. M., McHeyzer-Williams, L. J., Ngo, V. N., McHeyzer-Williams, M. G. & Cyster, J. G. In vivo-activated CD4 T cells upregulate CXC chemokine receptor 5 and reprogram their response to lymphoid chemokines. *J Exp Med* **190,** 1123–1134 (Oct. 1999).

118. Gunn, M. D. *et al.* A B-cell-homing chemokine made in lymphoid follicles activates Burkitt's lymphoma receptor-1. *Nature* **391,** 799–803 (Feb. 1998).

119. Dorfman, D. M., Brown, J. A., Shahsafaei, A. & Freeman, G. J. Programmed death-1 (PD-1) is a marker of germinal center-associated T cells and angioimmunoblastic T-cell lymphoma. *Am J Surg Pathol* **30,** 802–810 (July 2006).

120. Haynes, N. M. *et al.* Role of CXCR5 and CCR7 in follicular Th cell positioning and appearance of a programmed cell death gene-1high germinal center-associated subpopulation. *J Immunol* **179,** 5099–5108 (Oct. 2007).

121. Yu, D. *et al.* The transcriptional repressor Bcl-6 directs T follicular helper cell lineage commitment. *Immunity* **31,** 457–468 (Sept. 2009).

122. Johnston, R. J. *et al.* Bcl6 and Blimp-1 are reciprocal and antagonistic regulators of T follicular helper cell differentiation. *Science* **325,** 1006–1010 (Aug. 2009).

123. Nurieva, R. I. *et al.* Bcl6 mediates the development of T follicular helper cells. *Science* **325,** 1001–1005 (Aug. 2009).

124. Karnowski, A. *et al.* B and T cells collaborate in antiviral responses via IL-6, IL-21, and transcriptional activator and coactivator, Oct2 and OBF-1. *J Exp Med* **209,** 2049–2064 (Oct. 2012).

125. Eto, D. *et al.* IL-21 and IL-6 are critical for different aspects of B cell immunity and redundantly induce optimal follicular helper CD4 T cell (Tfh) differentiation. *PLoS One* **6,** e17739 (Mar. 2011).

126. Weber, J. P. *et al.* ICOS maintains the T follicular helper cell phenotype by down-regulating Krüppel-like factor 2. *J Exp Med* **212,** 217–233 (Feb. 2015).

127. Mordue, D. G., Monroy, F., La Regina, M., Dinarello, C. A. & Sibley, L. D. Acute toxoplasmosis leads to lethal overproduction of Th1 cytokines. *J Immunol* **167,** 4574–4584 (Oct. 2001).

128. Villarino, A. *et al.* The IL-27R (WSX-1) is required to suppress T cell hyperactivity during infection. *Immunity* **19,** 645–655 (Nov. 2003).

129. Wambre, E. *et al.* A phenotypically and functionally distinct human TH2 cell subpopulation is associated with allergic disorders. *Sci Transl Med* **9** (Aug. 2017).

130. Morimoto, Y. *et al.* Amphiregulin-Producing Pathogenic Memory T Helper 2 Cells Instruct Eosinophils to Secrete Osteopontin and Facilitate Airway Fibrosis. *Immunity* **49,** 134–150 (July 2018).

131. Endo, Y. *et al.* Eomesodermin controls interleukin-5 production in memory T helper 2 cells through inhibition of activity of the transcription factor GATA3. *Immunity* **35,** 733–745 (Nov. 2011).

132. Endo, Y. *et al.* The interleukin-33-p38 kinase axis confers memory T helper 2 cell pathogenicity in the airway. *Immunity* **42,** 294–308 (Feb. 2015).

133. Islam, S. A. *et al.* Mouse CCL8, a CCR8 agonist, promotes atopic dermatitis by recruiting IL-5+ T(H)2 cells. *Nat Immunol* **12,** 167–177 (Feb. 2011).

134. Murphy, C. A. *et al.* Divergent pro- and antiinflammatory roles for IL-23 and IL-12 in joint autoimmune inflammation. *J Exp Med* **198,** 1951–1957 (Dec. 2003).

135. Annunziato, F. *et al.* Phenotypic and functional features of human Th17 cells. *J Exp Med* **204,** 1849–1861 (Aug. 2007).

136. Cortelazzi, C., Campanini, N., Ricci, R. & De Panfilis, G. Inflammed skin harbours Th9 cells. *Acta Derm Venereol* **93,** 183–185 (Mar. 2013).

137. Böttcher, M. F., Bjurström, J., Mai, X. M., Nilsson, L. & Jenmalm, M. C. Allergen-induced cytokine secretion in atopic and non-atopic asthmatic children. *Pediatr Allergy Immunol* **14,** 345–350 (Oct. 2003).

138. Devos, S. *et al.* Allergen-induced interleukin-9 production in vitro: correlation with atopy in human adults and comparison with interleukin-5 and interleukin-13. *Clin Exp Allergy* **36,** 174–182 (Feb. 2006).

139. Li, H., Nourbakhsh, B., Ciric, B., Zhang, G. X. & Rostami, A. Neutralization of IL-9 ameliorates experimental autoimmune encephalomyelitis by decreasing the effector T cell population. *J Immunol* **185,** 4095–4100 (Oct. 2010).

140. Li, H., Nourbakhsh, B., Cullimore, M., Zhang, G. X. & Rostami, A. IL-9 is important for T-cell activation and differentiation in autoimmune inflammation of the central nervous system. *Eur J Immunol* **41,** 2197–2206 (Aug. 2011).

141. Nowak, E. C. *et al.* IL-9 as a mediator of Th17-driven inflammatory disease. *J Exp Med* **206,** 1653–1660 (Aug. 2009).

142. Elyaman, W. *et al.* IL-9 induces differentiation of TH17 cells and enhances function of FoxP3+ natural regulatory T cells. *Proc Natl Acad Sci U S A* **106,** 12885–12890 (Aug. 2009).

143. Gerlach, K. *et al.* TH9 cells that express the transcription factor PU.1 drive T cell-mediated colitis via IL-9 receptor signaling in intestinal epithelial cells. *Nat Immunol* **15,** 676–686 (July 2014).

144. Vitales-Noyola, M. *et al.* Pathogenic Th17 and Th22 cells are increased in patients with autoimmune thyroid disorders. *Endocrine* **57,** 409–417 (Sept. 2017).

145. Zhong, W., Zhao, L., Liu, T. & Jiang, Z. IL-22-producing CD4+T cells in the treatment response of rheumatoid arthritis to combination therapy with methotrexate and leflunomide. *Sci Rep* **7,** 41143 (Jan. 2017).

146. Justa, S., Zhou, X. & Sarkar, S. Endogenous IL-22 plays a dual role in arthritis: regulation of established arthritis via IFN- responses. *PLoS One* **9,** e93279 (2014).

147. Corneth, O. B. *et al.* Loss of IL-22 inhibits autoantibody formation in collagen-induced arthritis in mice. *Eur J Immunol* **46,** 1404–1414 (June 2016).

148. Block, K. E., Zheng, Z., Dent, A. L., Kee, B. L. & Huang, H. Gut Microbiota Regulates K/BxN Autoimmune Arthritis through Follicular Helper T but Not Th17 Cells. *J Immunol* **196,** 1550–1557 (Feb. 2016).

149. Teng, F. *et al.* Gut Microbiota Drive Autoimmune Arthritis by Promoting Differentiation and Migration of Peyer's Patch T Follicular Helper Cells. *Immunity* **44,** 875–888 (Apr. 2016).

150. Chevalier, N. *et al.* The Role of Follicular Helper T Cell Molecules and Environmental Influences in Autoantibody Production and Progression to Inflammatory Arthritis in Mice. *Arthritis Rheumatol* **68,** 1026–1038 (Apr. 2016).

151. Sakaguchi, S., Sakaguchi, N., Asano, M., Itoh, M. & Toda, M. Immunologic self-tolerance maintained by activated T cells expressing IL-2 receptor alpha-chains (CD25). Breakdown of a single mechanism of self-tolerance causes various autoimmune diseases. *J Immunol* **155,** 1151–1164 (Aug. 1995).

152. Fontenot, J. D., Gavin, M. A. & Rudensky, A. Y. Foxp3 programs the development and function of CD4+CD25+ regulatory T cells. *Nat. Immunol.* **4,** 330–336 (Apr. 2003).

153. Hori, S., Nomura, T. & Sakaguchi, S. Control of regulatory T cell development by the transcription factor Foxp3. *Science* **299,** 1057–1061 (Feb. 2003).

154. Jordan, M. S. *et al.* Thymic selection of CD4+CD25+ regulatory T cells induced by an agonist self-peptide. *Nat Immunol* **2,** 301–306 (Apr. 2001).

155. Apostolou, I., Sarukhan, A., Klein, L. & von Boehmer, H. Origin of regulatory T cells with known specificity for antigen. *Nat Immunol* **3,** 756–763 (Aug. 2002).

156. Hsieh, C. S., Lee, H. M. & Lio, C. W. Selection of regulatory T cells in the thymus. *Nat Rev Immunol* **12,** 157–167 (Feb. 2012).

157. Thorstenson, K. M. & Khoruts, A. Generation of anergic and potentially immunoregulatory CD25+CD4 T cells in vivo after induction of peripheral tolerance with intravenous or oral antigen. *J Immunol* **167,** 188–195 (July 2001).

158. Apostolou, I. & von Boehmer, H. In vivo instruction of suppressor commitment in naive T cells. *J Exp Med* **199,** 1401–1408 (May 2004).

159. Knoechel, B., Lohr, J., Kahn, E., Bluestone, J. A. & Abbas, A. K. Sequential development of interleukin 2-dependent effector and regulatory T cells in response to endogenous systemic antigen. *J Exp Med* **202,** 1375–1386 (Nov. 2005).

160. Chen, W. *et al.* Conversion of peripheral CD4+CD25- naive T cells to CD4+CD25+ regulatory T cells by TGF-beta induction of transcription factor Foxp3. *J Exp Med* **198,** 1875–1886 (Dec. 2003).

161. Mahnke, K., Qian, Y., Knop, J. & Enk, A. H. Induction of CD4+/CD25+ regulatory T cells by targeting of antigens to immature dendritic cells. *Blood* **101,** 4862–4869 (June 2003).

162. Vieira, P. L. *et al.* IL-10-secreting regulatory T cells do not express Foxp3 but have comparable regulatory function to naturally occurring CD4+CD25+ regulatory T cells. *J Immunol* **172,** 5986–5993 (May 2004).

163. Inobe, J. *et al.* IL-4 is a differentiation factor for transforming growth factor-beta secreting Th3 cells and oral administration of IL-4 enhances oral tolerance in experimental allergic encephalomyelitis. *Eur J Immunol* **28,** 2780–2790 (Sept. 1998).

164. Carrier, Y., Yuan, J., Kuchroo, V. K. & Weiner, H. L. Th3 cells in peripheral tolerance. I. Induction of Foxp3-positive regulatory T cells by Th3 cells derived from TGF-beta T cell-transgenic mice. *J Immunol* **178,** 179–185 (Jan. 2007).

165. Carrier, Y., Yuan, J., Kuchroo, V. K. & Weiner, H. L. Th3 cells in peripheral tolerance. II. TGF-beta-transgenic Th3 cells rescue IL-2-deficient mice from autoimmunity. *J Immunol* **178,** 172–178 (Jan. 2007).

166. Zeng, H., Zhang, R., Jin, B. & Chen, L. Type 1 regulatory T cells: a new mechanism of peripheral immune tolerance. *Cell Mol Immunol* **12,** 566–571 (Sept. 2015).

167. Nishimura, E., Sakihama, T., Setoguchi, R., Tanaka, K. & Sakaguchi, S. Induction of antigen-specific immunologic tolerance by in vivo and in vitro antigen-specific expansion of naturally arising Foxp3+CD25+CD4+ regulatory T cells. *Int Immunol* **16,** 1189–1201 (Aug. 2004).

168. Scheffold, A., Murphy, K. M. & Höfer, T. Competition for cytokines: T(reg) cells take all. *Nat Immunol* **8,** 1285–1287 (Dec. 2007).

169. Li, Z., Li, D., Tsun, A. & Li, B. FOXP3+ regulatory T cells and their functional regulation. *Cell Mol Immunol* **12,** 558–565 (Sept. 2015).

170. O'Garra, A., Vieira, P. L., Vieira, P. & Goldfeld, A. E. IL-10-producing and naturally occurring CD4+ Tregs: limiting collateral damage. *J Clin Invest* **114,** 1372–1378 (Nov. 2004).

171. Ouyang, W. & O'Garra, A. IL-10 Family Cytokines IL-10 and IL-22: from Basic Science to Clinical Translation. *Immunity* **50,** 871–891 (Apr. 2019).

172. Fiorentino, D. F., Bond, M. W. & Mosmann, T. R. Two types of mouse T helper cell. IV. Th2 clones secrete a factor that inhibits cytokine production by Th1 clones. *J Exp Med* **170,** 2081–2095 (Dec. 1989).

173. Yoon, S. I., Logsdon, N. J., Sheikh, F., Donnelly, R. P. & Walter, M. R. Conformational changes mediate interleukin-10 receptor 2 (IL-10R2) binding to IL-10 and assembly of the signaling complex. *J Biol Chem* **281,** 35088–35096 (Nov. 2006).

174. Yoon, S. I. *et al.* Structure and mechanism of receptor sharing by the IL-10R2 common chain. *Structure* **18,** 638–648 (May 2010).

175. Thompson-Snipes, L. *et al.* Interleukin 10: a novel stimulatory factor for mast cells and their progenitors. *J Exp Med* **173,** 507–510 (Feb. 1991).

176. Chen, W. F. & Zlotnik, A. IL-10: a novel cytotoxic T cell differentiation factor. *J Immunol* **147,** 528–534 (July 1991).

177. Rousset, F. *et al.* Interleukin 10 is a potent growth and differentiation factor for activated human B lymphocytes. *Proc Natl Acad Sci U S A* **89,** 1890–1893 (Mar. 1992).

178. Sage, P. T., Paterson, A. M., Lovitch, S. B. & Sharpe, A. H. The coinhibitory receptor CTLA-4 controls B cell responses by modulating T follicular helper, T follicular regulatory, and T regulatory cells. *Immunity* **41,** 1026–1039 (Dec. 2014).

179. Wing, J. B., Ise, W., Kurosaki, T. & Sakaguchi, S. Regulatory T cells control antigen-specific expansion of Tfh cell number and humoral immune responses via the coreceptor CTLA-4. *Immunity* **41,** 1013–1025 (Dec. 2014).

180. Guthmiller, J. J., Graham, A. C., Zander, R. A., Pope, R. L. & Butler, N. S. Cutting Edge: IL-10 Is Essential for the Generation of Germinal Center B Cell Responses and Anti-Plasmodium Humoral Immunity. *J Immunol* **198,** 617–622 (Jan. 2017).

181. Laidlaw, B. J. *et al.* Interleukin-10 from CD4+ follicular regulatory T cells promotes the germinal center response. *Sci Immunol* **2** (Oct. 2017).

182. De Waal Malefyt, R. *et al.* Interleukin 10 (IL-10) and viral IL-10 strongly reduce antigen-specific human T cell proliferation by diminishing the antigen-presenting capacity of monocytes via downregulation of class II major histocompatibility complex expression. *J. Exp. Med.* **174,** 915–924 (Oct. 1991).

183. Buelens, C. *et al.* Interleukin-10 differentially regulates B7-1 (CD80) and B7-2 (CD86) expression on human peripheral blood dendritic cells. *Eur J Immunol* **25,** 2668–2672 (Sept. 1995).

184. McBride, J. M., Jung, T., de Vries, J. E. & Aversa, G. IL-10 alters DC function via modulation of cell surface molecules resulting in impaired T-cell responses. *Cell Immunol* **215,** 162–172 (Feb. 2002).

185. Thibodeau, J. *et al.* Interleukin-10-induced MARCH1 mediates intracellular sequestration of MHC class II in monocytes. *Eur J Immunol* **38,** 1225–1230 (May 2008).

186. Chattopadhyay, G. & Shevach, E. M. Antigen-specific induced T regulatory cells impair dendritic cell function via an IL-10/MARCH1-dependent mechanism. *J Immunol* **191,** 5875–5884 (Dec. 2013).

187. Ding, L. & Shevach, E. M. IL-10 inhibits mitogen-induced T cell proliferation by selectively inhibiting macrophage costimulatory function. *J. Immunol.* **148,** 3133–3139 (May 1992).

188. Ding, L., Linsley, P. S., Huang, L. Y., Germain, R. N. & Shevach, E. M. IL-10 inhibits macrophage costimulatory activity by selectively inhibiting the up-regulation of B7 expression. *J. Immunol.* **151,** 1224–1234 (Aug. 1993).

189. De Waal Malefyt, R., Abrams, J., Bennett, B., Figdor, C. G. & de Vries, J. E. Interleukin 10(IL-10) inhibits cytokine synthesis by human monocytes: an autoregulatory role of IL-10 produced by monocytes. *J. Exp. Med.* **174,** 1209–1220 (Nov. 1991).

190. Fiorentino, D. F. *et al.* IL-10 acts on the antigen-presenting cell to inhibit cytokine production by Th1 cells. *J. Immunol.* **146,** 3444–3451 (May 1991).

191. Groux, H. *et al.* A CD4+ T-cell subset inhibits antigen-specific T-cell responses and prevents colitis. *Nature* **389,** 737–742 (Oct. 1997).

192. Akdis, M. *et al.* Immune responses in healthy and allergic individuals are characterized by a fine balance between allergen-specific T regulatory 1 and T helper 2 cells. *J Exp Med* **199,** 1567–1575 (June 2004).

193. Huber, S. *et al.* Th17 cells express interleukin-10 receptor and are controlled by Foxp3- and Foxp3+ regulatory CD4+ T cells in an interleukin-10-dependent manner. *Immunity* **34,** 554–565 (Apr. 2011).

194. Gagliani, N. *et al.* Coexpression of CD49b and LAG-3 identifies human and mouse T regulatory type 1 cells. *Nat. Med.* **19,** 739–746 (June 2013).

195. Brockmann, L. *et al.* IL-10 Receptor Signaling Is Essential for TR1 Cell Function In Vivo. *J. Immunol.* **198,** 1130–1141 (Feb. 2017).

196. Foulds, K. E., Rotte, M. J. & Seder, R. A. IL-10 is required for optimal CD8 T cell memory following Listeria monocytogenes infection. *J Immunol* **177,** 2565–2574 (Aug. 2006).

197. Cui, W., Liu, Y., Weinstein, J. S., Craft, J. & Kaech, S. M. An interleukin-21-interleukin-10-STAT3 pathway is critical for functional maturation of memory CD8+ T cells. *Immunity* **35,** 792–805 (Nov. 2011).

198. Laidlaw, B. J. *et al.* Production of IL-10 by CD4(+) regulatory T cells during the resolution of infection promotes the maturation of memory CD8(+) T cells. *Nat. Immunol.* **16,** 871–879 (Aug. 2015).

199. Roncarolo, M. G. *et al.* Autoreactive T cell clones specific for class I and class II HLA antigens isolated from a human chimera. *J. Exp. Med.* **167,** 1523–1534 (May 1988).

200. Bacchetta, R. *et al.* High levels of interleukin 10 production in vivo are associated with tolerance in SCID patients transplanted with HLA mismatched hematopoietic stem cells. *J. Exp. Med.* **179,** 493–502 (Feb. 1994).

201. Heinzel, F. P., Sadick, M. D., Mutha, S. S. & Locksley, R. M. Production of interferon gamma, interleukin 2, interleukin 4, and interleukin 10 by CD4+ lymphocytes in vivo during healing and progressive murine leishmaniasis. *Proc Natl Acad Sci U S A* **88,** 7011–7015 (Aug. 1991).

202. Ghalib, H. W. *et al.* Interleukin 10 production correlates with pathology in human Leishmania donovani infections. *J Clin Invest* **92,** 324–329 (July 1993).

203. Holaday, B. J. *et al.* Potential role for interleukin-10 in the immunosuppression associated with kala azar. *J Clin Invest* **92,** 2626–2632 (Dec. 1993).

204. Reiner, S. L., Zheng, S., Wang, Z. E., Stowring, L. & Locksley, R. M. Leishmania promastigotes evade interleukin 12 (IL-12) induction by macrophages and stimulate a broad range of cytokines from CD4+ T cells during initiation of infection. *J Exp Med* **179,** 447–456 (Feb. 1994).

205. Reed, S. G. *et al.* IL-10 mediates susceptibility to Trypanosoma cruzi infection. *J Immunol* **153,** 3135–3140 (Oct. 1994).

206. Hagenbaugh, A. *et al.* Altered immune responses in interleukin 10 transgenic mice. *J Exp Med* **185,** 2101–2110 (June 1997).

207. Noben-Trauth, N., Lira, R., Nagase, H., Paul, W. E. & Sacks, D. L. The relative contribution of IL-4 receptor signaling and IL-10 to susceptibility to Leishmania major. *J Immunol* **170,** 5152–5158 (May 2003).

208. Kamanaka, M. *et al.* Expression of interleukin-10 in intestinal lymphocytes detected by an interleukin-10 reporter knockin tiger mouse. *Immunity* **25,** 941–952 (Dec. 2006).

209. Wan, Y. Y. & Flavell, R. A. Identifying Foxp3-expressing suppressor T cells with a bicistronic reporter. *Proc Natl Acad Sci U S A* **102,** 5126–5131 (Apr. 2005).

210. Brockmann, L. *et al.* Molecular and functional heterogeneity of IL-10-producing CD4+ T cells. *Nat Commun* **9,** 5457 (Dec. 2018).

211. Cavani, A. *et al.* Human CD4+ T lymphocytes with remarkable regulatory functions on dendritic cells and nickel-specific Th1 immune responses. *J Invest Dermatol* **114,** 295–302 (Feb. 2000).

212. Levings, M. K., Sangregorio, R. & Roncarolo, M. G. Human cd25(+)cd4(+) t regulatory cells suppress naive and memory T cell proliferation and can be expanded in vitro without loss of function. *J Exp Med* **193,** 1295–1302 (June 2001).

213. Meiler, F. *et al.* In vivo switch to IL-10-secreting T regulatory cells in high dose allergen exposure. *J Exp Med* **205,** 2887–2898 (Nov. 2008).

214. Serafini, G. *et al.* Type 1 regulatory T cells are associated with persistent split erythroid/lymphoid chimerism after allogeneic hematopoietic stem cell transplantation for thalassemia. *Haematologica* **94,** 1415–1426 (Oct. 2009).

215. Gregori, S. *et al.* Differentiation of type 1 T regulatory cells (Tr1) by tolerogenic DC-10 requires the IL-10-dependent ILT4/HLA-G pathway. *Blood* **116,** 935–944 (Aug. 2010).

216. Bacchetta, R. *et al.* Host-reactive CD4+ and CD8+ T cell clones isolated from a human chimera produce IL-5, IL-2, IFN-gamma and granulocyte/macrophage-colony-stimulating factor but not IL-4. *J Immunol* **144,** 902–908 (Feb. 1990).

217. Roncarolo, M. G., Gregori, S., Bacchetta, R., Battaglia, M. & Gagliani, N. The Biology of T Regulatory Type 1 Cells and Their Therapeutic Application in Immune-Mediated Diseases. *Immunity* **49,** 1004–1019 (Dec. 2018).

218. Huang, W., Solouki, S., Koylass, N., Zheng, S. G. & August, A. ITK signalling via the Ras/IRF4 pathway regulates the development and function of Tr1 cells. *Nat Commun* **8,** 15871 (June 2017).

219. Huard, B., Prigent, P., Tournier, M., Bruniquel, D. & Triebel, F. CD4/major histocompatibility complex class II interaction analyzed with CD4- and lymphocyte activation gene-3 (LAG-3)-Ig fusion proteins. *Eur J Immunol* **25,** 2718–2721 (Sept. 1995).

220. Huang, C. T. *et al.* Role of LAG-3 in regulatory T cells. *Immunity* **21,** 503–513 (Oct. 2004).

221. Liang, B. *et al.* Regulatory T cells inhibit dendritic cells by lymphocyte activation gene-3 engagement of MHC class II. *J. Immunol.* **180,** 5916–5926 (May 2008).

222. Fan, X. *et al.* CD49b defines functionally mature Treg cells that survey skin and vascular tissues. *J Exp Med* **215,** 2796–2814 (Nov. 2018).

223. Yan, X., Johnson, B. D. & Orentas, R. J. Induction of a VLA-2 (CD49b)-expressing effector T cell population by a cell-based neuroblastoma vaccine expressing CD137L. *J Immunol* **181,** 4621–4631 (Oct. 2008).

224. Huang, W., Solouki, S., Carter, C., Zheng, S. G. & August, A. Beyond Type 1 Regulatory T Cells: Co-expression of LAG3 and CD49b in IL-10-Producing T Cell Lineages. *Front Immunol* **9,** 2625 (2018).

225. Cook, L. *et al.* Suppressive and Gut-Reparative Functions of Human Type 1 T Regulatory Cells. *Gastroenterology* **157,** 1584–1598 (Dec. 2019).

226. Arif, S. *et al.* Autoreactive T cell responses show proinflammatory polarization in diabetes but a regulatory phenotype in health. *J Clin Invest* **113,** 451–463 (Feb. 2004).

227. Chujo, D. *et al.* Adult-onset type 1 diabetes patients display decreased IGRP-specific Tr1 cells in blood. *Clin Immunol* **161,** 270–277 (Dec. 2015).

228. Petrich de Marquesini, L. G. *et al.* IFN-gamma and IL-10 islet-antigen-specific T cell responses in autoantibody-negative first-degree relatives of patients with type 1 diabetes. *Diabetologia* **53,** 1451–1460 (July 2010).

229. Battaglia, M. *et al.* Induction of tolerance in type 1 diabetes via both CD4+CD25+ T regulatory cells and T regulatory type 1 cells. *Diabetes* **55,** 1571–1580 (June 2006).

230. Yu, H. *et al.* Intestinal type 1 regulatory T cells migrate to periphery to suppress diabetogenic T cells and prevent diabetes development. *Proc Natl Acad Sci U S A* **114,** 10443–10448 (Sept. 2017).

231. Van Boxel-Dezaire, A. H. *et al.* Decreased interleukin-10 and increased interleukin-12p40 mRNA are associated with disease activity and characterize different disease stages in multiple sclerosis. *Ann Neurol* **45,** 695–703 (June 1999).

232. Waubant, E. *et al.* Relationship between serum levels of IL-10, MRI activity and interferon beta-1a therapy in patients with relapsing remitting MS. *J Neuroimmunol* **112,** 139–145 (Jan. 2001).

233. Vandenbark, A. A. *et al.* Diminished frequency of interleukin-10-secreting, T-cell receptor peptide-reactive T cells in multiple sclerosis patients might allow expansion of activated memory T cells bearing the cognate BV gene. *J Neurosci Res* **66,** 171–176 (Oct. 2001).

234. Bettelli, E. *et al.* IL-10 is critical in the regulation of autoimmune encephalomyelitis as demonstrated by studies of IL-10- and IL-4-deficient and transgenic mice. *J Immunol* **161,** 3299–3306 (Oct. 1998).

235. Fitzgerald, D. C. *et al.* Suppression of autoimmune inflammation of the central nervous system by interleukin 10 secreted by interleukin 27-stimulated T cells. *Nat Immunol* **8,** 1372–1379 (Dec. 2007).

236. Gagliani, N. *et al.* Th17 cells transdifferentiate into regulatory T cells during resolution of inflammation. *Nature* **523,** 221–225 (July 2015).

237. Karwacz, K. *et al.* Critical role of IRF1 and BATF in forming chromatin landscape during type 1 regulatory cell differentiation. *Nat. Immunol.* **18,** 412–421 (Apr. 2017).

238. Glocker, E. O. *et al.* Inflammatory bowel disease and mutations affecting the interleukin-10 receptor. *N Engl J Med* **361,** 2033–2045 (Nov. 2009).

239. Shim, J. O. *et al.* Interleukin-10 receptor mutations in children with neonatal-onset Crohn's disease and intractable ulcerating enterocolitis. *Eur J Gastroenterol Hepatol* **25,** 1235–1240 (Oct. 2013).

240. Shim, J. O. & Seo, J. K. Very early-onset inflammatory bowel disease (IBD) in infancy is a different disease entity from adult-onset IBD; one form of interleukin-10 receptor mutations. *J Hum Genet* **59,** 337–341 (June 2014).

241. Alfen, J. S. *et al.* Intestinal IFN-Î-producing type 1 regulatory T cells coexpress CCR5 and programmed cell death protein 1 and downregulate IL-10 in the inflamed guts of patients with inflammatory bowel disease. *J. Allergy Clin. Immunol.* **142,** 1537–1547 (Nov. 2018).

242. Jeon, S. G. *et al.* Probiotic Bifidobacterium breve induces IL-10-producing Tr1 cells in the colon. *PLoS Pathog* **8,** e1002714 (2012).

243. Bacchetta, R. *et al.* Immunological Outcome in Haploidentical-HSC Transplanted Patients Treated with IL-10-Anergized Donor T Cells. *Front Immunol* **5,** 16 (2014).

244. Blazar, B. R. *et al.* Interleukin-10 dose-dependent regulation of CD4+ and CD8+ T cell-mediated graft-versus-host disease. *Transplantation* **66,** 1220–1229 (Nov. 1998).

245. Morris, E. S. *et al.* Donor treatment with pegylated G-CSF augments the generation of IL-10-producing regulatory T cells and promotes transplantation tolerance. *Blood* **103,** 3573–3581 (May 2004).

246. Zhang, P. *et al.* Eomesodermin promotes the development of type 1 regulatory T (TR1) cells. *Sci Immunol* **2** (Apr. 2017).

247. Chatenoud, L. CD3-specific antibody-induced active tolerance: from bench to bedside. *Nat Rev Immunol* **3,** 123–132 (Feb. 2003).

248. Ferran, C. *et al.* Cytokine-related syndrome following injection of anti-CD3 monoclonal antibody: further evidence for transient in vivo T cell activation. *Eur J Immunol* **20,** 509–515 (Mar. 1990).

249. Jutel, M. *et al.* IL-10 and TGF-beta cooperate in the regulatory T cell response to mucosal allergens in normal immunity and specific immunotherapy. *Eur J Immunol* **33,** 1205–1214 (May 2003).

250. Matsuda, M. *et al.* Regulation of allergic airway inflammation by adoptive transfer of CD4+ T cells preferentially producing IL-10. *Eur J Pharmacol* **812,** 38–47 (Oct. 2017).

251. Matsuda, M. *et al.* Adoptive transfer of type 1 regulatory T cells suppressed the development of airway hyperresponsiveness in ovalbumin-induced airway inflammation model mice. *J Pharmacol Sci* **141,** 139–145 (Dec. 2019).

252. Montes de Oca, M. *et al.* IL-27 signalling regulates glycolysis in Th1 cells to limit immunopathology during infection. *PLoS Pathog* **16,** e1008994 (Oct. 2020).

253. Batten, M. *et al.* Cutting edge: IL-27 is a potent inducer of IL-10 but not FoxP3 in murine T cells. *J Immunol* **180,** 2752–2756 (Mar. 2008).

254. Anderson, C. F., Oukka, M., Kuchroo, V. J. & Sacks, D. CD4(+)CD25(-)Foxp3(-) Th1 cells are the source of IL-10-mediated immune suppression in chronic cutaneous leishmaniasis. *J Exp Med* **204,** 285–297 (Feb. 2007).

255. Jankovic, D. *et al.* Conventional T-bet(+)Foxp3(-) Th1 cells are the major source of host-protective regulatory IL-10 during intracellular protozoan infection. *J Exp Med* **204,** 273–283 (Feb. 2007).

256. Liu, F. D. *et al.* Timed action of IL-27 protects from immunopathology while preserving defense in influenza. *PLoS Pathog* **10,** e1004110 (May 2014).

257. Sun, J., Madan, R., Karp, C. L. & Braciale, T. J. Effector T cells control lung inflammation during acute influenza virus infection by producing IL-10. *Nat. Med.* **15,** 277–284 (Mar. 2009).

258. McKinstry, K. K. *et al.* IL-10 deficiency unleashes an influenza-specific Th17 response and enhances survival against high-dose challenge. *J. Immunol.* **182,** 7353–7363 (June 2009).

259. Sun, J., Dodd, H., Moser, E. K., Sharma, R. & Braciale, T. J. CD4+ T cell help and innate-derived IL-27 induce Blimp-1-dependent IL-10 production by antiviral CTLs. *Nat. Immunol.* **12,** 327–334 (Apr. 2011).

260. Sanda, S., Roep, B. O. & von Herrath, M. Islet antigen specific IL-10+ immune responses but not CD4+CD25+FoxP3+ cells at diagnosis predict glycemic control in type 1 diabetes. *Clin Immunol* **127,** 138–143 (May 2008).

261. Yao, Y. *et al.* Tr1 Cells, but Not Foxp3+ Regulatory T Cells, Suppress NLRP3 Inflammasome Activation via an IL-10-Dependent Mechanism. *J Immunol* **195,** 488–497 (July 2015).

262. Ristich, V., Liang, S., Zhang, W., Wu, J. & Horuzsko, A. Tolerization of dendritic cells by HLA-G. *Eur J Immunol* **35,** 1133–1142 (Apr. 2005).

263. Ristich, V., Zhang, W., Liang, S. & Horuzsko, A. Mechanisms of prolongation of allograft survival by HLA-G/ILT4-modified dendritic cells. *Hum Immunol* **68,** 264–271 (Apr. 2007).

264. Awasthi, A. *et al.* A dominant function for interleukin 27 in generating interleukin 10-producing anti-inflammatory T cells. *Nat. Immunol.* **8,** 1380–1389 (Dec. 2007).

265. Stumhofer, J. S. *et al.* Interleukins 27 and 6 induce STAT3-mediated T cell production of interleukin 10. *Nat. Immunol.* **8,** 1363–1371 (Dec. 2007).

266. Takeda, A. *et al.* Cutting edge: role of IL-27/WSX-1 signaling for induction of T-bet through activation of STAT1 during initial Th1 commitment. *J Immunol* **170,** 4886–4890 (May 2003).

267. Lucas, S., Ghilardi, N., Li, J. & de Sauvage, F. J. IL-27 regulates IL-12 responsiveness of naive CD4+ T cells through Stat1-dependent and -independent mechanisms. *Proc Natl Acad Sci U S A* **100,** 15047–15052 (Dec. 2003).

268. Owaki, T. *et al.* A role for IL-27 in early regulation of Th1 differentiation. *J Immunol* **175,** 2191–2200 (Aug. 2005).

269. Owaki, T., Asakawa, M., Fukai, F., Mizuguchi, J. & Yoshimoto, T. IL-27 induces Th1 differentiation via p38 MAPK/T-bet- and intercellular adhesion molecule-1/LFA-1/ERK1/2-dependent pathways. *J Immunol* **177,** 7579–7587 (Dec. 2006).

270. Pflanz, S. *et al.* IL-27, a heterodimeric cytokine composed of EBI3 and p28 protein, induces proliferation of naive CD4+ T cells. *Immunity* **16,** 779–790 (June 2002).

271. Yoshimura, T. *et al.* Two-sided roles of IL-27: induction of Th1 differentiation on naive CD4+ T cells versus suppression of proinflammatory cytokine production including IL-23-induced IL-17 on activated CD4+ T cells partially through STAT3-dependent mechanism. *J Immunol* **177,** 5377–5385 (Oct. 2006).

272. Wang, H. *et al.* IL-27 induces the differentiation of Tr1-like cells from human naive CD4+ T cells via the phosphorylation of STAT1 and STAT3. *Immunol Lett* **136,** 21–28 (Apr. 2011).

273. Pot, C. *et al.* Cutting edge: IL-27 induces the transcription factor c-Maf, cytokine IL-21, and the costimulatory receptor ICOS that coordinately act together to promote differentiation of IL-10-producing Tr1 cells. *J Immunol* **183,** 797–801 (July 2009).

274. Hutloff, A. *et al.* ICOS is an inducible T-cell co-stimulator structurally and functionally related to CD28. *Nature* **397,** 263–266 (Jan. 1999).

275. Apetoh, L. *et al.* The aryl hydrocarbon receptor interacts with c-Maf to promote the differentiation of type 1 regulatory T cells induced by IL-27. *Nat Immunol* **11,** 854–861 (Sept. 2010).

276. Liu, J., Guan, X. & Ma, X. Regulation of IL-27 p28 gene expression in macrophages through MyD88- and interferon-gamma-mediated pathways. *J Exp Med* **204,** 141–152 (Jan. 2007).

277. Liu, X. *et al.* The T cell response to IL-10 alters cellular dynamics and paradoxically promotes central nervous system autoimmunity. *J Immunol* **189,** 669–678 (July 2012).

278. Kumar, P. *et al.* IL-27 promotes NK cell effector functions via Maf-Nrf2 pathway during influenza infection. *Sci Rep* **9,** 4984 (Mar. 2019).

279. Neumann, C. *et al.* Role of Blimp-1 in programing Th effector cells into IL-10 producers. *J Exp Med* **211,** 1807–1819 (Aug. 2014).

280. Saraiva, M. *et al.* Interleukin-10 production by Th1 cells requires interleukin-12-induced STAT4 transcription factor and ERK MAP kinase activation by high antigen dose. *Immunity* **31,** 209–219 (Aug. 2009).

281. Gabrysova, L. *et al.* c-Maf controls immune responses by regulating disease-specific gene networks and repressing IL-2 in CD4+ T cells. *Nat Immunol* **19,** 497–507 (May 2018).

282. Xu, J. *et al.* c-Maf regulates IL-10 expression during Th17 polarization. *J Immunol* **182,** 6226–6236 (May 2009).

283. DeLong, J. H. *et al.* IL-27 and TCR Stimulation Promote T Cell Expression of Multiple Inhibitory Receptors. *Immunohorizons* **3,** 13–25 (Jan. 2019).

284. Chihara, N. *et al.* Induction and transcriptional regulation of the co-inhibitory gene module in T cells. *Nature* **558,** 454–459 (June 2018).

285. Zhang, H. *et al.* An IL-27-Driven Transcriptional Network Identifies Regulators of IL-10 Expression across T Helper Cell Subsets. *Cell Rep* **33,** 108433 (Nov. 2020).

286. Sawai, C. M. *et al.* Transcription factor Runx2 controls the development and migration of plasmacytoid dendritic cells. *J Exp Med* **210,** 2151–2159 (Oct. 2013).

287. Shaw, L. A. *et al.* Id2 reinforces TH1 differentiation and inhibits E2A to repress TFH differentiation. *Nat Immunol* **17,** 834–843 (July 2016).

288. Neptune, E. R. & Bourne, H. R. Receptors induce chemotaxis by releasing the betagamma subunit of Gi, not by activating Gq or Gs. *Proc Natl Acad Sci U S A* **94,** 14489–14494 (Dec. 1997).

289. Neptune, E. R., Iiri, T. & Bourne, H. R. Galphai is not required for chemotaxis mediated by Gi-coupled receptors. *J Biol Chem* **274,** 2824–2828 (Jan. 1999).

290. Vianello, F., Olszak, I. T. & Poznansky, M. C. Fugetaxis: active movement of leukocytes away from a chemokinetic agent. *J Mol Med (Berl)* **83,** 752–763 (Oct. 2005).

291. Gregor, C. E., Foeng, J., Comerford, I. & McColl, S. R. Chemokine-Driven CD4+ T Cell Homing: New Concepts and Recent Advances. *Adv Immunol* **135,** 119–181 (2017).

292. Wilbanks, A. *et al.* Expression cloning of the STRL33/BONZO/TYMSTRligand reveals elements of CC, CXC, and CX3C chemokines. *J Immunol* **166,** 5145–5154 (Apr. 2001).

293. Kuhn, R., Lohler, J., Rennick, D., Rajewsky, K. & Muller, W. Interleukin-10-deficient mice develop chronic enterocolitis. *Cell* **75,** 263–274 (Oct. 1993).

294. Roers, A. *et al.* T cell-specific inactivation of the interleukin 10 gene in mice results in enhanced T cell responses but normal innate responses to lipopolysaccharide or skin irritation. *J Exp Med* **200,** 1289–1297 (Nov. 2004).

295. Yoshida, H. *et al.* WSX-1 is required for the initiation of Th1 responses and resistance to L. major infection. *Immunity* **15,** 569–578 (Oct. 2001).

296. Batten, M. *et al.* Interleukin 27 limits autoimmune encephalomyelitis by suppressing the development of interleukin 17-producing T cells. *Nat Immunol* **7,** 929–936 (Sept. 2006).

297. Fitzgerald, D. C. *et al.* Suppressive effect of IL-27 on encephalitogenic Th17 cells and the effector phase of experimental autoimmune encephalomyelitis. *J Immunol* **179,** 3268–3275 (Sept. 2007).

298. Lund, J. M., Hsing, L., Pham, T. T. & Rudensky, A. Y. Coordination of early protective immunity to viral infection by regulatory T cells. *Science* **320,** 1220–1224 (May 2008).

299. Fulton, R. B., Meyerholz, D. K. & Varga, S. M. Foxp3+ CD4 regulatory T cells limit pulmonary immunopathology by modulating the CD8 T cell response during respiratory syncytial virus infection. *J Immunol* **185,** 2382–2392 (Aug. 2010).

300. Ruckwardt, T. J., Bonaparte, K. L., Nason, M. C. & Graham, B. S. Regulatory T cells promote early influx of CD8+ T cells in the lungs of respiratory syncytial virus-infected mice and diminish immunodominance disparities. *J Virol* **83,** 3019–3028 (Apr. 2009).

301. Suvas, S., Kumaraguru, U., Pack, C. D., Lee, S. & Rouse, B. T. CD4+CD25+ T cells regulate virus-specific primary and memory CD8+ T cell responses. *J Exp Med* **198,** 889–901 (Sept. 2003).

302. Veiga-Parga, T. *et al.* On the role of regulatory T cells during viral-induced inflammatory lesions. *J Immunol* **189,** 5924–5933 (Dec. 2012).

303. Sehrawat, S., Suvas, S., Sarangi, P. P., Suryawanshi, A. & Rouse, B. T. In vitro-generated antigen-specific CD4+ CD25+ Foxp3+ regulatory T cells control the severity of herpes simplex virus-induced ocular immunoinflammatory lesions. *J Virol* **82,** 6838–6851 (July 2008).

304. Loebbermann, J. *et al.* Regulatory T cells expressing granzyme B play a critical role in controlling lung inflammation during acute viral infection. *Mucosal Immunol* **5,** 161–172 (Mar. 2012).

305. Lanteri, M. C. *et al.* Tregs control the development of symptomatic West Nile virus infection in humans and mice. *J Clin Invest* **119,** 3266–3277 (Nov. 2009).

306. Arpaia, N. *et al.* A Distinct Function of Regulatory T Cells in Tissue Protection. *Cell* **162,** 1078–1089 (Aug. 2015).

307. Lu, C. *et al.* Memory regulatory T cells home to the lung and control influenza A virus infection. *Immunol Cell Biol* **97,** 774–786 (Oct. 2019).

308. Zou, Q. *et al.* CD8+ Treg cells suppress CD8+ T cell-responses by IL-10-dependent mechanism during H5N1 influenza virus infection. *Eur J Immunol* **44,** 103–114 (Jan. 2014).

309. McNally, A., Hill, G. R., Sparwasser, T., Thomas, R. & Steptoe, R. J. CD4+CD25+ regulatory T cells control CD8+ T-cell effector differentiation by modulating IL-2 homeostasis. *Proc Natl Acad Sci U S A* **108,** 7529–7534 (May 2011).

310. O'Gorman, W. E. *et al.* The initial phase of an immune response functions to activate regulatory T cells. *J Immunol* **183,** 332–339 (July 2009).

311. Betts, R. J. *et al.* Influenza A virus infection results in a robust, antigen-responsive, and widely disseminated Foxp3+ regulatory T cell response. *J. Virol.* **86,** 2817–2825 (Mar. 2012).

312. Liu, Z. *et al.* Immune homeostasis enforced by co-localized effector and regulatory T cells. *Nature* **528,** 225–230 (Dec. 2015).

313. Zaiss, D. M. *et al.* Amphiregulin, a TH2 cytokine enhancing resistance to nematodes. *Science* **314,** 1746 (Dec. 2006).

314. Zaiss, D. M. *et al.* Amphiregulin enhances regulatory T cell-suppressive function via the epidermal growth factor receptor. *Immunity* **38,** 275–284 (Feb. 2013).

315. Meulenbroeks, C. *et al.* Basophil-derived amphiregulin is essential for UVB irradiation-induced immune suppression. *J Invest Dermatol* **135,** 222–228 (Jan. 2015).

316. Collison, L. W. & Vignali, D. A. In vitro Treg suppression assays. *Methods Mol Biol* **707,** 21–37 (2011).

317. Ward, S. T., Li, K. K. & Curbishley, S. M. A method for conducting suppression assays using small numbers of tissue-isolated regulatory T cells. *MethodsX* **1,** 168–174 (2014).

318. Hornick, E. E., Zacharias, Z. R. & Legge, K. L. Kinetics and Phenotype of the CD4 T Cell Response to Influenza Virus Infections. *Front Immunol* **10,** 2351 (2019).

319. Maynard, C. L. *et al.* Regulatory T cells expressing interleukin 10 develop from Foxp3+ and Foxp3- precursor cells in the absence of interleukin 10. *Nat Immunol* **8,** 931–941 (Sept. 2007).

320. Barnes, M. J. & Powrie, F. Regulatory T cells reinforce intestinal homeostasis. *Immunity* **31,** 401–411 (Sept. 2009).

321. Van Wilgenburg, B. *et al.* MAIT cells contribute to protection against lethal influenza infection in vivo. *Nat Commun* **9,** 4706 (Nov. 2018).

322. Ho, L. P. *et al.* Activation of invariant NKT cells enhances the innate immune response and improves the disease course in influenza A virus infection. *Eur J Immunol* **38,** 1913–1922 (July 2008).

323. Torcia, M. G. *et al.* Sex differences in the response to viral infections: TLR8 and TLR9 ligand stimulation induce higher IL-10 production in males. *PLoS One* **7,** e39853 (2012).

324. Robinson, D. P., Lorenzo, M. E., Jian, W. & Klein, S. L. Elevated 17β-estradiol protects females from influenza A virus pathogenesis by suppressing inflammatory responses. *PLoS Pathog* **7,** e1002149 (July 2011).

325. Robinson, K. M. *et al.* The role of IL-27 in susceptibility to post-influenza Staphylococcus aureus pneumonia. *Respir Res* **16,** 10 (Feb. 2015).

326. Chihara, N., Madi, A., Karwacz, K., Awasthi, A. & Kuchroo, V. K. Differentiation and Characterization of Tr1 Cells. *Curr Protoc Immunol* **113,** 1–3 (Apr. 2016).

327. Akdis, M. *et al.* Immune responses in healthy and allergic individuals are characterized by a fine balance between allergen-specific T regulatory 1 and T helper 2 cells. *J. Exp. Med.* **199,** 1567–1575 (June 2004).

328. Umeshappa, C. S. *et al.* Ubiquitous antigen-specific T regulatory type 1 cells variably suppress hepatic and extrahepatic autoimmunity. *J Clin Invest* **130,** 1823–1829 (Apr. 2020).

329. Anderson, K. G. *et al.* Intravascular staining for discrimination of vascular and tissue leukocytes. *Nat Protoc* **9,** 209–222 (Jan. 2014).

330. Bacchetta, R. *et al.* Growth and expansion of human T regulatory type 1 cells are independent from TCR activation but require exogenous cytokines. *Eur J Immunol* **32,** 2237–2245 (Aug. 2002).

331. Haringer, B., Lozza, L., Steckel, B. & Geginat, J. Identification and characterization of IL-10/IFN-gamma-producing effector-like T cells with regulatory function in human blood. *J Exp Med* **206,** 1009–1017 (May 2009).

332. Volz, T. *et al.* Nonpathogenic bacteria alleviating atopic dermatitis inflammation induce IL-10-producing dendritic cells and regulatory Tr1 cells. *J Invest Dermatol* **134,** 96–104 (Jan. 2014).

333. Pot, C., Apetoh, L., Awasthi, A. & Kuchroo, V. K. Induction of regulatory Tr1 cells and inhibition of T(H)17 cells by IL-27. *Semin. Immunol.* **23,** 438–445 (Dec. 2011).

334. Zheng, S. G., Gray, J. D., Ohtsuka, K., Yamagiwa, S. & Horwitz, D. A. Generation ex vivo of TGF-beta-producing regulatory T cells from CD4+CD25- precursors. *J Immunol* **169,** 4183–4189 (Oct. 2002).

335. Magnani, C. F. *et al.* Killing of myeloid APCs via HLA class I, CD2 and CD226 defines a novel mechanism of suppression by human Tr1 cells. *Eur. J. Immunol.* **41,** 1652–1662 (June 2011).

336. Betts, M. R. *et al.* Sensitive and viable identification of antigen-specific CD8+ T cells by a flow cytometric assay for degranulation. *J Immunol Methods* **281,** 65–78 (Oct. 2003).

337. Tousa, S. *et al.* Activin-A co-opts IRF4 and AhR signaling to induce human regulatory T cells that restrain asthmatic responses. *Proc Natl Acad Sci U S A* **114,** E2891–E2900 (Apr. 2017).

338. Mascanfroni, I. D. *et al.* Metabolic control of type 1 regulatory T cell differentiation by AHR and HIF1-. *Nat Med* **21,** 638–646 (June 2015).

339. Gautron, A. S., Dominguez-Villar, M., de Marcken, M. & Hafler, D. A. Enhanced suppressor function of TIM-3+ FoxP3+ regulatory T cells. *Eur J Immunol* **44,** 2703–2711 (Sept. 2014).

340. Ji, F. & Sadreyev, R. I. RNA-seq: Basic Bioinformatics Analysis. *Curr Protoc Mol Biol* **124,** e68 (Oct. 2018).

341. Morgan M, Shepherd L. *AnnotationHub: Client to access AnnotationHub resources.* version R package version 3.2.0. 2021. 10.18129/B9.bioc.AnnotationHub.

342. Hoffman, G. E. & Schadt, E. E. variancePartition: interpreting drivers of variation in complex gene expression studies. *BMC Bioinformatics* **17,** 483 (Nov. 2016).

343. Law, C. W., Chen, Y., Shi, W. & Smyth, G. K. voom: Precision weights unlock linear model analysis tools for RNA-seq read counts. *Genome Biol* **15,** R29 (Feb. 2014).

344. Raivo Kolde. *Pheatmap: pretty heatmaps* version R package version 1.0.12. 2019. https://CRAN.%20R-project.%20org/package=%20pheatmap.

345. Wickham, H. *ggplot2: Elegant Graphics for Data Analysis* 1st ed. (Springer-Verlag New York, https://ggplot2.tidyverse.org, 2016).

346. Yu, G., Wang, L. G., Han, Y. & He, Q. Y. clusterProfiler: an R package for comparing biological themes among gene clusters. *OMICS* **16,** 284–287 (May 2012).

347. Sunnarborg, S. W. *et al.* Tumor necrosis factor-alpha converting enzyme (TACE) regulates epidermal growth factor receptor ligand availability. *J Biol Chem* **277,** 12838–12845 (Apr. 2002).

348. Sternlicht, M. D. *et al.* Mammary ductal morphogenesis requires paracrine activation of stromal EGFR via ADAM17-dependent shedding of epithelial amphiregulin. *Development* **132,** 3923–3933 (Sept. 2005).

349. Janssen, E. M. *et al.* CD4+ T cells are required for secondary expansion and memory in CD8+ T lymphocytes. *Nature* **421,** 852–856 (Feb. 2003).

350. Nakanishi, Y., Lu, B., Gerard, C. & Iwasaki, A. CD8(+) T lymphocyte mobilization to virus-infected tissue requires CD4(+) T-cell help. *Nature* **462,** 510–513 (Nov. 2009).

351. Shedlock, D. J. & Shen, H. Requirement for CD4 T cell help in generating functional CD8 T cell memory. *Science* **300,** 337–339 (Apr. 2003).

352. Sun, J. C. & Bevan, M. J. Defective CD8 T cell memory following acute infection without CD4 T cell help. *Science* **300,** 339–342 (Apr. 2003).

353. Novy, P., Quigley, M., Huang, X. & Yang, Y. CD4 T cells are required for CD8 T cell survival during both primary and memory recall responses. *J Immunol* **179,** 8243–8251 (Dec. 2007).

354. Ballesteros-Tato, A., León, B., Lund, F. E. & Randall, T. D. CD4+ T helper cells use CD154-CD40 interactions to counteract T reg cell-mediated suppression of CD8+ T cell responses to influenza. *J Exp Med* **210,** 1591–1601 (July 2013).

355. Elfaki, Y. *et al.* Tregs That Transiently Accumulate in Influenza A Virus-Infected Lungs. *Int J Mol Sci* **22** (July 2021).

356. Wehrens, E. J. *et al.* IL-27 regulates the number, function and cytotoxic program of antiviral CD4 T cells and promotes cytomegalovirus persistence. *PLoS One* **13,** e0201249 (2018).

357. Hamano, S. *et al.* WSX-1 is required for resistance to Trypanosoma cruzi infection by regulation of proinflammatory cytokine production. *Immunity* **19,** 657–667 (Nov. 2003).

358. Anderson, C. F., Stumhofer, J. S., Hunter, C. A. & Sacks, D. IL-27 regulates IL-10 and IL-17 from CD4+ cells in nonhealing Leishmania major infection. *J Immunol* **183,** 4619–4627 (Oct. 2009).

359. Brooks, D. G. *et al.* Interleukin-10 determines viral clearance or persistence in vivo. *Nat Med* **12,** 1301–1309 (Nov. 2006).

360. Hall, A. O. *et al.* The cytokines interleukin 27 and interferon- promote distinct Treg cell populations required to limit infection-induced pathology. *Immunity* **37,** 511–523 (Sept. 2012).

361. Stumhofer, J. S. *et al.* Interleukin 27 negatively regulates the development of interleukin 17-producing T helper cells during chronic inflammation of the central nervous system. *Nat Immunol* **7,** 937–945 (Sept. 2006).

362. O'Garra, A. & Vieira, P. T(H)1 cells control themselves by producing interleukin-10. *Nat Rev Immunol* **7,** 425–428 (June 2007).

363. Trinchieri, G. Interleukin-10 production by effector T cells: Th1 cells show self control. *J Exp Med* **204,** 239–243 (Feb. 2007).

364. Shin, J. S. *et al.* Surface expression of MHC class II in dendritic cells is controlled by regulated ubiquitination. *Nature* **444,** 115–118 (Nov. 2006).

365. Van Niel, G. *et al.* Dendritic cells regulate exposure of MHC class II at their plasma membrane by oligoubiquitination. *Immunity* **25,** 885–894 (Dec. 2006).

366. De Gassart, A. *et al.* MHC class II stabilization at the surface of human dendritic cells is the result of maturation-dependent MARCH I down-regulation. *Proc Natl Acad Sci U S A* **105,** 3491–3496 (Mar. 2008).

367. Walseng, E. *et al.* Dendritic cell activation prevents MHC class II ubiquitination and promotes MHC class II survival regardless of the activation stimulus. *J Biol Chem* **285,** 41749–41754 (Dec. 2010).

368. Mandapathil, M. *et al.* Adenosine and prostaglandin E2 cooperate in the suppression of immune responses mediated by adaptive regulatory T cells. *J Biol Chem* **285,** 27571–27580 (Sept. 2010).

369. Montes de Oca, M. *et al.* Blimp-1-Dependent IL-10 Production by Tr1 Cells Regulates TNF-Mediated Tissue Pathology. *PLoS Pathog* **12,** e1005398 (Jan. 2016).

370. Chen, P. P. *et al.* Alloantigen-specific type 1 regulatory T cells suppress through CTLA-4 and PD-1 pathways and persist long-term in patients. *Sci Transl Med* **13,** eabf5264 (Oct. 2021).

371. Hombrink, P. *et al.* lung-resident memory T cells. *Nat Immunol* **17,** 1467–1478 (Dec. 2016).

372. Mandai, Y. *et al.* Distinct Roles for CXCR6(+) and CXCR6(-) CD4(+) T Cells in the Pathogenesis of Chronic Colitis. *PLoS One* **8,** e65488 (2013).

373. Latta, M., Mohan, K. & Issekutz, T. B. CXCR6 is expressed on T cells in both T helper type 1 (Th1) inflammation and allergen-induced Th2 lung inflammation but is only a weak mediator of chemotaxis. *Immunology* **121,** 555–564 (Aug. 2007).

374. Di Pilato, M. *et al.* CXCR6 positions cytotoxic T cells to receive critical survival signals in the tumor microenvironment. *Cell* **184,** 4512–4530 (Aug. 2021).

375. Oghumu, S. *et al.* Distinct populations of innate CD8+ T cells revealed in a CXCR3 reporter mouse. *J Immunol* **190,** 2229–2240 (Mar. 2013).

376. Groux, H. *et al.* A transgenic model to analyze the immunoregulatory role of IL-10 secreted by antigen-presenting cells. *J Immunol* **162,** 1723–1729 (Feb. 1999).

377. Wakkach, A. *et al.* Characterization of dendritic cells that induce tolerance and T regulatory 1 cell differentiation in vivo. *Immunity* **18,** 605–617 (May 2003).

378. Maynard, C. L. *et al.* Contrasting roles for all-trans retinoic acid in TGF-beta-mediated induction of Foxp3 and Il10 genes in developing regulatory T cells. *J Exp Med* **206,** 343–357 (Feb. 2009).

379. Iwasaki, Y. *et al.* Egr-2 transcription factor is required for Blimp-1-mediated IL-10 production in IL-27-stimulated CD4+ T cells. *Eur J Immunol* **43,** 1063–1073 (Apr. 2013).

380. Wang, J. C. & Livingstone, A. M. Cutting edge: CD4+ T cell help can be essential for primary CD8+ T cell responses in vivo. *J Immunol* **171,** 6339–6343 (Dec. 2003).

381. Jankovic, D., Kugler, D. G. & Sher, A. IL-10 production by CD4+ effector T cells: a mechanism for self-regulation. *Mucosal Immunol* **3,** 239–246 (May 2010).

382. Wang, N. *et al.* CD226 deficiency attenuates the homeostasis and suppressive capacity of Tr1 cells. *Mol Immunol* (Jan. 2021).

383. Di Virgilio, F., Dal Ben, D., Sarti, A. C., Giuliani, A. L. & Falzoni, S. The P2X7 Receptor in Infection and Inflammation. *Immunity* **47,** 15–31 (July 2017).

384. Scheuplein, F. *et al.* NAD+ and ATP released from injured cells induce P2X7-dependent shedding of CD62L and externalization of phosphatidylserine by murine T cells. *J Immunol* **182,** 2898–2908 (Mar. 2009).

385. Borges da Silva, H. *et al.* The purinergic receptor P2RX7 directs metabolic fitness of long-lived memory CD8+ T cells. *Nature* **559,** 264–268 (July 2018).

386. Safford, M. *et al.* Egr-2 and Egr-3 are negative regulators of T cell activation. *Nat Immunol* **6,** 472–480 (May 2005).

387. Martinez, G. J. *et al.* The transcription factor NFAT promotes exhaustion of activated CD8 T cells. *Immunity* **42,** 265–278 (Feb. 2015).

388. Desreumaux, P. *et al.* Safety and efficacy of antigen-specific regulatory T-cell therapy for patients with refractory Crohn's disease. *Gastroenterology* **143,** 1207–1217 (Nov. 2012).

389. Gagliani, N. *et al.* Antigen-specific dependence of Tr1-cell therapy in preclinical models of islet transplant. *Diabetes* **59,** 433–439 (Feb. 2010).

390. Gagliani, N. *et al.* Transplant tolerance to pancreatic islets is initiated in the graft and sustained in the spleen. *Am J Transplant* **13,** 1963–1975 (Aug. 2013).

391. Rasch, S. *et al.* Increased extravascular lung water index (EVLWI) reflects rapid non-cardiogenic oedema and mortality in COVID-19 associated ARDS. *Sci Rep* **11,** 11524 (June 2021).

392. Matthay, M. A. *et al.* Acute respiratory distress syndrome. *Nat Rev Dis Primers* **5,** 18 (Mar. 2019).

393. Szabo, P. A. *et al.* Longitudinal profiling of respiratory and systemic immune responses reveals myeloid cell-driven lung inflammation in severe COVID-19. *Immunity* **54,** 797–814 (Apr. 2021).

394. Veeravagu, A. *et al.* Acute respiratory distress syndrome and acute lung injury in patients with vertebral column fracture(s) and spinal cord injury: a nationwide inpatient sample study. *Spinal Cord* **51,** 461–465 (June 2013).

395. Andrews, L. P. *et al.* conventional T cells. *Immunity* **54,** 2209–2217 (Oct. 2021).